Tampere University

TURO VÄLIKANGAS

Numerical Studies on Fin-and-Tube Heat Exchangers

Tampere University Dissertations 499

Tampere University Dissertations 499

TURO VÄLIKANGAS

Numerical Studies on Fin-and-Tube Heat Exchangers

ACADEMIC DISSERTATION
To be presented, with the permission of
the Faculty of Engineering and Natural Sciences
of Tampere University,
for public discussion in the auditorium TB109
of the Tietotalo, Korkeakoulunkatu 1, Tampere,
on 19 November 2021, at 12 o'clock.

ACADEMIC DISSERTATION
Tampere University, Faculty of Engineering and Natural Sciences
Finland
Collaborator Koja Oy

Responsible supervisor and Custos	Professor Miikka Dal Maso Tampere University Finland	
Supervisor	Assistant Professor Ville Vuorinen Aalto University Finland	
Pre-examiners	Associate Professor Emilie Sauret Queensland University of Technology Australia	Docent Esa Muurinen University of Oulu Finland
Opponent	Professor Esa Vakkilainen LUT University Finland	

Cover design: Roihu Inc.

ISBN 978-952-03-2165-9 (print)
ISBN 978-952-03-2166-6 (pdf)
ISSN 2489-9860 (print)
ISSN 2490-0028 (pdf)
http://urn.fi/URN:ISBN:978-952-03-2166-6

PunaMusta Oy – Yliopistopaino
Joensuu 2021

Abstract

Air handling units recirculate, filter, heat and cool the air inside buildings and cruise ships. One of the most commonly used type of heat exchanger is the fin-and-tube heat exchanger. Rapid development of computational resources and open source tools during the last decade have provided an opportunity to develop a framework for accurate, automated and computationally feasible simulations. In this thesis, these tools are utilized to predict the thermal-hydraulic efficiency and fouling propensity of new and traditional fin shapes. Then, a parametric variable sweep is performed to find the optimal tube pattern for a specific fin shape and operating condition. Most importantly the present thesis seeks to answer questions such as how to build an accurate model that describes the physics of the conjugate heat transfer process in a computationally reasonable manner. And, how the shape of the fin could be changed to improve the overall thermal-hydraulic performance in a production feasible manner. In the case of a specific fin shape, the aim is to show how many different data points with different design variations are needed to create accurate surrogate models for the industry. And finally, how to assess the risk of fouling involved with new enhanced fin types in an air conditioning application and how to quantify the risk.

The Publication I studies the significance of conjugate heat transfer in contrast to purely convective heat transfer simulations. The conjugate model was shown to be more accurate for fin-and-tube heat exchanger simulations than a purely convective one. In Publication II, the focus was to develop a novel enhanced fin type with a combined vortex generator and herringbone fin design. The fin design was adapted to increase the manufacturing feasibility as much as possible. After the previous study, a concern was raised that even though better thermal-hydraulic efficiency was observed with the selection of designs in the study, this is no guarantee of the goodness with other design combinations. Therefore, in the Publication III a parametric conjugate heat transfer study was performed to find out which combinations of fin pitch, transverse tube distance and longitudinal tube distance provide the best thermal-hydraulic efficiency for a fin shape. In Publication IV, a novel selection of material properties for the fouling particles is done so that a representative range of Reynolds numbers, Stokes numbers, elasticity and adhesion parameters is covered. This study illustrates how the fouling propensity of an enhanced fin shape can be quantified and the risk of fouling can be estimated. The results show that the applied and developed numerical methods can be used for accelerated and resource effective industrial product development of fin-and-tube heat exchangers.

Tiivistelmä

Ilmankäsittelykoneita käytetään rakennuksissa ja risteilijöissä suodattamaan, kierrättämään, jäähdyttämään ja lämmittämään ilmaa, jotta käyttäjän kokema sisäilmasto on sekä mieluinen että vaatimusten ja säädösten mukainen. Lamelliputkilämmönvaihdin on yksi yleisimmistä ilmankäsittelykoneissa käytetyistä lämmönvaihdintyypeistä. Lamelliputkilämmönvaihtimien valmistaminen ja kehittäminen vaatii paljon pääomaa, joten kehityssyklien ja uusien innovaatioiden teollistaminen on perinteisesti ollut isojen toimijoiden käsissä. Viime vuosien numeeristen menetelmien kehitys ja laskentaresurssien nopea kasvu ovat mahdollistaneet tarkkojen, automatisoitujen ja laskentakapasiteettivaatimuksiltaan kohtuullisten simulaatioiden tekemisen. Tämä tarkoittaa sitä, että innovaatioiden kokeilu ja testaaminen on mahdollista myös numeerisilla työkaluilla luotujen digitaalisten mallien avulla, mikä vähentää huomattavasti tuotekehityskuluja. Tässä väitöskirjassa näitä malleja ja numeerisia työkaluja käytettiin lamelliputkilämmönvaihtimien suoritusarvojen selvittämiseen erilaisissa käyttöolosuhteissa sekä kehitettiin menetelmä, jolla voidaan arvioida uusien lamellivaihtoehtojen likaantumisalttiutta. Tärkeimpänä tutkimuskohteena oli yhdistetyn lämmönsiirron virtauslaskentamallien luominen ja niiden parametrinen automatisointi. Työssä pyrittiin myös kehittämään uusia termohydrauliselta hyötysuhteeltaan parempia lamellivaihtoehtoja, joiden valmistettavuus olisi mahdollisimman korkealla tasolla. Tässä työssä osoitettiin, kuinka monen suunnittelumuuttujan suhteen potentiaalista uutta lamellivaihtoehtoa tulisi testata, jotta lämmönvaihtimen suoritusarvoja jäljittelemään voidaan valmistaa sen ominaisuuksia vastaava surrogaattimalli. Tätä mallia voidaan käyttää ilmankäsittelykoneiden mitoittamiseen sekä optimaalisten suunnittelu- ja olosuhdemuuttujayhdistelmien määrittämiseen. Viimeisenä osa-alueena tässä työssä kehitettiin uusi menetelmä, jonka avulla voidaan arvioida ja kvantifioida lamellivaihtoehtojen likaantumisriskiä.

Julkaisussa I kehitettiin avoimen lähdekoodin ohjelmistoja apuna käyttäen yhdistetyn lämmönsiirron virtauslaskentamalli. Tämän osoitettiin olevan tarkempi kuin mallin, joka ottaa huomioon vain konvektiivisen lämmönsiirron. Julkaisussa II kehitettiin uusi lamellityyppi, jossa virtausohjaimet sijoitetaan perinteiseen kalanruotolamelliin kasvattamaan sen termohydraulista hyötysuhdetta. Tämä toteutettiin siten, että valmistettavuus pysyi mahdollisimman korkealla tasolla. Julkaisussa II osoitettiin uudella lamellityypillä olevan korkeampi hyötysuhde yhdellä suunnittelumuuttujien yhdistelmällä. Tämä ei kuitenkaan tarkoita sitä, että saavutettu hyöty olisi saman suuruinen, jos lämmönvaihtimen muita ominaisuuksia muutetaan. Edellä mainitusta syystä julkaisussa III osoitettiin, kuinka yhdelle lamellityypille ja yhdelle otsapintanopeudelle on mahdollista löytää yhdistelmä suunnittelumuuttujia, jotka johtavat parhaaseen mahdolliseen hyötysuhteen korotukseen. Tätä varten tehtiin parametrinen yhdistetty lämmönsiirtomalli, jossa käytetään itsekehitettyä parametrista avoimen lähdekoodin verkotustyökalua. Julkaisussa IV kehitettiin numeerinen menetelmä, jonka avulla eri lamellityyppien likaantumisalttiutta

voidaan vertailla. Lisäksi julkaisussa ohjeistettiin, kuinka eri materiaaliominaisuudet tulisi valita, jotta ne edustaisivat mahdollisimman hyvin käytännössä havaittavia lämmönsiirtopinnoille deposoituvia aerosoleja. Saadut tulokset osoittavat, että työssä sovellettuja ja kehitettyjä menetelmiä voidaan käyttää putkilamellilämmönvaihtimen nopeaan ja resurssitehokkaaseen tuotekehitykseen.

Preface

First three years of this study were carried out at Tampere University of Technology (TUT) and the last year in Tampere University (TAU). This study was motivated and financially supported by Koja Oy. This thesis is a research continuation to my Master's Thesis *Simulation method development for Fin-and-Tube Heat Exchanger with Open-source software*, which I was honoured to do in Chalmers University under the supervision of Professor Håkan Nilsson. Håkan Nilsson is an active developer and teacher of OpenFOAM related topics and technologies. He has been a major source of inspiration in my endeavors to learn applied fluid dynamics with OpenFOAM.

First, I would like to thank Professor Reijo Karvinen for connecting me and Koja Oy for the first time in 2014. I would also like to thank Reijo for offering me the possibility to start my PhD project under his supervision. I am very grateful for the collaboration and guidance during my first publication process. I would also like to thank the colleagues during my time in the department of Mechanical Engineering and in the department of Chemistry and Bioengineering for creating a challenging and co-operative work environment. Specially I want to thank Dr. Seppo Syrjälä, Mr. Arttu Heininen, Mr. Pekka Pasanen, Dr. Kaj Lampio, Mr. Antti Mikkonen and Mr. Niko Niemelä for being the real powerhouse and faces for fluid dynamics and heat transfer research at Tampere during the challenging times. Thank you for the guidance and fellowship during the years. An even greater feeling of gratitude goes towards Mikko Folkersma, who has been a fantastic friend and co-author during these years. Thank you for helping me to develop my coding skills as well as for all the great discussions related to fluid dynamics and life in general.

Second, I want to thank Professor Thomas Condra and Professor Kim Sørensen for inviting me to Aalborg for an inspirational and educational research visit in spring 2017 at the Aalborg University. I am even more grateful to Dr. Shobhana Singh (Indian Institute of Technology Jodhpur) for answering to my visit enquiries and introducing me to the Aalborg University. I want to thank Shobhana for a major effort in supporting and guiding me during the process of my second publication in this thesis. Special thanks for the company and friendship for Professor Tuomas Messo, Professor Jakob Hærvig and Dr. Anna Jensen.

Third, I am deeply grateful for the opportunity to switch to Aerosol physics unit at the start of 2018 and restart my PhD project in a new environment. I want to thank Professor Jorma Keskinen and Professor Jyrki Mäkelä, who welcomed me with open arms and have led the Department of Physics and Aerosol physics unit with high standards and creating a truly efficient working environment. During the particle fouling study, Dr. Heino Kuuluvainen and Professor Jakob Hærvig were a major contributor to the novelty of the method developed in the publication and therefore I am greatly thankful for the help and discussions we had related to this topic. I want to thank Miikka Dal Maso for

believing in me and offering a place in his team to continue and bring my PhD project to a conclusion under his supervision.

Fourth, I am greatly thankful for Professor Ville Vuorinen and Mr. Petteri Peltonen from Aalto University for taking the time and effort to help me during the last three years of the project. With your help I have been able to reach a much higher level in terms of the computational knowledge and the quality of the scientific publications than I ever thought. Thank you for all the guidance and information about the scientific best practices related to the field of computational fluid dynamics.

Fifth, I want to thank Mrs. Taru Lähteenmäki for the industry supervision and guidance during the last six years. Special thanks to Mr. Petteri Sippola for the insightful discussion related to heat transfer development in general. I want to thank the executives at Koja; Mrs. Leena Aalto, Mr. Jorma Aalto, Mr. Matti Sippola, Mr. Esko Nousiainen and Mr. Joonas Lius for the opportunity to do this PhD project and especially for the financial support. I want to express my gratitude to all co-workers at Jalasjärvi, Tampere and Vantaa offices who have created the best possible work environment during these years working at Koja.

Sixth, I would like to thank the pre-examiners for their constructive comments and valuable feedback that has improved the quality of this thesis.

Finally, I like to also thank my parents Kari and Maria, as well as my little sisters, grandparents and other relatives who have supported me throughout my life. For Anna, thank you for the love and support, as well as guidance throughout these years to not only talk about my PhD project, but to also ask questions about other peoples lives.

Helsinki, 28 10 2021

Turo Välikangas

Contents

Acronyms

AC air conditioning

AGW anthropogenic global warming

AHU air handling unit

ASHRAE the american society of heating, refrigerating and air-conditioning engineers

CAD computer assisted design

CFD computational fluid dynamics

CFD-DEM computational fluid dynamics and discrete element method

COP coefficient of performance

DEM discrete element method

FTHE fin-and-tube heat exchanger

FVM finite volume method

HE heat exchanger

HVAC heating, ventilation, and air conditioning

IPCC intergovernmental panel of climate change

JKR Johnson-Kendall-Roberts

LES Large Eddy Simulation

NTP normal temperature and pressure

OpenFOAM open field operation and manipulation

RANS Reynolds-averaged Navier – Stokes

SFP specific fan power

SFPint internal specific fan power

TUT Tampere University of Technology

TAU Tampere University

UN United Nations

VG vortex generator

WALE Wall-adapting Local Eddy-viscosity

Nomenclature

Symbols

$\dot{m}$	Mass flow rate, kgs^{-1}
$\overline{h}$	Overall average heat transfer coefficient, $Wm^{-2}K^{-1}$
$\boldsymbol{F}_{\text{spring,n}}$	Spring force, normal to surface, N
$\boldsymbol{F}_{\text{spring,t}}$	Spring force, tangential to surface, N
$\boldsymbol{F}_{\text{damp,n}}$	Damping force, normal to surface, N
$\boldsymbol{F}_{\text{damp,t}}$	Damping force, tangential to surface, N
$\boldsymbol{F}_{\text{jkr,n}}$	Adhesive force, normal to surface, N
$\boldsymbol{F}_{\text{jkr,t}}$	Adhesive force, tangential to surface, N
A_t	Total heat transfer area, m^2
A_{inlet}	Inlet area, m^2
A_{min}	Minimum area of cross-section, m^2
C_f^p	Specific heat of the air, $Jkg^{-1}K^{-1}$
C_s	Specific heat of the fin, $Jkg^{-1}K^{-1}$
D	Tube diameter, m
d_{h}	Hydraulic diameter,m
D_c	Tube collar diameter,m
D_{out}	Tube outer diameter before expansio, mm
f	Fanning friction factor
F_h	Fin spacing,m
F_p	Fin pitch,m
$F_{i,con}$	Contact force
$F_{i,fluid}$	Combined fluid force
i	Unit vector to the first Cartesian direction
j	Colburn j-factor
j	Unit vector to the second Cartesian direction
k	Unit vector to the third Cartesian direction
m	Mass
P_l	Longitudinal tube pitch,m
P_t	Transversial tube pitch,m
Pr	Prandtl number
Q	Overall transferred heat to the air, W
Re	Reynolds number
$Re_{d_{\text{h}}}$	Reynolds number based on hydraulic diameter and core velocity
Re_{D_c}	Reynolds number based on tube collar diameter and core velocity
T	Temperature, K
t	Fin thickness, m

T_{inlet}	Air temperature at the inlet, K
T_{outlet}	Mass averaged air temperature at the outlet, K
T_w	Temperature of the inside diameter of the tube on the fin side, K
u	Velocity in the direction of x axis, ms^{-1}
$U_{\max,avg}$	Velocity in the minimum cross-sectional flow area, ms^{-1}
U_{core}	Core velocity, ms^{-1}
v	Velocity in the direction of y axis, ms^{-1}
w	Velocity in the direction of z axis, ms^{-1}
a	Radius of the contact area, m^2
E	Young's modulus, Nm^-2
E	Young's modulus, Pa
e	Restitution coefficient
n	Surface normal vector
R	Effective particle radius, m
S_n	Material properties parameter for normal direction
S_t	Material properties parameter for tangential direction
v_c	Critical velocity, ms^{-1}
v	Incident velocity, ms^{-1}
w	Adhesion work, Jm^-2
Greek symbols	
α_f	Thermal diffusivity of the fluid, $Wm^{-1}K^{-1}$
α_s	Thermal diffusivity of the solid, $Wm^{-1}K^{-1}$
β_f	Particle volume fraction
Δp	Pressure loss, Pa
ΔT_{lm}	Logarithmic mean temperature difference, K
μ	Dynamic viscosity of air, $kgm^{-1}s^{-1}$
ν	Kinematic viscosity of the air, m^2s^{-1}
β	Coefficient restitution parameter
δ_n	overlap distance in the contact area, m
γ	Surface energy density, Jm^-2
λ_T	Tabor parameter
ν	Poisson's ratio
ρ_f	Density of the air, kgm^{-3}
Subscripts	
f	Fluid
$inlet$	Into the simulation domain
lm	Logarithmic mean
max	Maximum
$outlet$	Out from the simulation domain
s	Solid
t	Total
w	Wall
i	Particle indicator
j	Target indicator
Superscripts	
p	Constant pressure

List of Publications

This thesis consists of an overview of the topics related to the following publications which are referred in the text by their Roman numerals.

I **Välikangas T.** and Karvinen R. (2017). Conjugated heat transfer simulation of a fin-and-tube heat exchanger. *Heat Transfer Engineering*, vol. 39, no. 13-14, pp. 1192-2000, DOI: 10.1080/01457632.2017.1363628

II **Välikangas T.**, Singh S., Sørensen K. and Condra T. (2018). Fin-and-tube heat exchanger enhancement with a combined herringbone and vortex generator design. *International Journal of Heat and Mass Transfer*, vol. 118, pp. 602-616, DOI: 10.1016/j.ijheatmasstransfer.2017.11.006

III **Välikangas T.**, Folkersma M., Dal Maso M., Keskitalo T., Peltonen P. and Vuorinen V. (2021). Parametric CFD study for finding the optimal tube arrangement of a fin-and-tube heat exchanger with plain fins in a marine environment. *Applied Thermal Engineering*, vol. 200, pp. 117642, DOI: 10.1016/j.applthermaleng.2021.117642

IV **Välikangas T.**, Hærvig J., Kuuluvainen H., Dal Maso M., Peltonen P. and Vuorinen V. (2020). Deposition of dry particles on a fin-and-tube heat exchanger by a coupled soft-sphere DEM and CFD. *International Journal of Heat and Mass Transfer*, vol 149., pp. 119046, DOI: 10.1016/j.ijheatmasstransfer.2019.119046

Author's contribution

Publication 1 Conjugated heat transfer simulation of a fin-and-tube heat exchanger: The importance of solving the heat equation in the solid at the same time as solving the convective heat transfer on the air side in a fin-and-tube heat exchanger fin design was illustrated. The author designed the study and conducted all the simulations and analysis of the results. The author wrote the main draft of the manuscript. Co-author Reijo Karvinen provided comments to improve the quality of the study and took part in the writing process by giving valuable feedback on how to improve the manuscript.

Publication 2 Fin-and-tube heat exchanger enhancement with a combined herringbone and vortex generator design: A new design of a combined vortex generator and herringbone fin shape was created. The aim of the design was to provide as good thermal-hydraulic efficiency as possible at the same time as keeping the manufacturing feasibility in mind. The author designed the study and conducted all the simulations and analysis of the results. The author wrote the main draft of the manuscript in collaboration with Shobhana Singh. Other co-authors provided valuable comments and important insights into the quality of the publication.

Publication 3 Parametric CFD study for finding the optimal tube arrangement of a fin-and-tube heat exchanger with plain fins in a marine environment: This study illustrates what is the optimal tube arrangements for a fin-and-tube (FTHE) heat exchanger with plain fins for two marine application specific fin pitches $F_p = 1.5\,\text{mm}$ and $3.5\,\text{mm}$. The computational data is used to create accurate surrogate models that can be used to find the optimal design in the applicable design space. The author designed the study and conducted all the simulations and analysis of the results. The author wrote the main draft of the manuscript. The meshing tool called SwiftBlock was originally developed by Karl-Johan Nogenmyr. Mikko Folkersma and Tuomo Keskitalo have since continued the development of the tool and the author has developed the features related to parametric meshing used in this publication. All co-authors provided valuable comments and important insights into the quality of the publication.

Publication 4 Deposition of dry particles on a fin-and-tube heat exchanger by a coupled soft-sphere DEM and CFD: A new method for the selection of material properties for simulating fouling in an air conditioning application was developed. The material properties are selected in a way that the critical velocity of the particles matches the available experimental data in the literature. Collection efficiencies of different fin types, particle types and operating conditions were simulated and the results were used to asses the risk of fouling between the conditions. The author invented the new method, designed the study and conducted all the simulations

and analysis of the results. Heino Kuuluvainen played an important role in the development process of the method. Jakob Hærvig played a vital role in the set up and validation of the CFD-DEM model as well as in the development process of the material properties selection method. Ville Vuorinen played a key role in the study design and model validation. All other co-authors provided valuable comments and important insights into the quality of the publication.

1 Introduction

The present thesis consists of a summary part and 4 journal publications. The scientific findings of the thesis have been reported in the publications. The main intention of this summary is to provide an introduction to the research area and summarize the major findings of the publications.

1.1 Scope of thesis

This thesis belongs to the research field of heat transfer modelling and applied computational fluid dynamics (CFD). The main application of interest is the FTHE in the air conditioning application. The results in this thesis are of numerical nature and the used models are validated against the available data in the literature. The major focus of this thesis is to develop better performing fins with higher thermal-hydraulic efficiency. Major part of the thesis is on performing fast converging and computationally cost effective accurate conjugate heat transfer simulations and automate the process of creating the computational models. This thesis introduces a new way to implement a vortex generator (VG) to a widely used fin type called the herringbone fin. Additionally, this thesis broadens the knowledge and provides important insight about the most traditional fin type called plain fin and its relation to other design variables. Finally, this thesis introduces a new method for assessing the fouling risk of a fin type.

1.2 Motivation and background

According to the report by the intergovernmental panel of climate change (IPCC), human activities are estimated to have caused a global warming of 1 °C [1] above the pre-industrial level. The anthropogenic global warming (AGW) is estimated to increase to the level of 1.5 °C between the years 2030-2052 if it continues to increase at the current rate. The consensus in the scientific community about the estimates of global warming being human-caused, is close to 97% [2]. According to the recent studies the increase induces severe risks to health [3], livelihoods [4], food security [5], water supply [6], human security [7], and economical growth [8].

One of the criticisms towards the IPCC report is that it underestimates the influence on population growth to AGW [9]. It was concluded that by the year 2100, according to the United Nations (UN) world population projections [10], the population on earth will reach its all time high of around 11 billion people. Most of the rise is expected to occur in warmer climate areas such as sub-Saharan Africa, Asia, and Latin America. These regions have been known to have a hot climate.

Following the example of the United States of America, where the percentage of households equipped with air conditioning (AC) has increased from 0.25% to 87% in just 80 years [11], the households in developing countries are going to install AC units with even higher pace. As the wealth of the working households continues to increase, AC is seen as one of the first improvements to the quality of life that parents will want to provide for their offspring. The need for AC is therefore high and is increasing in the future.

As the building sector is one of the largest contributors to the energy consumption and CO_2 emissions in the world [12], it is important to reduce the amount of energy used by the buildings in general [13]. The amount of energy used by heating and cooling of buildings varies highly in different parts of the world, the estimates varying from 17% to 73% of the total energy consumption [12]. Globally this constitutes for around 32% of the total energy usage (24% for residential and 8% for commercial). This corresponds to 30% of the energy production related CO_2 emissions [14]. As the need for more efficient air conditioning units is growing, it is essential to increase the research efforts to improve the thermal-hydraulic efficiency of the unit.

A device responsible for recirculating, filtering, heating and cooling of the air in a building is called an air handling unit (AHU) [15]. The most important components in the AHU are the fan that circulates the air, filters that are used to clean the air and different types of heat exchanger (HE), which are used to heat or cool the air. The heat exchanger type widely used in AHUs, which is studied in the thesis is a FTHE. An AHU with its components and different kind of FTHEs is illustrated in Fig. 1.1.

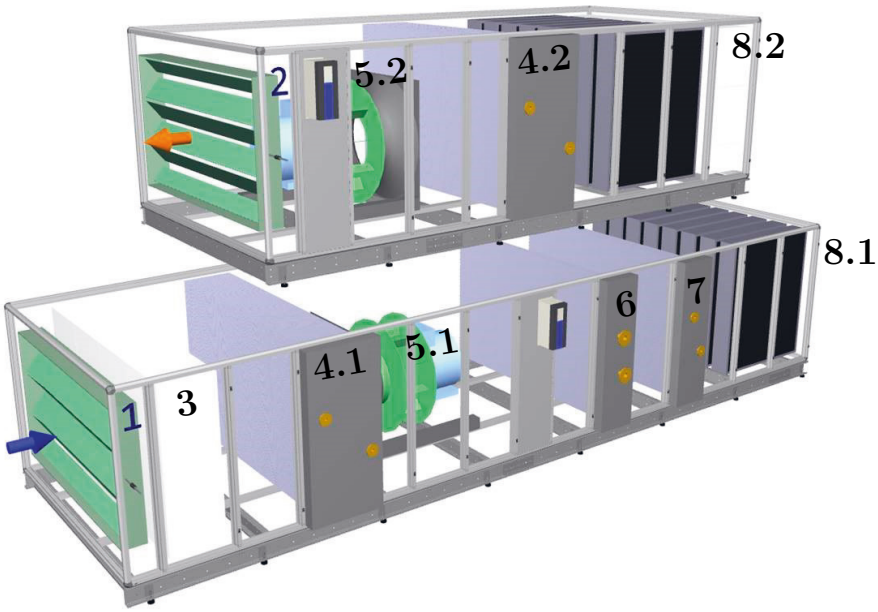

Figure 1.1: Illustration of the different components typically found in an air handling unit: 1. Fresh air damper, 2. Exhaust air damper, 3. Filter, 4.1 Fresh air heat recovery FTHE, 4.2 Exhaust air heat recovery FTHE, 5.1 Fresh air fan, 5.2 Exhaust air fan, 6. Heating FTHE 7. Cooling FTHE, 8.1 Fresh air attenuator and 8.2 Exhaust air attenuator

The energy consumption of an AHU consists of the power input of the fans illustrated in Fig. 1.1 and heat recovery pumps. The pump circulates the fluid medium, which is used for transporting the heat between the HE and the external heat source or a sink. The size and type of the fan depends on the size of the space and the requirement for the recirculation budget. If a higher pressure increase is required to push the air through the AHU and the following ducts, usually a centrifugal fan is used. For lower pressure increase, a higher efficiency axial fan can be used.

The running costs of ventilation are due to the pressure drop generated in the ducts and the AHU itself. The shorter the ducting is and the larger the cross-sectional area of the ducts and the AHU are, the smaller is the pressure drop for the flow. Despite increasing the efficiency of the fans, the only way to reduce the power consumption without increasing the size (and thus the price) of the system is to reduce the pressure loss caused by the components such as the FTHE.

1.3 Two driving factors in the development of fin-and-tube heat exchangers

The first driver for development of FTHE is the price of running an AHU. The pressure drop, and therefore the running cost, is accumulated by four main components: attenuators, filters, dampers and the heat exchangers. Dampers are used to restrict the amount of flowing air, filters are used to clean the air from impurities and the attenuators lower the noise level caused by the fan and its electric motor. The heat exchanger can be one of three different types; a thermal wheel, cross-flow plate heat exchanger or a finned tube heat exchanger. All the components generate a pressure drop, which is dependent on the design of the component and the speed of the flow through the AHU. In this thesis, the FTHE type of a heat exchanger is studied and efforts are made to show how to develop cost effective heat exchangers, in terms of the end user, and minimize the cost of manufacturing of the devices. The most important part of this is to illustrate the effect of the topological changes on the thermal-hydraulic efficiency and fouling propensity of different fin shapes on the air side of the FTHE. As was explained above, the energy consumption is generated by the fan that recirculates the air and the pump that recirculates the fluid medium inside the FTHE. The quality of the AHU is measured as the specific fan power (SFP) [16], which is calculated as the amount of energy consumed by the fan divided with the amount of supply or extract air heat capacity, which ever is higher. The main goal for the manufacturer of the AHU is to cool or heat the required amount of air so that the SFP number stays under the permissible maximum which was 1.8 kW/m^3s in 2018 building regulation [16].

The thermal-hydraulic efficiency requirements for AHUs in EU has increased due to the new ecodesign requirements for ventilation units [17] in 2014 developed by the European Parliament. First laws took effect in the beginning of 2016 and another in 2018. The new legislation's covers the minimum efficiency requirements for thermal and fan efficiency as well as for the internal specific fan power (SFPint), which on top of the power consumption takes into account the fans, filters and heat recovery systems. Currently, the ongoing negotiations for new, even more stricter legislation, brings challenges to the manufacturers of AHUs and FTHE in general. In practice, the new regulations have increased the thermal-hydraulic efficiency requirements of FTHEs. This drives the industry towards new solutions that are possibly more expensive to manufacture but meets the new requirements. On top of the EU-regulations the national legislation can implement new

restrictions and efficiency requirements [18–20] on top of the EU legislation. For example, in Finland the SFP has to consider individual heating and cooling coils on top of the SFPint related aspects, which leads to more comprehensive efficiency optimization of the whole heating, ventilation, and air conditioning (HVAC) system.

The second driver for development of FTHEs is the increasing cost of materials, such as aluminium, copper and steel. The FTHE inside the AHU consists of headers, which distributes the incoming fluid flow to the tubes inside the FTHE. The development of headers is left outside the scope of this thesis. Fins are added around the tubes for increased heat transfer surface. These fins can then be altered in such a way that the flow field on the air side can be manipulated to increase the heat transfer rate. An illustration of different sizes of FTHEs and the variables that define the heat exchanger is shown in Fig. 1.2.

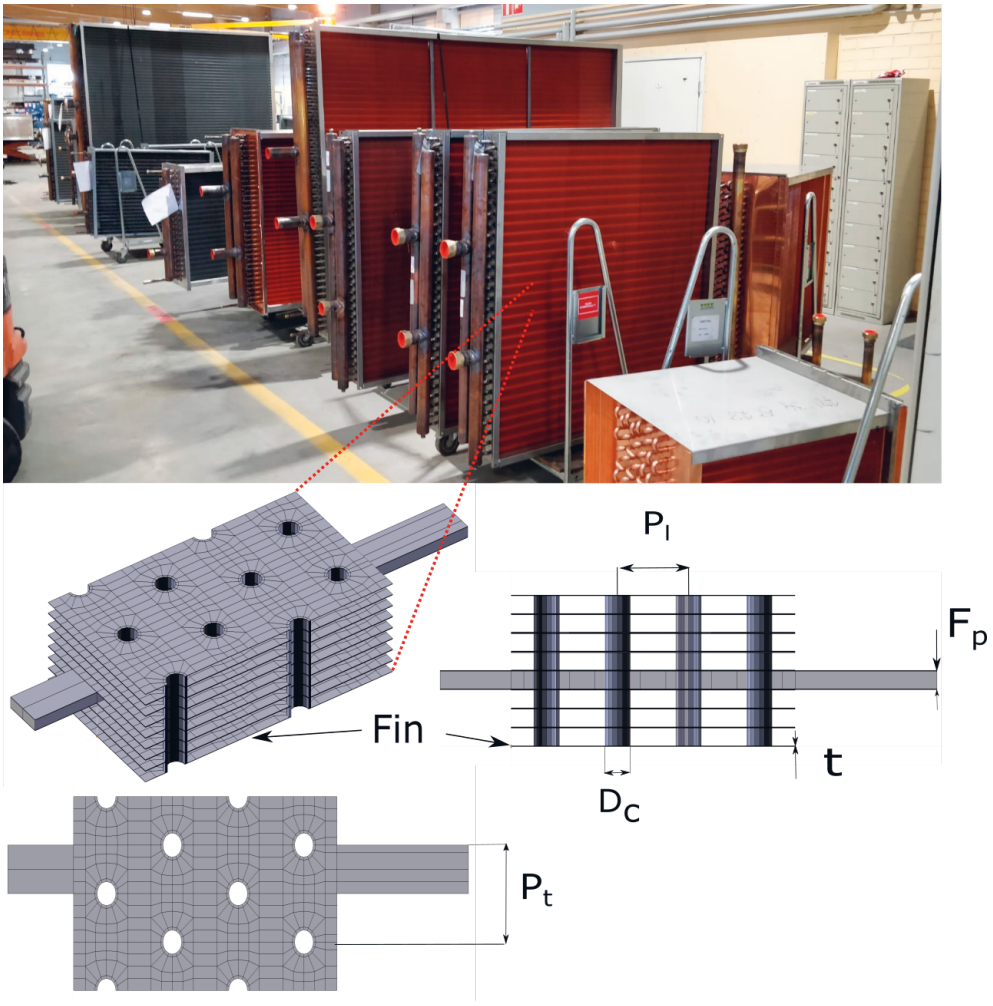

Figure 1.2: Illustration of different sizes of FTHE, the CFD domain and the design variables

All the variables used to define the heat exchanger are illustrated in the Fig. 1.2. Tube

Table 1.1: Material properties in NTP [22], prices in May 2019

Material	density $[kg/m^3]$	heat conductivity $[W/mK]$	price $[euro/kg]$
Copper	8960	397	5.58 [23]
Aluminium	2700	225	1.98 [23]
Steel	7870	14.6	0.58 [24]

collar diameter D_c, tube longitudinal pitch P_l, tube transverse pitch P_t, fin pitch F_p and the fin thickness t. Tube collar diameter is often defined as the tube diameter plus two times the fin thickness.

The headers and tubes in the FTHE are commonly manufactured from copper because of its malleability and ductility. The ductility refers to the ability of a material to stretch under tensile stress whereas the malleability refers to the ability to deform and change shape under compressive stress [21]. Both of these characteristics are required so that the material could be used for manufacturing of FTHEs. The fins are usually manufactured from copper, aluminium or steel. If the temperature level of the air is high ($> 300\,°C$), steel is the only viable option out of these tree. Otherwise, if the level of air impurities is low, aluminium fins are preferred due to their high heat transfer capacity to cost price ratio. An example of the material properties and prices of aluminium, copper and steel are shown in Table 1.1. As the density and the price per weight of copper are both around three times larger than those of aluminium, a copper fin will cost about nine times as much as a similar aluminium fin.

1.4 The manufacturing of fin-and-tube heat exchangers

This thesis focuses on the numerical simulation and development of the FTHEs. Still in the end, the numerical models are used to develop heat exchanger made out of real physical materials. Therefore it is important to discuss the tools and machines that are used to manufacture the heat exchanger parts before assembly.

The manufacturing process of the FTHE starts from the fin press machine. It is a machine that uses a roll of copper, aluminium or steel, cuts it into right length of strips, punctures holes to the fin for the tubes and forms the fin to the desired shape. Usually the fin thickness is between 0.1-0.3 mm. The fin press die has all the necessary tools, which perform the actual forming of the fin. Usually the die is the most expensive part of the machine. The thickness of the fin has an effect on the service intervals of the machine and the lifetime of the heat exchanger itself. It also affects the maximum possible fin pitch that can be manufactured, the thicker the fin the higher fin pitch can be made.

Next is a tube hairpin bender that takes a copper tube from a roll, bends it, and cuts the hairpins into the right length. Hairpin is a bent tube with a specific length. Then the hairpins are penetrated through the fin pack and the tube is expanded so that tubes and fins are connected. The circuiting strategy is implemented by soldering U-bend tubes to the opposite side of the heat exchanger. At the end of the manufacturing process the header is made. Header is connected to the tubes according to the circuiting strategy. Circuiting strategy can also be called a circuitry. The circuitry defines how many streams of fluid are flowing through the HE. If the heat exchanger has only one circuit, the same fluid stream will flow through all the tubes, if there is two circuits, one fluid stream will flow through half of the tubes and so forth.

1.5 Design parameters that affect the thermal-hydraulic performance of FTHE

In the FTHE, heat is transferred by convection on the air side, between the fins, and on the fluid side inside the tubes. Through the tubes and fins, heat is transferred by conduction and the connection between them. Because the heat transfer resistance on the air side can be around 80% [25] of the total heat transfer resistance, it is the most beneficial to direct the improvement efforts on that particular side. As a side note, in the air conditioning application, the temperature levels are low enough so that the radiation heat transfer can be neglected. [22]

Before further investigating different fin types, it is important to be aware of design parameters related to the FTHE design. Regardless of the fin type design, the FTHE thermal-hydraulic characteristics can be manipulated by changing the face area, number of tube rows, fin pitch and thickness, diameter and thickness of the tubes and the distance of the tubes from each other. Tube distances can be altered both in the direction of the air flow and perpendicular to it and the tubes can be arranged in an in-line or a staggered layout. All designs studied and discussed in this thesis are using the staggered tube layout.

Due to the constraints of the manufacturing process and production economics, FTHE manufacturers are forced to use a fixed combination of tube sizes, fin pitches and other design parameters. Often it is beneficial to specify different designs for distinct application. Very few data is found from the literature about the effect of the tube diameter and the distance pattern on the overall suitability of a design set for a specific application. Some studies suggest that smaller tubes, such as $D_{out} = 5\,\text{mm}$-$7\,\text{mm}$ with dens patterns $P_l = 12\,\text{mm}$-$20\,\text{mm}$ and $P_t = 20\,\text{mm}$-$30\,\text{mm}$ are commonly used in a residential air-handling products such as air-to-air and air-to-water heat pumps [26, 27]. The benefits from smaller tube size are gained in two different ways. On the air side, smaller tube size causes less form drag and have a higher heat transfer coefficient due to smaller hydraulic diameter of the flow. On the fluid side, smaller tubes require less refrigerant volume and enable the use of higher pressures in the process. As the price for the refrigerants continues to increase [28], it is reasonable that smaller tube sizes are becoming increasingly common in applications involving refrigerants. In the case of other working fluid, especially water, the benefits or of smaller tube size are more ambiguous.

1.5.1 Face area and face velocity

Together with air volume flow, the face area dictates the velocity of which the air encounters the heat exchanger, namely, the face velocity. The face area is dictated by space and economical limitations and the volume flow is usually implied by a fresh air flow requirement or other constraints independent of the actual heating or cooling demand. Therefore, face velocity often acts as a design point at which the thermal-hydraulic performance of the heat exchanger is to be examined.

The face (or frontal) area is the area of the cross section which the incoming air flows through the heat exchanger. The face area can be calculated as $A_{face} = HW$, where H is the height and W is the width of the heat exchanger. Most of the numerical results concerning FTHE efficiency are obtained by simulating only the air flow between two fins (or a flow around one fin) and the flow is restricted to consider only one or two adjacent tube rows. Most of the experimental results are instead obtained by measuring

the average flow temperature before and after and the pressure drop over the whole heat exchanger [25, 29−31]. It is clear that with a smaller face area, the ratio between the circumference and the face area is higher and therefore the effect on the boundary layer at the wall is higher. These experimental setups are conducted with various different face area sizes and no conclusions are made about the effect of the difference between different sizes of frontal areas.

Mao et al. [32], studied the effect of four different incoming flow distributions to the overall performance of the heat exchanger and concluded a 1-7% decrease in the heat transfer rate with a linear flow profile compared to a uniform profile. Yaïci et al. [33] have studied the maldistributed flow profile and its effect on the aforementioned channel flow. These studies illustrate the effect of the flow profile on the local heat transfer rates in each channel. The maldistribution of the incoming air and its effect on the performance of the FTHE in a residential application have been studied by Kærn et al. [34] who reported a decrease of 43% in the coefficient of performance (COP).

As all the simulations in this study are performed on the simplified piece of the heat exchanger, the effect of flow maldistribution cannot be taken into consideration when comparing the results to the experimental values found in the literature.

1.5.2 Effect of the number of tube rows to the FTHE thermal-hydraulic efficiency

The number of tube rows is one of the most important design variables in the FTHE design. Given a specific face area, fin pitch and tube arrangement, the heat transfer area both in the fluid side and the air side are directly proportional to the number of tube rows. Naturally, increasing the number of tube rows increases heat transfer capacity but, as a downside, also the pressure drop. The thermal-hydraulic efficiency of each tube row is different from each other. It is important to understand that the flow field will change inside the heat exchanger and is fully developed approximately after the sixth row, as shown experimentally by Wang and Liaw [35] and computationally Xie et al. [36]. Some studies claim that the thermal-hydraulic efficiency is constant after the forth row [37, 38], which is of course affected by the hydraulic length scale and the velocity of the flow. It is apparent that in addition to the hydraulic length scale and the velocity of the flow (and therefore the Reynolds number [39]), the shape of the fins affects the entrance length and thus the number of tubes required to achieve a fully developed flow. Unfortunately, no studies have been done to compare the differences according to the knowledge of the author. The important question is, how many tube rows should be studied so that the results would represent the characteristics of the whole spectrum of number of tube rows. Despite the possible informativity of such a study, higher number of tube rows are rarely considered in the literature. On the experimental side, the restrictive factor is that bigger heat exchanger requires higher heat loads in order to show differences in the results. The circuiting strategy on the experimental studies adds another layer of complexity and usually only very simple strategies are used. Whereas on the numerical side, the computational expenses increases almost linearly with the number of the rows. Also, on the numerical side, the circuiting strategy can be neglected by applying a constant temperature on the inner side of the tube. The computational as well as labour resources spent on the mesh generation process, despite the meshing strategy, increases linearly with the number of tube rows.

1.5.3 Effect of fin pitch on the FTHE thermal-hydraulic efficiency

Similarly to the other design properties of a FTHE, the fin pitch can be changed to manipulate the thermal-hydraulic efficiency. Usually in HVAC applications, fin pitch is varied between 1 mm - 5 mm. In case of simple shapes produced by pressing such as sine wave and herringbone, fin pitch can be varied rather freely as the fins fit inherently on top of each other. The exception from this is VGs and other guide vanes that are punched from the fin and erected upwards. The effect of the fin pitch to the normalised heat transfer and pressure drop depends on the inlet velocity of the flow [40]. Wongwises and Chokeman [41] reported that fin pitch does not have an effect to the heat transfer but the pressure drop increases with a higher fin pitch.

1.5.4 Enhanced fluid side heat transfer of a FTHE

Around 20-30 % [42, 43] of the resistance in the heat transfer process of a FTHE is related to the fluid side. The fluid flows forth and back through the heat exchanger a number of times. Each set of mutually connected tubes forms a circuit, which are usually designed to run as parallel to the air flow as possible in order to achieve maximum average temperature difference between the fluid and the air. If a heat exchanger has only one circuit, this means that one fluid stream will flow through every individual tube before exiting the heat exchanger. When the number of circuits is increased, the average length of a circuit is decreased. An illustration of a FTHE circuiting strategy with 23 circuits is shown in Fig. 1.3

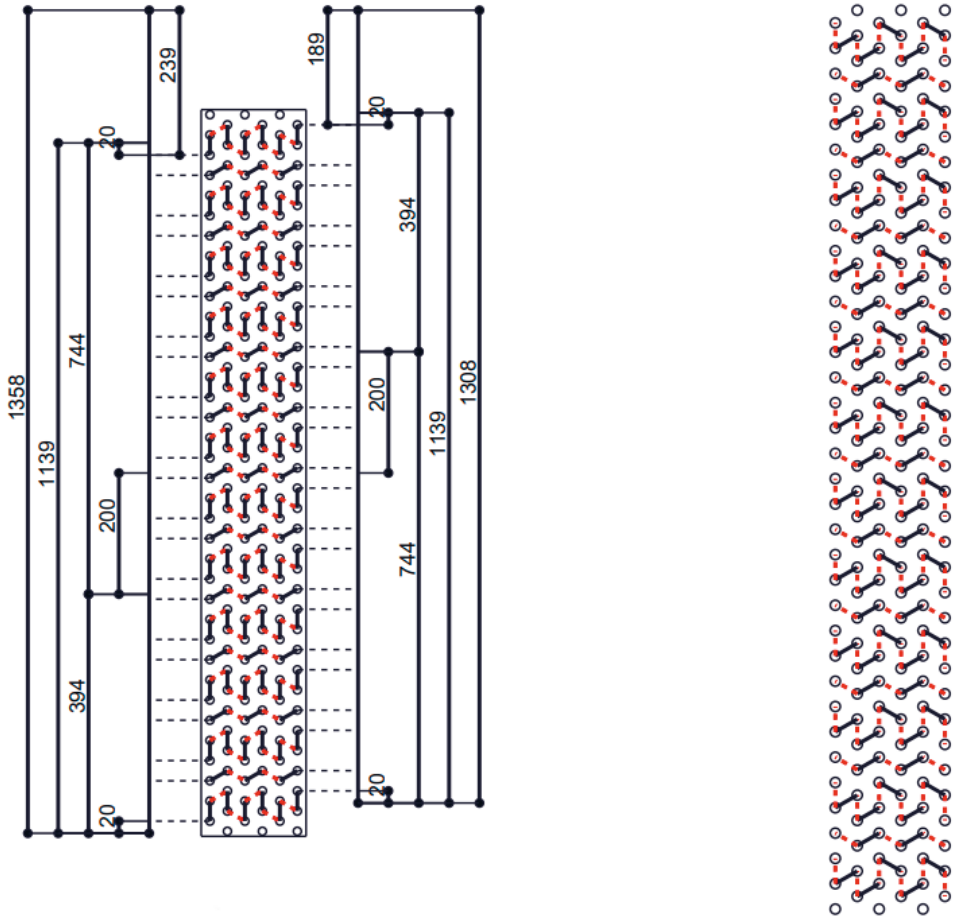

Figure 1.3: Illustration of the circuitting strategy with 23 circuits in the FTHE

The fluid side of the heat transfer process can be improved by implementing different kind of surface structures inside the tubes. Dimples can be added to the tubes [44] and tubes can be spirally corrugated [45] or ribbed [46]. Some enhanced tube surfaces can offer higher heat transfer rates with a relatively small increase in the pressure drop. As the fins are traditionally joined to the tubes by pulling a mechanical expander through the tubes, any pre-manufactured enhancement on the inner tube surfaces are diminished dramatically during the process. It is still uncommon to use enhanced tube types in the FTHE design because of the mechanical expanding process. In the future, the pressure expander technology can become more common and the use of enhanced tubes will increase. No academic literature is found on the pressure expander technology but prototypes have been seen in the industry.

1.5.5 The effect of tube size and tube pattern

The size of tubes and their location with respect to each other directly affects the hydraulic length scale and the core velocity of the flow. This means that in the case of two different heat exchangers with two different tube size-pattern combinations, the Reynolds number (based on the hydraulic length scale and the core velocity of the flow) inside the heat exchanger is different for the same face velocity. For example, in the case of the aforementioned two different heat exchangers, the non-dimensional heat transfer and pressure drop for these two designs can be made equal by using different face velocities. As the enhancement level of using a fin enhancement is a function of the Reynolds number, the benefit of using this enhancement is different for these two heat exchanger designs when the face velocity is kept constant. The same face velocity can be perceived as a specific application. In other words, the fin enhancement offers a larger improvement to use in one application than for some other application with completely different tube size-pattern combination and face velocity. Another angle to this discussion of fin enhancement and tube size-pattern combination is that some fin enhancements can be impossible to use with really small tube sizes. The smaller the tube-pattern combination is the smaller the absolute dimensions of the features in the fin enhancement are. This can be a challenge for the fin press tool manufacturer.

All these different design factors introduced before in this section are an essential part of the design process of a FTHE. When new enhanced fin designs are introduced, it is important to consider their effect on the whole design and other factors that impact the thermal-hydraulic efficiency of a FTHE.

1.6 Three generations of enhanced fin shapes

Tube banks without any attached fins have been thoroughly studied and their charasteristics are underlined by Zukauskas [47]. Originally fins were added around the tubes to increase the heat transfer surface and to make the volume of the heat exchanger smaller [48]. The fin type itself can be changed to manipulate the flow on the air side. These, are called the enhanced fin shapes. In general, higher turbulence levels are associated with higher heat transfer rates and higher pressure drops. [22] The enhancement mechanism can be divided into two different types, first one being the one that provides better mixing of the flow due to the boundary layer separation. This type of enhancement is seen in wavy fin shapes such as herringbone or sine-wave. The other mechanism is the repeated growth and wake destruction of the boundary layers. This can be said to be the main enhancement mechanism in slit, offset, louvered and even vortex generator fin types [49].

Plain fin shape is illustrated in Fig. 1.4. Different fin shape enhancements are divided into different generations of enhancements. First one being the transversial vortices, where wavy shapes such as sine wave or herringbone fins were used. Herringbone fin shape is illustrated in Fig. 1.5. These kind of transverse vortices that rotate perdendicular to the flow direction enabled the FTHE manufacturers to decrease the size of the heat exchanger but with the cost of an increase on the pressure drop over the heat exchanger. The second generation includes the chaotic turbulence fins such as louvered or slit fins that were generated by perforating the fin completely, twisting and elevating pieces of the fin to generate as much turbulence as possible. The X-slit fin shape is illustrated in Fig. 1.6. This enabled the manufacturers again to decrease the size of the heat exchanger but with an even larger increase on the pressure drop on the air side. The most recent methods of development have been the means of using intelligent turbulence management.

This means that only specific kind of turbulence is created in regions where it is the most beneficial for the heat transfer process. Such turbulence can be used by integrating vortex generators to the fin that guide the flow and generate longitudinal vortices. These type of vortices improve the heat transfer in regions where the pressure drop penalty for the increased heat transfer is the lowest. An illustration of the vortex generator fin shape with a herringbone fin shape can be seen in Fig. 1.7.

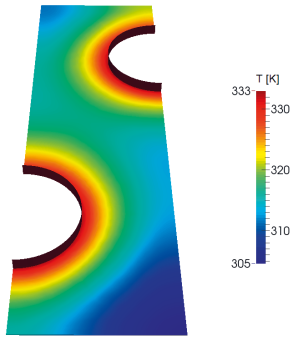

Figure 1.4: Plain fin (Figure adopted from **Publication I**)

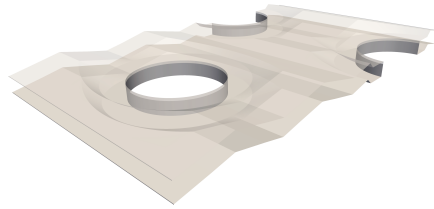

Figure 1.5: Herringbone fin with transverse turbulence

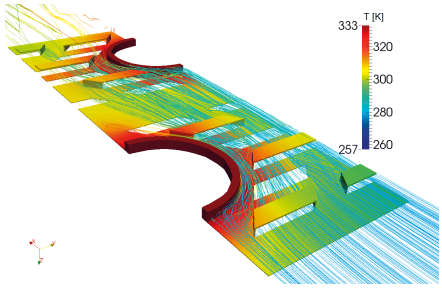

Figure 1.6: X-slit fin with chaotic turbulence (Figure adopted from **Publication I**)

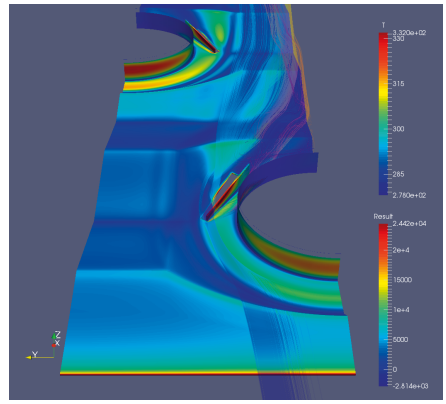

Figure 1.7: Combined herringbone and vortex generator fin with intelligent turbulence management

The challenge in comparing the performance of different fin shapes is the difficulty to express the thermal-hydraulic characteristics published in the literature in a comparable manner. The first challenge is the deviation of the results between experimental and numerical results. It is clear that there is no standardisation on the experimental setup in terms of frontal area, used temperature levels or in the turbulence levels of the inlet flow. Most of the older experimental studies are comprised into correlation studies [29, 50–53] where multiple experimental studies are expressed in terms of a correlation equation. It is clear that the effect of the experimental setup and error in the experimental setup is

averaged and obscured between the studies. As the original studies and publications are not accessible anymore [54, 55], at least not in the context of the agreement between the authors university and the publishers party, it is practically impossible to evaluate the credibility of the constructed correlations against the experimental data. Even if the original article is accessible, the thermal-hydraulic results are commonly presented as a scatter plot, where the exact value information is not tabulated and therefore can not be extracted easily. This creates an additional error in the interpretation of the values when transforming individual points to comparable data. Finally, there is the question of what combinations of the other variables affect the thermal-hydraulic efficiency, such as fin pitch, tube size, tube pattern and fin thickness. Naturally, the authors are studying and reporting values of real existing FTHE designs that are manufactured with applicable machinery. This means that data from uncommon combinations are absent. On top of this, not all possible combinations have been measured and therefore the complete relation between the fin shape and design parameters and their effect on the thermal-hydraulic efficiency is obscured. In Publication III, a computational study is performed to overcome this issue by providing data on all the possible design variable combinations that were under investigation. Such an approach should be expanded to all other studies in the future that investigate the thermal-hydraulic efficiency of fin type.

1.6.1 Vortex generators with wavy fin shapes

In the Publication II, a new vortex generator VG design is proposed on top of the traditional herringbone fin shape. Vortex generators have been a popular research topic during the last few years. As Li et al. [56] concluded, the use of vortex generators have been widely approved by the academic and industry partners in the recent years and a wide range of research for pure air has been conducted to study the effect of longitudinal vortices to the heat transfer characteristics of a FTHE [57–59]. On the other hand, studies with combined wavy fin and VG studies are very few. The academic results found on the wavy fin shape with VGs are tabulated in Table 1.2.

Table 1.2: Previous investigations on wavy fin-and-tube heat exchangers studies with vortex generators or delta winglets

Fin type	Tube type	Study type	Conjugate/Only convective	Authors
Smooth wavy	Elliptic	Numerical	Only convective	Lotfi et al. [60]
Smooth wavy	Elliptic	Numerical	Only convective	Lotfi et al. [61]
Smooth wavy	Round	Numerical	Only convective	Lotfi et al. [62]
Smooth wavy	Elliptic	Numerical	Only convective	Lotfi et al. [63]
Herringbone	Round	Numerical	Only convective	Lotfi et al. [64]
Herringbone	Round	Numerical	Only convective	Gong et al. [65]
Herringbone	Round	Numerical	Conjugate	Tian et al. [66]
Herringbone	Round	Numerical	Only convective	Tian et al. [67]
Herringbone	Round	Numerical	Only convective	Tian et al. [68]
Herringbone	Round	Numerical	Conjugate	Tian et al. [69]
Herringbone	Round	Numerical	Conjugate	Tian et al. [70]
Herringbone	Round	Numerical	Only convective	Li et al. [71]
Plain, Herringbone	Round	Numerical	Only convective	Ke et al. [72]
Herringbone	Elliptic	Numerical	Only convective	Damavandi et al. [73]
Herringbone	Flat	Experimental	Conjugate	Du et al. [74]
Herringbone	Round	Numerical	Conjugate	Gholami et al. [75]
Herringbone + VG	Round	Numerical	Conjugate	Publication II

It can be seen that only few of the computational studies uses a conjugate heat transfer

model. Possible reason for this is due to the sheer difficulty of meshing the computational domain and connecting the fluid and solid domain in a computationally feasible way. It was shown in the Publication II, that the temperature variations in the fin are very local and therefore global fin efficiency approximations can not be applied. In Table 1.3, is a brief illustration of the fin-and-tube heat exchanger studies found in the literature that are conducted in a conjugate manner.

Table 1.3: Conducted studies found on FTHEs with conjugate heat transfer models

Fin type	**Tube type**	**Solver sw**	**Meshing sw**	**Authors**
Herringbone+VG	Round	Fluent	Gambit	Tian et al. [68]
Plain/Louvered	Round	Phoenics	Ansys	Leu et al. [76]
Plain+VG	Oval	In-house	In-house	Chen et al. [77]
Plain+VG	Flat/Oval	Fluent	Gambit	Delač et al. [78]
Plain+VG	Oval	Fluent	Gambit	Chen et al. [79]
Plain+VG	Flat/Oval	Unknown	Unknown	Chen et al. [77]
Plain	Flat	Unknown	Unknown	Wang et al. [80]
Plain	Round	Fluent	Gambit	Tsai and Sheu [81]
Plain	Oval	Fluent	Unknown	Chu et al. [82]
Plain	Flat	Fluent	Gambit	Malapure et al. [83]
Plain/Slit	Round	Unknown	Unknown	Tsai et al. [84]
Louvered	Round	STAR-CD v3.15	Unknown	Perrotin and Clodic [85]
Plain	Round	OpenFOAM	Swiftblock+Salome	Publication I
Herringbone + VG	Round	OpenFOAM	Swiftblock	Publication II
Plain	Round	OpenFOAM	Swiftblock	Publication III

It is clear that the commercial code Fluent [86] combined with the meshing tool called Gambit is the most popular choice in the literature. Gambit is a product of ANSYS as well as Fluent and therefore offers a good match when licences are possessed. Unfortunately, in some articles, the solver or the meshing tool type is not revealed and therefore it is left unknown in the table. Few studies are conducted with an in-house code. Typically in these studies the temperature field in the fin is approximated with a two dimensional equation. In other words the temperature field in the fin is not calculated completely but its effect on the fluid side is approximated. This means that this way it would be very challenging to perform conjugate heat transfer simulations for a fin shape with three dimensional features. The authors guess is that overall the reason why there is only a handful of conjugate studies is due to two facts. First one is the level of difficulty of making the meshes for the domains. Second one is the ability to simulate the cases with a coupled solver architecture. In this context, segregated solver computes all the domains separately in an order and then interpolates the values on the borders. In a coupled solver, the field is solved at once in one matrix operation for all domains. If a segregated solver is used, the converge times of the cases are often infeasible long. Currently, the only solvers that have the matrix coupled heat transfer solver are Fluent and foam-extend [87]. As seen in the table, on top of the authors study II, there are only handful of conjugate studies with three-dimensional fin features [68, 76 – 79, 84, 85]. The reason for this is underlined above. An extensive introduction to conjugate heat transfer is given in Publications I and II.

1.6.2 From individual design points to a general model

In the industry, a collection of design and selection softwares are used to rapidly compare and select the correct utilities for the AHU. To make this possible, a set of libraries

are used inside the software to calculate the thermal and hydraulic performance of fans, heat exchangers and filters. These libraries can be called digital twins of the real world devices. They are a simplified version of the reality that predicts the performance based on the relation between inputs and outputs that have been either measured, simulated or calculated before hand. These digital twins consist of surrogate models that represent more in detail a subset of the physics inside the heat exchanger. [88] An example of this could be a heat transfer correlation for the air side heat transfer of a FTHE [89]. The surrogate model is based on features, which are the inputs of the model, such as the tube size, tube pattern, fin pitch, fin thickness and Reynolds number of the air flow. The models output is the rate of heat transfer with a specific collection of features.

Traditionally the experimental academic research has been circulating around finding model based equations that predict the heat transfer and pressure drop of the existing heat exchanger designs. First, individual authors have conducted experimental studies of a specific design [89–92]. Then a correlation study [52] was performed where an equation is developed, which combines the data from all these studies. These correlations are designed in a way that they describe most of the data with the smallest mean deviation as possible. They are then used in the industry to predict the thermal-hydraulic efficiency of a specific design and operation point. The main challenge with the experimental approach, as already mentioned before, is the bias in the data towards existing designs already manufactured in the industry. Another challenge is that there exists a collection of manufacturing restrictions that are followed in the industry. For example, one very common rule that is followed in the industry is to use a tube pattern that has the ratio of tranversial tube pitch to longitudinal tube pitch P_t/P_l =1.1547. This enables the manufacturer to use only one kind of U-bend tubes in the process of soldering the circuits. For example the experimental studies found in the literature on the thermal-hydraulic efficiency of FTHE with plain fins [50, 51, 55, 91, 93–95] have a 61% portion with the aforementioned ratio. This topic is discussed more in detail in Publication III.

When a study is conducted on a new fin shape such as the one in Publication II, possible higher thermal-hydraulic results are a good indication of a better performing fin shape. But this information is not enough because there is no guarantee of the goodness if some aspects of the design is changed. Therefore, to ensure the goodness, a complete data should be constructed for the whole design space. Such a study is performed in the Publication III for the traditional plain fins. In the study, a completely open source and parametric structured meshing tool developed by the authors was used to produce the computational meshes in this study. The parametric computational model was then used to simulate the thermal-hydraulic efficiency of a plain fin shape for a selection of different tube patterns. A regression model was created for the performance ratio JF, based on the CFD simulations for two different fin pitches $F_p = 1.5\,\text{mm}$ and $3.5\,\text{mm}$ and a selection of different tube patterns covering longitudinal tube pitch $P_l = 14{-}78\,\text{mm}$ and transverse tube pitch $P_t = 14{-}38\,\text{mm}$. The study illustrates that by not following any restrictions related to the tube pattern, it is possible to find combinations with higher thermal-hydraulic efficiency. It was also concluded that overall, the smaller fin pitch offers a higher efficiency with all tube patterns, which is consistent with the literature [96, 97].

1.7 Laminar and turbulent heat transfer

Next a short discussion about the level of turbulence, laminar flow and the Reynolds number is laid out. The velocity field inside the heat exchanger can be considered to

be laminar if the streamlines in the flow field are continuous [39]. When the velocity is increased, the hydraulic length scale is increased or the viscosity of the fluid is decreased, the level of turbulence increases [39]. The commonly used measure for turbulence is the Reynolds number $Re_{D_h} = \frac{u_{ref} D_{ref}}{\nu}$ [39], where u_{ref} is the reference velocity, D_{ref} is the reference length scale and ν is the dynamic viscosity of the fluid. When the Reynolds number is high enough the streamlines break up and the flow is considered to be turbulent. There exists no precise definition of what is turbulent flow and a clear separation between laminar and turbulent flow, cannot be drawn [39, 98, 99]. In a turbulent flow the velocity can be divided into two parts; the transient fluctuating velocity —*— and the mean velocity ——. An illustration of the local fluctuating velocity and the mean velocity in an arbitrary example is shown in Fig. 1.8

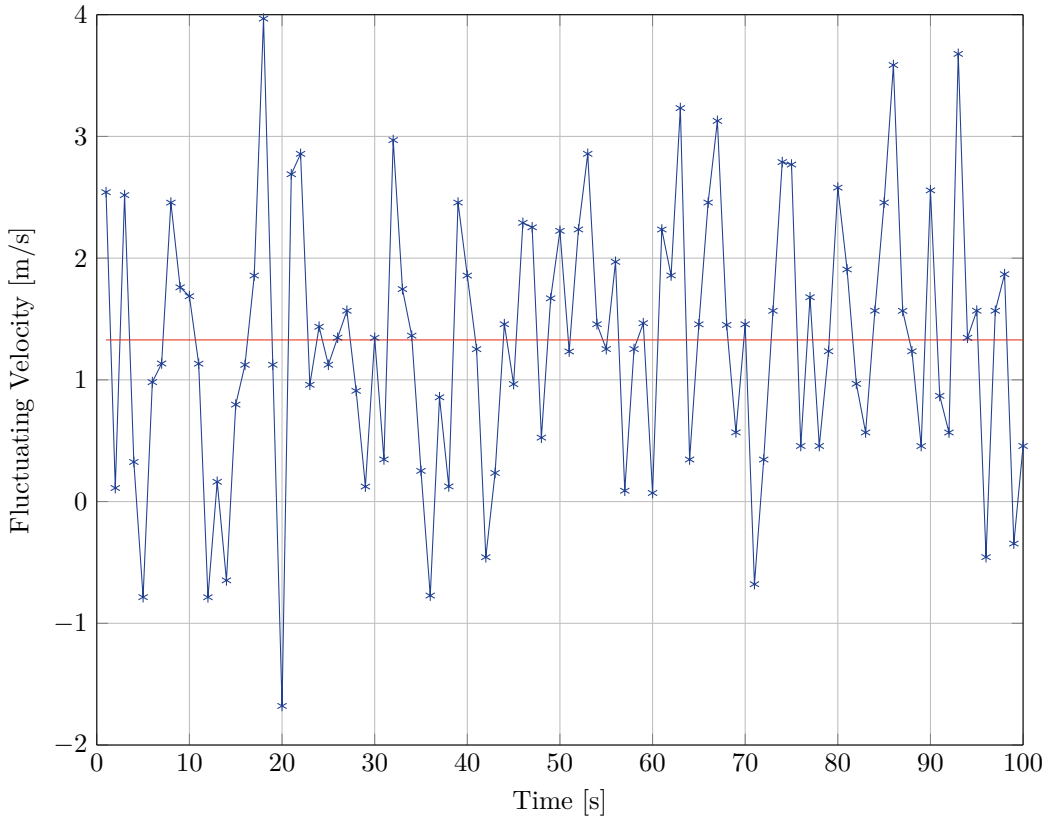

Figure 1.8: Two components of turbulent velocity: —*— is the transient fluctuating velocity and —— is the mean velocity

The fin type itself has a major effect on the level of turbulence inside the heat exchanger. But as is illustrated in Publication III, the turbulence level is also dependent on all the other design variables. In the literature, the Reynolds number is often used as a measure of the operating point in heat exchanger studies. This convention is also followed in Publications I, II and IV. But as is illustrated in Publication III for the same inlet velocity, and therefore the same operating point, a myriad of different values for Reynolds number is calculated with different design configurations. Therefore, not only in this thesis but

in the literature for heat exchangers in general, a careful readers discretion is advised regarding the relationship between turbulence level, operating point and the definition of the Reynolds number. [100]

1.7.1 Fundamentals of Heat Transfer

Heat transfer can be divided into conduction, convection and radiation. As mentioned before, due to low temperature levels in fin-and-tube heat exchangers the radiation is very often neglected. The law that governs heat conduction was first proposed by J.B. Fourier in 1822 [22]. It states that the heat will flow through the medium in the direction of decreasing temperature gradient. The heat flux can be defined as $\dot{q} = -k\nabla T$, where k is called the thermal conductivity of the medium.

Convective heat transfer can be considered to be a combination of conduction and advection. Advection is defined as the measure of mass that is transferred with the flow field. The heat transfer coefficient is based on the Newton's law of cooling which states that rate of heat loss of a body is proportional to the difference in temperature between the body and surroundings. The heat transfer coefficient based on the Newton's law of cooling can then be calculated as $h = \frac{\dot{q}}{A\Delta T}$, which is the amount of heat transferred $\dot{q}$ per the surface area A and the temperature difference ΔT between the object and the surroundings.

1.7.2 Boundary layer

Convective heat transfer can be defined as the integration of the velocity and temperature profiles over the flow medium. In the boundary layer, the value of the profile changes from the free flow value to the value at the wall. As was explained before, the repeated growth and wake destruction of the boundary layer increases heat transfer in the FTHE [49]. An illustration of the boundary layer profiles for temperature and velocity are shown in Fig. 1.9.

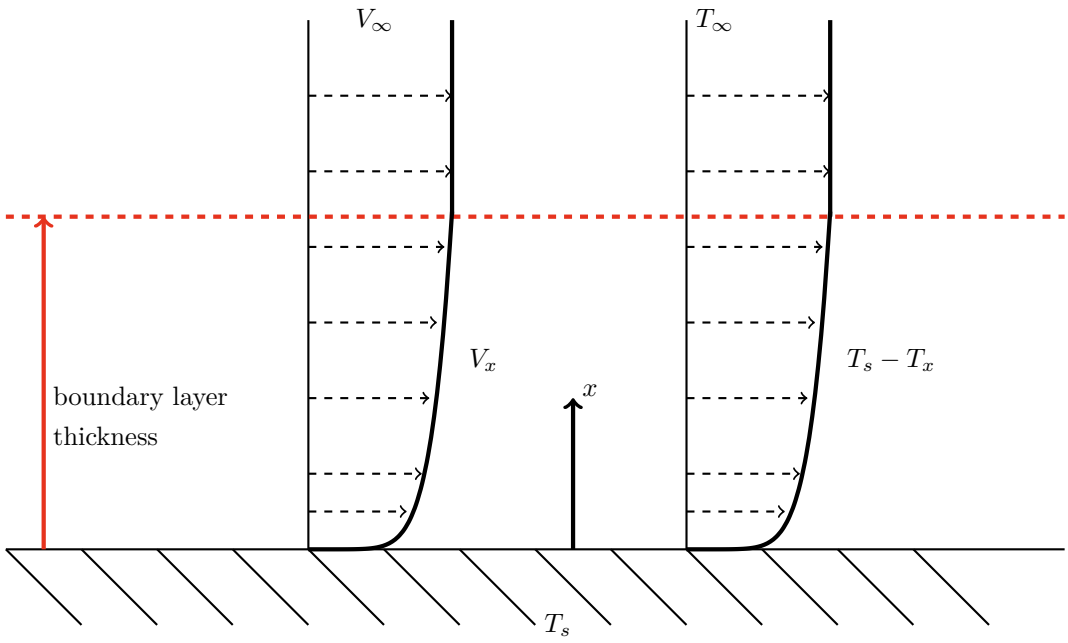

Figure 1.9: Velocity and temperature profiles of a fluid near the wall

The shape of these profiles is a function of the free stream speed V_∞ and temperature T_∞ as well as the surface roughness. Another factor that influences the shape of these profiles and is almost independent from the variables mentioned earlier is the Prandtl number $Pr = \frac{\nu}{\alpha}$ where ν is the viscous and α is the thermal diffusivity. For air the value of Prandtl number is around $Pr = 0.7$ for a wide temperature range. For an accurate heat transfer simulation it is essential to calculate correctly what happens in the boundary layer of the flow. In this thesis, this is assured by using a fine mesh near the wall at all times.

1.8 Fouling of heat transfer surfaces in a air conditioning application

In the continuous effort of making cheaper and more efficient FTHE, enhanced fin shapes are applied to the design as was discussed earlier. Contemporary development methods are focusing more on the numerical methods such as using CFD to predict the thermal-hydraulic efficiency of new designs. These studies typically consider pure air with material properties adopted in NTP conditions or similar. Therefore, the simulated efficiencies do not consider the impurities in the air and do not represent the real working conditions. Here lies a major risk for any heat exchanger manufacturer not limited to HVAC industry. In other heat exchanger applications, such as heat recovery boilers, the heat exchanger surfaces are exposed to ash and other secondary products of combustion processes [101–104]. The time scale of fouling in these applications can be considered to be hours or days and therefore the fouling is considered in the design by using wider and simpler geometries. On top of the design, necessary cleaning technologies are applied, which clean the heat transfer surfaces on a regular basis. Due to the large negative temperature gradient

between the flow and the heat exchangers, the deposition mechanism in these applications is dominated by thermophoresis [105]. In HVAC heat exchangers, thermophoresis is negligible due to much smaller temperature gradients [106].

Fouling can be described as accumulation of unwanted substances on the heat transfer surfaces. The fouling process itself can be divided into phases. Every fouling process will initially start with the nucleation regime where particles accumulate on the surface and form a deposition distribution. Later on, once the surfaces have been initially deposited by particles, the nucleation regime transitions typically towards the bulk fouling regime. At this stage the induced pressure drop from fouling is at its maximum in a specific operation point. The Publication IV focuses on the nucleation regime of the dry particle fouling as the bulk regime is still computationally too expensive. It should be noted here that as the wet-particle fouling layer can be up to 6.7 times the dry-particle fouling layer [107], in the future, as numerical tools for multiphysics modelling advance, it should be studied more in detail as well. The changes in the flow dynamics due to the fouling layer inside the air conditiong FTHE are very little in the nucleation phase and therefore will not be studied in detail in this study [108]. It was shown by Ahn et al. [108] that in the beginning, the particulate deposits on the surface of the fin actually increase the heat transfer, but the effect is reversed as the thermal resistance of the fouling layer decreases the heat transfer rate in the long run.

Before investigating the fouling process more in detail in the FTHE application, it is beneficial to look at the similar fouling studies conducted on tube bundles in general. Bouris and Bergeles [101] used the restitution coefficient and critical velocity to describe the solid deposition and rebound behaviour of a 2D tube bundle. A more recent 2D study was performed by Tang et al. [109], who compared numerically oval and round tube shapes and their effect on the fouling rate and heat transfer of a tube bundle. They concluded that the rate of fouling for oval tubes is much lower than for circular tube bundles. Han et al. [102] studied the effect of particle diameter, flow velocity and different heat exchanger geometries to the deposition characteristics of the tube bundle. On the authors knowledge, three dimensional numerical studies for FTHE exist only for plain fin heat exchanger types in the combustion application. Wang et al. [103] performed a parametric study of the geometry properties and their effect on the fouling rate of a H-type heat recovery FTHE. The mechanism of deposition as well as the removal process of fouling has been studied by Kern and Seaton [110] who proposed one of the earliest models of fouling. Another study by Pan et al. [111] also studied the fouling behaviour of an economizer by simulating the removal, rebound and deposition of particles. Zhan et al. [112] have studied the particle deposition on a wavy fin-and-tube heat exchanger with different fin pitches. They found that by decreasing the fin pitch from the 3.2 to 1.6 the deposition weight per unit area will increase by 13.1%.

The experimental fouling studies performed in the literature often deploy synthetic dust particles to represent real world fouling particles. Mass composition for such particles is 75 % silicon dioxide and 25 % carbon black powder, which is similar to the components of the the american society of heating, refrigerating and air-conditioning engineers (ASHRAE) standard dust [113] with the mean particle size being 10 µm and the density 2.3 $\mathrm{kg\,m^{-3}}$. Another article by Zhang et al. [114] uses ASHRAE standard 52.1 test dust, which contains 72 % of A2 fine Arizona test dust, 23 % carbon black powder and 5 % of second cut cotton liners milled in a Wiley mill. In their study, the mean diameter was 10 µm and the density 2.2 $\mathrm{kg\,m^{-3}}$. Yang et al. [115] performed a fouling study with dust 72% standardized air cleaner test dust that is predominantly silica and has a mass-mean

diameter of approximately 7.7 mm, 23% powdered carbon and 5% cotton linter. Bell et al. [116] used the ASHRAE dust according to the standard 52.1 with similar specs. It should be noticed here that of course, as the particles in the simulation model will be perfectly spherical, they will not represent all the shapes of the fouling particles that are encountered in real conditions. These are for example fibers and other arbitrary shapes and fractals.

The most difficult part in performing a fouling study of an HVAC heat exchanger is to define the type of the studied depositing aerosols. What is the appropriate size, size distribution, concentration, shape, density and other adhesion material properties. All the adhesion related material properties are discussed more in detail in Publication IV. For example in an indoor environment, submicron particles exist at much higher concentration than larger particles. The size range of 0.01-0.1 µm originates from combustion such as tobacco smoke, penetration from outdoor sources and gas-to-particle conversion [117]. Bioaerosols, soil grains and byproduct of cooking and other household activities are the source of aerosols in the range of 1-10 µm. Indoor dust can be considered as the largest particles with a diameter of around 10 to 100 µm [117]. Also smaller particles such as under 10 nm particles are found in the indoor air but their mass concentration is very low and therefore it is unlikely that they would have significant effect on the thermal insulation of the heat transfer surface or the increase in pressure drop [117]. Moreover, the microorganisms can cause indoor bio-aerosol problems as they colonize on moist surfaces inside the FTHEs [118, 119].

An illustration of the material properties used in different numerical studies in the literature and in this thesis are illustrated in Table 1.4.

Table 1.4: Material properties from different CFD-DEM studies related to indoor air particles

Application	Authors	d_p	**E (GPa)**	ν	ρ (**gcm**$^{-3}$)	γ_L (**Jm**$^{-2}$)	e
Fin-and-tube	Kuruneru et al. [120]	25 μm	70	0.345	2.4	0.59	-
Fin-and-tube	Zhan et al. [121]	50 μm	38	-	2.25	0.3	-
Fin-and-tube	Sauret and Hooman [122]	10-25 μm	-	-	2	-	-
Foam-and-tube, sawdust	Kuruneru et al. [123]	5-50	0.0005	0.3	0.5	-	0.5
Foam-and-tube, sandstone	Kuruneru et al. [123]	5-50	0.01	0.21	2.5	-	0.5
Metal foam, sand/sandstone	Kuruneru et al. [124]	5,10	-	-	2.4,0.5	-	0.5
Filter study	Qian et al. [125]	2.5-3 μm	0.05324	0.25	2.5	0.085	0.3-0.5
Filter study	Maddineni et al. [126]	0-10 μm	-	-	-	0.03-0.3	0.05-0.1
Filter study	Tao et al. [127]	2 μm	0.02	0.33	2.5	0.02	0.8
Fin-and-tube	Publication IV	5,10,20 μm	1.08	0.3	2.5	0.031,1.04	0.5

When conducting a computational fouling study, the most important decision, after choosing the studied geometry and operating condition, is the selection of material properties for the fouling particles. A natural choice would be to choose values for the adhesion material properties that would match the ASHRAE standard dust. This way a comparison between the computational and experimental fouling values could be performed. However, there is no experimental results about the critical velocity of the material pairs found in the ASHRAE standard dust and the FTHE fin materials. After an intensive testing of running the ASHRAE like dust particles in the computational fluid dynamics and discrete element method (CFD-DEM) FTHE model, it was found that the particles have very low adhesive levels and therefore don't deposit on the surface in the flow conditions related to the HVAC application at all. This is due to the differences between a ideally pure clean surface in a computational scheme and a real world surface with accumulated impurities. By using material properties for pure ASHRAE and aluminum surface the adhesive properties are not the same as are encountered in

real world applications where the adhesive properties are continuously changing as the heat exchanger is used. The heat transfer surfaces can be covered with different coatings, manufacturing related impurities such as oil or oxidation related end products of the fin material itself. This was the main motivation behind the process of developing a way to select the material properties for a FTHE fouling study as was done in Publication IV.

1.9 Recearch objectives

The research objectives in the publications I-IV are presented in each publication, respectively. The research objectives in a larger perspective that are answered in this thesis are formed as follows:

1. Build an accurate computational model which describes the physics of the conjugate heat transfer process in the FTHE in a computationally reasonable manner.
2. Develop an automated meshing process for FTHE that could be integrated to a design software in the future.
3. Illustrate how the fin shape can be improved so that the overall thermal-hydraulic performance is improved and how this can be manufactured in real applications.
4. For one fin shape, determine what is the required resolution of results for different combinations and what are maximum and minimum values for the tube distances so that accurate surrogate models can be created and use this to find the local optimal design combination.
5. Develop a method that can be used to quantify the risk of fouling involved with new enhanced fin types in an air conditioning application.

1.10 Innovations and significance of the research objectives to the industry

The four major innovations developed in this thesis and their significance to the industry are listed as follows.

First innovation is the developed open source meshing tool and its parametric meshing features. Due to the accelerated development cycles illustrated in this thesis, the major challenge in the development of FTHE is to forecast the thermal-hydraulic characteristics before investments to the new production equipment have to be made. Numerical methods have been used in the industry to decrease the cost of product development and innovation. Commercial CFD products are used increasingly by experts in various companies, but due to their high cost of ownership, they have not been implemented as an essential part of the companies' product design software systems. Therefore, there is a clear need for open source parametric meshing and automated conjugate heat transfer model creation. Such a software can enable the optimization of the FTHE for each application explicitly without any prior knowledge on numerical details behind the models. The parametric meshing tool developed during this thesis could be part of such a software in the future.

Second innovation developed in this thesis was to implement the vortex generator between the tube collar and the herringbone shape. No previous numerical study in the literature has taken into account the effects of machining the fins of FTHE. In this study, the novel

idea was to use this empty space between the tube collar and herringbone shape that was left from extruding the collar around the tubes. It was shown that the traditional herringbone fin shape performs better with the included vortex generators than without. This could encourage new studies to investigate other aspects of the manufacturing process that could be exploited in the development of vortex generator designs.

As third Publication III illustrates, the data and correlation equations in the literature are heavily biased towards the existing machinery currently used in the industry. Experimental studies will naturally follow this bias because it is very difficult to manufacture unconventional designs without appropriate mass production machinery. But for CFD studies, no such limitations exist. Therefore, CFD can be used to study the whole design space, when looking for the best performing combination of the geometric parameters. Publication III is one of the few studies found in the literature where the application specific boundary conditions and design restrictions are considered. This differs significantly from the convention how FTHE fin shapes are currently studied and analysed. Traditionally, the flow through the heat exchanger is simulated by alternating the inlet velocity boundary condition in an applicable range, for example between 1-5 m/s. Since special applications usually have a fixed inlet velocity boundary condition, it is better to keep the inlet velocity constant and vary other design aspects to save resources, as is done in Publication III.

Finally the fourth innovation in this thesis, is the method that was developed for the selection of adhesion properties of the fouling particles in an air conditioning application. Despite the major improvements in the design of FTHE, companies are still hesitant to invest in new designs because of increased fouling propensity of the new fin shapes. Thus, there is a clear need for a standardised method to analyse fouling propensity of different fin shapes. With such a method introduced in Publication IV, the fouling risk could be assessed before investing in a new technology. This decreases the product to market time significantly and speeds up the development cycle.

1.11 Outline

The rest of this thesis is organized as follows. In Chapter 2, an overview of the theory, methods and non-dimensional variables that are used to illustrate the results are presented. The Chapter 3 summarises the publications main contributions. In Chapter 4, conclusions are drawn in a broader context, the limitations are underlined and the direction of the future research is discussed. The main part of this thesis is contained in the attached Publications I-IV.

2 Methodology

Next, the methods used during the thesis will be briefly introduced while the more detailed description is found in the appended Publications I-IV and the citations therein.

2.1 Governing equations for fluid flow

When comparing different fin shapes and their effect on the air side heat transfer and the thermal-hydraulic performance of the whole FTHE, it is important to know the characteristics of the flow field with different inlet velocities. The governing equation for incompressible flow is thus the Navier-Stokes (N-S) equation [22]

$$\frac{\partial \boldsymbol{u}}{\partial t} + \nabla \cdot \boldsymbol{u}\boldsymbol{u} = -\nabla \hat{p} + \nu \Delta \boldsymbol{u}, \tag{2.1}$$

where $\boldsymbol{u}$ is the velocity, $\hat{p} = \frac{p}{\rho_f}$ is the pressure, ρ_f is the density of the fluid and ν is the kinematic viscosity. Conservation of mass is assured by using the continuity equation

$$\nabla \cdot \boldsymbol{u} = 0. \tag{2.2}$$

For the temperature T, an additional transport equation is solved

$$\frac{\partial T}{\partial t} + \nabla \cdot (\boldsymbol{u}T) - \Delta \alpha_f T = 0, \tag{2.3}$$

where α_f is the thermal diffusivity of the fluid.

The temperature field in the fin is governed by

$$\frac{\partial T}{\partial t} - \Delta \alpha_s T = 0 \tag{2.4}$$

where α_s is the thermal diffusivity of the fin.

The traditional method to solve the equations 2.1-2.4 in the FTHE is to do experimental studies. This can be done in two different ways. The first one being a "black box" type of study, where the inlet boundary conditions are known such as the temperature and velocity of the incoming air. The other boundary conditions for the flow and energy fields are the physical boundaries of the heat exchanger itself and the temperature of the fluid flow inside the tubes. Then the output values of the heat exchanger can be measured and the difference can be calculated by substracting the values from each other. This

difference can then be normalised by dividing the difference between inlet and outlet values with the amount of flow through the heat exchanger. This way the thermal-hydraulic efficiency of the whole FTHE can be determined. The problem with this method is that no insight to the flow characteristics and to the heat transfer process itself is achieved but only the average values of before, and after the heat exchanger are known. [89–92] The second experimental method is to do more local experiments and study the flow field directly inside the heat exchanger. This can be done by visualising the flow by inserting different substances to the flow and following the streamlines. [57, 128, 129] An excellent review of the naphthalene sublimation method is done by Goldstein and Cho [130]. The problem with these methods is to define how different topological changes in the heat transfer surface affect the heat transfer capacity because the differences are very difficult to measure. The amount of heat transfer can not be quantitatively measured in such a setup.

The biggest challenge with experimental development is the long and complex design and manufacturing cycles. The cycle starts from the decision of trying something new. Modifications and design is prepared in co-operation with mechanical and manufacturing engineers. The complexity of the new design highly affects the possibilities of manufacturing it. If the new design is a variation of something that has been already made by the fin press tool manufacturers, there might be a possibility to order directly from the original tool manufacturer. This tool is then designed and manufactured in such a way that it enables the tool to be utilized straight in the production line. Then a new version of the full sized FTHE can be made as fast as the old desing. The tool can be switched in a few hours. After this, full scale black box measurements can be performed on the design. The problem with this workflow is the cost of one design iteration. As the new prototype tool is manufactured with almost the same standards as the original tool, the costs are almost equal as well. A cheaper way is to do a smaller and slower fin press to perform the task of manufacturing a prototype fin shape. The manufacturing speed of this kind of press can be many times slower than the actual fin press machine. But so can be the difference in the price of the tool. This means that by paying a higher price for the prototype tool, a faster development cycle can be achieved. Unfortunately in the contemporary world with the scarcity of resource, only a fixed amount of resources can be invested in the development. Therefore a decision about the number of development cycles with respect to the development schedule needs to be made with given resources.

Third option is to try to find an explicit analytical solution to the Navier-Stokes equation and then integrate the temperature scalar over the flow medium. When an analytical solution can be found, the computational resources needed to solve the flow field are so low that a new design and its fields can be solved in fractions of a second. Unfortunately the solution can not be found to all different shapes that are encountered on the air side of the FTHE. Not to mention that the heat transfer process on the air side is a mix of different fundamental flow cases, most importantly flow over cylinder [131] and the channel flow [132]. This would correspond to the plain fin case where the fin shape is unaltered. Unfortunately even for these very simple cases separately, an analytical solution can only be found for the laminar case where the streamline of the flow is continuous. When the Reynolds number of the flow is increased and the fin shape is manipulated, for example by making it wavy, the turbulence can be very local and therefore it is impossible to solve the required fields directly with analytical means without making major simplifications. [133]

Because of the limitation in the experimental and analytical strategies, the numerical way

of solving the fields has increased popularity in the field of both academic and industry FTHE development [73, 134, 135]. In CFD, the domain, in this case the fluid air and the solid fin, are discretized (divided) into a finite number of computational cells. A set of equations (2.2, 2.1, 2.3 and 2.4) are solved in each cell and the information between cells is transferred by using a set of schemes, the accuracy of the solutions being proportional to the quality of the mesh and the diffusivity of the schemes. The more cells are generated in the mesh, the more computationally expensive it is to solve the flow field and more turbulence is resolved.

2.2 Computational fluid dynamics

When solving the governing equations that describe the heat transfer process in a FTHE, it is important to note that it is computationally too expensive to simulate the whole heat exchanger at once. This is why many engineering simplifications are made to overcome the scarcity of resource but still maintaining important features of the real world application. A common way is to first only simulate a smaller section of a heat exchanger that, when multiplied to the size of the real heat exchanger, represents the thermal-hydraulic characteristics of the entire FTHE. Illustration of the computational domain is illustrated in detail in every Publication I-IV. In this Thesis, finite volume method (FVM) is used to discretize the computational domain. It is a well-established approach in CFD codes. The governing equations are obtained by mathematically modelling the conservation laws of mass, momentum and energy. The steady-state discretization is followed in Publications I, II and III. In the Publication IV a transient discretization is required as well, which involves the integration of every term over time. This can be done with methods such as Euler and Runge-Kutta. [39] In all Publications, the discretization scheme used for the energy and velocity field was a second order upwind scheme called linearUpwind. For all the other fields a first order upwind scheme called upwind was used.

2.3 Turbulence modelling

When the flow is steady and the streamlines of the flow are continuous throughout the flow domain, the flow is said to be *laminar* [136]. The definition of turbulent flow is not so exact, but certain characteristics are used in the literature [39, 137, 138]. First the nature of turbulent flow is said to be random, irregular and chaotic. Regarding this thesis, the diffusivity of the turbulent flow can be said to be the most important factor of the turbulent flow since it increases the transfer of momentum, heat and mass. This feature is the most important from the heat exchanger design point of view since turbulent flow enables higher heat transfer rates. Another important aspect of turbulent flow is that the turbulence scales are always three-dimensional in their nature and the energy cascade process from bigger to smaller scales continues until the smaller Kolmogorov scales are dissipated and transformed to heat [39]. It should be noted here that in an HVAC application this dissipated heat from the smallest turbulence scales is negligible when compared to the amount of heat transferred in the FTHE [39].

When the flow field around a new enhanced fin shape is simulated, it is important to resolve enough turbulence scales so that their effect to the thermal-hydraulic properties are solved as accurately as needed. Despite the fact that Navier-Stokes equations do describe the full nature of the flow, often it is not computationally feasible to solve all the possible scales in the flow. Therefore, usually the smallest scales that have a minor effect on the whole domain can be modelled to save in computational resources.

For steady-state flow fields, it is beneficial to use Reynolds averaged formulation of the Navier-Stokes equation and model the Reynolds stress tensor [139]. Most commonly in the industry, the 2-equation models such as k-ω SST are used. In Publication I, II and III the aforementioned 2-equation model was used. If more turbulence scales are required to be resolved, for transient processes such as particle laden flow simulations, a Large Eddy Simulation (LES) approach can be used. In LES, larger scales are resolved, but the smallest isotropic scales, also called Kolmogorov scales, are modelled. In Publication IV, in this thesis, a model called Wall-adapting Local Eddy-viscosity (WALE) model with model constants $C_k = 0.094$, $C_e = 1.048$ and $C_\omega = 0.325$ was used. The sub-grid scale viscosity ν_{sgs} is therefore computed as follows:

$$\nu_{sgs} = (C_w V^{1/3})^2 \frac{(\overline{s}_{ij}^d \overline{s}_{ij}^d)^{3/2}}{(\overline{s}_{ij}^d \overline{s}_{ij}^d)^{5/2} + (\overline{s}_{ij}^d \overline{s}_{ij}^d)^{5/4}}, \tag{2.5}$$

where:

$$\overline{s}_{ij}^d = \frac{1}{2}(\overline{g}_{ij}^2 + \overline{g}_{ji}^2) - \frac{1}{3}\delta_{ij}\overline{g}_{kk}^2, \overline{s}_{ij} = \frac{1}{2}(\frac{\partial \overline{u}_i}{\partial x_j} + \frac{\overline{u}_j}{\partial x_i}), \tag{2.6}$$

$$g_{ij} = \frac{\partial \overline{u}_i}{\partial x_j}, \qquad g_{ij}^2 = g_{ik} g_{kj} \tag{2.7}$$

In equation 2.5, the V is referring to the size of every individual cell where the sub-grid scale viscosity is computed. Turbulence modelling is very efficient way to reduce the computational cost of the simulations since the characteristics of the flow resembles a constricted channel flow [140] and therefore the main stream through the middle of the flow channel is typically very laminar and turbulence is only seen behind tubes and other obstacles. The benefits of the WALE model in a wall-bounded flow such as the FTHE are highlighted in details by Mirzaei et al. [141] but most importantly, in the WALE model, the eddy-viscosity automatically approaches zero near the wall and therefore requires no additional dynamic damping functions such as the Smagorinsky model.

2.4 Meshing

2.4.1 Unstructured vs structured meshing

When new features are developed to an existing fin design, the development process starts from designing the topology of the feature. This must be done by describing the topology in a mathematical form. Utility software such as computer assisted design computer assisted design (CAD) softwares can be used to draw the fin geometry. This is the solid part of the computational model where only the temperature equation is solved. When the mesh for the computational domain is created, there is three different strategies that can be used. First one creates a completely structured mesh, the other one is called an unstructured mesh. If both these types of meshes are used, then it is called a hybrid mesh. An illustration of all these types can be seen in Fig. 2.1

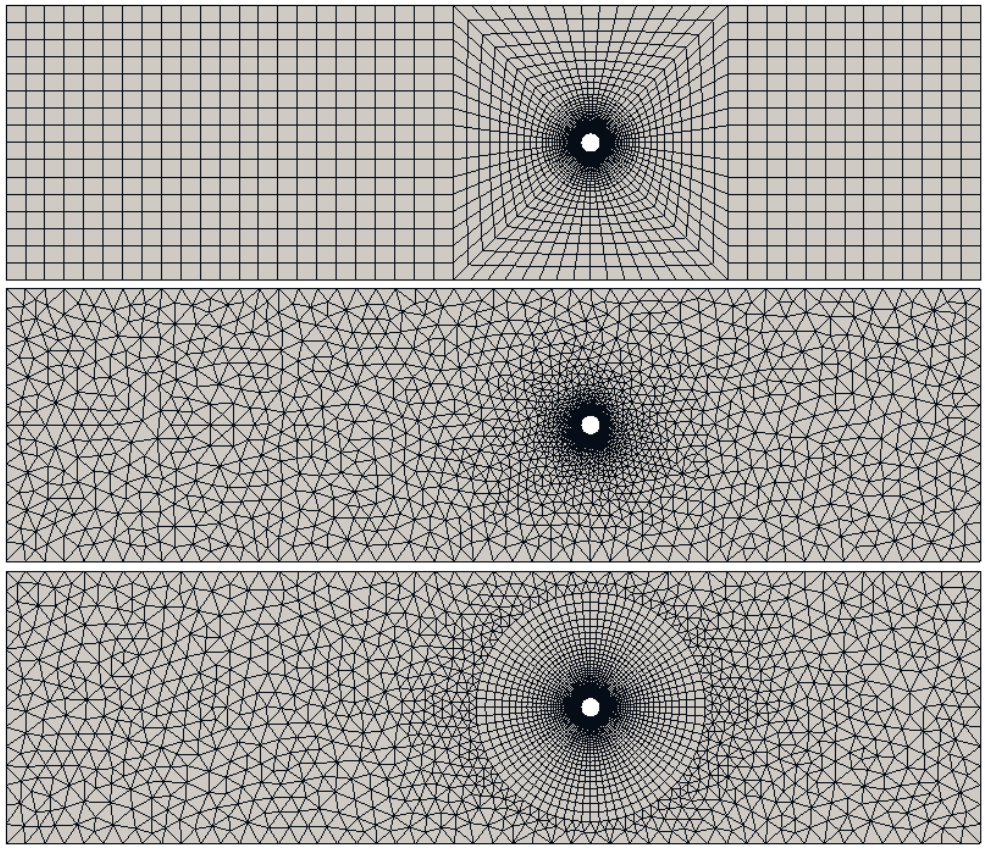

Figure 2.1: Illustration of the different mesh types; structured on top, unsctructured in the middle and a hybrid mesh on the bottom

A unstructured mesh usually consists of tetrahedra or polyhedra cells. The location of the cells, size and orientation, is created by a computer algorithm that follows some general guidelines that are given by the user. If the quality of the mesh is not satisfied after the algorithm has finished, the user has to change the user inputs or the boundaries (CAD model) in the effort to improve the quality and start the meshing process again. The benefit in an unstructured meshing strategy is the minimized time consumed on the meshing process on the first generation of the mesh. Especially if the CAD model is pre-existing before the meshing process starts. The downside of using unstructured meshing is that the efficiency of the meshing process does not improve after multiple design iterations. This means that every mesh takes equally long to create. Another downside is that the user does not have a complete control on the locations of fine and coarse mesh regions. The user can usually guide the algorithm to increase the mesh density around a boundary wall or a specific user defined region but the end product is always created by the algorithm.

When the user defines the blocking strategy, which is a framework that aligns the cells in the mesh. Then the refinement along every edge in each block can be adjusted to create coarse or fine regions where desired. The benefit in a structured meshing strategy is that when the blocking strategy is ready, it is very fast to generate different versions of the

mesh, in terms of mesh refinement and parametric topological changes. The downside is that in the beginning of creating the blocking strategy for the mesh, it can be a very time consuming process before the blocking is ready. For a manufacturer of a FTHE, structured meshing can offer great advantages over unstructured approach. Like in the case of the FTHE, the basic topology of the mesh stays the same; tubes and their distance from each other, fin thickness and spacing between the fins. When new enhanced fin shapes are created, the blocking strategy from the current fin design can most likely be reused and therefore a lot of time is saved. When different versions of the mesh are created for example to change the fin pitch, this can be done with a parametric structured mesh by just changing one value from example 2.0mm to 3.0mm and a new mesh is generated in seconds. This is why it is very beneficial for a product manufacturer to use structured meshing in their CFD workflow.

2.4.2 Multi-block structured mesh

A major part of this PhD project was to take part in developing an open source meshing tool called SwiftBlock. Swiftblock was an essential part of the computational workflow that enabled the process of creating Publications I-IV. Next is a short introduction to the basics of the meshing tool in question.

An open source software called open field operation and manipulation (OpenFOAM), includes a multi-block structured mesh generation utility called blockMesh. BlockMesh is a structured mesh generator only in a sense of meshing algorithms and the output is always an unstructured mesh from the computational point of view. BlockMesh, just like any other tool in OpenFOAM, does not come with a graphical user interface (GUI) and therefore it is usually used only for very simple geometries. The meshing capabilities are then restricted by the users ability to imagine the end product. BlockMesh is controlled by a dictionary file called blockMeshDict which user has to set-up manually.

In multi-block meshing, the user has to design the blocking structure by hand which consumes a lot of time. Blocking structure consists of hexahedral cells, which share faces with each other. The mesh is generated from the hexahedron blocks by splitting them into smaller cells. The user controls the resulting mesh by defining node distribution on the block edges. The internal node locations are calculated by an interpolation function which is usually transfinite interpolation (TFI). The vertices, edges and faces can be projected to follow a geometry.

SwiftBlock is a python based user add-on created inside a 3D creation suite called Blender [142]. SwiftBlock is a meshing tool that creates completely structured meshes. In this context structured means that the topology is defined with hexahedral blocks which are then filled with hexahedral cells. This means that in this context the structured mesh does not indicate anything about the file structure of the final mesh or how the solver uses the mesh. Actually if the mesh is used with OpenFOAM, it will be always used as an unstructured mesh from the computational point of view.

SwiftBlock is built around the block detecting algorithm described by Gaither [143]. Rather than keeping track of blocks as they are created by the user, and denoting them in a Cartesian structure (i,j,k), it is entirely up to the user to create a wire frame describing the desired block structure. How the block structure is created is not of importance; it can be built edge by edge, or imported into Blender from an external source. SwiftBlock will not examine or interfere with the wire frame until the user issues any of the functions that rely on the block detecting algorithm.

Adam [143], outlined an algorithm that detects hexahedral blocks out of a wire frame structure, consisting of edges joined together. The algorithm, denoted "cycleFinder", consists of a method that actually detects quad structures, i.e. four edges joined to form a closed loop. In SwiftBlock, the user defined wire frame is first fed to cycleFinder, which returns all the faces consisting of four edges forming a loop. Then, all faces that share one, and only one, common edge are connected in a new data structure. This data structure is then fed to the cycleFinder, which this time detects all loops consisting of four faces joined together. All such "face loops" are potentially the blocks the user wants. However, some substantial filtering is needed:

- Each block gives rise to many face loops, so first all unique blocks has to be singled out.
- A hexahedral block missing one edge is still detected as a block. These flawed blocks are ruled out by assuring that the first and third face in the face loop are connected by an edge; i.e. they do not share any edges, but there is at least one edge that connects them.

This is not enough for all possible cases for example the O-grid, which is commonly found in flow over cylinder related situations. The typical O-grid arrangement used to mesh for instance a cylinder contains two pitfalls for the algorithm. While the user typically wants five blocks (a center block surrounded by four blocks), the algorithm will find no less than eight formal hexahedral blocks. Except the obvious, and desired, ones there are two flat blocks, one at either end of the cylinder, and one block formed by the outer-most edges of the structure. The flat blocks are ruled out by their flatness. That is important because the user might actually be meshing a sphere, where he/she does want those end blocks to be present. In such cases those blocks wont be flat. The unwanted block is ruled out by counting how many blocks are located on each side of the faces. Each block face should have no more than one block at side. If a block face has more than one block on each side, those blocks are given a "fine". Initially all blocks have zero "fines", but for each face which have more than one block on each side, those blocks a fine is given. The unwanted block has a total fine of 4, while the four outer, wanted blocks, end up with 1 fine each. The unwanted block is then simply removed as it scored too high. The blocks remaining after this filtering process are used to define the blockMeshDict.

A walkthrough to the features of Swiftblock are laid out in the Appendix and the documentation can be found online [144].

2.5 Conjugate heat transfer

Conjugate heat transfer is a heat transfer process where the heat is transferred through both solid and fluid regions. In the fluid part, the continuity, momentum and heat equation is solved but in the solid part only the heat equation is solved. During the time of this PhD project, the development of open source CFD tools in general has been very significant. The solver development within the OpenFOAM C++ package and all of its different distributions has been very active. There exists different solvers that can be used to simulate conjugate heat transfer in a FTHE. The OpenFOAM foundation [145] distribution offers a solver called chtMultiRegionFoam, which is a segregated type of solver that allows unlimited number of solid and fluid regions to be created and solved. This was used in the Publication I. Segregated solver in this context means that every

region in the computational domain is computed separately in a user specific order and then an interpolation on the border is performed. This means that the information in one region, such as a fixed value boundary condition in a solid region, takes a relatively long time to reach a steady state in the fluid domain. This is especially troublesome for a FTHE simulation, where the flow field through the heat exchanger takes only a fraction of the time to converge that it takes for the temperature field. There exists few tricks to overcome this issue, such as increasing the relaxation for the temperature equation in a steady simulation and temporarily lowering the thermal capacity of the solid part in a transient simulation but only minor improvements can be achieved with these methods. In FOAM-extend [87], which is a community driven distribution of OpenFOAM, a solver called conjugateHeatFoam can be found. It is a block matrix based solver where the heat equation matrix from the solid region is included inside the matrix of the fluid region and solved simultaneously. This means that the information is distributed throughout the computational domain directly from the first iteration, no matter if a steady-state or a transient simulation is performed. This of course increases the convergence speed of the simulation significantly. During the PhD project, the author performed a comprehensive comparison of the different solvers between different OpenFOAM versions [146].

2.6 Data reduction and Performance metrics

The non-dimensional variables that are used to describe the characteristics of the FTHE, are based on fundamental features of the flow [22]. These features consists of the characteristic length scale and reference flow speed in the domain. Unfortunately, there is very little consistency in the definition of these features in the literature. It is very difficult to compare the results that are reported for different fin shapes and working conditions when the definition of the operating point is obscured. Some studies define the tube diameter as the characteristic length scale [29, 36, 147–151], some use fin entrance diameter [152], for others a fin enhancement specific value is used [153]. Kays and London [154] have proposed their own which is used by multiple studies [27, 155, 156] and its simplified version [157] or some even discuss Reynolds numbers based on multiple different length scales within the same context [158]. For the reference velocity, different authors use the face/frontal velocity [149, 150, 158], average flow velocity in the minimum cross-sectional area [27, 148, 151] or the maximum velocity in the minimum cross-sectional area [30, 36, 152, 153, 155–157]. This is one of the main reasons why the goodness of different fin shapes is hard to compare between different studies. Additionally the calculation steps are not shared with the original article and therefore the information about the calculations is lost. This is also pointed out by Webb [159] and Wang et al. [158] that the use of hydraulic diameter as characteristic length scale may not be successful at all in correlating the experimental data. Even in this thesis, three types of Reynolds number definition is used. In Publications III and IV, results are represented with the non-dimensional variables based on the hydraulic diameter d_h [154], defined in Eq. 2.8 and the average flow velocity in minimum cross sectional area of the FTHE as shown in Eq. 2.9.

$$\begin{aligned} D_\mathrm{h} = \frac{4 \cdot \text{free flow volume}}{\text{wetted area}} &= \frac{4 \cdot \text{free flow area} \cdot \text{depth of the FTHE}}{\text{fin surface area} + \text{tube surface area}} \\ &= \frac{4(F_\mathrm{h})(P_\mathrm{t} - D_\mathrm{c})(2P_\mathrm{l})}{(4P_\mathrm{l}P_\mathrm{t} - 4\pi(\frac{D_\mathrm{c}}{2})^2) + ((F_\mathrm{h})2\pi D_\mathrm{c})} \end{aligned} \tag{2.8}$$

$$U_{\mathrm{max,avg}} = U_{\mathrm{inlet}} \frac{A_{\mathrm{inlet}}}{A_{\mathrm{min}}} = U_{\mathrm{inlet}} \frac{P_{\mathrm{t}} F_{\mathrm{p}}}{(F_{\mathrm{p}} - t)(P_{\mathrm{t}} - D_{\mathrm{c}})} = U_{\mathrm{core}} \tag{2.9}$$

The Reynolds number $Re_{d_{\mathrm{h}}}$ defines the ratio of inertial forces to viscous forces and consequently quantifies the relative importance of these two types of forces for given flow conditions[39]. The Reynolds number is used as a measure of turbulence in the flow. There is no proof or theorem between the Reynolds number and turbulence, usually what happens is that flows with high Reynolds number contain a lot of turbulent structures in the flow and flows with low Reynolds number tend to stay laminar. Therefore the critical Reynolds number, above which the flow is turbulent, has to be defined separately for each case and condition individually. The Reynolds number of the flow inside the FTHE in Publication I, III and IV is defined as

$$Re_{d_{\mathrm{h}}} = \frac{U_{\mathrm{core}} d_{\mathrm{h}}}{\nu}. \tag{2.10}$$

Where as in Publication II the Reynolds number is defined as

$$Re_{D_c} = \frac{U_{\mathrm{core}} D_c}{\nu}. \tag{2.11}$$

where D_c is the collar tube diameter and ν is the kinematic viscosity of the air flowing through the heat exchanger.

For the FTHE, the overall average heat transfer coefficient is defined as:

$$\overline{h} = \frac{Q}{A_t \Delta T_{lm}} \tag{2.12}$$

where $Q = \dot{m} C_f^p (T_{inlet} - T_{outlet})$ is the overall transferred heat to the air, C_f^p is the specific heat of the air and ΔT_{lm} is the logarithmic mean temperature difference between the inside diameter of the tube and the air is defined as:

$$\Delta T_{lm} = \frac{(T_{inlet} - T_w) - (T_{outlet} - T_w)}{ln[(T_{inlet} - T_w)/(T_{outlet} - T_w))]} \tag{2.13}$$

When changing the fin pitch and the tube locations, the size of the inlet in the computational domain changes. Also, when the inlet velocity and the temperature difference is changed, the amount of transferred heat is changing. Because of this, it is essential to normalize the results when studying the effect of different fin shapes on thermal-hydraulic performance of the FTHE. In order to determine the heat transfer performance, non-dimensional Colburn j-factor, using the overall average heat transfer coefficient $\overline{h}$ of a fin-and-tube heat exchanger, it is calculated as [160]:

$$j = \frac{\overline{h}}{\rho_f U_{\mathrm{core}} C_f^p} Pr^{2/3}. \tag{2.14}$$

Colburn j-factor can be described as the amount of heat transferred to the flow divided with the total thermal capacity of the flow. In a similar manner the pressure loss in the

FTHE is evaluated using the non-dimensional fanning friction factor which is defined as [147]:

$$f = \frac{\Delta p}{\frac{1}{2}\rho_f U_{\text{core}}^2} \times \frac{A_{min}}{A_t} \tag{2.15}$$

which can be said to represent the pressure drop over the heat exchanger divided with the dynamic pressure of the flow. This is then multiplied with the ratio between the minimum cross sectional area and the wet area of the flow.

The performance of the FTHE can then be quantified with different performance-metrics. The two most important ones are the *area goodness factor/efficiency index* [49] defined as:

$$\frac{j}{f} = \frac{\frac{\overline{h}}{\rho_f U_{\text{core}} C_f^p} Pr^{2/3}}{\frac{\Delta p}{\frac{1}{2}\rho_f U_{\text{core}}^2} \times \frac{A_{min}}{A_t}}. \tag{2.16}$$

And the other one is the *volume goodness factor* proposed by Shah and London [161]:

$$\frac{j}{f^{1/3}} = \frac{\frac{\overline{h}}{\rho_f U_{\text{core}} C_f^p} Pr^{2/3}}{\left(\frac{\Delta p}{\frac{1}{2}\rho_f U_{\text{core}}^2} \times \frac{A_{min}}{A_t}\right)^{1/3}}. \tag{2.17}$$

These are used to represent the thermal-hydraulic efficiency in the Publications I and II. For a constant thermo-mechanical properties and given pumping power, a larger volume goodness factor yields to a smaller and lighter heat exchanger whereas a larger area goodness factor yields to a heat exchanger with smaller face/frontal area [162]. When comparison of different fin shapes, and their heat transfer and thermal-hydraulic performance is performed, it is essential that all results are post-processed in a similar manner using the same reference variables. When the format of the result is different, the comparison of the results to each other becomes very difficult and additional post-processing is required.

In general, increase in heat transfer yields an increase in pressure drop. This means that one must consider the trade off between the increase in heat transfer and increase on the pressure drop when evaluating the performance of the heat exchanger. The previously introduced area goodness [48, 163] or volume goodness [161, 163, 164] are sufficient to use when the design variables such as tube diameter, tube pattern and fin pitch are constant. However, there exist some difficulties in using these when the reference length and/or velocity scales are different between the cases [100]. In other words, area goodness factor comparison can only have some meaning either if the thermal hydraulic ratio is fixed or if the minimum free flow area is fixed [162]. In order to make a fair comparison between two different designs and their area and volume goodness they must have the same hydraulic diameters [48, 100, 162, 165]. In Publication III, all the reference variables changes between the cases. Therefore, one must use a performance criteria that takes this into consideration. In Publication III the performance criteria is defined based on the example of Shi et al. [97] where a modified JF-factor [166] is used. JF is defined as the ratio between a studied heat exchanger and a reference heat exchanger. One is the ratio

of the heat transfer rate per unit temperature difference, per unit surface area, and the other is the ratio of the friction power dissipated per unit surface area. JF performance ratio is a higher the better performance criteria in nature, which means that different fin types with different design variables and their thermal-hydraulic performance data can be compared to each other. Next, a short derivation of the JF performance ratio is laid out. The ratio of the heat transfer rate per unit temperature, per unit area of studied heat exchanger and reference heat exchanger is as follows.

$$\frac{\overline{h}}{\overline{h}_R} = \frac{j}{j_R} \times \frac{(Re_{d_\mathrm{h}}/d_\mathrm{h})}{(Re_{d_\mathrm{h}}/d_\mathrm{h})_R} \tag{2.18}$$

The ratio of the friction power dissipated per unit area of studied heat exchanger and reference heat exchanger.

$$\frac{(P/A_t)}{(P/A_t)_R} = \frac{f}{f_R} \times \frac{(Re_{d_\mathrm{h}}/d_\mathrm{h})^3}{(Re_{d_\mathrm{h}}/d_\mathrm{h})^3_R} \times \frac{A_{inlet}}{A_{inletR}} \times \frac{A_{tR}}{A_t} \tag{2.19}$$

Therefore, we define the JF performance ratio as

$$JF = \frac{\frac{\overline{h}}{\overline{h}_R}}{(\frac{(P/A)}{(P/A)_R})^{1/3}} = \frac{\frac{j}{j_R} \times \frac{(Re_{d_\mathrm{h}}/d_\mathrm{h})}{(Re_{d_\mathrm{h}}/d_\mathrm{h})_R}}{(\frac{f}{f_R} \times \frac{(Re_{d_\mathrm{h}}/d_\mathrm{h})^3}{(Re_{d_\mathrm{h}}/d_\mathrm{h})^3_R} \times \frac{A_{inlet}}{A_{inletR}} \times \frac{A_{tR}}{A_t})^{1/3}} \tag{2.20}$$

It should be pointed out here that it is evident that in cases where the Reynolds number Re_{d_h} is based on the same characteristic length scale d_h as the length scale used to define the JF performance ratio, the length scale can be substracted from the equation 2.20.

2.7 Adhesive particle flow

When considering methods to model the deposition of aerosols on a heat transfer surface, it is important to study the previous work done on the adhesive particle flows. In 1972 Dahneke [167] studied how elastic deformations affected the kinetic energy loss of the particle. Rogers and Reed [168] were the first ones to consider both elastic and plastic deformation in a particle-target impact. It was then Wall et al. [169] who discovered the effect of the adhesion surface energy of the target material to have a significant effect on the momentum energy loss of the particle in a low velocity impact. And Wall et al. [169] also pointed out that even in low velocity impacts the plastic deformation has a major contribution to the energy loss and that the original adhesion theory of Dahneke [170] did not predict correctly the critical velocity of when a particle will stick to the target. For different particle sizes, the adhesion phenomena changes as for the particles with a diameter in the order of micrometers, the van der Waals adhesion dominates, where as for millimeter diameter range, the liquid bridging becomes the most important mechanism. [106, 171] Moreover, Marshall et al. [106] pointed out that the surface roughness has a significant effect on the adhesion force so that a very high surface roughness usually leads to a lower level van der Waals forces.

The accumulated layer of fouling can be the result of many years of using the heat exchanger in an HVAC application. However, when we consider the time scale of the individual particle flowing through the heat exchanger and colliding to the fin surface, the

time scales can be as small as nano seconds. The time scales of the turbulent flow that carries the aerosol particles and the collision time scales of the particles can be as small as nano and piko seconds [172], respectively. The process of when a particle will deposit on a surface is both multiscale as well as a multiphysical problem. When the particle is advected by the air, the density of the particle and the density of the flow medium define the effect of gravity on the particle [173].

2.7.1 Governing equations for particles

When studying particle laden flows with models that include simplifications, a force comparison study is performed as was recommended by Marshall and Li [106]. If we look at the different type of forces encountered by the particles in the flow field in the Publication IV and compare them to the drag force, the Brownian force can be neglected since it is less than 0.01% with all Reynolds numbers used. The Saffmans lift force being $14-32\%$ and Magnus force $2-10\%$, it indicates that the particles are affected by the shear and rotational lift forces of the flow. This means that in order to compute the behaviour of the particles accurately it is important to solve the boundary layers correctly. The reduced gravity force is between $14-32\%$, which means that gravity is important to take into consideration. It should be noted still that the direction of the gravity force is perpendicular to the direction of the flow and the fin surface normal in Publication IV and therefore its effect on the fouling characteristics is very minimal. The most dominant force can be said to be the history force $233-1165\%$, which can be translated as the response time of the particle viscous shear force to the acceleration of the flow relative to the particle. This means that the particle trajectory and the forces acting on it are highly influenced by the history of the particles location inside the heat exchanger.

The collisions between the particles with each other and the fin surface are modelled with the soft-sphere discrete element method (DEM) approach [174]. The governing equation for the location $\boldsymbol{x}_\mathrm{i}$ is given by 2.21 :

$$m_\mathrm{i}\frac{\mathrm{d}^2\boldsymbol{x}_\mathrm{i}}{\mathrm{d}t^2} = \boldsymbol{F}_\mathrm{i,con} + \boldsymbol{F}_\mathrm{i,fluid} \tag{2.21}$$

where the $\boldsymbol{F}_\mathrm{con}$ is a contact force upon collision and $\boldsymbol{F}_\mathrm{fluid}$ is the combined fluid force acting on the particle.

2.7.2 Fluid forces on particles

If velocity difference exists between the particle and the carrier medium, the particle will experience a drag force that is caused by the pressure difference between the up- and downwind side of the particle, with respect to the flow direction. Depending on the particle's ability to follow local flow structures, the particle may collide with obstacles in the flow. This is the case of the tubes and the fins in the FTHE.

In the Publication IV, we use the particle drag formulation by Benyahia et al. [175], which is based on the simulations by Hill et al. [176] and Koch and Hill [177], where the modified Stokes drag is defined as $C_d = (24/Re_p)F$, where $F = f(Re_p, \beta_f)$. In the definition, Re_p corresponds to the particle Reynolds number while β_f corresponds to the particle volume fraction. By using this definition, a larger range of Reynolds numbers and particle volume fractions are covered.

2.7.2.1 Contact forces

The adhesive force between two spherical particles was originally studied by H.C. Hamaker in 1937 [178]. Hamaker concluded that the dominant forces of adhesion for two materials are the van der Waals and electrostatic forces. They originate from the continuous change of the electrical potential of atoms as the electrons circle around the core. The model that is used to describe these forces in Publication IV is the Johnson-Kendall-Roberts (JKR) model that was originally developed by Johnson et al. [179]. The JKR model is suitable for the specific type of collision for which the Tabor parameter $\lambda_T = (4R\gamma^2/E^2D_{min}^3) > 3$ [180], where γ is the surface energy density, which is defined as half of the energy required to separate two particles in contact and $D_{\min}$ is the minimum separation distance, usually assumed to be 1.65 Å [181, 182].

Since the surface energy density is defined for a specific material to interact with itself, it is important to notice that the value cannot be used directly in the collision computations between two different materials. For this a new property called adhesion work $w = \sqrt{\gamma_1\gamma_2}$ [106] is used.

When in contact, the radius of the contact surface can be calculated as $a = (9\pi\gamma R^2/E)^{1/3}$. According to the JKR theory, the relation between the contact radius a and normal overlap δ_n [182–184]

$$a^4 - 2R\delta_n a^2 - \frac{4\pi\gamma}{E_{eff}}R^2 a + R^2\delta_n^2 = 0 \tag{2.22}$$

The contact forces in the normal direction of the surface that are modelled with the JKR model are the spring force $\boldsymbol{F}_{\text{spring,n}}$, the adhesive force $\boldsymbol{F}_{\text{jkr,n}}$ and the damping force $\boldsymbol{F}_{\text{damp,n}}$:

$$\boldsymbol{F}_{\text{spring,n}} = -\frac{4E_{eff}}{3R}a^3\boldsymbol{n} \tag{2.23}$$

where n is the surface normal vector and a is the contact area.

$$\boldsymbol{F}_{\text{jkr,n}} = 4\sqrt{\pi\gamma E_{eff}a^3}\boldsymbol{n} \tag{2.24}$$

The effective Young's modulus is defined as $\frac{1}{E_{\text{eff}}} = \frac{1-\nu_{\text{i}}^2}{E_{\text{i}}} + \frac{1-\nu_j^2}{E_j}$ and the effective radius $\frac{1}{R} = \frac{1}{r_{\text{i}}} + \frac{1}{r_{\text{j}}}$ for particle collision between two materials where E and ν are the Young's modulus and Poisson's ratio and the subscript corresponds to the colliding materials i and j. In order to model the dissipation of kinetic energy upon collision, a damping force $\boldsymbol{F}_{\text{damp,n}}$ is used:

$$\boldsymbol{F}_{\text{damp,n}} = -2\sqrt{\frac{5}{6}}\beta\sqrt{S_{\text{n}}\boldsymbol{v}_{\text{n}}} \tag{2.25}$$

where $\boldsymbol{v}_{\text{n}}$ is the relative normal velocity, β is a parameter that takes into account the coefficient of restitution e as:

$$\beta = \frac{\ln(\text{e})}{\sqrt{\ln^2(2) + \pi^2}} \tag{2.26}$$

S_n is parameter that takes into account the material properties as:

$$S_\mathrm{n} = 2E_{eff}\sqrt{R\delta_\mathrm{n}} \tag{2.27}$$

where δ_n is the the overlap distance. In the tangential direction of the contact, the spring force $\boldsymbol{F}_\mathrm{spring,t}$ is used:

$$\mathbf{F}_\mathrm{spring,t} = -S_\mathrm{t}\Delta\mathrm{s}_\mathrm{t} \tag{2.28}$$

where $S_t = 8G\sqrt{R\delta_{s_t}}$ is a parameter for the particle properties and the δ_{s_t} is the tangential overlap. The effective shear modulus is calculated as $\frac{1}{G} = \frac{2-\nu_i}{G_i} + \frac{2-\nu_j}{G_j}$. As was done for the normal direction, a similar damping force $\boldsymbol{F}_\mathrm{damp,t}$ for the tangential direction is used:

$$\mathbf{F}_\mathrm{damp,t} = 2 - \sqrt{\frac{5}{6}}\beta\sqrt{S_\mathrm{t}m}\mathbf{v}_\mathrm{t} \tag{2.29}$$

where the $1/m = 1/m_i + 1/m_j$ is the effective mass and $\boldsymbol{v}_\mathrm{t}$ is the tangential velocity respect to the surface.

If the relative normal velocity v of the particle is lower than the critical velocity v_c in a collision between a particle of a material i and the target material j, then the particle will stick to the surface. Konstandopoulos et al. [185] concluded that the critical velocity is also a function of the incident angle and not only the incident velocity but due to simplicity this will be neglected in Publication IV.

The restitution coefficient can be expressed also as a ratio between the incident velocity after the collision divided with the velocity before the collision as is shown in Equation 2.30. It describes how much momentum will be lost in the impact if the particle will not stick to the surface.

$$e = \frac{v_i^{after}}{v_i^{before}} \tag{2.30}$$

The software that was used to calculate the particle laden flow and the adhesion process between the particles and the surfaces in Publication IV is called CFDEM (version 3.8.0) [186], which combines the CFD (Foundation version 5.0) toolbox OpenFOAM [145] with the DEM solver LIGGGHTS [187]. LIGGGHTS stands for LAMMPS improved for general granular and granular heat transfer simulations and LAMMPS stands for Large-scale Atomic/Molecular Massively Parallel Simulator [188]. The same solver that was used in the Publication IV is next compared against experimental data found in the literature. An illustration of the restitution coefficient between ammonium fluorescein particle and a polished silicon surface target for multiple particle sizes shown in Fig. 2.2. This figure illustrates how close the agreement between the model and real experiments can be in an ideal case when all the adhesion properties are known and are used according to the theory. Small discrepancies are seen in the values, which is caused by the imperfections of the experimental tests on unideal material properties. These are for example the surface roughness and the shape of the particles, which are never fully round in real life.

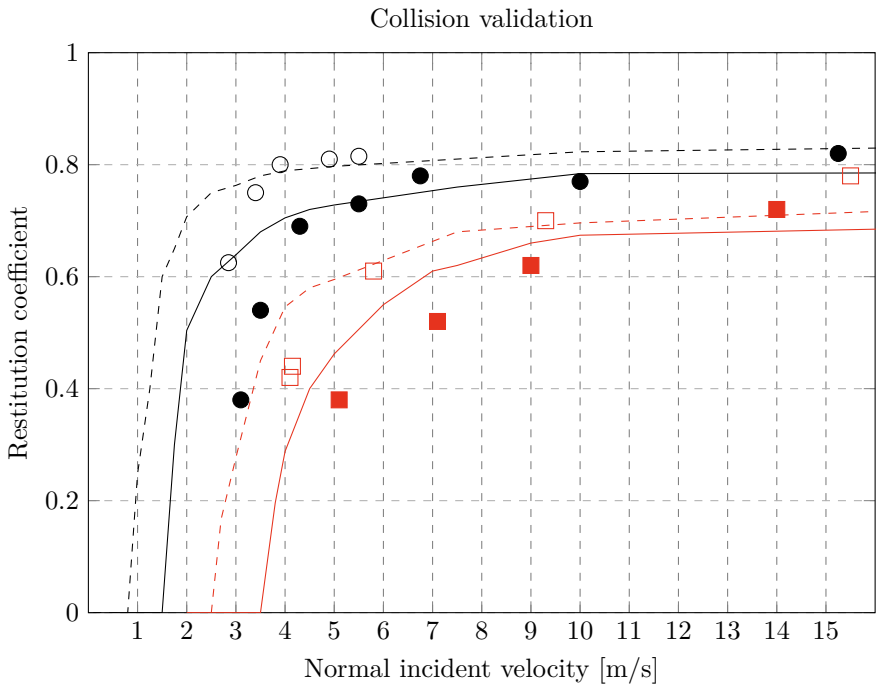

Figure 2.2: The restitution coefficients of the experimental results by Wall et al. [169] for ○ 6.89μm , ● 4.90μm , □ 3.44μm , ■ 2.58μm and the computed values with LIGGGHTS - - - 6.89μm , —— 4.90μm , - - - 3.44μm , —— 2.58μm

In the Publication IV, the boundary conditions for the flow field in the fouling simulations are designed so that the behaviour of the flow and its influence on the particle trajectories would be as close to the real working conditions as possible. On the sides of the inlet and outlet regions, periodic boundary conditions are used for all solved properties. For the pressure, a zero gradient inlet and constant outlet pressure condition are used. The velocity is adjusted at the inlet for every Reynolds number studied, outlet having a zero gradient boundary conditions. The turbulence levels at the inlet are kept zero, because of the arbitrary operating point and location of the heat exchanger respect to the fan. Extremities being a low velocity situation with the fan on the downwind side of the heat exchanger compared to a high velocity situation with the fan operating just before the heat exchanger on the upwind side. Therefore the turbulence level on the inlet side is neglected and a value of 0 for sub-grid scale viscosity is used. It should be noted here that the CFD-DEM fouling simulations do not consider temperature at all since it has been shown to not have any influence on the deposition rate [122].

2.8 Details on computational resources

During the thesis, two different clusters were used to perform the simulations. The simulations in the first Publication I were done with the now decommissioned Merope cluster at Tampere University. All the results in the rest of the Publications II, III and IV are simulated by using the cluster of CSC – IT Center for Science Finland. In all heat transfer publications (I, II, and III) a steady-state RANS simulation with k-ω SST turbulence model were performed. The simulations in Publication I were performed

for a two row plain fin FTHE with around 700 000 cells. The solid phase was meshed with 252 000 tetrahedral elements. This study was performed by using the segregated chtMultiRegionFoam solver and therefore the convergence times were seen to be very high of around 1000-2000 core hours per case. In the second Publication II, the two row herringbone with and without the vortex generators was simulated with around 600 000- 900 000 hexahedral cell meshes. On the solid side around 200 000 hexahedral cell mesh was used. In this study the matrix block coupled conjugateHeatSimpleFoam was used. The converged solution was found with around 300-400 core hours per case. In Publication III, a four row plain fin FTHE was studied with around 3 500 000 hexahedral cells on the air side and around 300 000 hexahedral cells on the solid side. The converged solution was found with around 800-1000 core hours. In the Publication IV, a two row herringbone and plain fin shape with 10 000 particles were simulated. The mesh used for the air side has around 2 000 000 cells. The computational resource in CFD-DEM fouling simulations are heavily related to the size and amount of the particles. With the current conditions used in the Publication IV, it took around 1200-2400 core hours in each case to compute the state were all particles have either deposited or flown through the heat exchanger. Overall, during the time of this thesis around 500 000 core hours were used.

3 Summary of results

The main scientific findings of this thesis are reported in Publications I-IV. Summaries of the publications are given below.

3.1 Publication I

In this study, pure convective simulations with only fluid side heat transfer and conjugate heat transfer with both fluid and solid side simulations were performed for fin-and-tube heat exchanger with plain fins. The results of these two type of heat transfer cases were compared to illustrate the importance of conjugate heat transfer.

The easiest way and most common strategy is to assume a constant temperature fin, which can result to correct results if fin heat conductivity and thickness are large. Usually an approximation of the fin efficiency is used for the calculation of global variables. However, often in practical applications this is not true, because fins are very thin in order to minimize material consumption as in our case. The results of our conjugate heat transfer simulations correlate well with experimental results. The results are not as good with only convective heat transfer. The main reason for this closer agreement in the plain fin geometry simulation is the lower heat flux rate both at the entrance and in the vicinity of the secondary vortex around the tubes. Especially, near the fin leading edge the fin temperature is much lower than in the neighborhood of the tube reducing heat flux as compared to an isothermal fin. The study shows that the errors for heat transfer and pressure drop in the conjugated simulation are, respectively, around 70 and 40 percent less than they are for the constant temperature simulation.

In this study, the meshing of the flow medium has been done by using open source tools called Swiftblock and Salome. This way structured good quality meshes with low computational cost are generated. Structured meshing strategy enables the user to define explicitly which directions the density of the mesh should be increased and therefore saves computational resources. Hexahedral cells are optimal for heat transfer simulations because the mesh density can be increased only in the direction of the highest temperature and velocity gradient, which is the direction of the surface normal. This meshing strategy enables the authors to parametrize different design variables in the blocking strategy of the meshing process. This is something that enables a fast and automated meshing when changing the design and is therefore used for a heat transfer optimization process in the future work.

An illustration of the wall heat flux and temperature of the fin are illustrated in Figs 3.1 and 3.2, respectively.

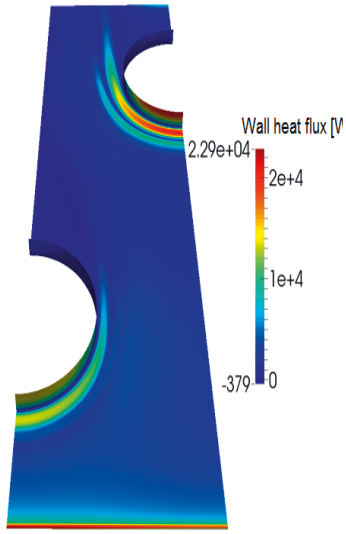

Figure 3.1: Heat flux through the heat transfer surface in the conjugate heat transfer model (Figure adopted from **Publication I**)

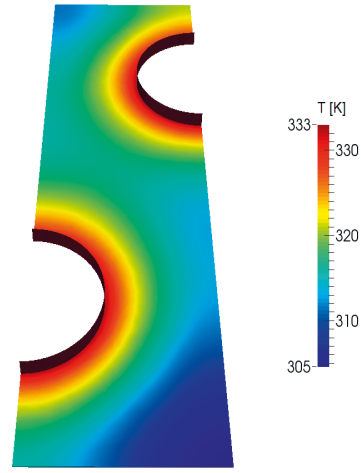

Figure 3.2: Temperature distribution on the fin in the conjugate heat transfer model (Figure adopted from **Publication I**)

3.2 Publication II

This article was motivated by discussions with fin press manufacturers. It was concluded that making the tooling for punching the vortex generator from the fin can be very difficult in the industrial scale. Especially inclined surfaces increase the difficulty and complexity of making the tool. By looking at the vortex generator studies conducted in the literature, it was clear that little to no consideration was given to the feasibility of manufacturing different VG designs that has been designed and studied during the last years.

Therefore, in this study six different punched longitudinal delta winglet VG designs and their heat transfer and pressure drop characteristics are investigated. The VG's are implemented in to the wavy herringbone fin shape. The design is restricted by the flat area around the tube, which is left from the collar forming tool in the fin press machine. Three-dimensional conjugate heat transfer simulations were performed by creating the meshes with Swiftblock and simulating the flow field as well as the temperature field in the air and in the fin with OpenFOAM.

From the results, the following conclusions can be made. The punched vortex delta winglets can enhance heat transfer in two ways; first one being the longitudinal vortices created in the downstream from the VG and the second one being the ability to direct high kinetic energy flow to the recirculation zone behind the tubes which leads to delay in the detachment of the flow from the tube as well as increase in the usage of heat transfer surface when the recirculation zone is decreased. Compared to the plain herringbone fin without VGs, herringbone fin with VG designs $s = 0.5D$ $H = 0.6F_p$ and the $s = 0.375D$ $H = 0.6F_p$ are found to have 5.23% and 4.97% higher volume goodness factor, respectively. From a manufacturing point of view the VG design can be made shorter $s = 0.375D$ but to ensure good thermal hydraulic enhancement the height of the VG should be kept closer to the height $H = 0.6F_p$. Shorter VG will perform better with higher Reynolds number where as the opposite will be encountered with lower velocities. The present investigation pursued the results considering conjugate heat transfer and its importance in heat transfer enhancement prediction with herringbone fin and VGs into account which is often neglected in many numerical studies. The effect of the VGs design on the temperature field in the fin is shown in Fig. 3.3. The present investigation provides important design performance data that could be useful to the heat exchanger design engineers and manufacturers in developing enhanced fin surfaces.

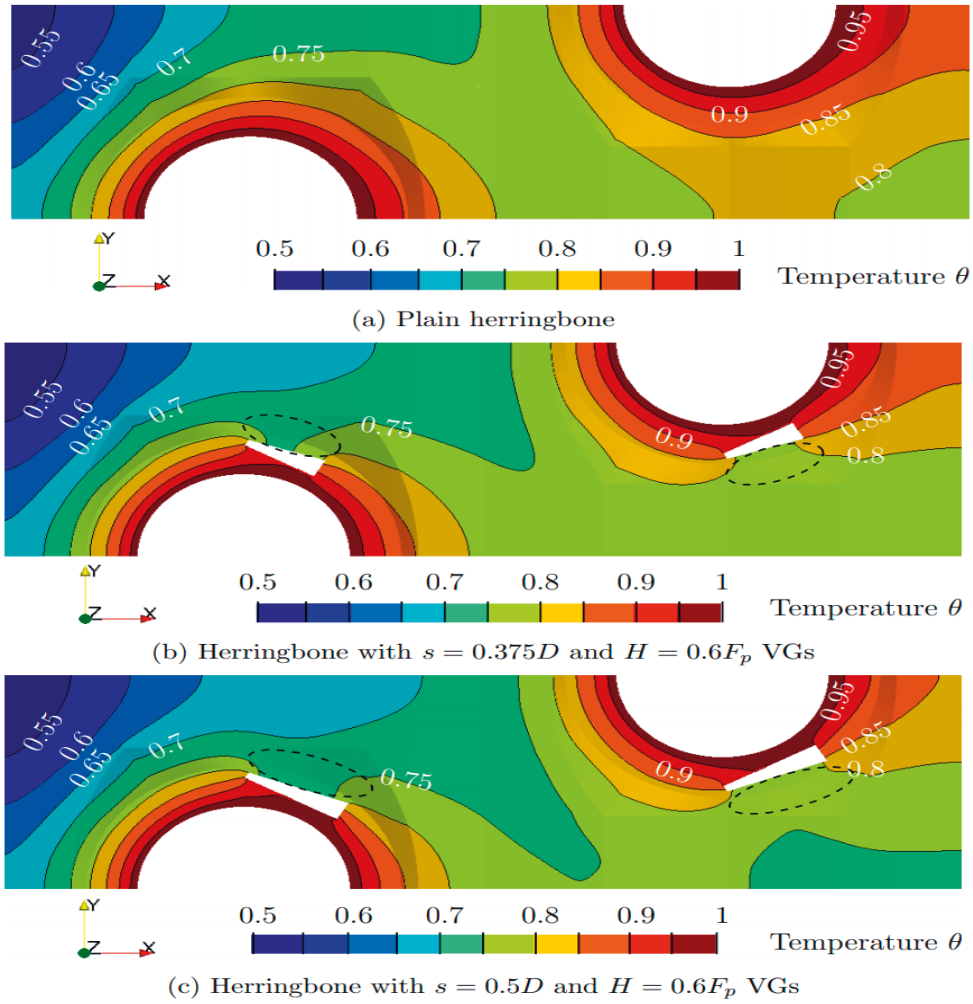

(a) Plain herringbone

(b) Herringbone with $s = 0.375D$ and $H = 0.6F_p$ VGs

(c) Herringbone with $s = 0.5D$ and $H = 0.6F_p$ VGs

Figure 3.3: Temperature distribution in the fin with diffeent vortex generator designs (Figure adopted from **Publication II**)

3.3 Publication III

It was evident from the experimental results found in the literature that most of the design factors in a FTHE have a profound effect on the thermal-hydraulic efficiency. For a constant tube size, the most important design variables are the fin pitch and the location of the tubes with respect to each other. The aim of this study was to investigate the optimal tube arrangements for a FTHE with plain fins in marine environments represented by two different air types; one for unfiltered air with high condensation rate and one for clean dry filtered air conditions. Second goal was to show how much the thermal-hydraulic efficiency could be improved by not following any manufacturing restrictions related to the tube arrangements in a FTHE. In this study the optimal tube arrangements for a fin-and-tube (FTHE) heat exchanger with plain fins for two application specific fin pitches $F_p = 1.5\,\text{mm}$ and $3.5\,\text{mm}$ was performed. Heat transfer and pressure drop over the heat exchanger is studied by performing conjugate heat transfer CFD simulations with varying longitudinal tube pitch $P_l = 14{-}78\,\text{mm}$ and transverse tube pitch $P_t = 14{-}38\,\text{mm}$. The thermal-hydraulic efficiency of the FTHE design is measured by comparing the JF performance criteria. The frontal velocity $u = 3\,\text{m}\,\text{s}^{-1}$, number of tube rows N =4, tube size D =10.00 mm and the fin thickness $t = 0.2\,\text{mm}$ was kept constant. The major findings of this study are summarized below.

Completely open source and parametric structured meshing tool developed by the authors was used to produce the computational meshes in this study. A regression model was created for the performance ratio JF based on the CFD simulations for two different fin pitches $F_p = 1.5\,\text{mm}$ and $3.5\,\text{mm}$ and a selection of different tube patterns covering longitudinal tube pitch $P_l = 14{-}78\,\text{mm}$ and transverse tube pitch $P_t = 14{-}38\,\text{mm}$. If application-specific additional constraints, related to air with high humidity or impurities, are not applied, the smaller fin pitch $F_p = 1.5\,\text{mm}$ may offer 36% better JF performance ratio than the design $F_p = 3.5\,\text{mm}$. For unconstrained tube arrangements, the local maximum performance ratio of $JF = 1.28$ for the fin pitch $F_p = 1.5\,\text{mm}$ is found and for the fin pitch $F_p = 3.5\,\text{mm}$ the maximum performance ratio of $JF = 0.94$ can be achieved. For constrained tube arrangements, $P_t/P_l = 1.1547$, the local maximum of the performance ratio is $JF = 1.24$ for the fin pitch $F_p = 1.5\,\text{mm}$ and for the fin pitch $F_p = 3.5\,\text{mm}$ the maximum performance ratio of $JF = 0.77$ can be achieved. Thus, by neglecting the manufacturing restrictions related to the radius of the hairpins in the soldering process of the tube circuits, a 4% higher JF performance ratio for fin pitch $F_p =$ 1.5 mm and 23% higher JF performance ratio for fin pitch $F_p = 3.5\,\text{mm}$ can be achieved. The results indicate that unconventional tube arrangement ratio values $P_t/P_l \neq 1.1547$ may offer better performance with regard to the JF performance ratio.

The regression models developed were used to visualise and locate the maximum value for the JF performance ratio for each fin pitch separately. In Fig.3.4, the JF performance ratio for $F_p = 1.5\,\text{mm}$ can be seen to reach its maximum value of $JF = 1.28$. This corresponds to the longitudinal tube pitch of $P_l = 38.04\,\text{mm}$ and the tranversial tube pitch of $P_t = 26.05\,\text{mm}$. In the Figs. 3.4 and 3.5, the black and red line represents a manufacturing restriction that is widely followed in the industry. By using tube patterns that corresponds to the ratio of P_t/P_l =1.1547, the transversial tube distance equals to the diagonal distance of the tube rows $P_t = P_d$ and therefore only one kind of U-bends can be used in the soldering process of the tube circuits. For better illustration please see Publication III.

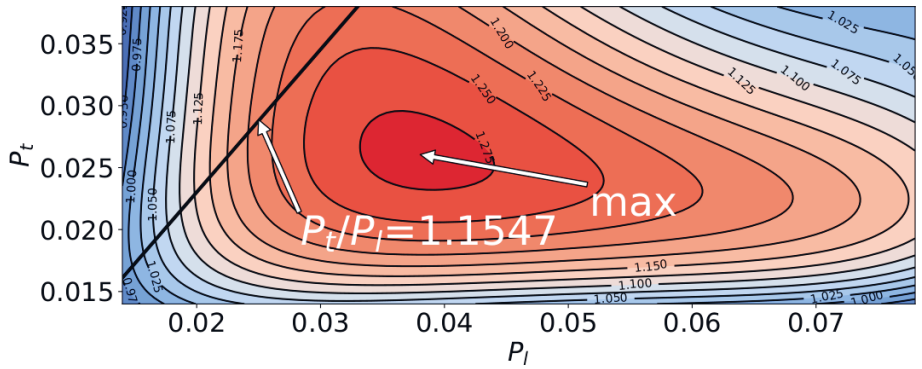

Figure 3.4: JF performance criteria response surface for F_p =1.5 mm (Figure adopted from **Publication III**)

In Fig.3.5, the JF performance ratio surface for F_p = 3.5 mm can be seen within the studied design space with the maximum value of JF =0.94 . This corresponds to the longitudinal tube pitch of P_l = 55.77 mm and the tranversial tube pitch of P_t = 21.56 mm.

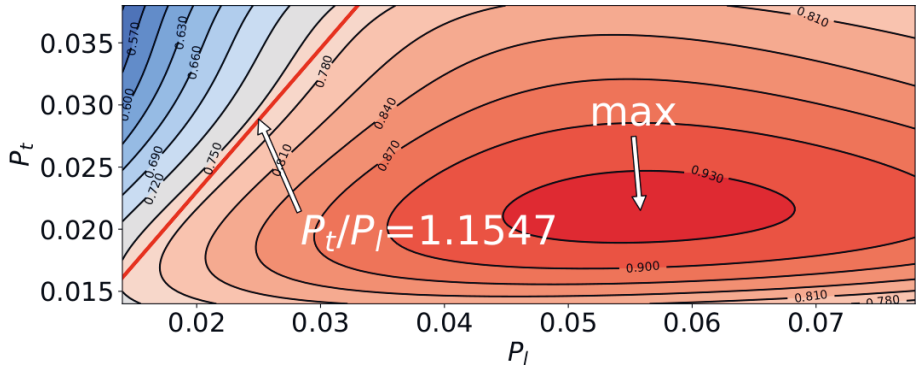

Figure 3.5: JF performance criteria response surface for F_p =3.5 mm (Figure adopted from **Publication III**)

Regarding all the numerical data with 198 value points in this study, a conclusion can be made that the maximum possible performance ratio JF for plain fins with a tube diameter of D = 10.00 mm is not found in the area of the current portfolio that is manufactured in the industry. Therefore comparison between the cost of manufacturing two sizes of U-bends and the benefits in the new unorthodox tube patterns with higher JF performance ratio illustrated in this study should be made.

3.4 Publication IV

This study was motivated by the uncertainty of assessing the risk of fouling with advanced fin types. It is an assumption in the air conditioning industry that enhanced fins with perforated and twisted fin shapes do accumulate more fouling but no methods have been developed to quantify this risk.

In this study, the deposition of dry particles on a fin-and-tube heat exchanger by a coupled soft-sphere discrete element method (DEM) and CFD was performed. The novel selection of material properties for the fouling particles is done so that a representative range of Reynolds numbers, Stokes numbers, elasticity and adhesion parameters is covered. The material selection in this study will lead to critical velocities between the particles and the fin surface that corresponds to the measurements performed for various material combinations and therefore different fouling characteristics. All the different models used for the calculation of the flow field and particle drag were validated. A comparison was carried out between low adhesive and high adhesive particle environments, with particle sizes of D_p = 5, 10, 20µm, with three typical FTHE Reynolds numbers Re_{D_h} =243, 528, 793 and two different fin shapes found in the contemporary HVAC industry. The major findings of this study are summarized below.

Novel method for the selection of adhesion properties such as particle size, particle density, effective Young's modulus, Poisson's ratio and adhesion work is demonstrated so that the corresponding critical velocity of the particles represent both ends of the spectrum in the real world fouling environments as illustrated in Fig. 3.6.

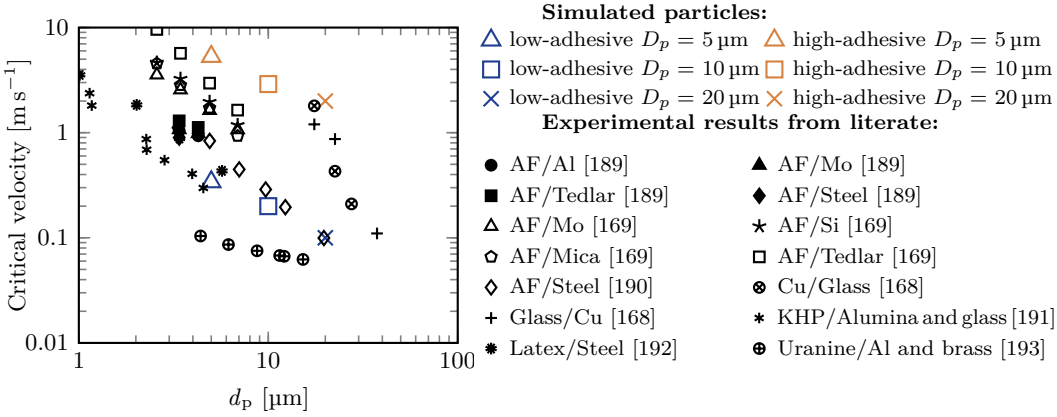

Figure 3.6: Critical velocity of the simulated particles and the measured values in the literature (Figure adopted from **Publication IV**)

The CFD code was validated by comparing the drag force and Strouhal numbers of a cylinder in a crossf flow against literature values. The CFD-DEM code was validated by comparing the particle drag to the analytical values and the DEM code was validated by comparing the critical velocity of the adhesion process to the experimental values reported in the literature. This method enables the comparison of the volume fouling rate of the fin-and-tube heat exchanger fin shapes in different environments. With low adhesive particles, plain fin volume fouling rate is 3.45 times higher with Re_{D_h} =793 than at Re_{D_h} =264. The herringbone fin shape has a volume fouling rate of 1.76 times

higher with Re_{D_h} =793 than at Re_{D_h} =264. With high adhesive particles, plain fin volume fouling rate is 5.4 times higher with Re_{D_h} =793 than at Re_{D_h} =264. This can be seen in Fig. 3.7. The herringbone fin shape has a volume fouling rate of 3.92 times higher with Re_{D_h} =793 than at Re_{D_h} =264. High adhesive particles will have 3.0 times higher volume fouling rate than low adhesive particles for both fin shapes, particle sizes and all Reynolds numbers combined. Herringbone fins have 1.74 higher volume fouling rate than plain fin shape for low adhesive type particles. For high adhesive particles, herringbone has 1.8 times higher volume fouling rate and when both particle types are summed together, herringbone has 1.78 times higher volume fouling rate than the plain fin shape.

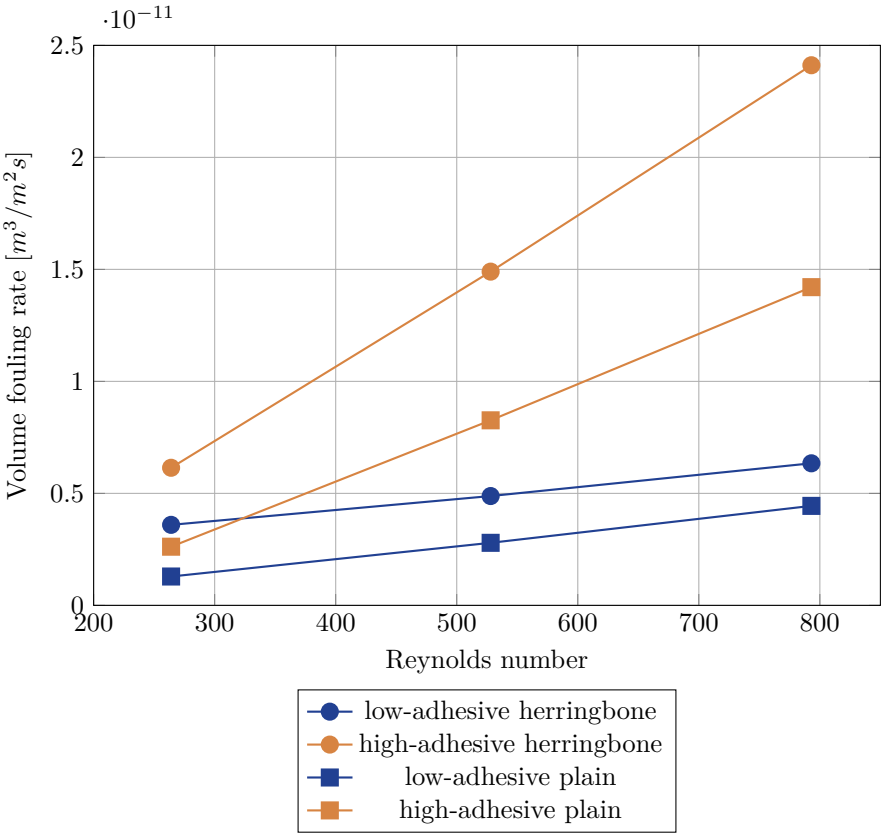

Figure 3.7: Volume fouling rate respect to the Reynolds number (Figure adopted from **Publication IV**)

If all new enhanced fin shapes that are shown to have an improved thermal-hydraulic efficiency were examined in a similar manner as was done in this study, a quantified estimation of the fouling risk could be determined.

4 Conclusions and Discussions

4.1 Conclusions

This thesis provides computational insight into fin-and-tube heat exchanger (FTHE) development in the air conditioning application. The work was motivated by the cost of running air conditioning appliances as well as the cost of manufacturing the heat exchangers for the air handling units. In the beginning, extensive research and development was done for finding a suitable open source framework that can be used for simulating the thermal-hydraulic efficiency of the FTHE in an accurate and computationally feasible way. Then, the focus shifted on to applying the framework for developing a novel vortex generator design with a traditional herringbone fin shape. Third, the aim was on studying the plain fin shape with all the feasible tube arrangements available to illustrate the designs with maximum performance ratio. Finally, a new method was developed for selecting the material properties for a computational particle fouling study so that the results represent both ends of the real world particles; high-adhesive and low-adhesive.

In publication I, pure convective simulations with only fluid side heat transfer was compared to conjugate heat transfer model with both fluid and solid side heat transfer for fin-and-tube heat exchanger with plain fins. The results of these two type of heat transfer cases were compared to illustrate the accuracy of conjugate heat transfer models. The present study clearly shows that the errors for heat transfer and pressure drop in the conjugated simulation are, respectively, around 70 and 40 percent less than they are for the constant temperature simulation. This initial research on conjugate heat transfer simulation of a FTHE was then extended to more advanced geometries and physics in following publications.

Using the knowledge from solvers, boundary conditions, meshing strategies and converge monitoring from the previous study, a much more topologically challenging fin shape study could be able to be performed. On the basis of the information about the thermal-hydraulic efficiency of the plain fin shape FTHE, a new type of an enhanced fin was develop. The aim was to take the well performing vortex generator (VG) design from a plain fin study and combine it with a herringbone fin shape commonly found in the industry. The inclusion was done in a way that the VG is punched to the flat surface between the collar and the herringbone shape. Compared to the plain herringbone fin without VGs, herringbone fin with VG designs $s = 0.5D$ $H = 0.6F_p$ and the $s = 0.375D$ $H = 0.6F_p$ are found to have 5.23% and 4.97% higher volume goodness factor, respectively.

In Publication III, a conjugate heat transfer model of plain fin FTHE is investigated in marine environment. By utilizing parametric meshing, a quadratic regression model was generated from the simulation data to describe the characteristics of the FTHE in the applicable range of design variables. The regression model was then used to locate the

maximum for each fin pitch separately. The smaller fin pitch $F_p = 1.5\,\text{mm}$ represents a FTHE design for dry filtered air. In contrast, the larger fin pitch $F_p = 3.5\,\text{mm}$ represents a typical design with high condensation rate and unfiltered air. It was demonstrated that it is possible to find the best tube pattern, which is unique for each application specific fin pitch. Second, the best tube pattern is different if the manufacturing restrictions are followed or not. Third, this means that, by neglecting the manufacturing restrictions related to the radius of the hairpins in the soldering process of the tube circuits, a 4% higher JF for $F_p = 1.5\,\text{mm}$ and 23% higher JF for $F_p = 3.5\,\text{mm}$ can be achieved. In a situation with no application specific or manufacturing restrictions on the fin pitch a $F_p = 1.5\,\text{mm}$ can have a 36% better JF than $F_p = 3.5\,\text{mm}$.

There is a deep concern about the increased fouling propensity of enhanced fin types in the industry. This concern was shared in the academic literature. Nevertheless, only a handful of studies have been conducted and most of them were experimental ones. It was clear that there is no standardized way of performing a fouling study of a FTHE and therefore the lack of data about the risks of enhanced fin types was evident. In this study, the deposition of dry particles on a fin-and-tube heat exchanger by a coupled soft-sphere DEM and CFD was performed. The novel selection of material properties for the fouling particles is done so that a representative range of Reynolds numbers, Stokes numbers, elasticity and adhesion parameters is covered. The material selection in this study will lead to critical velocities between the particles and the fin surface that corresponds to the measurements performed for various material combinations and therefore different fouling characteristics. All the different models used for the calculation of the flow field and particle drag were validated. A comparison was carried out between low adhesive and high adhesive particle environments, with particle sizes of $D_p = 5$, 10, 20µm, with three typical FTHE Reynolds numbers Re_{D_h} =243, 528, 793 and two different fin shapes found in the contemporary HVAC industry. The major findings of this study are summarized below.

With low adhesive particles, plain fin volume fouling rate is 3.45 times higher with Re_{D_h} =793 than at Re_{D_h} =264. The herringbone fin shape has a volume fouling rate of 1.76 times higher with Re_{D_h} =793 than at Re_{D_h} =264. With high adhesive particles, plain fin volume fouling rate is 5.4 times higher with Re_{D_h} =793 than at Re_{D_h} =264. The herringbone fin shape has a volume fouling rate of 3.92 times higher with Re_{D_h} =793 than at Re_{D_h} =264. High adhesive particles will have 3.0 times higher volume fouling rate than low adhesive particles for both fin shapes, particle sizes and all Reynolds numbers combined. Herringbone fins have 1.74 higher volume fouling rate than plain fin shape for low adhesive type particles. For high adhesive particles, herringbone has 1.8 times higher volume fouling rate and when both particle types are summed together, herringbone fin shape has a 1.78 times higher volume fouling rate than the plain fin shape.

Regarding the research objectives, in this dissertation it was illustrated how a computational model can be created for a FTHE to study multiple aspects of the design in a computationally reasonable manner. Essential part of this was to use the matrix coupled open source solver found in the FOAM-Extend library. The meshing process was automated by using and developing an open source structured parametric meshing tool called SwiftBlock. By then combining a vortex generator to a traditional herringbone fin shape, it was shown how much the thermal-hydraulic efficiency can be improved with different inlet velocities compered to the pure herringbone design. The design was also considered to be more feasible to manufacture than other vortex generator designs found in the industry. After this, by performing a parametric study on the tube arrangement of

a specific plain fin FTHE design it was illustrated how many data points are required to represent the thermal-hydraulic characteristics of a fin type and a local maximum can be located. It was also evident that this local maximum is not close to the FTHE designs currently manufactured in the industry. Finally a computational method to quantify the risk of fouling involved with different fin shapes was developed. It was then applied to compare the fouling propensity of two popular fin shape designs to illustrate what is the effect of the operating point, fin design and the size and adhesiveness level of the fouling particles to the fouling risk of the FTHE.

4.2 Limitations and challenges

The two major challenges and two limitations related to the topics studied in this thesis are listed as follows.

First challenge is related to the methods and models used and developed in this thesis. A major one is the steep learning curve related to the software's used to generate the meshes for the simulations. The open source software called Blender is known for its complexity and the large amount of hours required to master it. The difficulty is not related to the poor design of the software, but rather its the vast scope and feature rich design. Typically, when creating blocking strategies for the meshes, the user does not need most of the available features. Therefore, to enhance the use of the tools developed in this thesis, a major effort should be put on creating documentation and introduction materials to improve the learning experience.

Second challenge is related to the computational resources required to run similar simulations as was done during the studies in this thesis. Multiple different compromises were made in relation to the accuracy of the numerical models, such as the choice to run Reynolds-averaged Navier–Stokes (RANS) simulations instead of using more turbulence resolving techniques. Also in all studies in this thesis, only the air side of the heat transfer process is considered. This is of course due to the overwhelming computational resources required for a full scale FTHE simulation, which will not be available in a long time. Another example of challenges in computational resources, is the decision to simulate only the nucleation regime of the fouling process in Publication IV, instead of simulating all the way to the bulk regime and possibly running enough particles through the heat exchanger that the whole air way would get clogged. Nevertheless, even with the simplifications, the simulations require vast amounts of computational resources that are only available through high-performance computing.

The first limitation is related to the regression models developed for the data set in the Publication III. Regression models are a common way in science to represent a group of data in a form of an equation, often called a correlation-equation. The drawbacks of regression model -based equations is that every point in the data is considered to have an equal contribution to the model. This means that regression models do not classify the data in any way and the reliability of the data needs to be ensured in other methods. Therefore, the regression models are very diffusive and smooth out features as it tries to represent every data point equally well. Of course an argument could be made that by excluding all the outlier values from the data, this would not be a problem. But in practice, it is very hard to define which values are outliers. Also if the polynomial degree of the regression model is too high, the model starts to overfit to the data and does not generalize well for new data or subsets of the data. Therefore a compromise has to be made with the overfitting and accurate general representation of the data.

Second limitation is related to the fact that even if the numerical results indicate that a better performing heat exchanger design is found in the studied design space, still, the FTHE manufacturer requires experimental proof of its performance. Therefore, one can never solely rely on computational methods and still needs to invest in experimental measurement setups and tools to manufacture prototype heat exchangers.

4.3 Benefits for the broader community

The benefits are divided in to three different categories; CFD community, FTHE manufacturers and society in general and are laid out as follows.

First, the direct benefit for the CFD community comes from the developed meshing tool called SwiftBlock. It is one of the few open source structured meshing tools available. In authors knowledge, it is currently used in industrial scale as well and is gaining more users everyday. The most common use case for it is when the user already knows how to use blockMesh but wants to create a bit more complex blocking structures and therefore uses SwiftBlock to design the blocking strategy.

Second, the results and key findings of this thesis can be utilized in many ways for the benefit of the broader community. The key is to define the performance criteria that is used to measure the goodness of the heat exchanger. The computational models developed in this thesis can be used to find the optimal heat exchanger design for each application specific operating condition in such a way that it leads to the maximum possible values of the chosen performance criteria. If a performance criterion is chosen, that measures the cost to manufacture the heat exchanger per amount of transferred heat, the computational models and workflows can be used to develop heat exchanger designs that fulfill the requirements and at same time maximize the profits for the manufacturers.

Finally, if a performance criteria is used that represents the cost of running the heat exchanger per a required heat load. This would benefit the user of the heat exchanger by minimizing the cost of running the heat exchanger and minimizing the amount of emissions created by the usage of the device. Note that then other design aspects such as manufacturing costs or size of the heat exchanger are not taken into consideration. Neither does it guarantee that the overall environmental load caused by the heat exchanger are lower. This is because sourcing the materials and manufacturing the device can still cause more emissions than using the device through its lifetime, that can be up to 30 years.

4.4 Future work

In Publication I, it is shown that by solving the heat equation in the fin at the same time while solving the flow and temperature field on the air side, higher accuracy can be achieved. Using fin efficiency accompanied with a pure convective heat transfer simulation can lead to equally good results in some cases. But no quantified data about the suitability of the fin efficiency in respect to all the different fin generations is available. Therefore, a study should be made by varying the Reynolds number, fin type, design parameters and the conductivity of the fin to see where the two dimensional fin efficiency is applicable. It is possible that as the fin type has increasing amount of three dimensional features, the fin efficiency starts to deviate from the brute force strategy where everything is solved as is.

The combined vortex generator and herringbone design study in Publication II should be expanded to include all the other design variables as was illustrated in Publication III so that a complete comparison of the goodness of the fin can be performed. This of course applies to all other studies conducted for just one combination of design variables in the literature.

A comprehensive series of studies should be performed for all other enhanced fin types and their fouling characteristics. This should then be linked to the cost of running the enhanced fin types. This way the trade-off between increased thermal-hydraulic efficiency and higher fouling rate can be quantified and a reasoned decision can be made, should the enhanced fin types be used or not.

As the computational resources increase in the future, the Publication IV should be expanded to include the bulk regime as well. This is the point where the balance between depositing incoming particles and re-entrained particles is equal. This is the maximum additional pressure drop induced by the fouling layer for a specific design of FTHE in a certain fouling environment after years of usage. The thermal-hydraulic efficiency between the bulk regime and a clear new heat exchanger should then be taken into account by simulating the effect of the insulating fouling layer between the air and the fin.

Bibliography

[1] T. Stocker, *Climate change 2013: the physical science basis: Working Group I contribution to the Fifth assessment report of the Intergovernmental Panel on Climate Change*. Cambridge University Press, 2014.

[2] J. Cook, N. Oreskes, P. T. Doran, W. R. L. Anderegg, B. Verheggen, E. W. Maibach, J. S. Carlton, S. Lewandowsky, A. G. Skuce, S. A. Green, D. Nuccitelli, P. Jacobs, M. Richardson, B. Winkler, R. Painting, and K. Rice, "Consensus on consensus: a synthesis of consensus estimates on human-caused global warming," *Environmental Research Letters*, vol. 11, no. 4, p. 048002, 2016. [Online]. Available: http://stacks.iop.org/1748-9326/11/i=4/a=048002

[3] N. S. Diffenbaugh, D. Singh, J. S. Mankin, D. E. Horton, D. L. Swain, D. Touma, A. Charland, Y. Liu, M. Haugen, M. Tsiang *et al.*, "Quantifying the influence of global warming on unprecedented extreme climate events," *Proceedings of the National Academy of Sciences*, vol. 114, no. 19, pp. 4881–4886, 2017.

[4] A. Damm, W. Greuell, O. Landgren, and F. Prettenthaler, "Impacts of+ 2 c global warming on winter tourism demand in europe," *Climate Services*, vol. 7, pp. 31–46, 2017.

[5] R. Warren, J. Price, E. Graham, N. Forstenhaeusler, and J. VanDerWal, "The projected effect on insects, vertebrates, and plants of limiting global warming to 1.5° c rather than 2° c," *Science*, vol. 360, no. 6390, pp. 791–795, 2018.

[6] P. Döll, T. Trautmann, D. Gerten, H. M. Schmied, S. Ostberg, F. Saaed, and C.-F. Schleussner, "Risks for the global freshwater system at 1.5° c and 2° c global warming," *Environmental Research Letters*, vol. 13, no. 4, p. 044038, 2018.

[7] H.-B. Xie, Y.-F. Wang, J. Gong, M.-H. Liu, and X.-Y. Yang, "Effect of global warming on chloride ion erosion risks for offshore rc bridges in china," *KSCE Journal of Civil Engineering*, pp. 1–7, 2018.

[8] S. Hsiang, R. Kopp, A. Jina, J. Rising, M. Delgado, S. Mohan, D. Rasmussen, R. Muir-Wood, P. Wilson, M. Oppenheimer *et al.*, "Estimating economic damage from climate change in the united states," *Science*, vol. 356, no. 6345, pp. 1362–1369, 2017.

[9] J. Bongaarts and B. C. O'Neill, "Global warming policy: Is population left out in the cold?" *Science*, vol. 361, no. 6403, pp. 650–652, 2018.

[10] U. N. D. of International Economic, *World Population Prospects as Assessed in...* UN, 1982.

[11] S. Buranyi. (2019) The air conditioning trap: how cold air is heating the world. [Online]. Available: https://www.theguardian.com/environment/2019/aug/29/the-air-conditioning-trap-how-cold-air-is-heating-the-world

[12] D. Ürge Vorsatz, L. F. Cabeza, S. Serrano, C. Barreneche, and K. Petrichenko, "Heating and cooling energy trends and drivers in buildings," *Renewable and Sustainable Energy Reviews*, vol. 41, pp. 85 – 98, 2015. [Online]. Available: http://www.sciencedirect.com/science/article/pii/S1364032114007151

[13] A. Allouhi, Y. E. Fouih, T. Kousksou, A. Jamil, Y. Zeraouli, and Y. Mourad, "Energy consumption and efficiency in buildings: current status and future trends," *Journal of Cleaner Production*, vol. 109, pp. 118 – 130, 2015, special Issue: Toward a Regenerative Sustainability Paradigm for the Built Environment: from vision to reality. [Online]. Available: http://www.sciencedirect.com/science/article/pii/S0959652615007581

[14] I. E. Agency, *Energy Technology Perspectives 2014: Harnessing Electricity's Potential*. OECD Publishing, 2012.

[15] P. Jaboyedoff, C.-A. Roulet, V. Dorer, A. Weber, and A. Pfeiffer, "Energy in air-handling units—results of the airless european project," *Energy and Buildings*, vol. 36, no. 4, pp. 391 – 399, 2004, proceedings of the International Conference on Solar Energy in Buildings CISBAT 2001. [Online]. Available: http://www.sciencedirect.com/science/article/pii/S0378778804000477

[16] D. of the Ministry of the Environment, "On the energy performance of new buildings," Ministry of Environment Finland, Tech. Rep., 2019.

[17] E. Parliament and Council, "Commission regulation (eu) no 1253/2014 of 7 july 2014 implementing directive 2009/125/ec of the european parliament and of the council with regard to ecodesign requirements for ventilation units text with eea relevance," *OJ*, vol. 1253/2014, 2014-7-5.

[18] F. M. of the Environment, "National building code of finland, d2. indoor climate and ventilation in buildings, regulations and guidelines," 1987.

[19] F. M. of the Environment, "National building code of finland 2012 – section d3 on energy management in buildings, regulations and guidelines," 2012.

[20] F. M. of the Environment, "National building code of finland 2012 – section d5 on guidelines for the calculation of power and energy needs for heating of buildings, regulations and guidelines," 2008.

[21] W. D. Callister, D. G. Rethwisch *et al.*, *Materials science and engineering: an introduction*. John wiley & sons New York, 2007, vol. 7.

[22] A. F. Mills and A. Mills, *Basic heat and mass transfer*. Prentice hall Upper Saddle River, 1999, vol. 2.

[23] U. G. Survey, "Mineral commodity summaries (2020)," U.S. Geological Survey, Tech. Rep., 2020. [Online]. Available: https://minerals.usgs.gov/minerals/pubs/commodity/

[24] J. Allwood, C. Dunant, R. Lupton, and A. Serrenho, "Steel arising: Opportunities for the uk in a transforming global steel industry," *Steel arising*, 2019.

[25] C. Wang, W. Fu, and C. Chang, "Heat transfer and friction characteristics of typical wavy fin-and-tube heat exchangers," *Experimental Thermal and Fluid Science*, vol. 14, no. 2, pp. 174 – 186, 1997.

[26] C.-C. Wang and C.-T. Chang, "Heat and mass transfer for plate fin-and-tube heat exchangers, with and without hydrophilic coating," *International Journal of Heat and Mass Transfer*, vol. 41, no. 20, pp. 3109 – 3120, 1998. [Online]. Available: http://www.sciencedirect.com/science/article/pii/S001793109800060X

[27] C.-C. Wang, W.-S. Lee, and W.-J. Sheu, "A comparative study of compact enhanced fin-and-tube heat exchangers," *International Journal of Heat and Mass Transfer*, vol. 44, no. 18, pp. 3565 – 3573, 2001. [Online]. Available: http://www.sciencedirect.com/science/article/pii/S0017931001000114

[28] L. Pigani, M. Boscolo, and N. Pagan, "Marine refrigeration plants for passenger ships: Low-gwp refrigerants and strategies to reduce environmental impact," *International Journal of Refrigeration*, vol. 64, pp. 80 – 92, 2016. [Online]. Available: http://www.sciencedirect.com/science/article/pii/S0140700716000220

[29] C.-C. Wang, K.-Y. Chi, and C.-J. Chang, "Heat transfer and friction characteristics of plain fin-and-tube heat exchangers, part ii: Correlation," *International Journal of Heat and Mass Transfer*, vol. 43, no. 15, pp. 2693 – 2700, 2000.

[30] C.-C. Wang and K.-Y. Chi, "Heat transfer and friction characteristics of plain fin-and-tube heat exchangers, part i: new experimental data," *International Journal of Heat and Mass Transfer*, vol. 43, no. 15, pp. 2681 – 2691, 2000.

[31] J.-Y. Jang, M.-C. Wu, and W.-J. Chang, "Numerical and experimental studies of threedimensional plate-fin and tube heat exchangers," *International Journal of Heat and Mass Transfer*, vol. 39, no. 14, pp. 3057 – 3066, 1996.

[32] J. Mao, H. Chen, H. Jia, Y. Wang, and H. Hu, "Effect of air-side flow maldistribution on thermal–hydraulic performance of the multi-louvered fin and tube heat exchanger," *International Journal of Thermal Sciences*, vol. 73, pp. 46 – 57, 2013. [Online]. Available: http://www.sciencedirect.com/science/article/pii/S1290072913001257

[33] W. Yaïci, M. Ghorab, and E. Entchev, "3d cfd analysis of the effect of inlet air flow maldistribution on the fluid flow and heat transfer performances of plate-fin-and-tube laminar heat exchangers," *International Journal of Heat and Mass Transfer*, vol. 74, pp. 490 – 500, 2014. [Online]. Available: http://www.sciencedirect.com/science/article/pii/S0017931014002403

[34] M. R. Kærn, W. Brix, B. Elmegaard, and L. F. S. Larsen, "Performance of residential air-conditioning systems with flow maldistribution in fin-and-tube evaporators," *International Journal of Refrigeration*, vol. 34, no. 3, pp. 696 – 706, 2011. [Online]. Available: http://www.sciencedirect.com/science/article/pii/S0140700710002859

[35] C.-C. Wang and J.-S. Liaw, "Air-side performance of herringbone wavy fin-and-tube heat exchangers under dehumidifying condition – data with larger diameter tube," *International Journal of Heat and Mass Transfer*, vol. 55, no. 11, pp. 3054 – 3060, 2012. [Online]. Available: http://www.sciencedirect.com/science/article/pii/S0017931012000889

[36] G. Xie, Q. Wang, and B. Sunden, "Parametric study and multiple correlations on air-side heat transfer and friction characteristics of fin-and-tube heat exchangers with large number of large-diameter tube rows," *Applied Thermal Engineering*, vol. 29, no. 1, pp. 1 – 16, 2009. [Online]. Available: http://www.sciencedirect.com/science/article/pii/S135943110800029X

[37] S. Panse, "A numerical investigation of thermal and hydraulic characteristics in 3d plate and wavy fin-tube heat exchangers for laminar and transitional flow regimes," *Montana State University*, 2005.

[38] M. Tutar and A. Akkoca, "Numerical analysis of fluid flow and heat transfer characteristics in three-dimensional plate fin-and-tube heat exchangers," *Numerical Heat Transfer, Part A: Applications*, vol. 46, no. 3, pp. 301–321, 2004.

[39] S. B. Pope, *Turbulent flows*. Cambridge university press, 2000.

[40] G. Zhang, B. Wang, X. Li, W. Shi, and Y. Cao, "Review of experimentation and modeling of heat and mass transfer performance of fin-and-tube heat exchangers with dehumidification," *Applied Thermal Engineering*, vol. 146, pp. 701–717, 2019.

[41] S. Wongwises and Y. Chokeman, "Effect of fin pitch and number of tube rows on the air side performance of herringbone wavy fin and tube heat exchangers," *Energy Conversion and Management*, vol. 46, no. 13, pp. 2216 – 2231, 2005. [Online]. Available: http://www.sciencedirect.com/science/article/pii/S0196890404002584

[42] J. Jeong, C. N. Kim, and B. Youn, "A study on the thermal contact conductance in fin–tube heat exchangers with 7mm tube," *International Journal of Heat and Mass Transfer*, vol. 49, no. 7, pp. 1547 – 1555, 2006.

[43] C.-C. Wang, R. L. Webb, and K.-Y. Chi, "Data reduction for air-side performance of fin-and-tube heat exchangers," *Experimental Thermal and Fluid Science*, vol. 21, no. 4, pp. 218 – 226, 2000.

[44] J. Chen, H. Müller-Steinhagen, and G. G. Duffy, "Heat transfer enhancement in dimpled tubes," *Applied Thermal Engineering*, vol. 21, no. 5, pp. 535 – 547, 2001. [Online]. Available: http://www.sciencedirect.com/science/article/pii/S1359431100000673

[45] P. Vicente, A. Garcia, and A. Viedma, "Experimental investigation on heat transfer and frictional characteristics of spirally corrugated tubes in turbulent flow at different prandtl numbers," *International Journal of Heat and Mass Transfer*, vol. 47, no. 4, pp. 671 – 681, 2004. [Online]. Available: http://www.sciencedirect.com/science/article/pii/S001793100300454X

[46] N. Zheng, P. Liu, F. Shan, Z. Liu, and W. Liu, "Effects of rib arrangements on the flow pattern and heat transfer in an internally ribbed heat exchanger tube," *International Journal of Thermal Sciences*, vol. 101, pp. 93 – 105, 2016. [Online]. Available: http://www.sciencedirect.com/science/article/pii/S1290072915003361

[47] A. Zukauskas, "Heat transfer from tubes in cross flow vol. 8," 1972.

[48] R. L. Webb and N. Kim, "Enhanced heat transfer," *Taylor and Francis, NY*, 2005.

[49] A. A. Bhuiyan and A. S. Islam, "Thermal and hydraulic performance of finned-tube heat exchangers under different flow ranges: A review on modeling and experiment," *International Journal of Heat and Mass Transfer*, vol. 101, pp. 38 – 59, 2016. [Online]. Available: http://www.sciencedirect.com/science/article/pii/S001793101630134X

[50] C.-C. Wang, K.-Y. Chi, and C.-J. Chang, "Heat transfer and friction characteristics of plain fin-and-tube heat exchangers, part ii: Correlation," *International Journal of Heat and mass transfer*, vol. 43, no. 15, pp. 2693–2700, 2000.

[51] C.-C. Wang, Y.-J. Chang, Y.-C. Hsieh, and Y.-T. Lin, "Sensible heat and friction characteristics of plate fin-and-tube heat exchangers having plane fins," *International Journal of Refrigeration*, vol. 19, no. 4, pp. 223–230, 1996.

[52] C.-C. Wang, Y.-M. Hwang, and Y.-T. Lin, "Empirical correlations for heat transfer and flow friction characteristics of herringbone wavy fin-and-tube heat exchangers," *International Journal of Refrigeration*, vol. 25, no. 5, pp. 673–680, 2002.

[53] C.-C. Wang, W.-S. Lee, and W.-J. Sheu, "A comparative study of compact enhanced fin-and-tube heat exchangers," *International Journal of Heat and Mass Transfer*, vol. 44, no. 18, pp. 3565–3573, 2001.

[54] F. McQuiston, "Heat, mass and momentum transfer data for five plate-fin-tube heat transfer surfaces," *ASHRAE Trans*, vol. 84, no. 1, pp. 266–293, 1978.

[55] Y. Seshimo and M. Fujii, "An experimental study on the performance of plate fin and tube heat exchangers at low reynolds numbers," in *Proceedings of the 1991 ASME JSME thermal engineering joint conference*, 1991.

[56] M. Li, H. Zhang, J. Zhang, Y. Mu, E. Tian, D. Dan, X. Zhang, and W. Tao, "Experimental and numerical study and comparison of performance for wavy fin and a plain fin with radiantly arranged winglets around each tube in fin-and-tube heat exchangers," *Applied Thermal Engineering*, vol. 133, pp. 298 – 307, 2018.

[57] C.-C. Wang, J. Lo, Y.-T. Lin, and C.-S. Wei, "Flow visualization of annular and delta winlet vortex generators in fin-and-tube heat exchanger application," *International Journal of Heat and Mass Transfer*, vol. 45, no. 18, pp. 3803 – 3815, 2002.

[58] A. Joardar and A. Jacobi, "Impact of leading edge delta-wing vortex generators on the thermal performance of a flat tube, louvered-fin compact heat exchanger," *International Journal of Heat and Mass Transfer*, vol. 48, no. 8, pp. 1480 – 1493, 2005.

[59] J. Wu and W. Tao, "Numerical study on laminar convection heat transfer in a rectangular channel with longitudinal vortex generator. part a: Verification of field synergy principle," *International Journal of Heat and Mass Transfer*, vol. 51, no. 5, pp. 1179 – 1191, 2008.

[60] B. Lotfi, M. Zeng, B. Sundén, and Q. Wang, "3d numerical investigation of flow and heat transfer characteristics in smooth wavy fin-and-elliptical tube heat exchangers using new type vortex generators," *Energy*, vol. 73, pp. 233–257, 2014.

[61] B. Lotfi, B. Sund??n, and Q. Wang, "An investigation of the thermo-hydraulic performance of the smooth wavy fin-and-elliptical tube heat exchangers utilizing new type vortex generators," *Applied Energy*, vol. 162, pp. 1282–1302, 2016.

[62] B. Lotfi, M. Zeng, B. Sundén, and Q. Wang, "3d numerical investigation of flow and heat transfer characteristics in smooth wavy fin-and-elliptical tube heat exchangers using new type vortex generators," *Energy*, vol. 73, pp. 233 – 257, 2014. [Online]. Available: http://www.sciencedirect.com/science/article/pii/S0360544214007142

[63] B. Lotfi, B. Sunden, and Q.-W. Wang, "3d fluid-structure interaction (fsi) simulation of new type vortex generators in smooth wavy fin-and-elliptical tube heat exchanger," *Engineering Computations*, 2016.

[64] B. Lotfi, B. Sundén, and Q. Wang, "An investigation of the thermo-hydraulic performance of the smooth wavy fin-and-elliptical tube heat exchangers utilizing new type vortex generators," *Applied Energy*, vol. 162, pp. 1282 – 1302, 2016. [Online]. Available: http://www.sciencedirect.com/science/article/pii/S0306261915009058

[65] J. Gong, C. Min, C. Qi, E. Wang, and L. Tian, "Numerical simulation of flow and heat transfer characteristics in wavy fin-and-tube heat exchanger with combined longitudinal vortex generators," *International Communications in Heat and Mass Transfer*, vol. 43, pp. 53 – 56, 2013. [Online]. Available: http://www.sciencedirect.com/science/article/pii/S0735193313000146

[66] L. Tian, Y. He, Y. Tao, and W. Tao, "A comparative study on the air-side performance of wavy fin-and-tube heat exchanger with punched delta winglets in staggered and in-line arrangements," *International Journal of Thermal Sciences*, vol. 48, no. 9, pp. 1765–1776, 2009. [Online]. Available: http://dx.doi.org/10.1016/j.ijthermalsci.2009.02.007

[67] L. Tian, Y. He, P. Chu, and W. Tao, "Numerical Study of Flow and Heat Transfer Enhancement by Using Delta Winglets in a Triangular Wavy Fin-and-Tube Heat Exchanger," *Journal of Heat Transfer*, vol. 131, no. 9, pp. 11–19, 2009.

[68] L. Tian, Y. He, Y. Tao, and W. Tao, "A comparative study on the air-side performance of wavy fin-and-tube heat exchanger with punched delta winglets in staggered and in-line arrangements," *International Journal of Thermal Sciences*, vol. 48, no. 9, pp. 1765 – 1776, 2009.

[69] L. Tian, Y. He, Y. Tao, and W. Tao, "A comparative study on the air-side performance of wavy fin-and-tube heat exchanger with punched delta winglets in staggered and in-line arrangements," *International Journal of Thermal Sciences*, vol. 48, no. 9, pp. 1765 – 1776, 2009. [Online]. Available: http://www.sciencedirect.com/science/article/pii/S1290072909000234

[70] L. Tian, Y. He, P. Chu, and W. Tao, "Numerical study of flow and heat transfer enhancement by using delta winglets in a triangular wavy fin-and-tube heat exchanger," *Journal of heat transfer*, vol. 131, no. 9, 2009.

[71] W. Li, T. A. Khan, W. Tang, and W. Minkowycz, "Numerical study and optimization of corrugation height and angle of attack of vortex generator in the wavy fin-and-tube heat exchanger," *Journal of Heat Transfer*, vol. 140, no. 11, 2018.

[72] H. Ke, T. A. Khan, W. Li, Y. Lin, Z. Ke, H. Zhu, and Z. Zhang, "Thermal-hydraulic performance and optimization of attack angle of delta winglets in plain and wavy finned-tube heat exchangers," *Applied Thermal Engineering*, vol. 150, pp. 1054 – 1065, 2019. [Online]. Available: http://www.sciencedirect.com/science/article/pii/S1359431118319847

[73] M. D. Damavandi, M. Forouzanmehr, and H. Safikhani, "Modeling and pareto based multi-objective optimization of wavy fin-and-elliptical tube heat exchangers using cfd and nsga-ii algorithm," *Applied Thermal Engineering*, vol. 111, pp. 325 – 339, 2017. [Online]. Available: http://www.sciencedirect.com/science/article/pii/S1359431116318191

[74] X. Du, L. Feng, Y. Yang, and L. Yang, "Experimental study on heat transfer enhancement of wavy finned flat tube with longitudinal vortex generators," *Applied Thermal Engineering*, vol. 50, no. 1, pp. 55 – 62, 2013. [Online]. Available: http://www.sciencedirect.com/science/article/pii/S1359431112003870

[75] A. Gholami, M. A. Wahid, and H. Mohammed, "Heat transfer enhancement and pressure drop for fin-and-tube compact heat exchangers with wavy rectangular winglet-type vortex generators," *International Communications in Heat and Mass Transfer*, vol. 54, pp. 132 – 140, 2014. [Online]. Available: http://www.sciencedirect.com/science/article/pii/S0735193314000566

[76] J.-S. Leu, M.-S. Liu, J.-S. Liaw, and C.-C. Wang, "A numerical investigation of louvered fin-and-tube heat exchangers having circular and oval tube configurations," *International Journal of Heat and Mass Transfer*, vol. 44, no. 22, pp. 4235 – 4243, 2001. [Online]. Available: http://www.sciencedirect.com/science/article/pii/S0017931001000813

[77] Y. Chen, M. Fiebig, and N. Mitra, "Conjugate heat transfer of a finned oval tube with a punched longitudinal vortex generator in form of a delta winglet—parametric investigations of the winglet," *International Journal of Heat and Mass Transfer*, vol. 41, no. 23, pp. 3961 – 3978, 1998.

[78] B. Delač, A. Trp, and K. Lenić, "Numerical investigation of heat transfer enhancement in a fin and tube heat exchanger using vortex generators," *International Journal of Heat and Mass Transfer*, vol. 78, pp. 662 – 669, 2014. [Online]. Available: http://www.sciencedirect.com/science/article/pii/S0017931014006164

[79] Y. Chen, M. Fiebig, and N. Mitra, "Heat transfer enhancement of finned oval tubes with staggered punched longitudinal vortex generators," *International Journal of Heat and Mass Transfer*, vol. 43, no. 3, pp. 417 – 435, 2000. [Online]. Available: http://www.sciencedirect.com/science/article/pii/S001793109900157X

[80] Y. Wang, L.-C. Wang, Z.-M. Lin, Y.-H. Yao, and L.-B. Wang, "The condition requiring conjugate numerical method in study of heat transfer characteristics of tube bank fin heat exchanger," *International Journal of Heat and Mass Transfer*, vol. 55, no. 9, pp. 2353 – 2364, 2012. [Online]. Available: http://www.sciencedirect.com/science/article/pii/S0017931012000415

[81] S. Tsai and T. W. Sheu, "Some physical insights into a two-row finned-tube heat transfer," *Computers & Fluids*, vol. 27, no. 1, pp. 29 – 46, 1998. [Online]. Available: http://www.sciencedirect.com/science/article/pii/S004579309700025X

[82] P. Chu, Y. He, Y. Lei, L. Tian, and R. Li, "Three-dimensional numerical study on fin-and-oval-tube heat exchanger with longitudinal vortex generators," *Applied Thermal Engineering*, vol. 29, no. 5, pp. 859 – 876, 2009. [Online]. Available: http://www.sciencedirect.com/science/article/pii/S1359431108002032

[83] V. Malapure, S. K. Mitra, and A. Bhattacharya, "Numerical investigation of fluid flow and heat transfer over louvered fins in compact heat exchanger," *International Journal of Thermal Sciences*, vol. 46, no. 2, pp. 199 – 211, 2007. [Online]. Available: http://www.sciencedirect.com/science/article/pii/S1290072906000688

[84] S. Tsai, T. Sheu, and S. Lee, "Heat transfer in a conjugate heat exchanger with a wavy fin surface," *International Journal of Heat and Mass Transfer*, vol. 42, no. 10, pp. 1735 – 1745, 1999. [Online]. Available: http://www.sciencedirect.com/science/article/pii/S0017931098002920

[85] T. Perrotin and D. Clodic, "Thermal-hydraulic cfd study in louvered fin-and-flat-tube heat exchangers," *International Journal of Refrigeration*, vol. 27, no. 4, pp. 422 – 432, 2004. [Online]. Available: http://www.sciencedirect.com/science/article/pii/S0140700703001749

[86] A. Fluent, "Ansys fluent theory guide," *ANSYS Inc., USA*, vol. 15317, pp. 724–746, 2011.

[87] FOAM-extend, "Foam-extend." [Online]. Available: http://foam-extend.org/

[88] A. Forrester, A. Sobester, and A. Keane, *Engineering design via surrogate modelling: a practical guide*. John Wiley & Sons, 2008.

[89] C.-C. Wang, "Investigation of wavy fin-and-tube heat exchangers: a contribution to databank," *Experimental Heat Transfer*, vol. 12, no. 1, pp. 73–89, 1999.

[90] C.-C. Wang, Y.-M. Tsai, and D.-C. Lu, "Comprehensive study of convex-louver and wavy fin-and-tube heat exchangers," *Journal of Thermophysics and Heat transfer*, vol. 12, no. 3, pp. 423–430, 1998.

[91] C.-C. Wang, J.-Y. Chang, and N.-F. Chiou, "Effects of waffle height on the air-side performance of wavy fin-and-tube heat exchangers," *Heat Transfer Engineering*, vol. 20, no. 3, pp. 45–56, 1999.

[92] C. Wang, J.-Y. Jang, and N. Chiou, "A heat transfer and friction correlation for wavy fin-and-tube heat exchangers," *International Journal of Heat and Mass Transfer*, vol. 42, no. 10, pp. 1919–1924, 1999.

[93] C.-C. Wang, C.-J. Lee, C.-T. Chang, and Y.-J. Chang, "Some aspects of plate fin-and-tube heat exchangers: with and without louvers," *Journal of Enhanced Heat Transfer*, vol. 6, no. 5, 1999.

[94] D. G. Rich, "The effect of fin spacing on the heat transfer and friction performance of multi-row, smooth plate fin-and-tube heat exchangers," *AsHRAE Trans*, vol. 79, no. 2, pp. 135–145, 1973.

[95] D. G. Rich, *The effect of the number of tube rows on heat transfer performance of smooth plate fin-and-tube heat exchangers*. Pascal and Francis, 1975.

[96] B. Raja, V. Patel, and R. Jhala, "Thermal design and optimization of fin-and-tube heat exchanger using heat transfer search algorithm," *Thermal Science and Engineering Progress*, vol. 4, pp. 45–57, 2017.

[97] B. Shi, L. Wang, F. Gen, and Y. Zhang, "The optimal fin spacing for three-row flat tube bank fin mounted with vortex generators," *Heat and mass transfer*, vol. 43, no. 1, pp. 91–101, 2006.

[98] H. Tennekes and J. L. Lumley, *A first course in turbulence*. MIT press, 1972.

[99] L. Davidson, *Fluid mechanics, turbulent flow and turbulence modeling*. Division of Fluid Dynamics, Chalmers University of Technology, 2015.

[100] K. Stone, "Review of literature on heat transfer enhancement in compact heat exchangers," Air Conditioning and Refrigeration Center. College of Engineering ..., Tech. Rep., 1996.

[101] D. Bouris and G. Bergeles, "Numerical calculation of the effect of deposit formation on heat-exchanger efficiency," *International Journal of Heat and Mass Transfer*, vol. 40, no. 17, pp. 4073 – 4084, 1997.

[102] H. Han, Y.-L. He, W.-Q. Tao, and Y.-S. Li, "A parameter study of tube bundle heat exchangers for fouling rate reduction," *International Journal of Heat and Mass Transfer*, vol. 72, pp. 210 – 221, 2014.

[103] F.-L. Wang, Y.-L. He, S.-Z. Tang, and Z.-X. Tong, "Parameter study on the fouling characteristics of the h-type finned tube heat exchangers," *International Journal of Heat and Mass Transfer*, vol. 112, no. Supplement C, pp. 367 – 378, 2017.

[104] Y. Wang and G. Tang, "Numerical investigation on the coupling of ash deposition and acid vapor condensation on the h-type fin tube bank," *Applied Thermal Engineering*, vol. 139, pp. 524 – 534, 2018.

[105] A. Leppänen, H. Tran, R. Taipale, E. Välimäki, and A. Oksanen, "Numerical modeling of fine particle and deposit formation in a recovery boiler," *Fuel*, vol. 129, pp. 45–53, 2014.

[106] J. S. Marshall and S. Li, *Adhesive particle flow*. Cambridge University Press, 2014.

[107] S. Kaiser, D. Antonijevic, and E. Tsotsas, "Formation of fouling layers on a heat exchanger element exposed to warm, humid and solid loaded air streams," *Experimental Thermal and Fluid Science*, vol. 26, no. 2, pp. 291 – 297, 2002.

[108] Y.-C. Ahn, J.-M. Cho, H.-S. Shin, Y.-J. Hwang, C.-G. Lee, J.-K. Lee, H.-U. Lee, and T.-W. Kang, "An experimental study of the air-side particulate fouling in fin-and-tube heat exchangers of air conditioners," *Korean Journal of Chemical Engineering*, vol. 20, no. 5, pp. 873–877, 2003.

[109] S.-Z. Tang, Y.-L. He, F.-L. Wang, and Y.-B. Tao, "Parametric study on fouling mechanism and heat transfer characteristics of tube bundle heat exchangers for reducing fouling considering the deposition and removal mechanisms," *Fuel*, vol. 211, pp. 301 – 311, 2018.

[110] D. Kern and R. Seaton, "A theoretical analysis of thermal surface fouling," *British Chemical Engineering*, vol. 4, no. 5, pp. 258–262, 1959.

[111] Y. Pan, F. Si, Z. Xu, and C. E. Romero, "An integrated theoretical fouling model for convective heating surfaces in coal-fired boilers," *Powder Technology*, vol. 210, no. 2, pp. 150 – 156, 2011.

[112] F. Zhan, J. Tang, G. Ding, and D. Zhuang, "Experimental investigation on particle deposition characteristics of wavy fin-and-tube heat exchangers," *Applied Thermal Engineering*, vol. 99, pp. 1039 – 1047, 2016.

[113] F. Zhan, D. Zhuang, G. Ding, P. Ju, and J. Tang, "Influence of wet-particle deposition on air-side heat transfer and pressure drop of fin-and-tube heat exchangers," *International Journal of Heat and Mass Transfer*, vol. 124, pp. 1230 – 1244, 2018.

[114] C. Zhang, Z. Tang, Z. Zhang, J. Shi, J. Chen, and M. Zhang, "Impact of airside fouling on microchannel heat exchangers," *Applied Thermal Engineering*, vol. 128, no. Supplement C, pp. 42 – 50, 2018.

[115] L. Yang, J. E. Braun, and E. A. Groll, "The impact of fouling on the performance of filter–evaporator combinations," *International Journal of Refrigeration*, vol. 30, no. 3, pp. 489 – 498, 2007.

[116] I. H. Bell, E. A. Groll, and H. König, "Experimental analysis of the effects of particulate fouling on heat exchanger heat transfer and air-side pressure drop for a hybrid dry cooler," *Heat Transfer Engineering*, vol. 32, no. 3-4, pp. 264–271, 2011.

[117] J. A. Siegel and W. W. Nazaroff, "Predicting particle deposition on hvac heat exchangers," *Atmospheric Environment*, vol. 37, no. 39, pp. 5587 – 5596, 2003, indoor Air Chemistry and Physics: Papers from Indoor Air 2002.

[118] P. Hugenholtz and J. A. Fuerst, "Heterotrophic bacteria in an air-handling system." *Applied and environmental microbiology*, vol. 58, no. 12, pp. 3914–3920, 1992.

[119] P. Morey, "Microorganisms in buildings and hvac systems: A summary of 21 environmental studies," *ASHRAE IAQ'88*, pp. 10–24, 1988.

[120] S. T. Kuruneru, E. Sauret, S. C. Saha, and Y. Gu, "Coupled cfd-dem simulation of oscillatory particle-laden fluid flow through a porous metal foam heat exchanger: Mitigation of particulate fouling," *Chemical Engineering Science*, vol. 179, pp. 32 – 52, 2018.

[121] F. Zhan, D. Zhuang, G. Ding, and J. Tang, "Numerical model of particle deposition on fin surface of heat exchanger," *International Journal of Refrigeration*, vol. 72, pp. 27 – 40, 2016.

[122] E. Sauret and K. Hooman, "Particle size distribution effects on preferential deposition areas in metal foam wrapped tube bundle," *International Journal of Heat and Mass Transfer*, vol. 79, pp. 905 – 915, 2014.

[123] S. T. Kuruneru, E. Sauret, S. C. Saha, and Y. T. Gu, "A coupled finite volume & discrete element method to examine particulate foulant transport in metal foam heat exchangers," *International Journal of Heat and Mass Transfer*, vol. 115, pp. 43 – 61, 2017.

[124] S. Kuruneru, S. Saha, E. Sauret, and Y. Gu, "Transient heat transfer and non-isothermal particle-laden gas flows through porous metal foams of differing structure," *Applied Thermal Engineering*, vol. 150, pp. 888 – 903, 2019. [Online]. Available: http://www.sciencedirect.com/science/article/pii/S1359431118345307

[125] F. Qian, N. Huang, J. Lu, and Y. Han, "Cfd–dem simulation of the filtration performance for fibrous media based on the mimic structure," *Computers & Chemical Engineering*, vol. 71, pp. 478 – 488, 2014.

[126] A. K. Maddineni, D. Das, and R. M. Damodaran, "Air-borne particle capture by fibrous filter media under collision effect: A cfd-based approach," *Separation and Purification Technology*, vol. 193, pp. 1 – 10, 2018.

[127] R. Tao, M.-m. Yang, and S.-q. Li, "Filtration of micro-particles within multi-fiber arrays by adhesive dem-cfd simulation," *Journal of Zhejiang University-SCIENCE A*, vol. 19, no. 1, pp. 34–44, 2018.

[128] R. Romero-Méndez, M. Sen, K. Yang, and R. McClain, "Effect of fin spacing on convection in a plate fin and tube heat exchanger," *International Journal of Heat and Mass Transfer*, vol. 43, no. 1, pp. 39 – 51, 2000. [Online]. Available: http://www.sciencedirect.com/science/article/pii/S0017931099001209

[129] B. Sahin, N. A. Ozturk, and C. Gurlek, "Horseshoe vortex studies in the passage of a model plate-fin-and-tube heat exchanger," *International Journal of Heat and Fluid Flow*, vol. 29, no. 1, pp. 340 – 351, 2008. [Online]. Available: http://www.sciencedirect.com/science/article/pii/S0142727X07000860

[130] R. Goldstein and H. Cho, "A review of mass transfer measurements using naphthalene sublimation," *Experimental Thermal and Fluid Science*, vol. 10, no. 4, pp. 416 – 434, 1995, experimental methods in Thermal and Fluid Science. [Online]. Available: http://www.sciencedirect.com/science/article/pii/089417779400071F

[131] A. G. Kravchenko and P. Moin, "Numerical studies of flow over a circular cylinder at re d= 3900," *Physics of fluids*, vol. 12, no. 2, pp. 403–417, 2000.

[132] M. H. Chaudhry, *Open-channel flow*. Springer Science & Business Media, 2007.

[133] W. M. Kays, *Convective heat and mass transfer*. Tata McGraw-Hill Education, 2012.

[134] W. Yaïci, M. Ghorab, and E. Entchev, "3d cfd study of the effect of inlet air flow maldistribution on plate-fin-tube heat exchanger design and thermal–hydraulic performance," *International Journal of Heat and Mass Transfer*, vol. 101, pp. 527 – 541, 2016. [Online]. Available: http://www.sciencedirect.com/science/article/pii/S0017931016303544

[135] S. Ryuichi *et al.*, "Turbulence model-free approach for predictions of air flow dynamics and heat transfer in a fin-and-tube exchanger," *Energy conversion and management*, 2017.

[136] F. M. White, "Fluid mechanics, 1999," *Google Scholar*, pp. 367–375, 1979.

[137] H. Tennekes, J. L. Lumley, J. Lumley *et al.*, *A first course in turbulence*. MIT press, 1972.

[138] L. Davidson, "Fluid mechanics, turbulent flow and turbulence modeling," 2015.

[139] T. J. Välikangas, *Simulation method development for Fin-and-Tube Heat Exchanger with Open-source software*. Chalmers University / Tampere University of Technology, 2015.

[140] A. V. Hirtum, B. Wu, H. Gao, and X. Luo, "Constricted channel flow with different cross-section shapes," *European Journal of Mechanics - B/Fluids*, vol. 63, pp. 1 – 8, 2017. [Online]. Available: http://www.sciencedirect.com/science/article/pii/S0997754615303241

[141] M. Mirzaei, A. Sohankar, L. Davidson, and F. Innings, "Large eddy simulation of the flow and heat transfer in a half-corrugated channel with various wave amplitudes," *International Journal of Heat and Mass Transfer*, vol. 76, pp. 432 – 446, 2014.

[142] B. O. Community, "Blender – a 3d modelling and rendering package." [Online]. Available: http://www.blender.org

[143] A. Gaither, "An efficient block detection algorithm for structured grid generation," in *Pro ceedings of the 5th international conference on numerical grid generation in computa tional field simulations, held at Mississippi State University*, 1996, pp. 443–450.

[144] Swiftblock, "Swiftblock," 2020. [Online]. Available: https://swiftblock.readthedocs.io/

[145] T. O. Foundation, "The openfoam documentation," 2019. [Online]. Available: https://openfoam.org/

[146] T. Välikangas, "Conjugate heat transfer in openfoam," *Proceedings of CFD with OpenSource Software Edited by Nilsson H.*, 2015. [Online]. Available: http://dx.doi.org/10.17196/OS_CFD#YEAR_2015

[147] W. C.-C., C. Y.-J., H. Y.-C., and Y.-T. Lin, "Sensible heat and friction characteristics of plate fin-and-tube heat exchangers having plane fins," *International Journal of Refrigeration*, vol. 19, no. 4, pp. 223 – 230, 1996.

[148] C.-C. Wang, Y.-T. Lin, and C.-J. Lee, "Heat and momentum transfer for compact louvered fin-and-tube heat exchangers in wet conditions," *International Journal of Heat and Mass Transfer*, vol. 43, no. 18, pp. 3443 – 3452, 2000. [Online]. Available: http://www.sciencedirect.com/science/article/pii/S0017931099003750

[149] L. Tang, M. Zeng, and Q. Wang, "Experimental and numerical investigation on air-side performance of fin-and-tube heat exchangers with various fin patterns," *Experimental Thermal and Fluid Science*, vol. 33, no. 5, pp. 818 – 827, 2009. [Online]. Available: http://www.sciencedirect.com/science/article/pii/S0894177709000387

[150] C.-C. Wang, Y.-M. Hwang, and Y.-T. Lin, "Empirical correlations for heat transfer and flow friction characteristics of herringbone wavy fin-and-tube heat exchangers," *International Journal of Refrigeration*, vol. 25, no. 5, pp. 673 – 680, 2002. [Online]. Available: http://www.sciencedirect.com/science/article/pii/S0140700701000494

[151] Y. Tao, Y. He, J. Huang, Z. Wu, and W. Tao, "Three-dimensional numerical study of wavy fin-and-tube heat exchangers and field synergy principle analysis," *International Journal of Heat and Mass Transfer*, vol. 50, no. 5, pp. 1163 – 1175, 2007. [Online]. Available: http://www.sciencedirect.com/science/article/pii/S0017931006002298

[152] D. Junqi, C. Jiangping, C. Zhijiu, Z. Yimin, and Z. Wenfeng, "Heat transfer and pressure drop correlations for the wavy fin and flat tube heat exchangers," *Applied Thermal Engineering*, vol. 27, no. 11, pp. 2066 – 2073, 2007. [Online]. Available: http://www.sciencedirect.com/science/article/pii/S1359431106004121

[153] J. Dong, J. Chen, Z. Chen, W. Zhang, and Y. Zhou, "Heat transfer and pressure drop correlations for the multi-louvered fin compact heat exchangers," *Energy Conversion and Management*, vol. 48, no. 5, pp. 1506 – 1515, 2007. [Online]. Available: http://www.sciencedirect.com/science/article/pii/S0196890406003608

[154] W. M. Kays and A. L. London, *Compact heat exchangers*. McGraw-Hill, New York, NY, 1984.

[155] D. Taler and P. Ocłoń, "Thermal contact resistance in plate fin-and-tube heat exchangers, determined by experimental data and cfd simulations," *International Journal of Thermal Sciences*, vol. 84, pp. 309 – 322, 2014. [Online]. Available: http://www.sciencedirect.com/science/article/pii/S1290072914001513

[156] D. Taler and P. Ocłoń, "Determination of heat transfer formulas for gas flow in fin-and-tube heat exchanger with oval tubes using {CFD} simulations," *Chemical Engineering and Processing: Process Intensification*, vol. 83, pp. 1 – 11, 2014.

[157] J. Dong, L. Su, Q. Chen, and W. Xu, "Experimental study on thermal–hydraulic performance of a wavy fin-and-flat tube aluminum heat exchanger," *Applied Thermal Engineering*, vol. 51, no. 1, pp. 32 – 39, 2013. [Online]. Available: http://www.sciencedirect.com/science/article/pii/S1359431112006308

[158] C.-C. Wang, W.-H. Tao, and C.-J. Chang, "An investigation of the airside performance of the slit fin-and-tube heat exchangers," *International Journal of Refrigeration*, vol. 22, no. 8, pp. 595 – 603, 1999. [Online]. Available: http://www.sciencedirect.com/science/article/pii/S0140700799000316

[159] R. Webb, "Externally finned tubes, principles of enhanced heat transfer," 1994.

[160] G. C., *Transport processes and separation process principles (includes unit operations)*. Prentice Hall Press, 2003.

[161] R. K. Shah and A. L. London, *Flow Forced Convection Heat Transfer and Flow Friction in Straight and Curved Ducts - A Summary of Analytical Solutions*, ser. 1. Academic Press, 1972, no. 1.

[162] J. Doo, M. Ha, J. Min, R. Stieger, A. Rolt, and C. Son, "An investigation of cross-corrugated heat exchanger primary surfaces for advanced intercooled-cycle aero engines (part-i: Novel geometry of primary surface)," *International Journal of Heat and Mass Transfer*, vol. 55, no. 19, pp. 5256 – 5267, 2012. [Online]. Available: http://www.sciencedirect.com/science/article/pii/S0017931012003559

[163] W. M. Kays and A. L. London, *Compact heat exchangers*. McGraw-Hill New York, 1958, vol. 196.

[164] A. London and C. Ferguson, "Test results of high-performance heat exchanger surfaces used in aircraft intercoolers and their significance for gas-turbine regenerator design," *Trans. ASME*, vol. 71, pp. 17–26, 1949.

[165] T. Cowell, "A general method for the comparison of compact heat transfer surfaces," -, 1990.

[166] J.-Y. Yun and K.-S. Lee, "Influence of design parameters on the heat transfer and flow friction characteristics of the heat exchanger with slit fins," *International Journal of Heat and Mass Transfer*, vol. 43, no. 14, pp. 2529 – 2539, 2000.

[167] B. Dahneke, "The influence of flattening on the adhesion of particles," *Journal of Colloid and Interface Science*, vol. 40, no. 1, pp. 1 – 13, 1972.

[168] L. Rogers and J. Reed, "The adhesion of particles undergoing an elastic-plastic impact with a surface," *Journal of Physics D: Applied Physics*, vol. 17, no. 4, p. 677, 1984.

[169] S. Wall, W. John, H.-C. Wang, and S. L. Goren, "Measurements of kinetic energy loss for particles impacting surfaces," *Aerosol Science and Technology*, vol. 12, no. 4, pp. 926 – 946, 1990.

[170] B. Dahneke, "Measurements of bouncing of small latex spheres," *Journal of Colloid and Interface Science*, vol. 45, no. 3, pp. 584 – 590, 1973.

[171] S. Li, J. S. Marshall, G. Liu, and Q. Yao, "Adhesive particulate flow: The discrete-element method and its application in energy and environmental engineering," *Progress in Energy and Combustion Science*, vol. 37, no. 6, pp. 633 – 668, 2011.

[172] J. Hærvig, U. Kleinhans, C. Wieland, H. Spliethoff, A. Jensen, K. Sørensen, and T. Condra, "On the adhesive jkr contact and rolling models for reduced particle stiffness discrete element simulations," *Powder Technology*, vol. 319, pp. 472 – 482, 2017.

[173] W. C. Hinds, *Aerosol technology: properties, behavior, and measurement of airborne particles*. John Wiley & Sons, 2012.

[174] P. A. Cundall and O. D. Strack, "A discrete numerical model for granular assemblies," *geotechnique*, vol. 29, no. 1, pp. 47 – 65, 1979.

[175] S. Benyahia, M. Syamlal, and T. J. O'Brien, "Extension of hill – koch – ladd drag correlation over all ranges of reynolds number and solids volume fraction," *Powder Technology*, vol. 162, no. 2, pp. 166 – 174, 2006.

[176] R. J. Hill, D. L. Koch, and A. J. Ladd, "The first effects of fluid inertia on flows in ordered and random arrays of spheres," *Journal of Fluid Mechanics*, vol. 448, pp. 213 – 241, 2001.

[177] D. L. Koch and R. J. Hill, "Inertial effects in suspension and porous-media flows," *Annual Review of Fluid Mechanics*, vol. 33, no. 1, pp. 619 – 647, 2001.

[178] H. Hamaker, "The london—van der waals attraction between spherical particles," *physica*, vol. 4, no. 10, pp. 1058 – 1072, 1937.

[179] K. L. Johnson, K. Kendall, and A. Roberts, "Surface energy and the contact of elastic solids," *Proc. R. Soc. Lond. A*, vol. 324, no. 1558, pp. 301 – 313, 1971.

[180] D. Tabor, "Surface forces and surface interactions," in *Plenary and Invited Lectures*. Elsevier, 1977, pp. 3 – 14.

[181] J. N. Israelachvili, *Intermolecular and surface forces*. Academic press, 2011.

[182] E. J. Parteli, J. Schmidt, C. Blümel, K.-E. Wirth, W. Peukert, and T. Pöschel, "Attractive particle interaction forces and packing density of fine glass powders," *Scientific reports*, vol. 4, p. 6227, 2014.

[183] X. Deng, J. V. Scicolone, and R. N. Davé, "Discrete element method simulation of cohesive particles mixing under magnetically assisted impaction," *Powder Technology*, vol. 243, pp. 96 – 109, 2013. [Online]. Available: http://www.sciencedirect.com/science/article/pii/S0032591013002416

[184] J. Hærvig, K. Sørensen, and T. Condra, "Early stages of agglomeration of adhesive particles in fully-developed turbulent pipe flows," *International Journal of Multiphase Flow*, vol. 106, pp. 254 – 267, 2018. [Online]. Available: http://www.sciencedirect.com/science/article/pii/S0301932217307036

[185] A. G. Konstandopoulos, "Particle sticking/rebound criteria at oblique impact," *Journal of Aerosol Science*, vol. 37, no. 3, pp. 292 – 305, 2006.

[186] C. Goniva, C. Kloss, N. G. Deen, J. A. Kuipers, and S. Pirker, "Influence of rolling friction on single spout fluidized bed simulation," *Particuology*, vol. 10, no. 5, pp. 582–591, 2012.

[187] C. Kloss, C. Goniva, A. Hager, S. Amberger, and S. Pirker, "Models, algorithms and validation for opensource dem and cfd–dem," *Progress in Computational Fluid Dynamics, an International Journal*, vol. 12, no. 2-3, pp. 140–152, 2012.

[188] S. Plimpton, "Fast parallel algorithms for short-range molecular dynamics," *Journal of Computational Physics*, vol. 117, no. 1, pp. 1 – 19, 1995. [Online]. Available: http://www.sciencedirect.com/science/article/pii/S002199918571039X

[189] H. Kuuluvainen, A. Arffman, A. Järvinen, J. Harra, and J. Keskinen, "The effect of materials and obliquity of the impact on the critical velocity of rebound," *Aerosol Science and Technology*, vol. 51, no. 3, pp. 301–310, 2017.

[190] H.-C. Wang and W. John, "Dynamic contact charge transfer considering plastic deformation," *Journal of aerosol science*, vol. 19, no. 4, pp. 399–411, 1988.

[191] T. D'Ottavio and S. L. Goren, "Aerosol capture in granular beds in the impaction dominated regime," *Aerosol Science and Technology*, vol. 2, no. 2, pp. 91–108, 1982.

[192] Y.-S. Cheng and H.-C. Yeh, "Particle bounce in cascade impactors." *Environmental Science & Technology*, vol. 13, no. 11, pp. 1392–1396, 1979.

[193] N. A. Esmen, P. Ziegler, and R. Whitfield, "The adhesion of particles upon impaction," *Journal of Aerosol Science*, vol. 9, no. 6, pp. 547–556, 1978.

[194] Karl-Johan Nogenmyr, "Swiftblock," 2012. [Online]. Available: https://openfoamwiki.net/index.php/Contrib/SwiftBlock

[195] Mikko Folkersma, "Swiftblock," 2016. [Online]. Available: https://github.com/flowkersma/swiftBlock

Appendix

Appendix

SwiftBlock - A walk-through to the features

In this section an introduction to the features of the meshing tool called SwiftBlock developed by Karl-Johan Nogenmyr [194] is given. The section is divided into three segments. First the original features that Nogenmyr created are illustrated and explained. Then in the second section the new features and improvements developed by Mikko Folkersma [195] are laid out. The third part will consist of the usability feature, most importantly a boundary flag system that allows the user to define boundary layer cell size and expansion ratio as well as the max cell size in the domain globally. In the third part the parametric feature of the meshing tool is introduced briefly as well. SwiftBlock [194] is a graphical user interface for blockMesh, a meshing tool integrated in the OpenFOAM package [145]. It is an addon in the Blender software that is an open source 3D creation suite developed by the Blender Foundation [142].

Karl-Johan Nogenmyr has created the original version of SwiftBlock. He started the development in 2011, and the first public release came in April 2012. The latest version from Nogenmyr is from February 2015. In this section the original features of the program are explained because this has not been done in any published articles in the authors knowledge. In CFD, the boundary conditions for the calculated equations are inserted in the faces of the cells. In SwiftBlock, these boundary patches can be inserted straight through the user interface with the Patch settings platform. In Fig. 1a the Patch settings is shown and for an example the left side of the cube is set to wall, front into patch and upper side of the box is set so symmetryPlane. These are some of the most used boundary conditions in OpenFOAM. The two faces of the cube that are not shown in the figure are not pointed into any patch so they will be automatically put into defaultName group. If the user requires to have a hole in the mesh, it is possible by disabling blocks that will not be meshed by blockMesh. This will be illustrated in Fig. 1b, where first a block is selected from the middle of the blocking, then these points are assigned in the same group with *Block's name settings* tool. Then when the mesh is created, blockMesh will not make cells in this block.

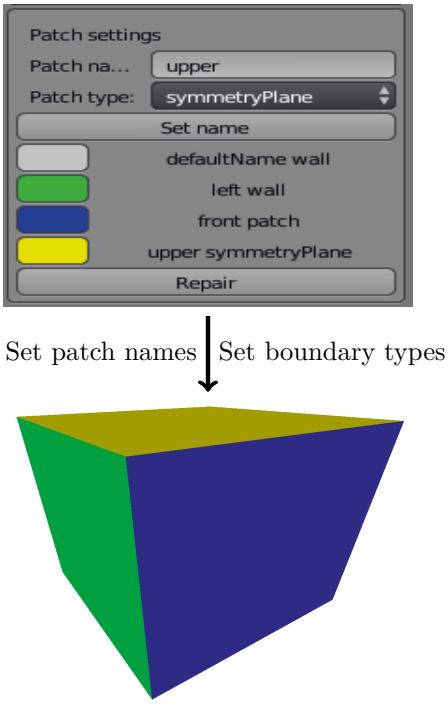

(a) Illustration of the patch definition system

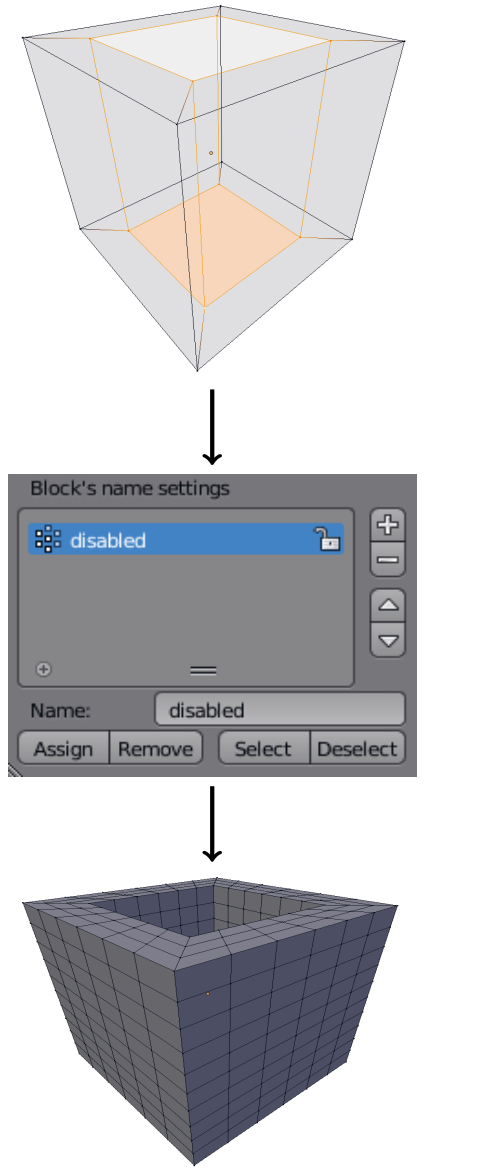

(b) Illustration of the disabled-block feature

Figure 1: Illustration of the patch definition and disabled-block feature

In Fig. 2a is an illustration how the edges of the block can be made to follow any kind of polyline created with Blender. With the OpenFOAM version 2.4.x, the blockMesh tool got a new *multigrading* feature, which allows one edge to have grading rules in multiple direction [145]. This saves the user for the effort of creating multiple blocks with different single grading per edge, but now the user can specify two different gradings for both ends of the edge. In Fig. 2b, the basic idea of specifying gradings for both ends of one edge with the first cell size $dx = 0.05$ and the expansion ratio $exp = 1.3$ is illustrated. This means that in this example the size of the cell will be 1.3 times larger for every cell from

the end or start of the edge until it reaches the maximum cell size max $dx = 1$.

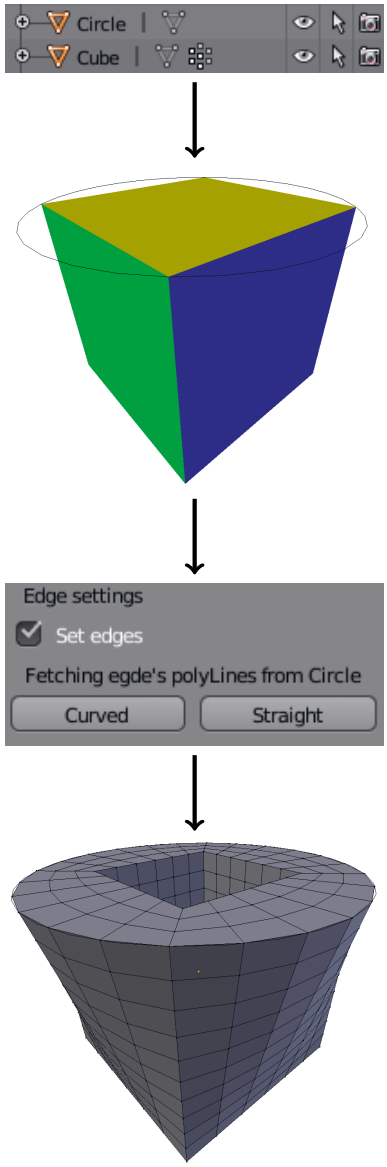

(a) Illustration of the snapping feature

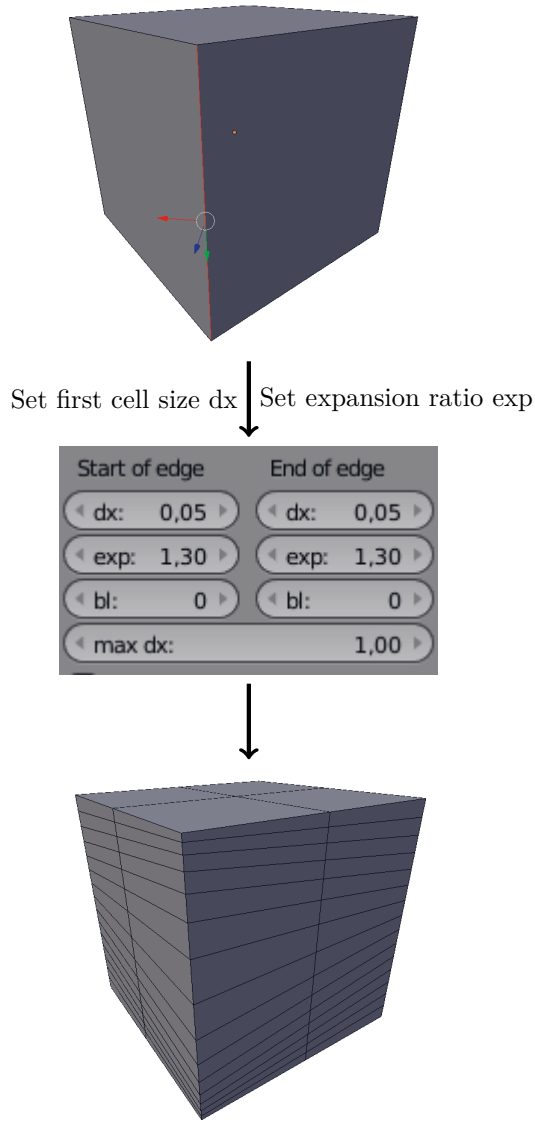

(b) Illustration of the edge settings

Figure 2: Illustration of the snapping and the multigrading feature

To illustrate how the edge is oriented in Blender, the user should press **space** → **type & select *select orientation*** → **then select *Normal***.

Another very important feature developed by Mikko Folkersma is the block alignment algorithm. It is a very useful tool to align all the edges of the blocks to the same direction which makes defining boundary layer rules for parallel blocks much easier. In figure 3a an

illustration of the alignment of non-aligned edges is shown. The first feature that was developed by the author is a simple button to control the maximum cell size in all edges of the blocking. This feature is illustrated in figure 3b. The figure shows two examples of what happens to the cell structure when the global maximum cell size is limited in two different cases. On the left the maximum is set to $dx = 1$ and on the right the $dx = 0.2$.

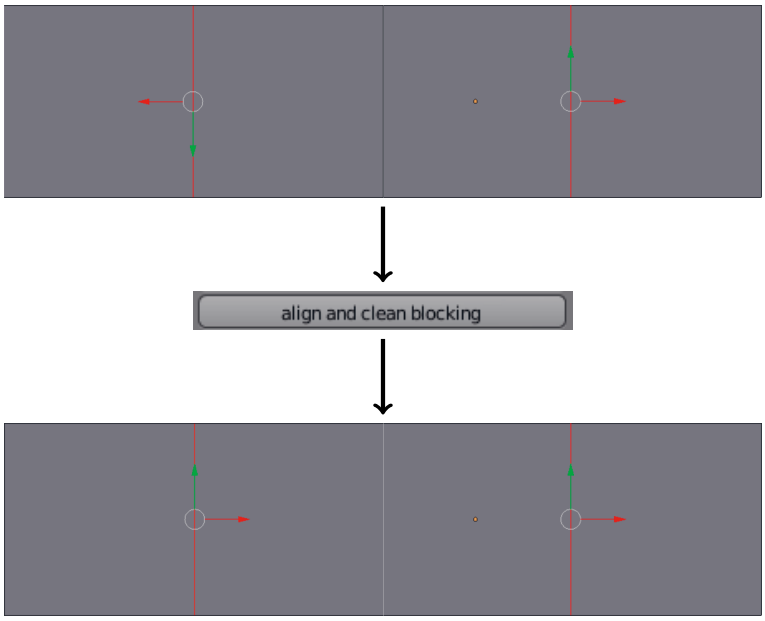

(a) Illustration of the block alignment feature

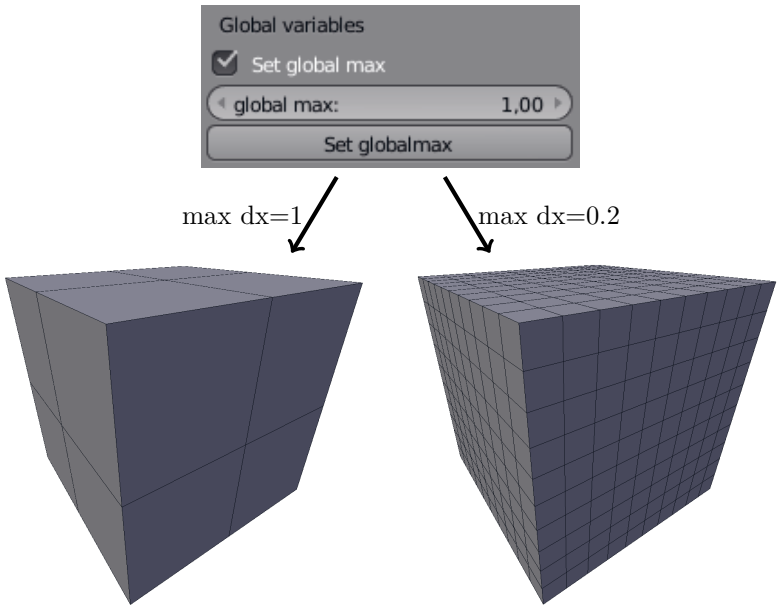

(b) Illustration of the global max feature

Figure 3: Illustration of the block alignment and the global maximum feature

The second feature called the *boundary layer flags* introduces a new entity *bl* that can be defined for every edge in the blocking. Every edge has two corresponding ends, start and end of the edge, and both of these ends can be defined with four different values for *bl*.

- $bl = 1$ means that this edge is part of the type 1 group which can be globally changed from the interface.

- $bl = 2$ means that this edge is part of the type 2 group which can be globally changed from the interface.

- $bl = 3$ means that the global boundary layer system or the global max cell size rules do not apply to neither ends of the edge.

- $bl = 0$ (or any other than the previously explained) means that global boundary layer system does not affect the dx or exp of the edge but the maximum cell size can be changed from the interface.

In Fig. 4 the boundary layer flag system is illustrated. First the edges are selected, then *bl* values are changed for desired boundary layer structures.

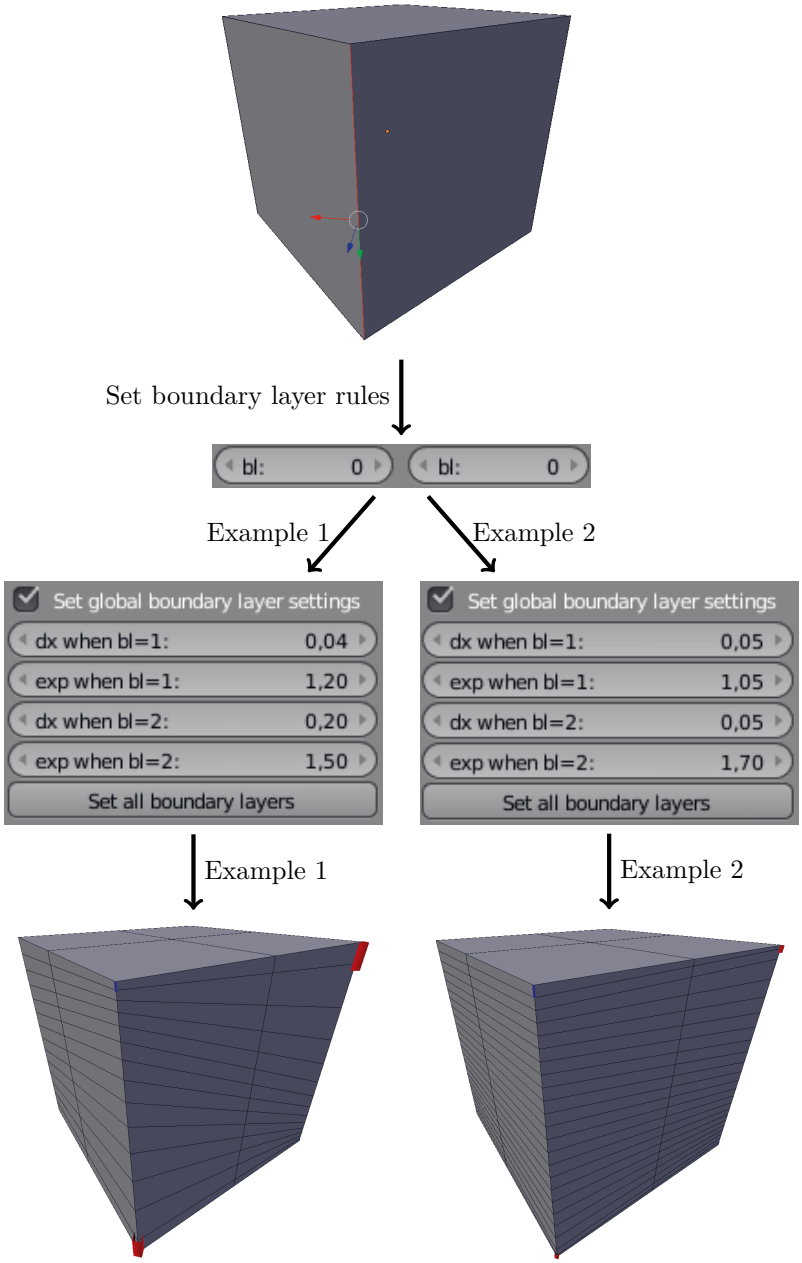

Figure 4: Illustration of the boundary layer flag system

On the bottom of the figure 4, two different examples of boundary layer flags are shown, the other one on the right shows a case where the $dx = 0.05$ on both type 1 and 2, but the expansion ratio is different. In the figure the $bl = 1$ is shown with a blue and $bl = 2$ with a red flag. The height of the flag indicates the first cell size in the final mesh.

Finally the most important feature developed by the author is the parametric features of

the meshing tool. An illustration of the blockMeshDict is shown below, where the values x, y, z, zz can be changed arbitrarily.

```
FoamFile
{
    version     2.0;
    format      ascii;
    class       dictionary;
    object      blockMeshDict;
}
// * * * * * * * * * * * * * * * * * * * * * * * * * * * * * * * * * * * * * * * * //
x 2.0;
y -4.50;
z 1.0;
zz 0;

convertToMeters 0.001;

vertices #codeStream
{
    codeInclude
    #{
       #include "vectorField.H"
    #};
    code
    #{
       double x = readScalar(dict.lookup("x"));
       double y = readScalar(dict.lookup("y"));
       double z = readScalar(dict.lookup("z"));
       double zz = readScalar(dict.lookup("zz"));
       vectorField v(306);
       #include "/PATH_TO/verticesFile.H"
     #};
};
```

These values are then compiled in to the file as the utility blockMesh is used. Example of the verticesFile is given below.

```
v[0] = vector(4.0*x + 112.0 , -1.0*y + 0 , 0.0*z + 1.0*zz + 0.1  );
v[1] = vector(4.0*x + 112.0 , -1.0*y + 0 , 1.0*z + -1.0*zz + 3.4  );
v[2] = vector(1.5*x + 42 , -1.0*y + -0.006, 1.0*z + -1.0*zz + 3.4  );
v[3] = vector(1.5*x + 42 , -1.0*y + -0.006, 0.0*z + 1.0*zz + 0.1  );
v[4] = vector(0.7*x + 23 , -1.0*y + -0 , 1.0*z + -1.0*zz + 3.4  );
```

The parametric meshing feature of Swiftblock was fully utilized in constructing the computational meshes for Publication III, where multiple different designs are created from one blocking strategy.

During the last years, Tuomo Keskitalo has done major modifications and improvements to the structure of the code and created an improved documentation for SwiftBlock [144]. Mikko Folkersma has also made some informative videos about the usage of SwiftBlock to Youtube that can be found by searching the word "SwiftBlock".

Publications

Publication I

Välikangas T. and Karvinen R. (2017). Conjugated heat transfer simulation of a fin-and-tube heat exchanger. *Heat Transfer Engineering*, vol. 39, no. 13-14, pp. 1192-2000, DOI: 10.1080/01457632.2017.1363628

Conjugated heat transfer simulation of a fin-and-tube heat exchanger

Turo Välikangas[1], Reijo Karvinen[1]

[1]Tampere University of Technology, Tampere, Finland

Address correspondence to Turo Välikangas, Tampere University of Technology, Korkeakoulunkatu 10, 33720 Tampere, Finland. E-mail: turo.valikangas@tut.fi
Phone Number: (+358) 456704201

ABSTRACT

Heat transfer and pressure drop of a fin-and-tube heat exchanger are studied by taking into account the conjugated heat transfer between the flow and the fin. The temperature distribution of the fin is calculated in respect to the convective heat transfer of the air flowing through the tube bank channel. Contemporary enhancement methods emphasize the importance of local turbulence augmentation which effects the convective heat transfer. In this paper, the importance of conjugated heat transfer, where the temperature of the flow and fin are coupled together is emphasized and compared with a constant surface temperature boundary condition simulation and experiment, which are found in the literature.

INTRODUCTION

The fin-and-tube heat exchangers (FTHE) shown schematically in Figure 1 are widely used in air conditioning. In FTHEs, heat is transferred between the fluid flowing in the tubes and the air flowing in the channels between the fins and they are a popular choice with Air Handling Unit manufacturers because of their flexible design and relatively straightforward manufacturing process.

The ideal FTHE is one in which the pressure drop, volume and material consumption are low but the heat transfer rate is high. This presents a multi-objective problem because of the competing criteria. The hydro-thermal performance of the fin-and-tube heat exchanger is affected by geometrical parameters, such as the tube diameters and their locations, as well as the pitch and thickness of the fins [1]. Because most of the heat transfer resistance, (over 60 % [2][3]), is on the air side, understanding the air flow structures is essential. Finned-tubes increase the heat transfer by 60-90 % [4] over smooth tubes, so although finned tubes are more expensive, their use is justified in cases where the extra weight of the heat exchanger is not harmful to its utilization for the application in question, such as it would be in a jet-fighter intercooler [5], for example.

The most important aspect of optimizing FTHEs is to decide on which optimization criteria are of interest. Different results are achieved depending on whether the design is optimized in respect to manufacturing costs, operational costs or if the goal is to maximize heat transfer [6]. One essential criterion is the space that the heat exchanger must fit into, which means that the volume goodness factor needs to be optimized [4].

The enhancement methods for FTHEs can be divided into three generations. The first generation concentrated on the merging of herringbone [7] and sine-wave [8] fin shapes. The main idea of these shapes is to create transversal vortices in the flow field, so that the air flow

is forced to zig-zag through the channels. The second generation concentrated on making compact FTHEs. In order to make the heat exchangers smaller, a set of slits [9] or louvered [10] fins are used to create chaotic turbulence on the air side. However, although these slits enhance the heat-transfer coefficient on the air side, they do so at the expense of creating an almost proportionally equivalent increase in the pressure drop. The third generation concentrated on thermal flow management strategies [6]. Thermal management of the flow inside FTHEs, especially in the wake behind the tubes, means that the goal of the enhancement is to create the required turbulence only where it is needed. Two contemporary methods have used longitudinal vortex generators [11] accompanied by oval tubes [12]. It has been conclusively proven that longitudinal vortices, as illustrated in Figure 2, create higher hydro-thermal enhancement than transverse vortices with the same pressure drop [13].

Given a specific inlet flow velocity, the optimal shape and location of the vortex generator (VG) can be defined. The best overall performance results have been achieved with delta winglets [14] at a 45% angle of attack [15]. For one type of vortex generator, the heat transfer augmentation progresses asymptotically to a maximum point, after which the heat transfer cannot be enhanced any further. Thereafter, changing the attack angle does not affect the heat transfer but only results in an increase in the pressure drop [6]. Up-wash delta winglet pairs seem to offer the best hydro-thermal efficiency [6].

Whatever type of VG is used, the most important thing is to create the right-sized longitudinal vortex in the right place, thus achieving the optimum local heat transfer coefficient with the minimum pressure drop.

Oval tubes have distinct advantages over round ones. Experiments have proved that they provide 50 % higher heat transfer augmentation with the same pressure drop as round tubes [16]. Oval tubes have also been studied in combination with first- and second-generation enhancement methods. In these studies, sine-wave [17] and louvered fins [18] have given very

good results, for example. One big advantage that oval tubes have over circular ones is that in the absence of competitive design criteria, they always reduce pressure drop and increase heat transfer regardless of the operating conditions [17].

The average heat-transfer coefficient of a heat exchanger is obtained from integrating the local heat transfer over the heat transfer area. The overall performance of the exchanger can be experimentally measured with minimum effort simply by measuring only the input and output variables. However, measuring the local heat-transfer coefficient is not so simple, and is almost impossible in real conditions. This means that the cause and effect relationships between the various augmentation strategies are difficult to pinpoint. Recent experimental methods for the study of local heat transfer have utilized infrared cameras combined with the heated-thin-foil technique (constant heat flux boundary condition) [19], the naphthalene sublimation technique [20] and the lumped capacitance method [21].

The theoretical method is to generate numerical models of both the fluid flows and the heat transfer. If the flow is laminar, then the importance of the fin temperature distribution on the convective heat transfer must be considered. When comparing different thermal augmentation methods by experimental or numerical means, it is essential to take account of the conjugated heat transfer from the fluid in the tubes to the air flowing through the channel. The conduction in the fin and the convection are coupled together because the local heat-transfer rate is highly dependent on the fin surface temperature. This is especially true for the enhancement method called slit fins [22], where a piece of fin is erected from the surface to create turbulence on the air side. In Figure 3 a typical arrangement calculated by the authors of the present paper is shown.

When the material of the fin itself is used to create the slits or louvers, for example by punching or pressing shapes out of the fin, it disturbs the heat conduction path from the fluid in the tubes to the erected slit. This is because when the slit is erected, it creates an air gap

which acts as insulation. Therefore, the overall conductive heat transfer resistance in the fin is increased. Thus the slits can also decrease the overall heat-transfer rate of the fin. This fact has been largely ignored in the papers published in this field, especially in heating, ventilation and air conditioning applications. Usually, only flue-gas FTHE simulations have considered the temperature variation, due to the greater temperature difference between the air and the fluid [26].

An open source c++ library called Open Field Operation And Manipulation (OpenFOAM) [24] has been utilized for this paper to solve the fin temperature field and the flow field in the channel between the fins. OpenFOAM was chosen because of its computational transparency, it is easily modifiable, object-oriented implementation, and its accompanying computational capabilities. All the solvers, boundary conditions, thermal-property libraries and discretization methods etc. can be changed, and their implementation can be modified at will. This gives the required control over whichever CFD-solver is used, but at the same time, its object-oriented programming makes the implementation easy to understand. OpenFOAM is also highly parallelizable without the need for any high-performance computing licenses.

A solver called conjugate heat transfer multi region simple foam (chtMultiRegionSimpleFoam) [25] was used to study the effect of the temperature distribution on the local convective heat transfer. ChtMultiRegionSimpleFoam is a conjugated solid-fluid heat transfer solver with an unlimited number of fluid or solid regions. A compressible solver with the energy equation and buoyancy term is selected for the air side, while only a solver for the temperature was needed on the fin side. Due to the small temperature differences between the studied mediums, the effect of buoyancy is negligible and therefore the effect of gravity can be neglected. With chtMultiRegionSimpleFoam, the coupling of different regions can be done with a mappedWall boundary condition, which means that the values from the master side

are mapped to the slave side, and different thermophysical properties can be applied for each region individually. The mesh in the coupling region does not have to be conformal when interpolative mapping is used between the regions. The coupling between fins and fluid, i.e. conjugated heat transfer, has been dealt in papers when the fin thickness is reasonable [26][27]. If the fin thickness is very small as in our case, the treatment of convection –conduction coupling gives extra difficulties at least in optimization cases [28].

VARIABLES IN RESULTS

Heat transfer can be divided into three different modes: conduction, convection, and radiation. Only the first two are considered in this paper because of the low temperature levels in fin-and-tube heat exchangers. The characteristic length scale used in the Reynolds number in the paper is based on an approximation developed for FTHE simulations in refs. [29] and [30]. The characteristic length is calculated by the ratio of four times the free flow volume divided by the wetted area:(see Figure 1 for the definitions of the variables).

$$D_h = \frac{4V_0}{A_t} = \frac{4(F_p - t)(P_t - D_c)P_l}{2\left(P_l P_t - \frac{\pi D_c^2}{4}\right) + \pi D_c\left(F_p - t\right)} \tag{1}$$

where F_p, t, P_t, P_l and D_c are the fin pitch, the thickness of the fin, the transverse distance of the tubes, the longitudinal distance of the tubes and the outside diameter of the collar around the tubes, respectively.

The Reynolds number is defined as:

$$Re_{D_h} = \frac{u_{max} D_h}{\nu} \tag{2}$$

where u_{max} is the mean velocity in a minimum cross-sectional flow area and ν is the kinematic viscosity of air.

The amount of heat that is transferred from a surface to the flowing medium can be described with a local heat transfer coefficient, defined as:

$$\alpha_{x,y,z} = \frac{q_{x,y,z}}{\Delta T} \tag{3}$$

where $q_{x,y,z}$ is the local heat flux and ΔT, the local temperature difference between the surface and the flow. When studying the overall performance of the fin-tube channel, a set of non-dimensional variables are defined. The temperature difference between the bulk air and the fin is defined with a logarithmic mean temperature difference:

$$\Delta T_{lm} = \frac{(T_{in} - T_w) - (T_{out} - T_w)}{\ln[(T_{in} - T_w)/(T_{out} - T_w)]} \tag{4}$$

where the T_{in}, T_{out} and T_w are the temperatures of the air at the inlet, the air at the outlet, and the temperature of the tube wall, respectively. The overall average heat transfer coefficient in the case of an FTHE is calculated as follows:

$$\bar{\alpha} = \frac{Q}{A_t \Delta T_{lm}} \tag{5}$$

Where $Q = \dot{m} C_p (T_{in} - T_{out})$ is the overall transferred heat, A_t is the heat transfer area, $\dot{m}$ is the mass flow rate, C_p is the specific heat capacity, and T_{in} and T_{out} are the mass flow averaged temperature of the air of the inlet and outlet, respectively.

Finally, the non-dimensional Colburn j-factor of the heat exchanger is defined [30]:

$$j = \frac{\bar{\alpha}}{\rho u_{max} C_p} Pr^{2/3} \tag{6}$$

where $Pr = \frac{\nu}{\alpha_f}$ is the Prandtl number, which is defined as the kinematic viscosity ν divided with the thermal diffusivity $\alpha_f = \frac{\lambda_f}{\rho C_p}$, ρ is the density of the fluid, λ_f is the thermal conductivity of the fluid and u_{max} is the mean velocity in the minimum cross-sectional flow area. A constant value of $Pr = 0.7$ and

$C_p = 1005 \frac{kj}{kgK}$ was used for the Prandtl number and the specific heat of the air, respectively. For the viscosity of the air, an approximation of Sutherland's law was used.

The non-dimensional pressure drop in the flow channel is expressed with the Fanning friction factor according to [29][31]:

$$f = \frac{\Delta p}{\frac{1}{2}\rho u_{max}^2} \frac{A_c}{A_t} \tag{7}$$

where A_c is the minimum cross-sectional area, which can be calculated as follows:

$$A_c = (F_p - t)(min\left(P_t, \sqrt{{P_l}^2 + \left(\frac{P_t}{2}\right)^2}\right) - D_c) \tag{8}$$

This means that the minimum cross-sectional flow area can be found between transversal tubes or between the diagonal distance of two corresponding tubes in staggered rows depending on the transverse P_t, and longitudinal distance, P_l, of the tubes.

The maximum velocity u_{max} can then be calculated according to the continuity equation from the face velocity by multiplying the face velocity U with the ratio of face area to the minimum flow area as follows:

$$u_{max} = \frac{A}{A_c} U = \frac{P_t F_p}{A_c} U \tag{9}$$

COMPUTATIONAL MODEL

The computational model of convective heat transfer simulations with a constant temperature boundary condition is illustrated in ref. [32]. The geometry of the fin shape is shown in Figure 1. The dimensions used in the simulations for the plain fin geometry are given in Table 1. In the present study, the simulation includes the first two tube rows, shown in Figure 4 and Figure 1. Figure 4 also shows the boundary conditions used in the OpenFOAM simulations and they are also tabulated in Table 2.

Cyclic Arbitrary Mesh Interface (CyclicAMI) is an interpolative periodic boundary condition and symmetryPlane is a symmetry boundary condition. A constant value of 100kPa was used for the pressure at the outlet, and a zero gradient boundary condition for the inlet. The computation model of the fin only has the solver for the temperature field. The interface between the air and the fin is interpolated with an OpenFOAM mappedWall boundary condition. This means that after the solver loop for the air side is finished, the temperature values are mapped to the fin side, after which the temperature distribution of the fin is solved. The inner diameters of the tubes have a constant temperature boundary condition and the rest of the model is set as insulated.

The conduction in the fin and the convection in the channel are coupled, which is why they need to be calculated simultaneously. If we assume that the temperature is of a thin fin as shown in Figure 5 is constant across the fin, the equation that governs its temperature distribution in other dimensions is:

$$\lambda t\left(\frac{\partial^2 T}{\partial x^2}+\frac{\partial^2 T}{\partial y^2}\right)+q(x,y)=0 \tag{10}$$

where λ is the heat conductivity of the fin material, t the fin thickness and $q_{(x,y)}$ the convection heat flux. In this paper, the heat conductivity of the aluminum alloy, $\lambda = 220$ $W.m^{-1}.K^{-1}$, is used.

The inlet temperature of the air was 278K and the constant temperature of the inner side of the tube was set to 333K.

The turbulence model used in this paper is the $k-\omega$ SST model which has been proven to give good overall results with fin-and-tube simulations [33]. A second order upwind scheme was used for the velocity and enthalpy field, and a first order upwind scheme was used for the turbulence quantities.

Grid independence test:

A grid independence test was done for the air-side mesh. Four different meshes were tested to see how much the results changed when the mesh density was increased and to see what density is required for mesh-independent results. The meshing strategies for all the meshes were identical, so only the density of the mesh was changed. The mesh was created with a Blender [34] add-on called Swiftblock, which is an open-source meshing program created by Nogenmyr & Folkersma [35]. It is based on Blender, which is a 3D creation suite software that provides a graphical interface for creating the blocking structures in three dimensions, as shown in Figure 6. The mesh is then created according to these blocks with blockMesh, a novel meshing tool integrated into OpenFOAM.

The time consuming part in a structured mesh creation is to develop a good blocking strategy. The blocks define the alignment of the cells inside the mesh. Structured meshing strategy enables the user to define explicitly which directions the density of the mesh is increased. Hexahedral cells are optimal for heat transfer simulations because the mesh density can be increased only in the direction of the highest temperature and velocity gradient, which is the direction of the surface normal.

The results of these simulations are shown in in Table 3, where the flow-averaged temperature of air at the channel outlet is shown for each of the 4 different mesh sizes. The values in Table 3 are the percentage differences from the finest mesh, which had 2.9 million cells.

We can see that the mesh with 7×10^5 cells gives a result that differs only 1.9% from the results with the mesh that has 29×10^5 cells. This means that the density of the mesh is fine enough to resolve the turbulence scales that contribute the most to the heat transfer process. With the finest mesh, no new turbulence scales needed to be resolved, and therefore the results are same as for the 7×10^5 mesh. This mesh can be used for all the simulations. The fin mesh with 252000 tetrahedral elements was created with Salome open source CAD software [36].

RESULTS AND DISCUSSION

Before the era of computational fluid dynamics, fin-and-tube heat exchanger research and development was based on analytical equations which were based on measurements. Results were reasonably correct for plain geometries but fail to predict subsequent boundary layer formations. Measurements, on the other hand, give results about the overall characteristics of the heat exchanger when the average temperatures and pressures of the inlet and outlet flows are measured, but give no information about the flow structures and heat transfer mechanisms. This leads to obscure cause and effect relationships between the design variables and the results of the measurements. CFD offers a way to simulate what are the most important heat transfer mechanisms that affect the characteristics of the heat exchanger. Next we look at the heat transfer and pressure drop characteristics of both the conjugated model and only the convective heat transfer simulation and see how they compare against measurements found from the literature.

Heat transfer and pressure drop comparison

The j-factor of the constant temperature simulation and the conjugated heat transfer is shown in Figure 7 [32], with experimental results from Wang et al. [31] for the same geometry with similar boundary conditions. We can see that the constant temperature overpredicts heat transfer, whereas the conjugated model predicts heat transfer quite well.

This is mainly because of unrealistically high temperature levels of the fin with the constant temperature boundary condition. When the coupling between convection and conduction is taken into account, the results are seen to be much more realistic. If we look at the pressure drop characteristics in the form of the Fanning friction factor in Figure 8 [32], we see that the pressure drop decreases slightly compared to the constant temperature simulation and agrees quite well with the experiments.

The reason for the smaller decrease in the pressure drop could be the lower value of air density as it flows through the channel. For example, with the highest velocity at the Reynolds number 7000, the temperature of the outlet air with a constant temperature boundary condition is 304K, whereas

for the conjugated heat transfer model it was 295K, the corresponding densities being 1.196 kg.m^{-3} and 1.16 kg.m^{-3}, respectively. This means that when the density decreases, the velocity increases and creates more pressure drop. The difference in densities have an effect on the turbulence levels in RANS equations. The result errors of the conjugated simulation are 68 and 39 percent smaller than the constant temperature simulation for heat transfer and pressure drop, respectively.

Heat flux, temperature and velocity distributions

Figure 9 [32] shows the heat flux distribution on the fin surface using a constant surface-temperature model. The effect of the primary and secondary horseshoe vortices can be seen next to the tubes with the Reynolds number 7000, as has been observed in previous experimental studies [20]. These swirling longitudinal vortices have been reported to increase heat transfer in the vicinity of the tubes [18].

The results of both the wall heat flux distributions are scaled to the result of the conjugated simulation model in order to give a clear visual illustration of their significance. In the constant-temperature simulation there was no negative heat flux because the fin is always at a higher temperature than the moving fluid. However, if we look at the wall heat flux of the conjugated heat transfer model in Figure 10, with the same Reynolds number of 7000, we can see that the primary horseshoe vortices next to the tubes are visible, but the secondary vortices are much smaller. The secondary vortex is most likely equal in size in the flow field in both cases, but because the temperature is closer to the fluid temperature, the heat transfer between these two mediums is shown as lower in the conjugated model.

Figure 11 shows the temperature distribution on the fin surface of the conjugated heat transfer model.

The greatest effect of the more realistic temperature distribution of the conjugated heat transfer can be seen around the air inlet area. If we compare the constant temperature model to the conjugated heat-transfer model and the heat flux levels at the entrance, we notice that the maximum heat flux is 3 times higher in the constant temperature simulation. This difference occurs because, in the

conjugated heat transfer simulation, the temperature of the fin is dependent on the conductive heat transfer rate in the fin and the convective heat transfer rate from the fin to the air. The higher the convective heat transfer rate is in comparison to the conductive heat transfer rate, the closer the temperature of the fin is to the air. The heat flux is very small behind the tubes in Figure 10, even though the temperature of the fin is relatively high, as can be seen in Figure 11. This is because of the low velocity in the wake of the tubes, as can be seen in Figure 12.

The above observations can be said to be the reason for the more realistic and better agreement with respect to the available experimental data for the heat transfer and pressure drop characteristics. Therefore, this emphasizes the importance of using conjugated heat transfer simulations when studying different enhancement methods for FTHEs numerically.

CONCLUSIONS

In the study, it has been shown by numerical simulation with the OpenFoam code that the treatment of fin heat transfer affects the performance of fin-and-tube heat exchangers (FTHE). The easiest way is to assume a constant temperature fin, which is correct if fin heat conductivity and thickness are large. However, often in practical applications this is not true, because fins are very thin in order to minimize material consumption as in our case. In addition, the pressure drop should be small.

If there is no coupling between the fin and fluid temperature distribution, both heat transfer and pressure drop are higher than few experimental values in the literature [31]. The results of our conjugated heat-transfer simulations correlate with experimental results much more closely than the ones with an isothermal fin. The main reason for this closer agreement in the plain fin geometry simulation is the lower heat flux rate both at the entrance and in the vicinity of the secondary vortex around the tubes. Especially, near the fin leading edge the fin temperature is much lower than in the neighborhood of the tube reducing heat flux as compared to an isothermal fin. The present study clearly shows that the errors for heat transfer and pressure drop in the conjugated simulation are, respectively, around 70 and 40 percent less than they are for the constant temperature simulation.

In the present study, the meshing of the flow medium has been done in a structured manner with hexahedral cell mesh by using tools called Swiftblock and blockMesh. Structured meshing strategy enables the user to define explicitly which directions the density of the mesh should be increased and therefore saves computational costs. Hexahedral cells are optimal for heat transfer simulations because the mesh density can be increased only in the direction of the highest temperature and velocity gradient, which is the direction of the surface normal. This meshing strategy enables the authors to parametrize different design variables in the blocking strategy of the meshing process. This is something that enables a fast and automated meshing when changing the design and is therefore used for a heat transfer optimization process in the future work.

Experimental data of local heat transfer coefficients needed to validate the simulations but experiments are not easy to perform. As to optimization, when heat transfer rate should be large and pressure drop and mass small, the coupling of flow convection and conduction requires special attention. Present solution methods in commercial computer codes are not are not suitable for multi-objective optimization.

ACKNOWLEDGEMENTS

The authors greatly acknowledge the financial support of Koja Oy and the computational resources provided by the Tampere University of Technology.

NOMENCLATURE

A	Local heat transfer area, m^2
A_t	Overall heat transfer area on the fin, m^2
A_c	Minimum cross-sectional area, m^2
C_p	Specific heat capacity, $J.kg^{-1}.K^{-1}$
D_c	tube collar diameter after expansion, m
D_h	hydraulic diameter, m
F_p	Fin pitch, m
f	Fanning friction factor, dimensionless
j	Chilton and Coburn j-factor, dimensionless
$\dot{m}$	Mass flow rate, $kg.s^{-1}$
n	Normal to the surface, dimensionless
Pr	Prandtl number, dimensionless
P_l	Longitudinal tube distance, m
P_t	Transverse tube distance, m
Q	Overall heat transferred to the air, W
$q_{x,y,z}$	Local heat flux, $W.m^{-2}$
Re_{D_h}	Reynolds number according to the corresponding hydraulic diameter, dimensionless
t	Fin thickness, m

T	Temperature, K
U	Face velocity, the average air velocity approaching the face of the tube bank, $m.s^{-1}$
u,v,w	Velocities in the orthogonal coordinate system, $m.s^{-1}$
u_{max}	Mean velocity in the minimum cross-sectional flow area, $m.s^{-1}$
V_0	Free flow volume, m^3
x,y,z	Location in the orthogonal coordinate system, m

Greek Symbols

$\alpha_{x,y,z}$	Local heat transfer coefficient, $W.m^{-2}.K^{-1}$
$\bar{\alpha}$	Average heat transfer coefficient, $W.m^{-2}.K^{-1}$
α_f	Thermal diffusivity of the fluid, $m^2.s^{-1}$
λ	Thermal conductivity, $W.m^{-1}.K^{-1}$
ν	Kinematic viscosity, $kg.m^{-1}.s^{-1}$
ρ	Density, $kg.m^{-3}$
ΔT	Temperature difference, K
Δp	Pressure difference, Pa

Subscripts

f	fluid
lm	logarithmic mean
i	index notation to sum over x,y and z
in	inlet temperature

out	outlet temperature
w	wall temperature
s	solid

Superscripts

$\bar{}$	average data

REFERENCES

[1] Cobian-Iñiguezand J., Wu A., Dugastand F., and Pacheco-Vega A., Numerically-based parametric analysis of plain fin and tube compact heat exchangers, *Applied Thermal Engineering*, vol. 86, pp. 1-13, 2015.

[2] Jeong J., Nyung C.K., and Youn B., A study on the thermal contact conductance in fin–tube heat exchangers with 7 mm tube, *Int. J. of Heat and Mass Transfer*, vol. 49, no. 7-8, pp. 1547-1555, 2006.

[3] Wang C.-C., Webb R.L., and Chi K.-Y., Data reduction for air-side performance of fin-and-tube heat exchangers, Experimental Thermal and Fluid Science ,vol. 21, no. 4, pp. 218-226, 2000.

[4] Kumar A., Joshi J. B., Nayak A. K., and Vijayan P. K., 3D CFD simulations of air cooled condenser-iii: Thermal–hydraulic characteristics and design optimization under forced convection conditions, *Int. J. of Heat and Mass Transfer*, vol. 93, pp. 1227-1247, 2016.

[5] Xin Z. and Grönstedt T., Aero engine intercooling optimization using a variable flow path, in: *Proceedings of the 22nd International Symposium on Air Breathing Engines*, Phoenix, United States of America, 2015.

[6] Arora A., Subbarao P.M.V., and Agarwal R.S. , Development of parametric space for the vortex generator location for improving thermal compactness of an existing inline fin and tube heat exchanger, *Applied Thermal Engineering,* vol. 98, pp. 727-742*,* 2016.

[7] Wang C.-C., Hwang Y.-M., and Lin Y.-T., Empirical correlations for heat transfer and flow friction characteristics of herringbone wavy fin-and-tube heat exchangers, *Int. J. Refrigeration*, vol. 25, no. 5 pp. 673-680, 2002.

[8] Choi B.-N., Yi F., Sim H.-M., and Kim N.-H., Air-side performance of fin-and- tube heat exchangers having sine wave fins and oval tubes,
Korean J. of Air-Conditioning and Refrigeration Engineering, vol. 25, no. 5, pp. 279-288, 2013.

[9] Wang C.-C., Tao W.-H., and Chang C.-J., An investigation of the airside performance of the slit fin-and-tube heat exchangers, *Int. J. of Refrigeration*, vol. 22, no.8, pp. 595-603, 1999.

[10] Wang C.-C., Chi K.-Y., Chang Y.J., and Chang Y.-P., An experimental study of heat transfer and friction characteristics of typical louver fin-and-tube heat exchangers, *Int. J. of Heat and Mass transfer*, vol. 41, no. 4, pp. 817-822, 1998.

[11] Q.-W., Wang, B., Sundén, Y., Chen, Z., Guo, and P., Stehlík, Selected papers from the 2nd international workshop on heat transfer advances for energy conservation and pollution control, *Heat Transfer Engineering*, vol. 37, no. 3-4, pp. 243-245, 2016.

[12] Webb R. L., Air-side heat transfer in finned tube heat exchangers, *Heat Transfer Engineering*, vol. 1, no. 3, pp. 33-49, 1980.

[13] Fiebig M., Embedded vortices in internal flow: heat transfer and pressure loss enhancement, *Int. J. Heat and Fluid Flow*, vol. 16, no. 5, pp. 376-388, 1995.

[14] Mitra N.K., and Fiebig M., Comparison of wing-type vortex generators for heat transfer enhancement in channel flows*, J. of Heat Transfer*, vol. 116, no. 4, pp. 880-885, 1994.

[15] Li L., Xiaoze D., Yuwen Z., Lijun Y., and Yongping Y., Numerical simulation on flow and heat transfer of fin-and-tube heat exchanger with longitudinal vortex generators, *Int. J. Thermal Sciences*, vol. 92, pp. 85-96, 2015.

[16] Jang J.-Y., and Yang J.-Y., Experimental and 3D numerical analysis of the thermal-hydraulic characteristics of elliptic finned-tube heat exchangers, *Heat Transfer Engineering*, vol. 19, no. 4, pp. 55-67, 1998.

[17] Lotfi B., Zeng M., Sundén B., and Wang Q., Thermo-hydraulic characterization of the smooth wavy fin-and-elliptical tube heat exchangers using new type vortex generators. *Energy Procedia*, vol. 61, pp. 2343-2346, Int. Conf. on Applied Energy, Taipei City, Taiwan, 30.5-2.6.2014.

[18] Tiggelbeck S., Mitra N., and Fiebig M., Flow structure and heat transfer in a channel with multiple longitudinal vortex generators, *Experimental Thermal and Fluid Science*, vol. 5, no. 4, pp. 425-436, 1992.

[19] Astarita T., Cardone G., Carlomagno G.M., and Meola C., A survey on infrared thermography for convective heat transfer measurements, *Optics Laser Technology*, vol. 32, no. 7-8, pp. 593-610, 2000.

[20] Kim J.-Y., and Song, T.H., Microscopic phenomena and macroscopic evaluation of heat transfer from plate fins/circular tube assembly using naphthalene sublimation technique, *Int. J. of Heat and Mass Transfer*, vol. 45, no. 16, pp. 3397-3404, 2002.

[21] Kim Y. Y., Kim K. S., Jeong G. H., and Jeong S., An experimental study on the quantitative interpretation of local convective heat transfer for a plate fin and tube heat exchanger using the lumped capacitance method, *Int. J. of Heat and Mass Transfer*, vol. 49, no. 1-2, pp. 230-239, 2006.

[22] Wu X., Zhang W., Gou Q., Luo Z., and Lu Y., Numerical simulation of heat transfer and fluid flow characteristics of composite fin, *Int. J. of Heat and Mass Transfer*, vol. *75*, pp. 414-424, 2014.

[23] Stanisław Ł., and Paweł O, Numerical study of the effect of fouling on local heat transfer conditions in a high-temperature fin-and-tube heat exchanger, *Energy,* vol. 92, no. 1, pp. 100-116, 2015.

[24] Weller H. G., Tabor G., Jasak H., Fureby C., A tensorial approach to computational continuum mechanics using object-oriented techniques, *Computer in physics*, 1998.

[25] The OpenFOAM Foundation, The OpenFOAM Documentation, 2017

[26] Singh S., Sørensen K., Condra T.J., Influence of the degree of thermal contact in fin and tube heat exchanger: A numerical analysis, *Applied Thermal Engineering*, vol 107, pp 612-624, 2016

[27] Chen H.-T., Lin Y.-S., Chen P.-C. and Chang J.-R., Numerical and experimental study of natural convection heat transfer characteristics for vertical plate fin and tube heat exchangers with various tube diameters, *International Journal of Heat and Mass Transfer*, vol. 100, pp. 320-331, 2016.

[28] Damavandi M.D., Forouzanmehr M. and Safikhani M., Modeling and Pareto based multi-objective optimization of wavy fin-and-elliptical tube heat exchangers using CFD and NSGA-II algorithm, *Applied Thermal Engineering*, vol. 111, pp. 325-339, 2017.

[29] Fornasieri E., and Mattarolo L., Air-side heat transfer and pressure loss in finned tube heat exchangers: state of art, in: *Proceedings of the European Conference on Finned Tube Heat Exchangers,* ITT of Stuttgart University, Stuttgart, Germany, 1991.

[30] Geankoplis C., Transport processes and separation process principles (includes unit operations), *Prentice Hall Press*, New Jersey, 2003.

[31] Wang C.-C., Chang Y.-J., Hsieh Y.-C., and Y.-T. Lin., Sensible heat and friction characteristics of plate fin-and-tube heat exchangers having plane fins., *Int. J. of Refrigeration*, vol. 19, no. 4, pp. 223-230, 1996.

[32] Välikangas T., Simulation method development for fin-and-tube heat exchanger with open source software, *Master's Thesis*, Chalmers University of Technology, Sweden Tampere University of Technology, Finland, 2015.

[33] Hansen A.M., CFD simulation of a fin-and-tube heat exchanger, *Master's Thesis,* Aalborg Universitet, Esbjerg, Denmark, 2008.

[34] Blender Online Community, Blender – a 3D modelling and rendering package, URL http://www.blender.org , 2017

[35] Nogenmyr, K.J., Folkersma, M., Swiftblock, *URL* https:// openfoamwiki.net/index.php/Contrib/SwiftBlock, 2016.

[36] Open Cascade, Salome platform, *URL* http://www.salome-platform.org/, 2016.

Table 1 Fin dimensions

Fin name	Plain
Dimension	(mm)
t	0.13
F_p	2
D_c	13.5
P_l	28.84
P_t	33.3

Table 2 Boundary conditions for the computational domain

Inlet	$u = constant., v = w = 0, T = 278K$
Outlet	$\frac{\partial u_i}{\partial x} = \frac{\partial T}{\partial x} = 0$
Inflow and outflow regions	
Top and bottom	$\frac{\partial u}{\partial z} = \frac{\partial v}{\partial z} = 0, w = 0, \frac{\partial T}{\partial z} = 0$
Left and right	$\frac{\partial u}{\partial y} = \frac{\partial v}{\partial y} = 0, v = 0, \frac{\partial T}{\partial y} = 0$
Fin region	
Top and bottom	$\frac{\partial u}{\partial z} = \frac{\partial v}{\partial y} = 0, w = 0, \frac{\partial T}{\partial z} = 0$
Left and right	Tube inner surface: $u = v = w = 0, T = 333K$
	Fin region: $u = v = w = 0, \frac{\partial T}{\partial y} = 0$
	Fluid region: $\frac{\partial u}{\partial y} = \frac{\partial z}{\partial y} = 0, v = 0, \frac{\partial T}{\partial y} = 0$
Fluid-Solid interface	$T_s = T_f, -\lambda_s \frac{\partial T_s}{\partial n} = -\lambda_f \frac{\partial T_f}{\partial n}$

Table 3 Grid independence study with Re_{D_h}= 7000

Number of cells	Mass flow averaged temperature at outlet	Percentage difference in respect to the finest mesh	Processor hours
	[K]	%	hours
$75*10^3$	284.85	63	15
$350*10^3$	295.07	7.5	357
$700*10^3$	296.10	1.9	731
$2900*10^3$	296.46	0	1752

List of Figure Captions

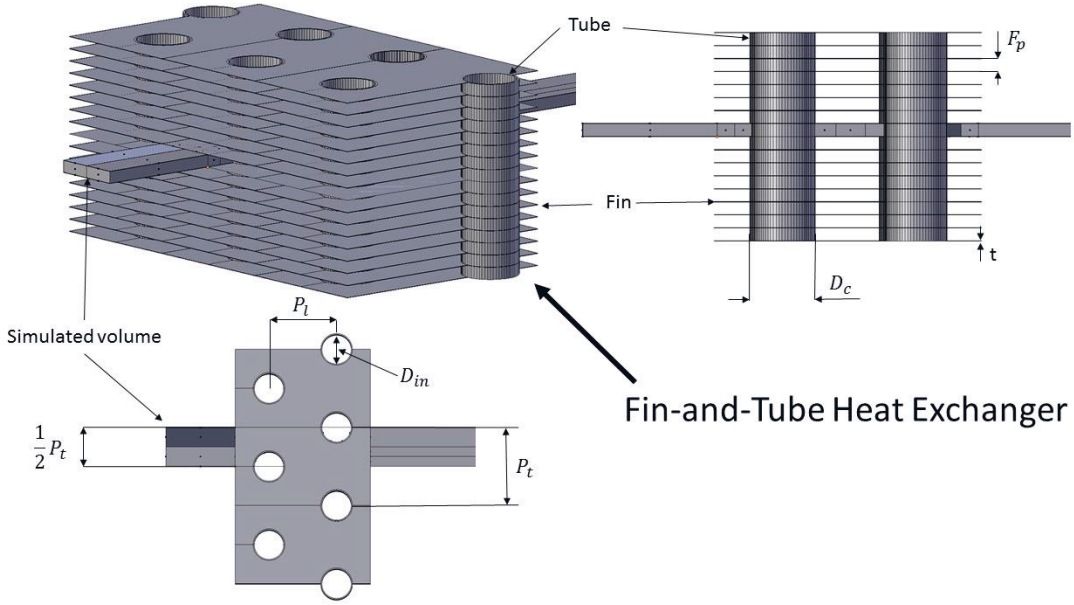

Figure 1 Schematic figure of fin-and-tube heat exchanger

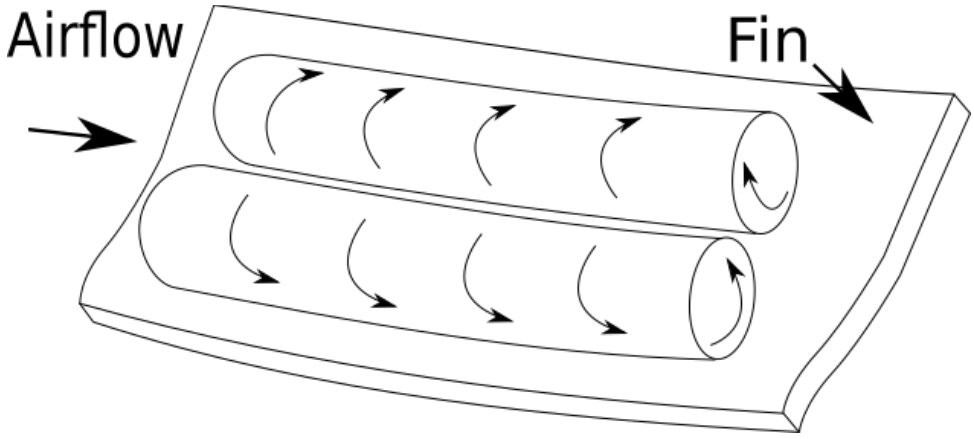

Figure 2 Longitudinal vortices on fin surface

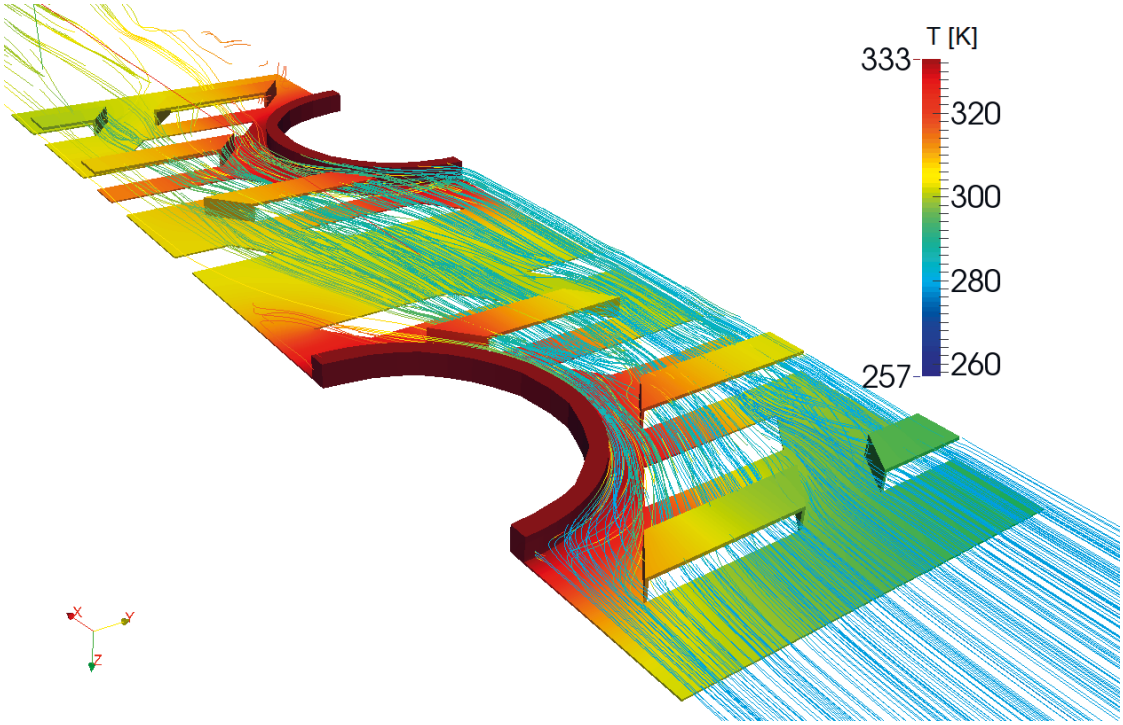

Figure 3 Example of slit fin enhancement method

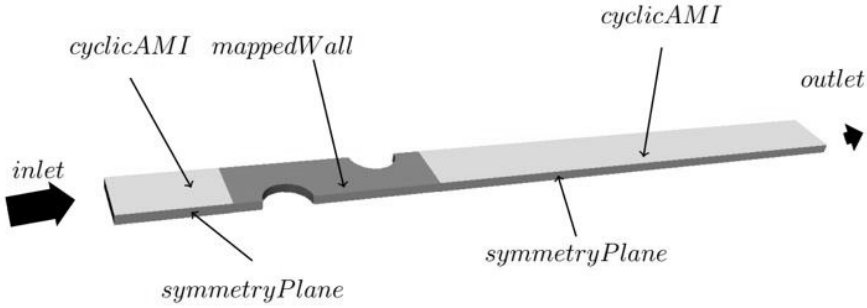

Figure 4 Calculation domain

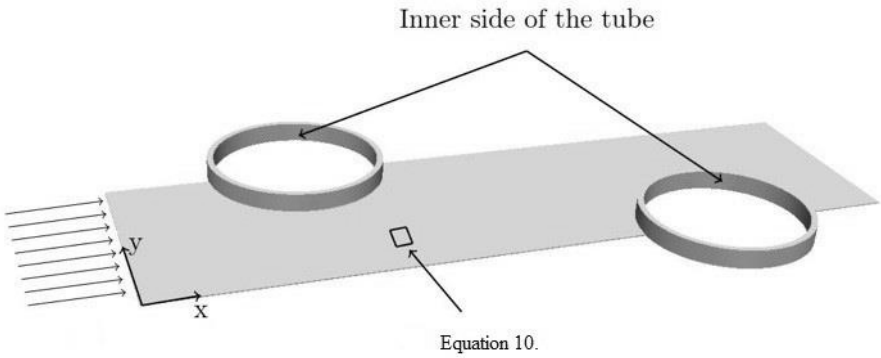

Figure 5 Illustration of the fin and the tubes

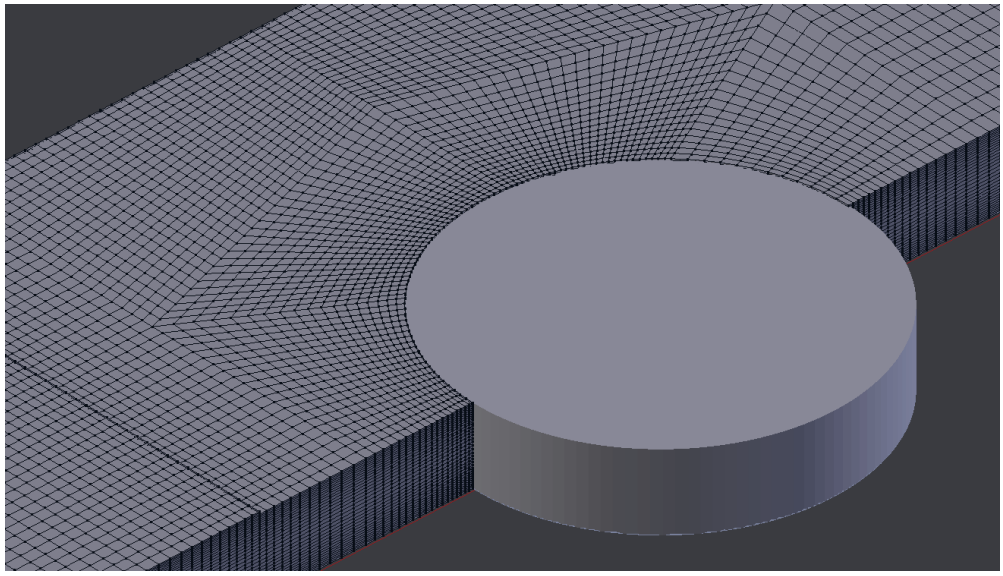

Figure 6 Blocking strategy used for the airside mesh

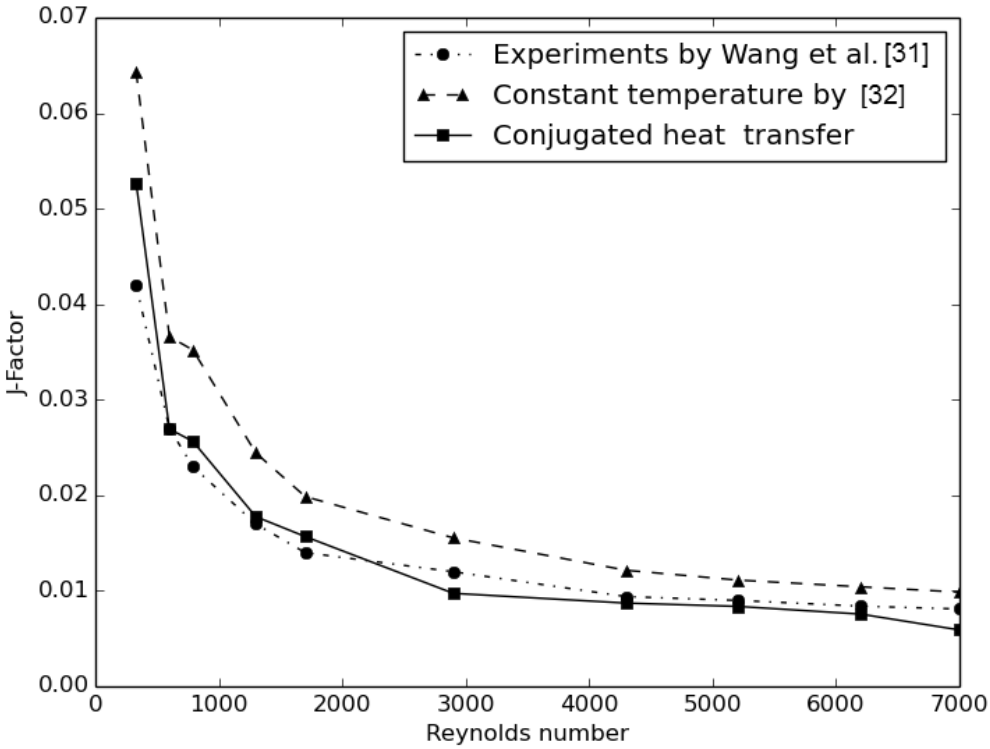

Figure 7 Comparison of j-factor with constant fin temperature, coupled solution and measurements

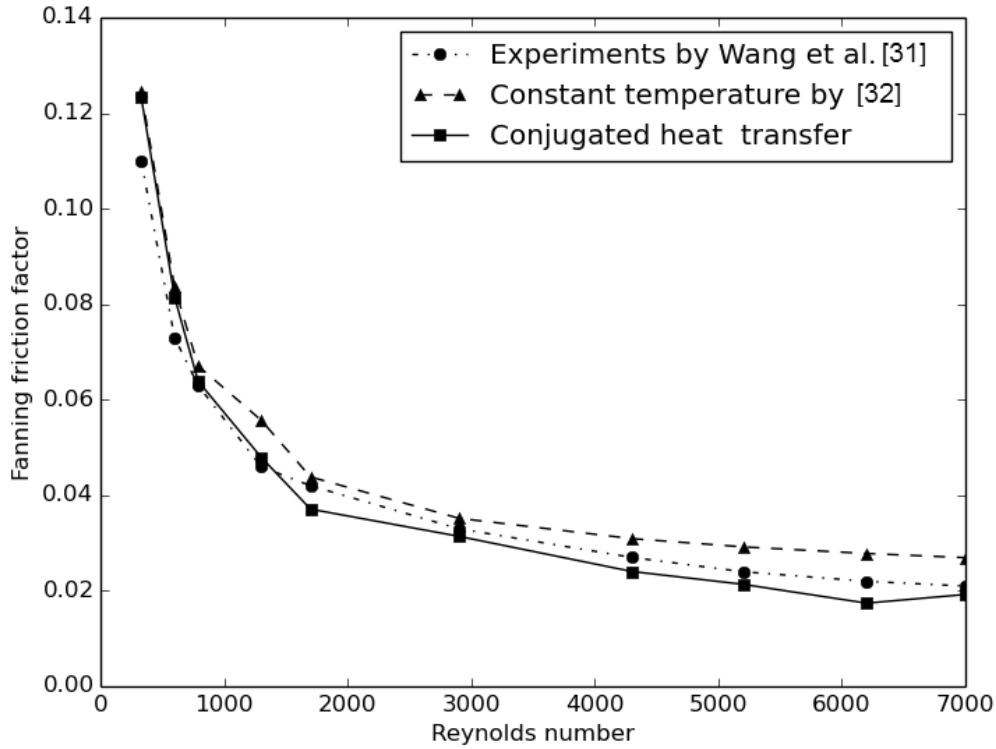

Figure 8 Comparison of the fanning friction factor with constant fin temperature, coupled solution and measurements

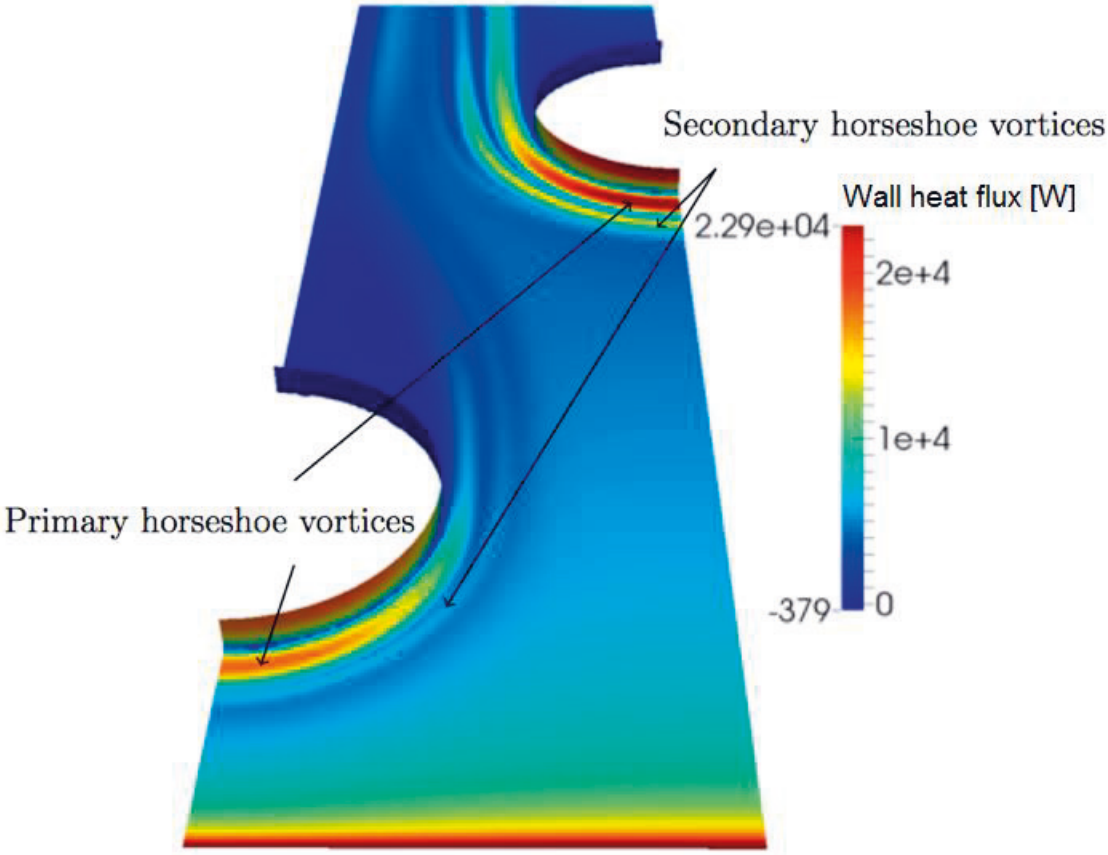

Figure 9 Fin heat flux distribution of constant temperature model [32]

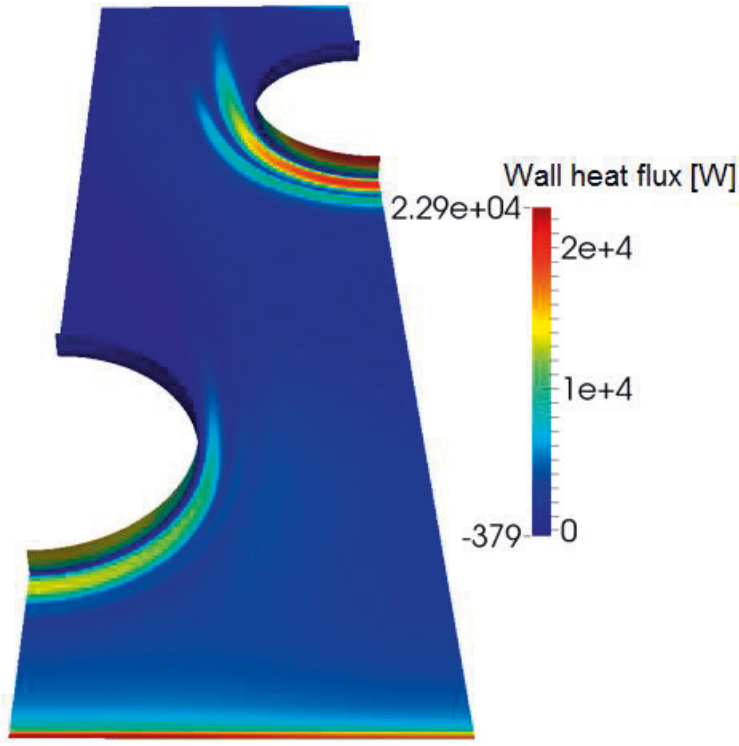

Figure 10 Fin heat flux distribution of conjugated heat transfer model

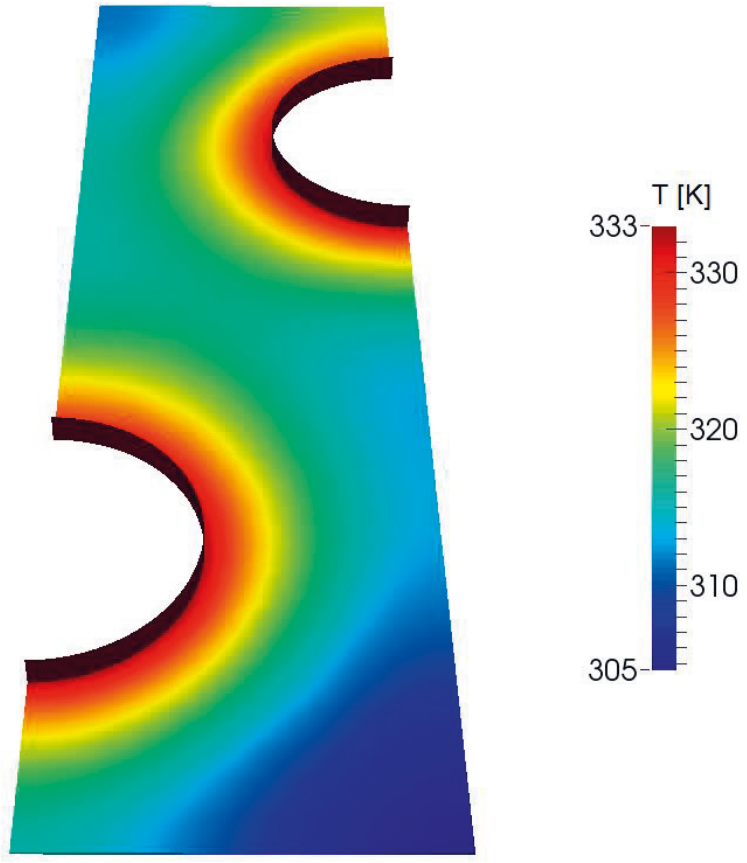

Figure 11 Temperature distribution of fin in conjugated heat transfer simulation

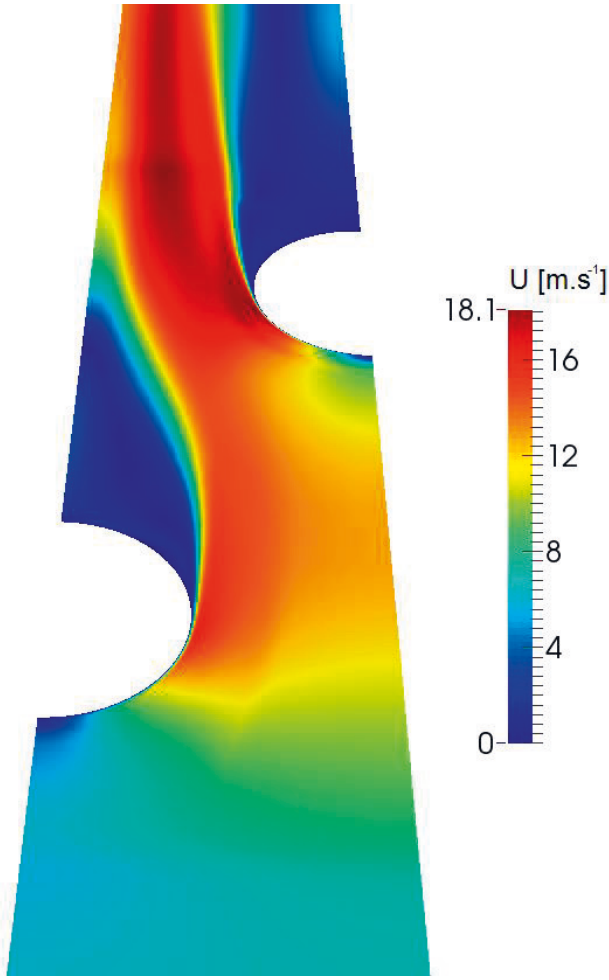

Figure 12 Velocity distribution in the middle of the channel in conjugated heat transfer simulation

Turo Välikangas is a Ph.D. student at Tampere University of Technology (TUT), Tampere, Finland, under the supervision of Prof. Reijo Karvinen. He graduated with honors from TUT with a Master's Degree in Science from the field of Mechanical engineering. He was majoring in fluid dynamics and heat transfer. He is currently working on fin-and-tube heat exchangers both numerically and experimentally.

Reijo Karvinen made his Ph.D. Thesis in conjugated heat transfer forty years ago and has been Prof. of Heat Transfer and Fluid Dynamics at Tampere University of Technology in Finland very long time. Most important results in research are in the fields of equipment development for pulp and paper industry, boilers, cooling of electronics and glass processing. Energy efficient research has resulted in credits such as for Reward of Clean Environment by Suomen Messut and the Innovation Reward of Tampere City.

Publication 2

Välikangas T., Singh S., Sørensen K. and Condra T. (2018). Fin-and-tube heat exchanger enhancement with a combined herringbone and vortex generator design. *International Journal of Heat and Mass Transfer*, vol. 118, pp. 602-616,
DOI: 10.1016/j.ijheatmasstransfer.2017.11.006

International Journal of Heat and Mass Transfer 118 (2018) 602–616

Contents lists available at ScienceDirect

International Journal of Heat and Mass Transfer

journal homepage: www.elsevier.com/locate/ijhmt

Fin-and-tube heat exchanger enhancement with a combined herringbone and vortex generator design

Turo Välikangas [a,b,*], Shobhana Singh [c], Kim Sørensen [c], Thomas Condra [c]

[a] Tampere University of Technology, Laboratory of Chemistry and Bioengineering, Finland
[b] Tampere University of Technology, Laboratory of Physics, Finland
[c] Department of Energy Technology, Aalborg University, Pontoppidanstræde, 9220 Aalborg East, Denmark

ARTICLE INFO

Article history:
Received 12 June 2017
Received in revised form 12 October 2017
Accepted 2 November 2017
Available online 14 November 2017

Keywords:
Fin-and-tube heat exchanger
Herringbone fin
Vortex generator
Conjugate heat transfer

ABSTRACT

Vortex generators (VGs) are the most commonly investigated enhancement methods in the field of improved heat exchangers. The aim of present work is to study the effect of VGs in a fin-and-tube heat exchanger (FTHE) with herringbone fin shape. The delta winglet VG design with length (s) and height (H) is selected based on previous studies. The investigated VG design is simple and considered realistic from the manufacturing point of view. The combined enhancement with herringbone fin and the VG is evaluated by simulating the conjugate heat transfer and the air flow. The structured mesh is created for both solid and fluid domains to solve the model numerically using a coupled open source solver in OpenFOAM. The influence of flow condition on the performance enhancement is studied by changing the Reynolds number in a range $Re = 1354–6157$. The study showed that VGs not only increase the heat transfer in the herringbone fin but also decrease the pressure drop. The highest and longest investigated VG design is found to perform the best because of its ability to delay the flow detachment from the tube, to feed high kinetic energy flow to the recirculation zone and to create longitudinal vortices in the downstream region from the VG. The fin with VG design $s = 0.5D$ and $H = 0.6F_p$ enhances the overall performance by 5.23% in comparison to the fin without VG. The results demonstrated the usefulness of VGs for the performance enhancement in connection with a herringbone fin design.

1. Introduction

Fin-and-tube heat exchangers (FTHE) are widely used in different applications for exchanging heat between a fluid and air domains. Highly reliable operation, customizable size, relatively lower cost and easy cleaning/maintenance characteristics make FTHEs a suitable design choice for many applications, for example, air conditioning, refrigeration, power generation and waste heat recovery from exhaust gases [1]. Fig. 1 shows FTHEs of different dimensions; depth, face area and size of the headers that can vary dramatically from design to another based on required applications of different characteristics.

The heat transfer process between the fluid in the tubes and the air flowing through the tube bank consist of different heat transfer resistances. These are the convective heat transfer in the fluid inside the tubes, conduction through the tubes and fins, the contact resistance between the tubes and the fins and the convective heat transfer in the air. The largest covering 60–80% of the total resistance has been shown to be found on the air side of the heat exchanger [2,3] due to which the heat transfer enhancement strategies are traditionally focused on the air side.

1.1. Heat transfer enhancement

The heat transfer enhancement strategies in FTHE's can be divided into three different generations based on the period of their introduction and the goal of the enhancement method. The first one being the most traditional one where the fin is corrugated to achieve a wavy shape so that transverse vortices are formed to the flow field. These fin shapes are called the herringbone [4] and sine wave [5]. These transverse vortices increase heat transfer but at the same time increase the pressure drop and are therefore not beneficial if the goal of the design is to achieve the best possible thermal hydraulic efficiency. Increased heat transfer will increase the pressure drop and will not lead to improvement in the overall efficiency. In a transverse vortex, there will always be a stream of flow towards the main free flow direction, which then

* Corresponding author at: Tampere University of Technology, Laboratory of Chemistry and Bioengineering, Finland.
E-mail addresses: turo.valikangas@tut.fi (T. Välikangas), ssi@et.aau.dk (S. Singh), kso@et.aau.dk (K. Sørensen), tc@et.aau.dk (T. Condra).

https://doi.org/10.1016/j.ijheatmasstransfer.2017.11.006
0017-9310/

Nomenclature

Symbols

Δp	pressure loss, Pa
ΔT_{lm}	logarithmic mean temperature difference, K
$\dot{m}$	mass flow rate, kg s^{-1}
$\overline{h}$	overall average heat transfer coefficient, W m^{-2} K^{-1}
A_c	minimum area of cross-section, m^2
A_t	total heat transfer area, m^2
C_f^p	specific heat of the air, J kg^{-1} K^{-1}
C_s	specific heat of the fin, J kg^{-1} K^{-1}
D	tube diameter, m
f	fanning friction factor
G_k	production term for k, kg m^{-1} s^{-3}
G_ω	production term for ω, kg m^{-3} s^{-2}
j	colburn j-factor
k	turbulence kinetic energy, m^2 s^{-2}
Pr	Prandtl number
Q	overall transferred heat to the air, W
Re	Reynolds number
T	temperature, K
t	fin thickness, m
T_{inlet}	air temperature at the inlet, K
T_{outlet}	mass averaged air temperature at the outlet, K
T_w	temperature of the inside diameter of the tube on the fin side, K
u	velocity in the direction of x axis, m s^{-1}
u_{max}	velocity in the minimum cross-sectional flow area, m s^{-1}
v	velocity in the direction of y axis, m s^{-1}
w	velocity in the direction of z axis, m s^{-1}
E_k	inlet kinetic energy, Pa
U_{inlet}	velocity at the inlet, m s^{-1}
y	distance from the wall, m

Greek symbols

α	attack angle of delta winglet VG, °
Γ	turbulent viscosity, kg m^{-1} s^{-1}
λ_f	thermal conductivity of the air, W m^{-1} K^{-1}
λ_s	thermal conductivity of the fin, W m^{-1} K^{-1}
μ	dynamic viscosity of air, kg m^{-1} s^{-1}
ν	kinematic viscosity of the air, m^2 s^{-1}
ω	turbulence specific dissipation, s^{-1}
ρ	density of the air, kg m^{-3}
τ_w	wall shear stress, Pa
θ	non-dimensionalised temperature

Subscripts

f	fluid
h	hydraulic
$inlet$	into the simulation domain
lm	logarithmic mean
max	maximum
$outlet$	out from the simulation domain
p	pitch
s	solid
t	total
w	wall

Superscripts

p	constant pressure

creates a high pressure drop because of the abrupt change in the direction of momentum energy.

The second generation of enhancement strategies was focused on creating as much heat transfer from a heat exchanger volume as possible. This lead to the introduction of louvered [6] and slit fins [7]. The main goal for these enhancement strategies is to create chaotic turbulence on the air side irrespective of the change in the pressure drop. This is of course justified in cases where there is a surplus of pressure on the air side or the most important design criterion is the size of the heat exchanger.

The third generation has the main focus on thermal flow management strategies [8]. These strategies focus on enhancing the flow in a way that turbulence is created only in areas where it is the most beneficial. This is done by utilizing vortex generators or other guide vanes to create longitudinal vortices to the flow field that are proven to give higher thermal hydraulic performance [9].

1.1.1. Herringbone fin shape

Herringbone wave fin-and-tube heat exchanger is one of the most common configurations which have been used extensively in many air-conditioning or process industries. Numerous studies, experimental as well as numerical, investigating the air-side performance of herringbone wavy fin-and-tube heat exchangers are available in the literature [10–13]. Series of experimental studies investigating the effect of fin thickness, pitch and pattern on the heat transfer and friction characteristics of herringbone wavy fin-and-tube heat exchangers has been reported by Wongwises and Chokeman [14,15]. Similar tests for herringbone wave fin heat exchangers investigating the effect of tube row, fin spacing, tube diameter, waffle height, etc. have been conducted by Wang et al. [16–19] They found that the heat transfer coefficient is almost independent of the fin spacing; however, waffle height has a significant effect, the heat transfer coefficient and the friction factor both increase as the waffle height increases. Moreover, Wang and Liaw [20] examines the air-side performance of the herringbone wavy fin-and-tube heat exchangers having a larger tube diameter (16.59 mm) in dehumidifying condition and compared the results with dry conditions. It has been found that the heat transfer performance of herringbone wavy fin-and-tube heat exchangers in a wet condition normally exceeds than in a dry condition in contrast to the plain fin geometry where the heat transfer coefficient in wet condition is slightly lower than that in a dry condition. Furthermore, several correlations have been developed for both in-line and staggered tube configurations in order to predict the air-side heat transfer coefficient and friction factor [21,17].

1.2. Vortex generators as an enhancement method

The use of oval tubes instead of round ones has proven to give higher heat transfer rates with the same pressure drop with similar hydraulic diameter regardless of the free flow velocity [22–24]. The main reason for this is the delayed detachment of the flow from the tube which then leads to larger heat transfer area utilisation and a smaller wake region down stream from the tube. In an attempt to achieve the similar heat enhancement characteristics that oval tubes would provide, different guide vanes and vortex generators are utilized to delay the detachment of the flow from the tubes and guide the flow of higher kinetic energy to the wake region to minimize the recirculation zone. Vortex generators are the passive flow enhancement devices, which facilitate the transfer of momentum in the boundary layer. The effect of using VG's to enhance the thermal hydraulic properties in fin-and-tube heat exchangers has been studied by several authors in the past. The level of enhancement varying depending on the Reynolds number, the angle of

Fig. 1. Illustration of different sizes of fin-and-tube heat exchangers.

attack, placement of the wing, the aspect ratio and the shape of the wing. [25]. Lotfi et al. [26] studied the thermal hydraulic performance of four different kinds of VG's used with smooth wave fin shape and oval tubes. The four different designs Rectangular Trapezoidal Winglet (RTW), Angle Rectangular Winglet (ARW), Curved Angle Rectangular Winglet (CARW) and Wheeler Wishbone (WW) are illustrated in Fig. 2.

They concluded that for the attack angle 30°, the CARW VG shape provides the best thermal hydraulic performance because of the biggest projected face area confronted by the impinging flow. The punched winglet type VG's, on the other hand, was studied by He et al. [27] and they concluded that the continuous winglet shape gives the best heat transfer augmentation with 33.8–70.6% higher heat transfer coefficient and with a pressure drop penalty of 43.4–97.2% in the range of 0.54–2.3 m/s in flow velocity.

1.3. Problem analysis

The temperature distribution in the fin is especially influenced by the heat transfer rate on the air side near the tubes as was concluded by Mosayebidorcheh et al. [28]. Moreover, the temperature distribution is dependent on the flow structure itself, and therefore, needs to be computed at the same time as the flow field [29–31]. This means that the temperature fields in solid and fluid in FTHE are coupled and should be treated as a conjugate heat transfer (CHT) problem. The assumption of a constant temperature boundary condition may lead to unrealistic results [32]. Therefore, it is important to acknowledge the effect of non-uniform temperature field in the fin and the conduction of the heat from the inside of the tube to the fin while comparing different passive fin heat enhancement methods with each other.

Several researchers have started to analyze the fluid flow with CHT in FTHEs [33–35]. Chen et al. [36] conducted parametric investigations on the fin and oval tube heat exchanger with punched longitudinal VG to explore the influence of angle of attack and the aspect ratio of the delta winglet on the heat transfer enhancement and flow loss. Lin and Jang [18] investigated CHT in fin-and-tube heat exchanger with embedded vortex generators and performed 3D turbulence analysis to identify improvements in the heat transfer coefficient. In addition, Singh et al. [37,1] investigated

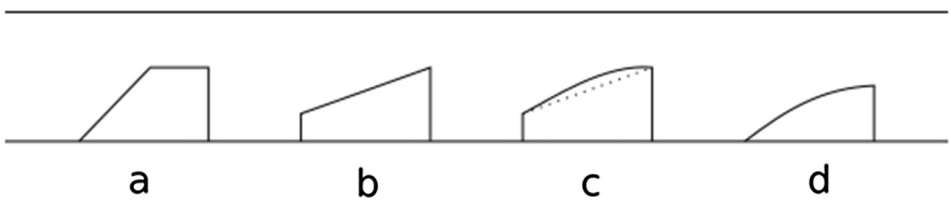

Fig. 2. Illustration of the different VG design studied by Lotfi et al. [26], (a) rectangular Trapezoidal Winglet (RTW), (b) Angle Rectangular Winglet (ARW), (c) Curved Angle Rectangular Winglet (CARW) and (d) Wheeler Wishbone (WW).

CHT mechanism coupled with the turbulent gas flow to elucidate temperature and velocity fields in double fin-and-tube heat exchanger for the waste heat recovery applications. Numerous studies, both experimental and numerical, have been carried out on wavy surface FTHE without VGs [14,20,38,39], and with VGs [40–43]. Despite the extensive research on herringbone FTHEs, very limited work focusing on CHT and flow performance has been reported so far. The main objective of the present study is to bridge this information gap by numerically investigating the enhancement in the herringbone FTHE combined with VG and taking conjugate nature of the heat transfer phenomenon into account.

2. Model development

2.1. Governing equations and boundary conditions

The governing equations that are solved in the fluid region for a steady-state, incompressible, three-dimensional flow using $k-\omega$ Shear-Stress Transport (SST) model, with no dissipative or source terms and in the solid region the three-dimensional heat equation without any source terms can be expressed as follows:

1. Continuity equation

$$\frac{\partial(\rho u_i)}{\partial x_i} = 0 \tag{1}$$

2. Momentum equation

$$\frac{\partial}{\partial x_i}(\rho u_i u_j) = \frac{\partial}{\partial x_i}\left(\mu \frac{\partial u_j}{\partial x_i}\right) - \frac{\partial p}{\partial x_j} \tag{2}$$

3. Energy equation for fluid region

$$\frac{\partial}{\partial x_i}(\rho C_f^p u_i T) = \frac{\partial}{\partial x_i}\left(\lambda_f \frac{\partial T}{\partial x_i}\right) \tag{3}$$

4. Transport equation for the turbulence kinetic energy, k

$$\frac{\partial}{\partial x_i}(\rho k u_i) = \frac{\partial}{\partial x_j}\left(\Gamma_k \frac{\partial k}{\partial x_j}\right) + G_k \tag{4}$$

5. Transport equation for the specific turbulence dissipation rate, ω

$$\frac{\partial}{\partial x_i}(\rho \omega u_i) = \frac{\partial}{\partial x_j}\left(\Gamma_\omega \frac{\partial \omega}{\partial x_j}\right) + G_\omega \tag{5}$$

6. Energy equation for solid region

$$\frac{\partial}{\partial x_i}\left(\lambda_s \frac{\partial T}{\partial x_i}\right) = 0 \tag{6}$$

In this study, the boundary condition used inside the tube of the solid region is a constant temperature of $T = 333$ K due to the relatively high heat transfer rate of the fluid flowing inside the tubes. The heat conductivity will be kept constant and is chosen to be similar to an aluminium alloy of $\lambda_s = 220\ \mathrm{W\,m^{-1}\,K^{-1}}$. For the temperature field between the fluid and the solid region, the Neumann-Dirichlet boundary condition is applied in a way that both the value and the gradient at the boundary is obeyed, other boundaries being set to zero gradients. The inlet condition on air side is set to $T = 278$ K for the temperature of the fluid and a uniform inlet velocity conditions in a range 1.1–5 m s^{-1} is applied. At the outlet of the outflow region, a fixed pressure condition is applied. For the upper and lower boundaries of the fluid region, a periodic boundary condition is used as for the left and right symmetric boundary condition is applied. In the fluid region, the fin surface has a non-slip boundary condition for the velocity field. This study focuses on dry conditions and therefore the humidity of the air and its effect on heat transfer can be neglected [44]. A summary of all the boundary conditions can be seen in Table 1.

2.2. Data reduction and performance parameters

In the present study, Reynolds number is based on the hydraulic diameter of the collar around the tube and is defined as:

$$Re_{D_h} = \frac{u_{max} D_h}{\nu} \tag{7}$$

where the hydraulic diameter is calculated as:

$$D_h = D + 2 * t \tag{8}$$

The overall average heat transfer coefficient in the case of a FTHE is calculated as:

$$\overline{h} = \frac{Q}{A_t \Delta T_{lm}} \tag{9}$$

where $Q = \dot{m} C_f^p (T_{inlet} - T_{outlet})$ is the overall transferred heat to the air and ΔT_{lm} is the logarithmic mean temperature difference between the inside diameter of the tube and the air.

In order to determine the heat transfer performance, non-dimensional Colburn j-factor using overall average heat transfer coefficient of a fin-and-tube heat exchanger is calculated as [45]:

$$j = \frac{\overline{h}}{\rho u_{max} C_f^p} Pr^{2/3} \tag{10}$$

The pressure loss in the FTHE is evaluated using the non-dimensional fanning friction factor which is defined as [46]:

$$f = \frac{\Delta p}{\frac{1}{2}\rho u_{max}^2} \times \frac{A_c}{A_t} \tag{11}$$

Different enhancement methods, operating conditions and mechanical design in heat exchanger design influences performance to a great extent, therefore, it is necessary to consider the resulting heat transfer and pressure loss simultaneously in the selection. Moreover, large scale applications require minimum heat exchanger volume in addition to the pressure loss. In the present study, *volume goodness factor* and proposed by Shah and London [47] are calculated. The factor compares the thermal performance of different exchanger surfaces in terms of heat transfer as well as frictional loss.

The *volume goodness factor* is defined as:

$$\frac{j}{f^{1/3}} = \frac{\frac{\overline{h}}{\rho u_{max} C_f^p} Pr^{2/3}}{\left(\frac{\Delta p}{\frac{1}{2}\rho u_{max}^2} \times \frac{A_c}{A_t}\right)^{1/3}} \tag{12}$$

Table 1
Boundary conditions used for the computational model.

Boundary name	Boundary condition
Inlet	$u = constant,\ v = w = 0,\ T = 289$ K
Outlet	$\frac{\partial u_i}{\partial x} = \frac{\partial T}{\partial x} = 0$
Inflow and outflow regions	
Top and bottom	$\frac{\partial u}{\partial z} = \frac{\partial v}{\partial z}, w = 0, \frac{\partial T}{\partial z} = 0$
Left and right	$\frac{\partial u}{\partial y} = \frac{\partial v}{\partial y}, v = 0, \frac{\partial T}{\partial y} = 0$
Fin region	
Top and bottom	$\frac{\partial u}{\partial z} = \frac{\partial v}{\partial z}, w = 0, \frac{\partial T}{\partial z} = 0$
Left and right	Tube inner surface $u = v = w = 0, T = 333$ K
	Fin region $u = v = w = 0, \frac{\partial T}{\partial y} = 0$
	Fluid region $\frac{\partial u}{\partial y} = \frac{\partial w}{\partial y}, \frac{\partial T}{\partial y} = 0$
Fluid-Solid interface	$T_s = T_f, -\lambda_s \frac{\partial T_s}{\partial n} = -\lambda \frac{\partial T_f}{\partial n}$

A larger value of *volume goodness factor* leads to reduced heat exchanger volume and weight which is required in light weight heat exchanger demands.

3. Computational model

3.1. Herringbone fin-and-tube heat exchanger

The computational geometry of the FTHE that is simulated in this study is shown in Fig. 3. The enhancement method that was chosen to be studied is the inclusion of VGs in the herringbone fin shape. Herringbone is one of the most commonly used fin shapes in the industry and can be said to be part of the first generation enhancement methods as explained in Section 1.1. As can be seen, the computational geometry consists of the air flowing between two fins and therefore the solid domain consists of half of the fin thickness on both sides of the fluid domain. The dimensions that characterize the design of the heat exchanger such as longitudinal P_l and transverse distance P_t of the tubes, as well as the diameter of the tubes D_c, fin pitch F_p and the thickness of the fin t are illustrated in Fig. 3 and the simulated values are given in Table 2. Geometric details of the herringbone FTHE are presented in Fig. 4a. It is important to mention that the inner and outer diameter of the tubes, the location of the VG and the characteristic dimensions of the herringbone fin shape i.e. the wave length and the amplitude of the herringbone shape are kept constant for all the simulations in this study. The characteristic length scale used for the hydraulic diameter in the Reynolds number calculation is also illustrated in the figure and the value $D_h = 9.76$ mm for collar diameter is kept constant for all the simulations.

The strong wall bounded flow inside the fin-and-tube heat exchanger and the passive scalar temperature field that is formed by the flow field is highly affected by two different kind of design parameters. The first ones are those that are kept constant for a specific heat exchanger design such as the tube diameter D and the longitudinal and transfer tube distance P_l and P_t, respectively. These parameters often stay the same for one specific fin press tool and are not changed in the design phase. The second set of parameters that can be changed in the design process and does not require major changes in the fin press are the thickness of the fin t and the fin pitch F_p. In the present design, the thickness can be changed by choosing a different roll of fin while the fin pitch can be changed by manipulating the settings in the fin press. These are related to each other in a way that the thicker the fin thickness is the higher fin pitches can be created from it. This is due to the stretching of the material in the process. All of these affect the hydro-thermal characteristics of the heat exchanger with plain fin shapes which is studied numerically [48–51] and experimentally [52,49,50] by numerous authors in the past.

Table 2
Geometric dimensions for herringbone fin shape

Parameter	Symbol/unit	Value
Outside diameter of tube collar	D_c/mm	9.76
Inside diameter of tube	D_{in}/mm	9.16
Longitudinal tube distance	P_l/mm	22
Transverse tube distance	P_t/mm	25.4
Number of tube row	n	2
Fin length along flow direction	L/mm	44
Fin pitch	F_p/mm	1.81
Fin thickness	t/mm	0.115
Herringbone amplitude	P_d/mm	1.19
Herringbone half wave length	X_f/mm	5.5
Location of the vortex generator	L_p/mm	6.5
Attack angle of delta winglet VG	α / °	30

3.2. Vortex generators

When designing VGs for fin-and-tube heat exchangers, it is important to analyse how it will be manufactured. One option is to use the material of the fin as the basis of the VG. In this case, the VG would be punched or twisted out from the fin in the fin press. The benefits in this way of manufacturing the VG is that no additional processes are needed, only one extra set of press tools is needed to be integrated to the fin press. Another option would be to manufacture the VGs before hand and then attach them to the fin afterwards. This method would require one extra phase in the manufacturing process of the heat exchanger and, therefore, it can be seen as a less beneficial way to produce the VG. This is why, the first option where the VGs are punched from the fin, is chosen to enhance the heat transfer in the recirculation zone behind the tubes. The design of the delta winglet VG that was chosen in the present study can be seen in Fig. 4b. The figure shows the hole that is left in the fin, after the VG is punched out as

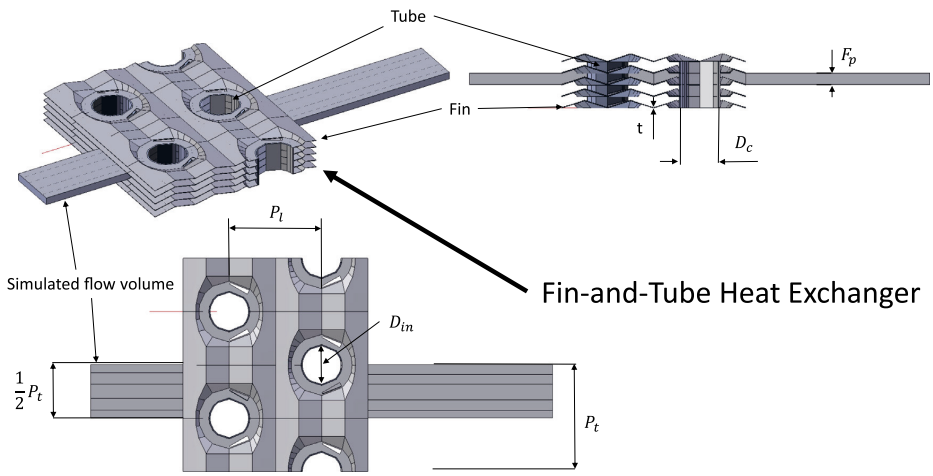

Fig. 3. Illustration of the simulated geometry of the fin-and-tube heat exchanger.

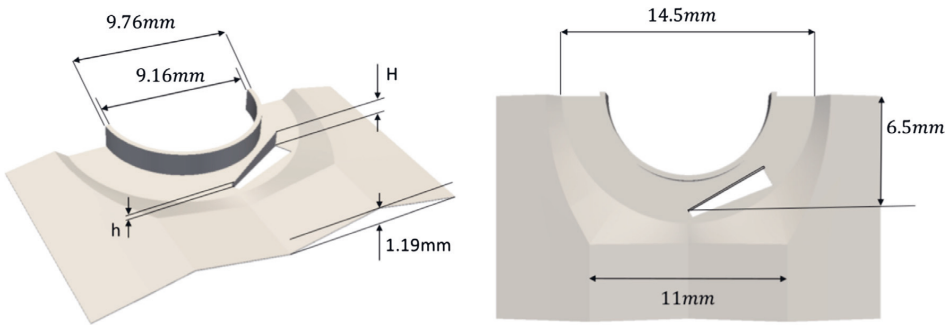

(a) Herringbone corrugation amplitude and wavelength

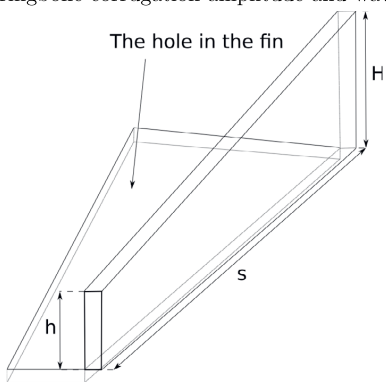

(b) The variables that are used to describe the design of the vortex generator

Fig. 4. Geometry details of the herringbone fin shape, VG locations and variables used in the study.

a winglet. Furthermore, it is important to know the dimensions of the VG so that it would enhance heat transfer but still be small enough so that it can be easily manufactured and the hole in the fin that is left from the process does not disturb the conduction of heat too much. This is why different sizes of VGs are studied in the present work. The variables that are varied are the length (s) and the height of the VG (H), where as the location of VG is kept constant. The dimensions of the VG that are simulated are shown in Table 3.

3.3. Grid generation

When solving a CHT problem, both the fluid and the solid regions need to be solved together and, therefore, a numerical mesh needs to be created for both mediums [32]. All the meshes used in the study are created with an open source meshing software called Swiftblock, which is a add-on tool in Blender. Blender is a 3D modelling software that is created and developed by the Blender Online Community [53]. Swiftblock is a graphical user interface to the generic meshing tool blockMesh that is distributed with the OpenFOAM package [54]. The following steps demonstrate the creation of the mesh:

1. First, the blocking strategy is created in the Swiftblock as shown in Fig. 5. The blocks define that in which direction the mesh will be aligned.

Table 3
Vortex generator parameters to be studied.

Variation	Lenght (s)	Downwind height (H)	Upwind height (h)
1	1/2D	$0.60F_p$	$0.20F_p$
2	1/2D	$0.45F_p$	$0.15F_p$
3	1/2D	$0.30F_p$	$0.10F_p$
4	3/8D	$0.60F_p$	$0.20F_p$
5	3/8D	$0.45F_p$	$0.15F_p$
6	3/8D	$0.30F_p$	$0.10F_p$

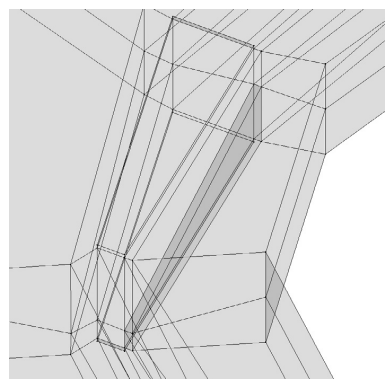

Fig. 5. Blocking strategy.

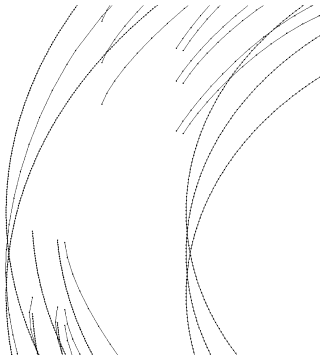

Fig. 6. Guide polylines.

2. In order to create hexahedral blocks, polylines following the round shapes need to be described in a separate object as can be seen in Fig. 6. The mesh will follow these lines when the corner of the block is connected to it.
3. Finally, the density of the mesh is defined by the grading of the cells on each edge of the blocks. The mesh will then be created by running the program blockMesh. The final mesh is then optimized in a way that boundary layers are computed with a finer mesh density than the free flow volume and, therefore, some computational resources are saved. Fig. 7 is an illustration of the mesh for the case with the length and height of the VG being $s = 0.375D$ and $H = 0.6F_p$, respectively.

The same procedure is followed to create the mesh of both regions, the fluid and the solid.

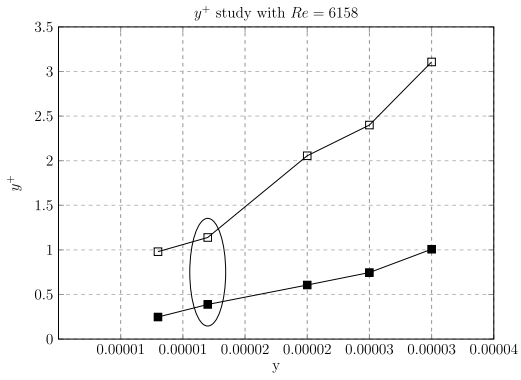

Fig. 8. The y^+ study for the plain herringbone fin shape with the chosen values for the simulations highlighted: Maximum y^+ —□— and the average y^+ —■— on all the heat transfer surfaces.

3.4. Computation procedure

The computational model that has been built for solving the conjugate heat transfer problem between the fluid and the solid region is solved by using an open-source C++ library called FOAM-Extend. FOAM-Extend is a community driven version of OpenFOAM [54], which is a finite volume method (FVM) based numerical solver for fluid dynamic problems. OpenFOAM is an open-source computational fluid dynamics (CFD) toolbox. Unlike other commercially available software's, it is free to use. It includes several numerical solvers for a wide range of applications. We use OpenFOAM for the present work because the source codes can be easily accessible, the cost of scalability is free and tailored for

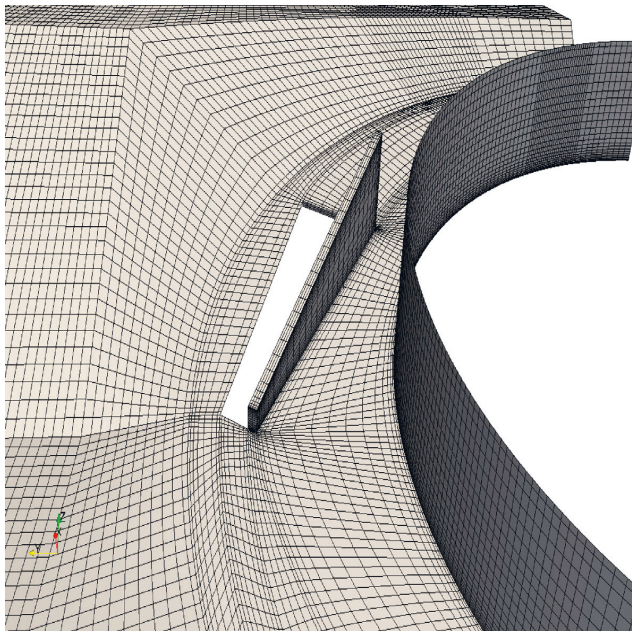

Fig. 7. Mesh illustration of grid independent mesh which results to average $y^+ = 0.35$ with $Re = 6158$.

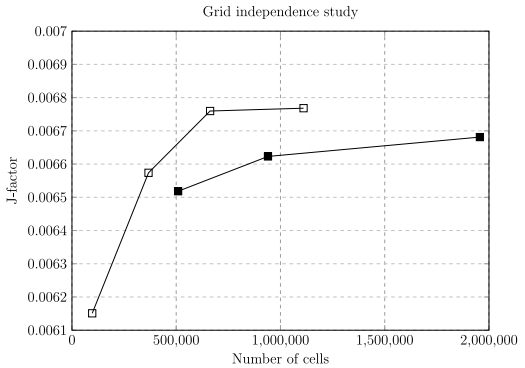

Fig. 9. Grid independence study with $Re = 6157$ for the herringbone fin shape mesh with and without vortex generators: Plain herringbone fin shape —□— and herringbone with VGs —■— ($s = 0.5D$ & $H = 0.45F_p$).

desired simulation and boundary conditions. The solver that was chosen is called conjugate heat simple foam (conjugateHeatSimpleFoam), which is an incompressible steady-state solver with the Boussinesq approximation for the buoyancy term. The solver is a block coupled matrix solver which solves the temperature equation in the solid and the fluid domain at the same time. It facilitates faster convergence of the CHT problem than in the traditional segregated solvers. A study of the convergence speeds and a break down of the solvers was done by Välikangas [55].

The small scale turbulence eddies are captured using $k - \omega$ SST model. Bhuiyan et al. [56] have shown that it performs best for fin-and-tube heat exchanger simulations with a wide range of inlet velocities taking different turbulence levels into account from fully laminar through the transitional phase into fully turbulent flow regime. The flow around a cylinder and other bluff bodies is by no means a steady-state situation when taking into account, the low frequency vortex-shedding eddies, the turbulence related large-eddies within the flow and the high frequency dissipation eddies. However, comparing these frequencies/timescales to the much longer thermal inertia time constants of the solid material leads to a conclusion that an assumption of an essentially steady flow field is accurate enough to elucidate the differences between enhancement strategies. Nagaosa [57] conducted a turbulence model free approach study, with the same tube diameter and fin pitch as in the present study, and concluded that turbulence structure started to appear after the inlet velocity value of 3 m/s.

3.5. Validation

The numerical mesh used in this study is validated in two ways, by performing a grid independence study and comparing the numerical results with the experimental data.

3.5.1. Grid independence study

The mesh independence measurements were done for a herringbone fin shape without the use of any VG. All the other design parameters were kept similar as described in Section 3.1. To find a grid independent mesh, the procedure developed by Roache [58] was used. First, a set of different meshes with different y-values (size of the cell normal from the wall) were compared to each other. The highest inlet velocity with Reynolds number of $Re = 6158$ was used and the results can be seen in Fig. 8.

A mesh with an average y^+-value of 0.38 was chosen which corresponds to the y-value of 0.000012 m to keep the maximum y^+-value in the whole domain close to 1. This is essential because no wall functions were used in any of the simulations for k or omega. All the meshes in this study, therefore, have a $y = 0.000012$ or smaller on all the heat transfer surfaces. Then the maximum cell size in the whole medium was varied to find a mesh that gives a grid independent solution with the smallest amount of cells possible. The Colburn j-factor value is monitored at four different mesh sizes to verify the grid independence. The results of mesh independence study for the design without and with VGs can be seen in Fig. 9. It can be seen that with the herring-

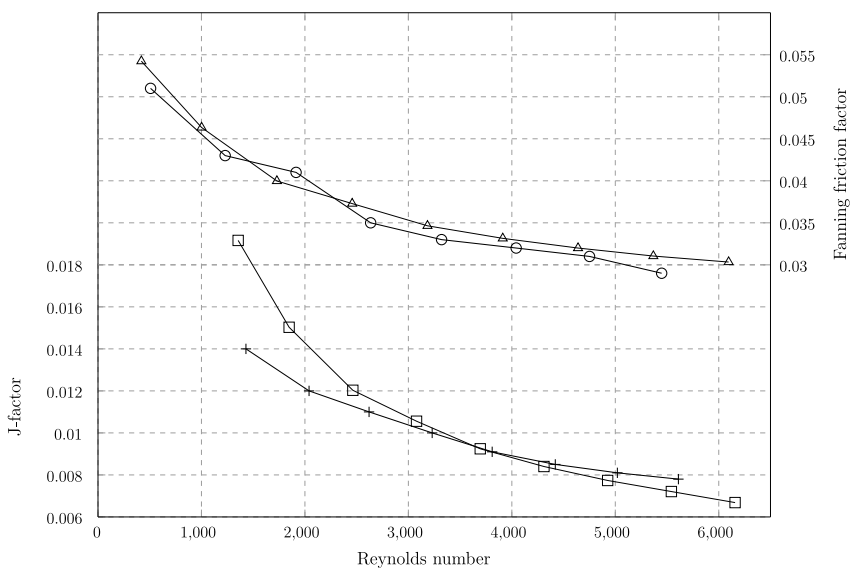

Fig. 10. Model validation comparison with experimental values done by Chokeman and Wongwises [15]: CFD j-factor —□—, Experimental j-factor —+—, CFD Fanning friction factor —△— and Experimental Fanning friction factor —○—.

bone shape without VG, around 625,000 cells are needed to reach the same value of j-factor as with the mesh that has 1,100,000 cells. Therefore, mesh with a lower number of cells can be used for the model validation.

For the mesh with VGs, if the same y^+-value and the same maximum cell size in the flow medium was used as in the design without the VGs, the total number of cells was 940,114. As can be seen from the grid independence study results, the j-factor value deviates by only 0.87% from the mesh that has double amount of cells, therefore to save computational resources the same maximum cell size and same y^+-values were used for all the different VG designs.

3.5.2. Comparison with experimental data

To validate the used mesh and the numerical choices in the simulation setup, a model validation study was conducted where the results of the simulations with different inlet velocities were compared to the measurements done by Chokeman and Wongwises [15]. When the pressure is non-dimensionalised into Fanning friction factor as in Eq. (11) and compared against the measured values in the upper part of Fig. 10, it can be seen that the CFD results correlate well with the measured values.

The Chilton and Coburn j-factor is also computed and compared to the measured values and the comparison can be seen in the lower part of Fig. 10. It can be seen that the non-dimensionalised heat transfer and pressure drop of the herringbone fin shape are really close to the measured ones and therefore it can be concluded that if the same numerical choices are used for the case of herringbone fin shape with the integration of VGs, similar results can be obtained.

4. Results and discussion

In this section, the results from six different designs of VGs as shown in Table 3 are compared with each other to find out which one has the highest volume goodness factor for best overall performance. First, the fanning friction factors are compared to each other, following the comparison of Colburn j-factors. For a more comprehensive comparison of the characteristics of the flow field, the volume goodness factor of the different designs is compared.

4.1. Herringbone with $s = 0.5D$ VGs

The VGs of the length $s = 0.5D$ is the longest of the two VG lengths that were simulated in this study. The length was found as the maximum size that could be punched from the herringbone fin when the starting location and the angle of attack was kept constant. The maximum length and height are restricted by the space between the collar around the tubes and the edge of the herringbone corrugation. When the VG is punched from the fin the surface should be flat so that the manufacturing process would be as secure as possible. The fanning friction factor values of the herringbone with VGs of $s = 0.5D$ at three different heights are shown Fig. 11. It can be seen that with lower velocities the higher VG design $H = 0.6F_p$ gives higher values than the lower designs with $H = 0.45F_p$ and $H = 0.3F_p$. But when the inlet velocity is increased the results turn around, and higher VG design shows lower friction factor values than the lower ones.

The heat transfer characteristics of the VG with $s = 0.5D$ in terms of j-factor are shown in Fig. 12. It can be seen that the trends with all the designs are very similar with the highest one $H = 0.6F_p$ having the highest values for the analysed Reynolds numbers.

When these two values are combined together into a volume goodness factor as explained in Eq. (12), we can observe that in Fig. 13 the overall performance of the VG design with $s = 0.5D$ and $H = 0.6F_p$ has higher values than the lower VG designs.

4.2. Herringbone with $s = 0.375D$ VGs

When the design of the VG is considered from the manufacturing point of view, it is important to know how small the VG can be

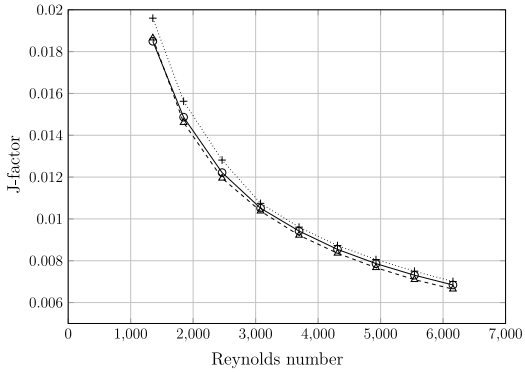

Fig. 12. j-factor comparison between Herringbone fin shape with $s = 0.5D$ VGs: herringbone with $H = 0.6F_p$ ··+··, herringbone with $H = 0.45F_p$ —○— and herringbone with $H = 0.3F_p$ – △ –.

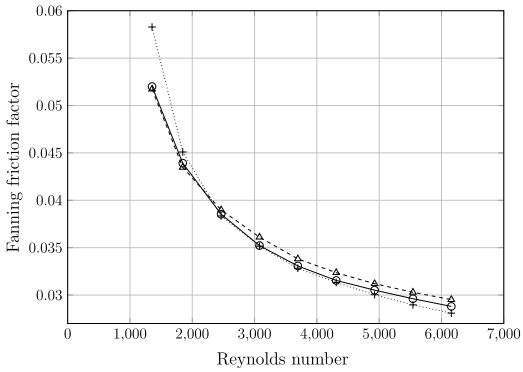

Fig. 11. Fanning friction factor comparison of Herringbone fin shape with $s = 0.5D$ VGs: herringbone with $H = 0.6F_p$ ··+··, herringbone with $H = 0.45F_p$ —○— and herringbone with $H = 0.3F_p$ – △ –.

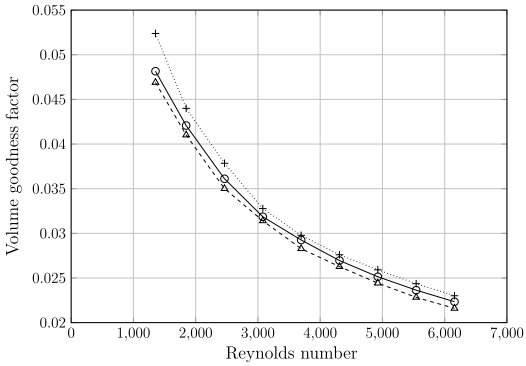

Fig. 13. Volume goodness factor comparison between Herringbone fin shape with $s = 0.5D$ VGs: herringbone with $H = 0.6F_p$ ··+··, herringbone with $H = 0.45F_p$ —○— and herringbone with $H = 0.3F_p$ – △ –.

made without compromising the improvement potential of its thermal hydraulic performance. This is why another set of simulations was made for a shorter VG design with $s = 0.375D$ to see how it affects the heat transfer process. When the VG is shorter it means that a smaller hole needs to made into the fin and therefore the manufacturing process of punching the VG requires less force. With the shorter VG, an interesting trend can be seen in Fig. 14. The lower design with $H = 0.3F_p$ gives a higher friction factor than the one with $H = 0.45F_p$ at different inlet velocities. With the highest case where $H = 0.6F_p$, a similar trend can be found that was seen with the longer VG in Section 4.1, so that the friction factor is higher at lower Reynolds number and lower at higher Reynolds numbers when compared to the shorter VG designs.

The comparison of j-factor for different VG designs can be observed in Fig. 15. It can be seen that with the j-factor shows a decreasing trend with the increasing Reynolds number. Also, with the increase in the height of VG, the j-factor decreases for a given value of Reynolds number. The highest VG design $H = 0.6F_p$ is found to perform superior at all Reynolds numbers and gives a higher j-factor than the lower designs.

To see the overall thermal hydraulic performance of the different height of VGs the volume goodness factor is compared. The results can be seen in Fig. 16. It is observed that the highest VG with $H = 0.6F_p$ has the highest value with all the other Reynolds number values except for $Re = 1354$.

4.3. Plain herringbone comparison with the best VG designs

To compare the impact of VG on overall performance, volume goodness factor of VG designs with the highest volume goodness factor i.e. VGs with length $s = 0.5$ and $s = 0.375D$ and plain herringbone fin shape is determined. The comparison is shown in Fig. 17.

The Volume goodness factor for Herringbone design with $s = 0.375D$ $H = 0.6F_p$ VGs is 4.97% and $s = 0.5D$ $H = 0.6F_p$ VGs 5.23% higher on average compared to the plain herringbone design without the use of VGs. This means that by using the new design with $s = 0.5D$ $H = 0.6F_p$ VGs, the same heat load can be achieved at the same pressure drop while saving 5.23% in the volume and material costs compared to the plain herringbone fin shape.

4.4. Temperature distribution

In the attempt to visualise the reasons why the VG designs have a higher thermal hydraulic performance than the plain herringbone fin shape, both the $s = 0.375D$ $H = 0.6F_p$ in Fig. 18b and the

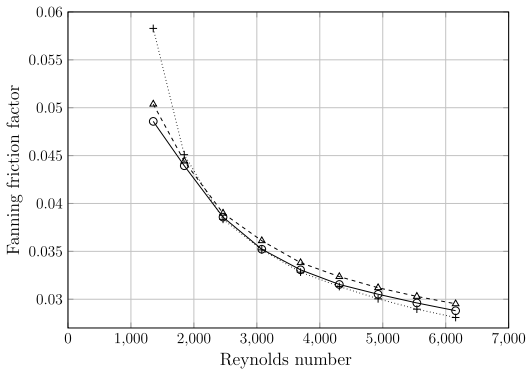

Fig. 14. Fanning friction factor comparison of Herringbone fin shape with $s = 0.375D$ VGs: herringbone with $H = 0.6F_p$ ··+··, herringbone with $H = 0.45F_p$ —○— and herringbone with $H = 0.3F_p$ – △ –.

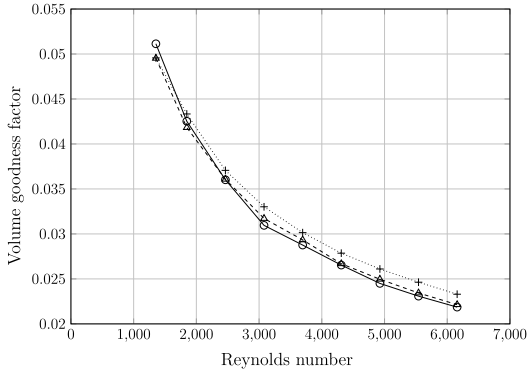

Fig. 16. Volume goodness factor comparison between Herringbone fin shape with $s = 0.375D$ VGs: herringbone with $H = 0.6F_p$ ··+··, herringbone with $H = 0.45F_p$ —○— and herringbone with $H = 0.3F_p$ – △ –.

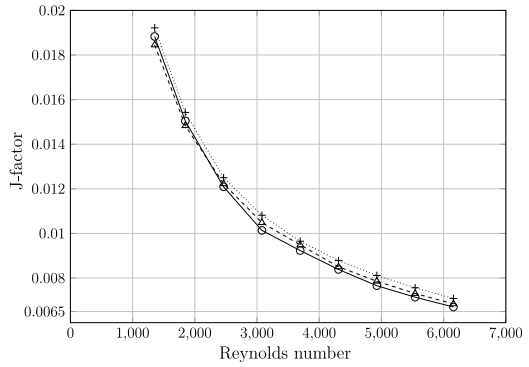

Fig. 15. j-factor comparison between Herringbone fin shape with $s = 0.375D$ VGs: herringbone with $H = 0.6F_p$ ··+··, herringbone with $H = 0.45F_p$ —○— and herringbone with $H = 0.3F_p$ – △ –.

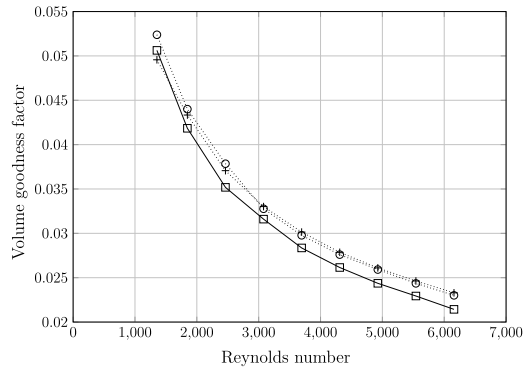

Fig. 17. Volume goodness factor comparison between the plain herringbone fin shape and two different VG designs: plain herringbone —□—, herringbone with $s = 0.375D$ $H = 0.6F_p$ ··+·· and herringbone with $s = 0.5D$ $H = 0.6F_p$ – △ –.

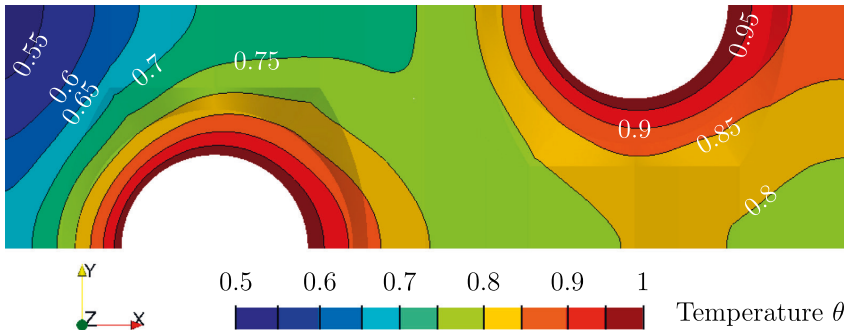

(a) Plain herringbone

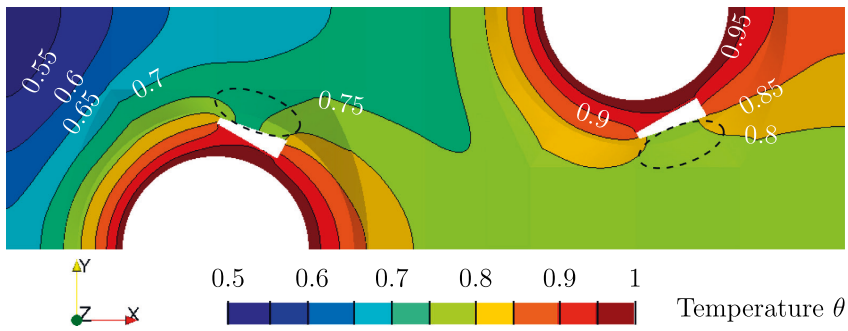

(b) Herringbone with $s = 0.375D$ and $H = 0.6F_p$ VGs

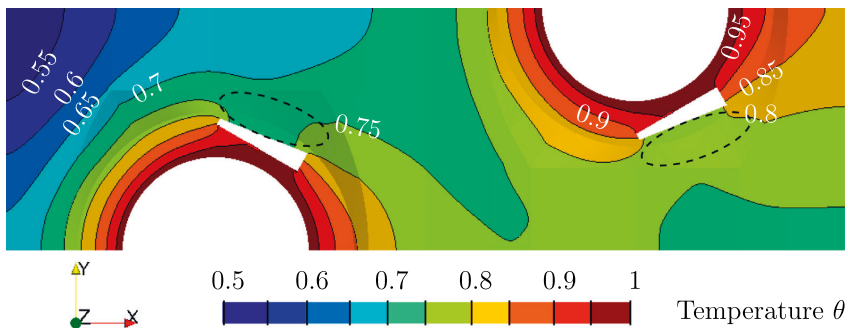

(c) Herringbone with $s = 0.5D$ and $H = 0.6F_p$ VGs

Fig. 18. Temperature distribution of the fin in the plain herringbone case in Fig. 18a, herringbone with $s = 0.375D$ and $H = 0.6F_p$ VGs in Fig. 18b and herringbone with $s = 0.5D$ and $H = 0.6F_p$ VGs in Fig. 18c.

$s = 0.5D$ $H = 0.6F_p$ in Fig. 18c and their corresponding temperature distributions of the fin are shown next to the plain herringbone fin shape in Fig. 18a.

The temperature is non-dimensionalised according to the Eq. (13).

$$\theta = \frac{T - T_{inlet}}{T_w - T_{inlet}} \tag{13}$$

It can be concluded that the difference in the temperature field can already been seen upstream from the first tube due to different distribution of the flow caused by the VGs.

As expected the air gaps that are left out from punching and lifting up the vortex generators, are acting as an insulation and prevents the heat from the inside of the tube to be transferred on the other side of the gap. This is why the temperature levels are lower behind the VG gaps as highlighted in the figures with dashed circles. It should be noted that even if the flow field were enhanced behind the gaps (when observed from the direction of the tubes), the improved heat transfer capabilities in the air would not lead to an improved heat transfer because of the obstructed conduction path caused by the gap. Another noticeable difference between the temperature distributions is that the downstream region behind the tubes is colder in the VG designs than in the original plain her-

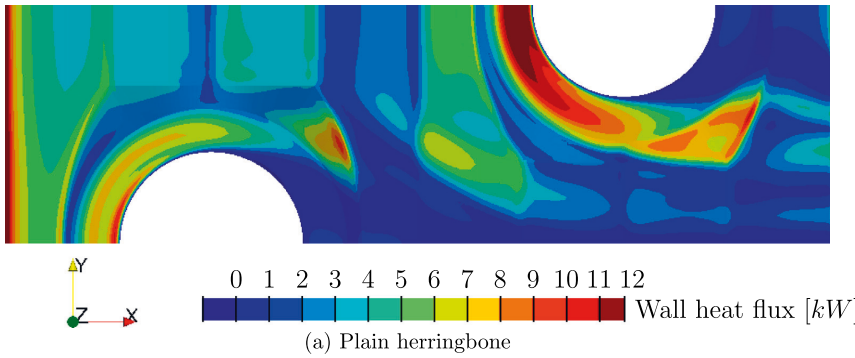

(a) Plain herringbone

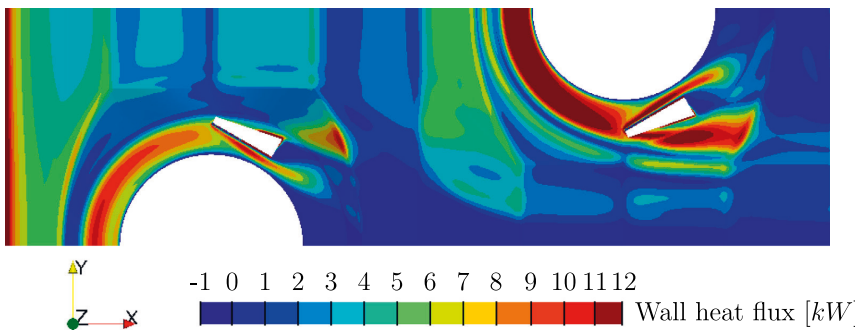

(b) Herringbone with $s = 0.375D$ and $H = 0.6F_p$ VGs

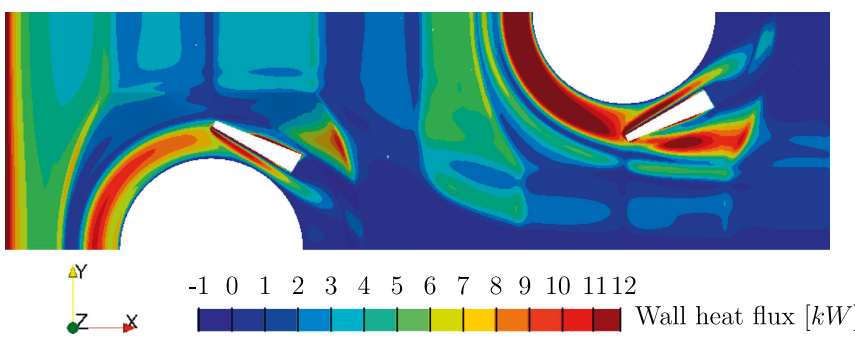

(c) Herringbone with $s = 0.5D$ and $H = 0.6F_p$ VGs

Fig. 19. Wall heat flux distribution of the fin in the plain herringbone case in Fig. 19a, herringbone with $s = 0.375D$ and $H = 0.6F_p$ VGs in Fig. 19b and herringbone with $s = 0.5D$ and $H = 0.6F_p$ VGs in Fig. 19c.

ringbone case. As was discussed in Section 1.3 the temperature distribution in the fin is asymmetrical and therefore, the usage of a fin efficiency with a constant boundary condition would lead to totally wrong results.

4.5. Wall heat flux

To see which parts of the fin is distributing the heat better to the air, the wall heat flux distribution on the boundary surface of VGs with $s = 0.375D$ $H = 0.6F_p$, $s = 0.5D$ $H = 0.6F_p$, and the plain herringbone fin shape are shown in Fig. 19b, c, and a, respectively. All the values are scaled from −1000 W to 12,000 W which is based on the plain herringbone case. It can be concluded that some negative heat flux is found in the recirculation zone behind the tubes. The heat transfer enhancement in the down stream region behind the VGs can be clearly seen from the figures.

It can be seen from the figures that the inclusion of VGs is guiding some of the flow to the recirculation zone behind the tube and, therefore, delaying the detachment of the flow from tube which increases the heat transfer and lowers the pressure drop.

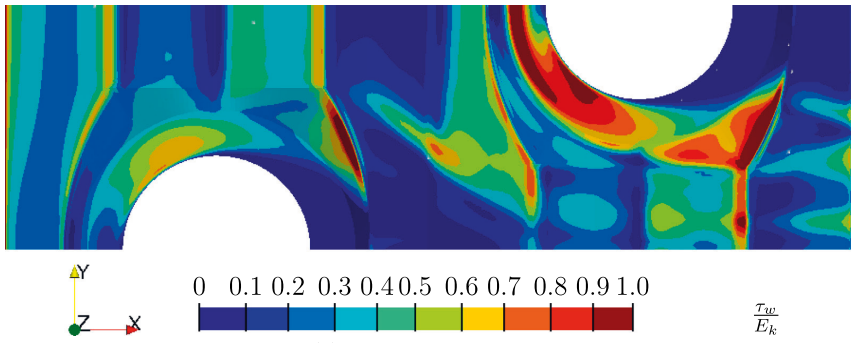

(a) Plain herringbone

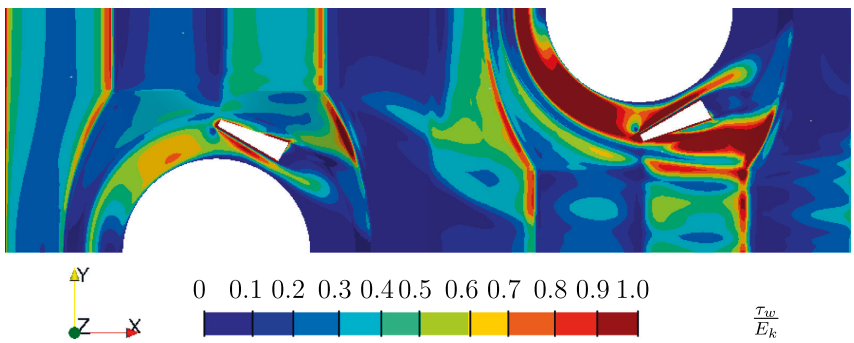

(b) Herringbone with $s = 0.375D$ and $H = 0.6F_p$ VGs

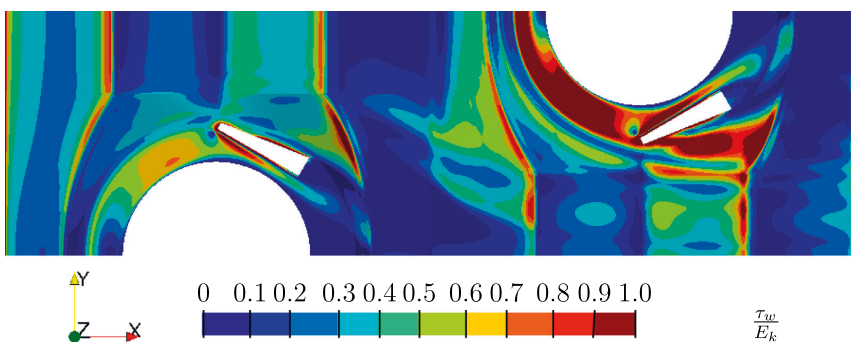

(c) Herringbone with $s = 0.5D$ and $H = 0.6F_p$ VGs

Fig. 20. Non-dimensionalised wall shear stress distribution on the fin in the plain herringbone case in Fig. 20a, herringbone with $s = 0.375D$ and $H = 0.6Fp$ VGs in Fig. 20b and herringbone with $s = 0.5D$ and $H = 0.6F_p$ VGs in Fig. 20c.

4.6. Wall shear stress

Finally, the $s = 0.375D$ $H = 0.6F_p$ in Fig. 20b and the $s = 0.5D$ $H = 0.6F_p$ in Fig. 20c and their corresponding wall shear stress distribution at the wall on the air side are shown next to the plain herringbone fin shape in Fig. 20a. The shear stress is normalised with the free flow kinetic energy as shown in Eq. (14).

$$\frac{\tau_w}{E_k} = \frac{\mu\left(\frac{\partial u}{\partial y}\right)_{y=0}}{\frac{1}{2}\rho_{inlet}U^2_{inlet}} \tag{14}$$

It is known that the wall shear stress is directly related to the heat transfer process because it is a measure of the fluid speed at the wall. Similar conclusions can be made for the wall shear stress as was concluded from the wall heat flux comparison. The detachment of the flow from the tube is delayed and more high kinetic energy flow is directed behind the tubes decreasing the size of the recirculation zone. Before the tube and VGs a clear stagnation point can be seen in the figures. Even though the VGs create longitudinal vortices that can be seen with high wall shear stress values between the tubes where the distance to the tube is the highest, the wall heat flux in these areas is not as high as it would be if

the conjugate heat transfer process with the conduction in the fin would not be solved. This shows the importance of the coupled heat transfer process between the conduction heat transfer in the fin and the convection on the air side.

The present investigation shows that the bigger the VG is, the higher performance it seems to have as more flow is directed behind the tubes. The size of the VG is limited due to two main reasons. First one, being the manufacturing and design limitations. For example, the fixed fin pitch that limits the height of the VG and the collar around the tube that defines the area available for the VG to be punched from the fin. The second form of limitation comes from the heat transfer process itself; if too much material is punched from the fin, the heat conduction path from the tubes to the other side of the VG can be disrupted which may decrease the heat transfer more than increasing it. Present work is limited to analyse the performance enhancement tendencies of different VG designs. However, these tendencies are useful in defining the design constraints and can be used for future optimization studies on herringbone fin-and-tube heat exchanger.

5. Conclusions

In this paper, six different punched longitudinal delta winglet VG designs and their heat transfer and pressure drop characteristics are investigated. Three-dimensional conjugate heat transfer and flow numerical model is developed in OpenFOAM. From the results, the following conclusions can be made.

1. The punched vortex delta winglets can enhance heat transfer in two ways; first one being the longitudinal vortices created in the downstream from the VG and the second one being the ability to direct high kinetic energy flow to the recirculation zone behind the tubes which leads to delay in the detachment of the flow from the tube as well as increase in the usage of heat transfer surface when the recirculation zone is decreased.
2. Compared to the plain herringbone fin without VGs, herringbone fin with VG designs $s = 0.5D$ $H = 0.6F_p$ and the $s = 0.375D$ $H = 0.6F_p$ are found to have 5.23% and 4.97% higher volume goodness factor, respectively.
3. From a manufacturing point of view the VG design can be made shorter $s = 0.375D$ but to ensure good thermal hydraulic enhancement the height of the VG should be kept closer to the height $H = 0.6F_p$. Shorter VG will perform better with higher Reynolds number where as the opposite will be encountered with lower velocities.
4. The present investigation pursued the results considering conjugate heat transfer and its importance in heat transfer enhancement prediction with herringbone fin and VGs into account which is often neglected in many numerical studies.
5. The present investigation is limited to the specific VG designs that are possible to manufacture in the existing herringbone fin design. In the future studies, the design parameters will be extended and varied to find the optimum design combination for the best overall performance.

The present investigation provides important design performance data that could be useful to the heat exchanger design engineers and manufacturers in developing enhanced fin surfaces.

Conflict of interests

We wish to confirm that there are no known conflicts of interest associated with this publication.

Acknowledgments

The authors greatly acknowledge the financial support of Koja Oy and the computational resources provided by the Tampere University of Technology.

References

[1] S. Singh, K. Sørensen, T.J. Condra, Influence of the degree of thermal contact in fin and tube heat exchanger: a numerical analysis, Appl. Therm. Eng. 107 (2016) 612–624, https://doi.org/10.1016/j.applthermaleng.2016.07.022. <http://www.sciencedirect.com/science/article/pii/S1359431116311516>.
[2] J. Jeong, C.N. Kim, B. Youn, A study on the thermal contact conductance in fin-tube heat exchangers with 7 mm tube, Int. J. Heat Mass Transfer 49 (7–8) (2006) 1547–1555, https://doi.org/10.1016/j.ijheatmasstransfer.2005.10.042. <http://www.sciencedirect.com/science/article/pii/S001793100500685X>.
[3] C.-C. Wang, R.L. Webb, K.-Y. Chi, Data reduction for air-side performance of fin-and-tube heat exchangers, Exp. Therm. Fluid Sci. 21 (4) (2000) 218–226, https://doi.org/10.1016/S0894-1777(00)00005-4. <http://www.sciencedirect.com/science/article/pii/S0894177700000054>.
[4] C.-C. Wang, Y.-J. Du, Y.-J. Chang, W.-H. Tao, Airside performance of herringbone fin-and-tube heat exchangers in wet conditions, Can. J. Chem. Eng. 77 (6) (1999) 1225–1230, https://doi.org/10.1002/cjce.5450770620.
[5] C. Wang, W. Fu, C. Chang, Heat transfer and friction characteristics of typical wavy fin-and-tube heat exchangers, Exp. Therm. Fluid Sci. 14 (2) (1997) 174–186, https://doi.org/10.1016/S0894-1777(96)00056-8. <http://www.sciencedirect.com/science/article/pii/S0894177796000568>.
[6] Z. Čarija, B. Franković, M. Perčić, M. Čavrak, Heat transfer analysis of fin-and-tube heat exchangers with flat and louvered fin geometries, Int. J. Refrig. 45 (2014) 160–167, https://doi.org/10.1016/j.ijrefrig.2014.05.026. <http://www.sciencedirect.com/science/article/pii/S0140700714001388>.
[7] C.-C. Wang, W.-H. Tao, C.-J. Chang, An investigation of the airside performance of the slit fin-and-tube heat exchangers, Int. J. Refrig. 22 (8) (1999) 595–603, https://doi.org/10.1016/S0140-7007(99)00031-6. <http://www.sciencedirect.com/science/article/pii/S0140700799000316>.
[8] A. Arora, P. Subbarao, R. Agarwal, Development of parametric space for the vortex generator location for improving thermal compactness of an existing inline fin and tube heat exchanger, Appl. Therm. Eng. 98 (2016) 727–742, https://doi.org/10.1016/j.applthermaleng.2015.12.117. <http://www.sciencedirect.com/science/article/pii/S1359431116000089>.
[9] M. Fiebig, Embedded vortices in internal flow: heat transfer and pressure loss enhancement, Int. J. Heat Fluid Flow 16 (5) (1995) 376–388, https://doi.org/10.1016/0142-727X(95)00043-P. <http://www.sciencedirect.com/science/article/pii/0142727X9500043P>.
[10] T. Kuvannarat, C.C. Wang, S. Wongwises, Effect of fin thickness on the air-side performance of wavy fin-and-tube heat exchangers under dehumidifying conditions, Int. J. Heat Mass Transfer 49 (15–16) (2006) 2587–2596, https://doi.org/10.1016/j.ijheatmasstransfer.2006.01.020.
[11] N.H. Kim, J.H. Ham, J.P. Cho, Experimental investigation on the airside performance of fin-and-tube heat exchangers having herringbone wave fins and proposal of a new heat transfer and pressure drop correlation, J. Mech. Sci. Technol. 22 (3) (2008) 545–555, https://doi.org/10.1007/s12206-007-1116-4.
[12] N.H. Kim, T. Kim, An experimental investigation on the airside performance of fin-and-tube heat exchangers having slit fins under wet condition, J. Mech. Sci. Technol. 29 (11) (2015) 5011–5019, https://doi.org/10.1007/s12206-015-1049-2.
[13] N.H. Kim, T. Kim, An experimental investigation on the airside performance of fin-and-tube heat exchangers having slit fins under wet condition, J. Mech. Sci. Technol. 29 (11) (2015) 5011–5019, https://doi.org/10.1007/s12206-015-1049-2.
[14] S. Wongwises, Y. Chokeman, Effect of fin pitch and number of tube rows on the air side performance of herringbone wavy fin and tube heat exchangers, Energy Convers. Manage. 46 (13–14) (2005) 2216–2231, https://doi.org/10.1016/j.enconman.2004.09.011.
[15] Y. Chokeman, S. Wongwises, Effect of fin pattern on the air-side performance of herringbone wavy fin-and-tube heat exchangers, Heat Mass Trans./Waerme- Stoffuebertragung 41 (7) (2005) 642–650, https://doi.org/10.1007/s00231-004-0578-5.
[16] Chi-Chuan Wang, Jiin-Yuh Chang Nie, Effects of waffle height on the air-side performance of wavy fin-and-tube heat exchangers, Heat Transfer Eng. 20 (3) (1999) 45–56, https://doi.org/10.1080/014576399271411. <http://www.tandfonline.com/doi/abs/10.1080/014576399271411>.
[17] C.C. Wang, Y.M. Hwang, Y.T. Lin, Empirical correlations for heat transfer and flow friction characteristics of herringbone wavy fin-and-tube heat exchangers, Int. J. Refrig. 25 (5) (2002) 673–680, https://doi.org/10.1016/S0140-7007(01)00049-4.
[18] Y.T. Lin, Y.M. Hwang, C.C. Wang, Performance of the herringbone wavy fin under dehumidifying conditions, Int. J. Heat Mass Transfer 45 (25) (2002) 5035–5044, https://doi.org/10.1016/S0017-9310(02)00193-X.
[19] C.-c. Wang, J.-s. Liaw, B.-c. Yang, Airside performance of herringbone wavy fin-and-tube heat exchangers - data with larger diameter tube, Int. J. Heat Mass

Transfer 54 (5–6) (2011) 1024–1029, https://doi.org/10.1016/j.ijheatmasstransfer.2010.11.038.
[20] C.C. Wang, J.S. Liaw, Air-side performance of herringbone wavy fin-and-tube heat exchangers under dehumidifying condition - data with larger diameter tube, Int. J. Heat Mass Transfer 55 (11–12) (2012) 3054–3060, https://doi.org/10.1016/j.ijheatmasstransfer.2012.02.025.
[21] N. Kim, J. Yun, R. Webb, Heat transfer and friction correlations for wavy plate fin-and-tube heat exchangers, Heat Transfer (1997) 560–567. <http://heattransfer.asmedigitalcollection.asme.org/article.aspx?articleid=144288>.
[22] D. Taler, P. Ocłoń, Determination of heat transfer formulas for gas flow in fin-and-tube heat exchanger with oval tubes using {CFD} simulations, Chem. Eng. Process.: Process Intens. 83 (2014) 1–11, https://doi.org/10.1016/j.cep.2014.06.011. <http://www.sciencedirect.com/science/article/pii/S0255270114001305>.
[23] H. Han, Y.-L. He, Y.-S. Li, Y. Wang, M. Wu, A numerical study on compact enhanced fin-and-tube heat exchangers with oval and circular tube configurations, Int. J. Heat Mass Transfer 65 (2013) 686–695, https://doi.org/10.1016/j.ijheatmasstransfer.2013.06.049. <http://www.sciencedirect.com/science/article/pii/S0017931013005176>.
[24] C.-N. Lin, Y.-W. Liu, J.-S. Leu, Heat transfer and fluid flow analysis for plate-fin and oval tube heat exchangers with vortex generators, Heat Transfer Eng. 29 (7) (2008) 588–596, https://doi.org/10.1080/01457630801922279.
[25] Y.-G. Lei, Y.-L. He, L.-T. Tian, P. Chu, W.-Q. Tao, Hydrodynamics and heat transfer characteristics of a novel heat exchanger with delta-winglet vortex generators, Chem. Eng. Sci. 65 (5) (2010) 1551–1562, https://doi.org/10.1016/j.ces.2009.10.017. <http://www.sciencedirect.com/science/article/pii/S0009250909007325>.
[26] B. Lotfi, M. Zeng, B. Sundén, Q. Wang, 3d numerical investigation of flow and heat transfer characteristics in smooth wavy fin-and-elliptical tube heat exchangers using new type vortex generators, Energy 73 (2014) 233–257, https://doi.org/10.1016/j.energy.2014.06.016. <http://www.sciencedirect.com/science/article/pii/S0360544214007142>.
[27] Y. He, H. Han, W. Tao, Y. Zhang, Numerical study of heat-transfer enhancement by punched winglet-type vortex generator arrays in fin-and-tube heat exchangers, Int. J. Heat Mass Transfer 55 (21–22) (2012) 5449–5458, https://doi.org/10.1016/j.ijheatmasstransfer.2012.04.059. <http://www.sciencedirect.com/science/article/pii/S0017931012003109>.
[28] S. Mosayebidorcheh, M. Rahimi-Gorji, D.D. Ganji, T. Moayebidorcheh, O. Pourmehran, M. Biglarian, Transient thermal behavior of radial fins of rectangular, triangular and hyperbolic profiles with temperature-dependent properties using dtm-fdm, J. Central South Univ. 24 (3) (2017) 675–682, https://doi.org/10.1007/s11771-017-3468-y.
[29] H.-T. Chen, J.-P. Song, Y.-T. Wang, Prediction of heat transfer coefficient on the fin inside one-tube plate finned-tube heat exchangers, Int. J. Heat Mass Transfer 48 (13) (2005) 2697–2707, https://doi.org/10.1016/j.ijheatmasstransfer.2005.01.035. <http://www.sciencedirect.com/science/article/pii/S0017931005001195>.
[30] H.-T. Chen, J.-C. Chou, H.-C. Wang, Estimation of heat transfer coefficient on the vertical plate fin of finned-tube heat exchangers for various air speeds and fin spacings, Int. J. Heat Mass Transfer 50 (1–2) (2007) 45–57, https://doi.org/10.1016/j.ijheatmasstransfer.2006.06.038. <http://www.sciencedirect.com/science/article/pii/S0017931006004406>.
[31] H.-T. Chen, J.-R. Lai, Study of heat-transfer characteristics on the fin of two-row plate finned-tube heat exchangers, Int. J. Heat Mass Transfer 55 (15–16) (2012) 4088–4095, https://doi.org/10.1016/j.ijheatmasstransfer.2012.03.050. <http://www.sciencedirect.com/science/article/pii/S0017931012001998>.
[32] T. Välikangas, R. Karvinen, Conjugated heat transfer simulation of a fin-and-tube heat exchanger, in: Selected Papers from the 9th International Conference on Computational Heat and Mass Transfer, Heat Transfer Eng.
[33] W.M. Yan, T.F. Fin, T.L. Lee, Steady conjugate heat transfer in turbulent channel flows, Wärme Stoffübertragung 25 (4) (1990) 215–220, https://doi.org/10.1007/BF01785408.
[34] M. Fiebig, A. Grosse-Gorgemann, Y. Chen, N.K. Mitra, Conjugate heat transfer of a finned tube part a: heat transfer behavior and occurrence of heat transfer reversal, Numer. Heat Transfer, Part A: Appl. 28 (2) (1995) 133–146, https://doi.org/10.1080/10407789508913737.
[35] M. Fiebig, Y. Chen, A. Grosse-Gorgemann, N.K. Mitra, Conjugate heat transfer of a finned tube part b: heat transfer augmentation and avoidance of heat transfer reversal by longitudinal vortex generators, Numer. Heat Transfer, Part A: Appl. 28 (2) (1995) 147–155, https://doi.org/10.1080/10407789508913738, doi:http://dx.doi.org/10.1080/10407789508913738.
[36] Y. Chen, M. Fiebig, N. Mitra, Conjugate heat transfer of a finned oval tube with a punched longitudinal vortex generator in form of a delta winglet-parametric investigations of the winglet, Int. J. Heat Mass Transfer 41 (23) (1998) 3961–3978, https://doi.org/10.1016/S0017-9310(98)00076-3. <http://www.sciencedirect.com/science/article/pii/S0017931098000763>.
[37] S. Singh, K. Sørensen, A.S. Simonsen, T.J. Condra, Implications of fin profiles on overall performance and weight reduction of a fin and tube heat exchanger, Appl. Therm. Eng. 115 (2017) 962–976, https://doi.org/10.1016/j.applthermaleng.2017.01.043. <http://www.sciencedirect.com/science/article/pii/S1359431116332069>.
[38] Y.B. Tao, Y.L. He, J. Huang, Z.G. Wu, W.Q. Tao, Three-dimensional numerical study of wavy fin-and-tube heat exchangers and field synergy principle analysis, Int. J. Heat Mass Transfer 50 (5–6) (2007) 1163–1175, https://doi.org/10.1016/j.ijheatmasstransfer.2006.03.019.
[39] M. Darvish Damavandi, M. Forouzanmehr, H. Safikhani, Modeling and Pareto based multi-objective optimization of wavy fin-and-elliptical tube heat exchangers using CFD and NSGA-II algorithm, Appl. Therm. Eng. 111 (2017) 325–339, https://doi.org/10.1016/j.applthermaleng.2016.09.120.
[40] L. Tian, Y. He, Y. Tao, W. Tao, A comparative study on the air-side performance of wavy fin-and-tube heat exchanger with punched delta winglets in staggered and in-line arrangements, Int. J. Therm. Sci. 48 (9) (2009) 1765–1776, https://doi.org/10.1016/j.ijthermalsci.2009.02.007.
[41] B. Lotfi, B. Sundén, Q. Wang, An investigation of the thermo-hydraulic performance of the smooth wavy fin-and-elliptical tube heat exchangers utilizing new type vortex generators, Appl. Energy 162 (2016) 1282–1302, https://doi.org/10.1016/j.apenergy.2015.07.065.
[42] L. Tian, Y. He, P. Chu, W. Tao, Numerical study of flow and heat transfer enhancement by using delta winglets in a triangular wavy fin-and-tube heat exchanger, J. Heat Transfer 131 (9) (2009) 11–19, https://doi.org/10.1115/1.3139106.
[43] L. Tian, Y. He, Y. Tao, W. Tao, A comparative study on the air-side performance of wavy fin-and-tube heat exchanger with punched delta winglets in staggered and in-line arrangements, Int. J. Therm. Sci. 48 (9) (2009) 1765–1776, https://doi.org/10.1016/j.ijthermalsci.2009.02.007. <http://www.sciencedirect.com/science/article/pii/S1290072909000234>.
[44] W. Pirompugd, S. Wongwises, Partially wet fin efficiency for the longitudinal fins of rectangular, triangular, concave parabolic, and convex parabolic profiles, J. Franklin Inst. 350 (6) (2013) 1424–1442, https://doi.org/10.1016/j.jfranklin.2013.02.019. <http://www.sciencedirect.com/science/article/pii/S0016003213000896>.
[45] C.J. Geankoplis, Transport Processes and Separation Process Principles (Includes Unit Operations), Springer, 2003. <http://cds.cern.ch/record/1508328/files/013101367X_TOC.pdf>.
[46] C.C. Wang, Y.J. Chang, Y.C. Hsieh, Y.T. Lin, Sensible heat and friction characteristics of plate fin-and-tube heat exchangers having plane fins, Int. J. Refrig. 19(4) (1996) 223–230. <http://www.sciencedirect.com/science/article/pii/0140700796000217>.
[47] R.K. Shah, A.L. London, Flow Forced Convection Heat Transfer and Flow Friction in Straight and Curved Ducts - A Summary of Analytical Solutions, vol. 1, Academic Press, 1972.
[48] J. Cobian-Iñiguez, A. Wu, F. Dugast, A. Pacheco-Vega, Numerically-based parametric analysis of plain fin and tube compact heat exchangers, Appl. Therm. Eng. 86 (2015) 1–13, https://doi.org/10.1016/j.applthermaleng.2015.03.072. <http://www.sciencedirect.com/science/article/pii/S1359431115003312>.
[49] R. Romero-Méndez, M. Sen, K. Yang, R. McClain, Effect of fin spacing on convection in a plate fin and tube heat exchanger, Int. J. Heat Mass Transfer 43 (1) (2000) 39–51, https://doi.org/10.1016/S0017-9310(99)00120-9. <http://www.sciencedirect.com/science/article/pii/S0017931099001209>.
[50] J.-Y. Jang, M.-C. Wu, W.-J. Chang, Numerical and experimental studies of threedimensional plate-fin and tube heat exchangers, Int. J. Heat Mass Transfer 39 (14) (1996) 3057–3066, https://doi.org/10.1016/0017-9310(95)00341-X. <http://www.sciencedirect.com/science/article/pii/001793109500341X>.
[51] A. Erek, B. Özerdem, L. Bilir, Z. İlken, Effect of geometrical parameters on heat transfer and pressure drop characteristics of plate fin and tube heat exchangers, Appl. Therm. Eng. 25 (14–15) (2005) 2421–2431, https://doi.org/10.1016/j.applthermaleng.2004.12.019. <http://www.sciencedirect.com/science/article/pii/S1359431105000268>.
[52] C.-C. Wang, K.-Y. Chi, C.-J. Chang, Heat transfer, Heat transfer and friction characteristics of plain fin-and-tube heat exchangers, Part ii: Correlation, Int. J. Heat Mass Transfer 43 (15) (2000) 2693–2700, https://doi.org/10.1016/S0017-9310(99)00333-6. <http://www.sciencedirect.com/science/article/pii/S0017931099003336>.
[53] B.O. Community, Blender - A 3d Modelling and Rendering Package. <http://www.blender.org>.
[54] T.O. Foundation, The Openfoam Documentation, 2017. <https://openfoam.org/>.
[55] T. Välikangas, H. Nilsson, Conjugate heat transfer in openfoam, in: Proceedings of CFD with OpenSource Software.
[56] A. Bhuiyan, A. Islam, M. Amin, Numerical study of 3d thermal and hydraulic characteristics of wavy fin-and-tube heat exchanger, Front. Heat Mass Transfer (FHMT) 3(3) (2012).
[57] R. Nagaosa, Turbulence model-free approach for predictions of air flow dynamics and heat transfer in a fin-and-tube exchanger, Energy Convers. Manage. 142 (2017) 414–425, https://doi.org/10.1016/j.enconman.2017.03.063.
[58] P.J. Roache, Perspective: a method for uniform reporting of grid refinement studies, J. Fluids Eng. 116 (1994) 405–413, https://doi.org/10.1115/1.2910291.

Publication 3

Välikangas T., Folkersma M., Dal Maso M., Keskitalo T., Peltonen P. and Vuorinen V. (2021). Parametric CFD study for finding the optimal tube arrangement of a fin-and-tube heat exchanger with plain fins in a marine environment. *Applied Thermal Engineering*, vol. 200, pp. 117642, DOI: 10.1016/j.applthermaleng.2021.117642

Applied Thermal Engineering 200 (2022) 117642

Contents lists available at ScienceDirect

Applied Thermal Engineering

journal homepage: www.elsevier.com/locate/ate

Research Paper

Parametric CFD study for finding the optimal tube arrangement of a fin-and-tube heat exchanger with plain fins in a marine environment

Turo Välikangas [a,*], Mikko Folkersma [b], Miikka Dal Maso [a], Tuomo Keskitalo [c], Petteri Peltonen [d], Ville Vuorinen [e]

[a] Aerosol Physics Laboratory, Physics Unit, Tampere University, Finland
[b] Faculty of Aerospace Engineering, Delft University of Technology, Netherlands
[c] Neste Engineering Solutions Oy, Finland
[d] Technical Research Centre of Finland, FI-02044 VTT, Finland
[e] Department of Mechanical Engineering, Aalto University, Finland

ARTICLE INFO

Keywords:
Fin-and-tube
Heat exchanger
Plain fin
Conjugate heat transfer

ABSTRACT

In the past, fin-and tube heat exchanger (FTHE) tube pattern ratios have been largely based on ad-hoc design principles. Here, we investigate the optimal tube arrangements for a FTHE with plain fins in marine environments represented by two different air types; one for unfiltered air with high condensation rate and one for clean dry filtered air conditions. The thermal-hydraulic efficiency of the FTHE design is measured by comparing a modified ratio of Colburn j-factor and Fanning friction factor. The regression model generated from the CFD data is then used to identify the maximum efficiency for two design specific fin pitches separately. We identified two optimal tube patterns: one for a large fin pitch for unfiltered air, and another for a small fin pitch for filtered air. Manufacturing restrictions were found to significantly limit the maximum achievable efficiency of a tube pattern. By neglecting the related manufacturing restrictions, 4% higher efficiency for a fin pitch of 1.5 mm and 23% higher efficiency for a fin pitch of 3.5 mm is achieved. Without any application specific limitations or manufacturing restrictions the fin pitch 1.5 mm can have a 36% increased efficiency than fin pitch 3.5 mm. These novel results show that development in manufacturing have potential for significant improvements in thermal-hydraulic efficiency.

1. Introduction

The heating ventilation and air conditioning (HVAC) system is the second largest energy consumer in a cruiser ship following the propulsion system [1]. The energy consumption of the HVAC system is highly dependent on the outside temperature, but in some estimates the energy consumption of the HVAC system can be up to 13%–16% [2,3]. Due to the COVID19 pandemic, it is possible that the use of fully separated fresh-exhaust air conditioning systems will increase in the future. Such designs can be achieved by using fin-and-tube heat exchanger (FTHE) -based heat recovery systems. In a FTHE-based heat recovery system the heat is transferred by a fluid in such a way that no mixing between fresh and exhaust air occurs. Unfortunately, this may lead to the overall decrease of efficiency in HVAC systems due to lack of recycled air. As the need for more efficient air conditioning units is evident, it is essential to improve the thermal-hydraulic efficiency of the heat exchanger inside the units.

The performance of the FTHE can be adjusted by changing the fin pitch [4], size of the tubes [5], longitudinal tube pitch [6], transverse tube pitch [7], number of tube rows [8], number of fluid circuits [9], the mass flow of the fluid [10] or the fin shape itself [11]. The challenge in comparing the performance of different fin shapes is the difficulty to reproduce the thermal-hydraulic efficiencies in a comparable manner. Experimental results of the performance of different fin types by multiple authors have been compiled into correlation studies [12–16]. In these, the results of multiple experimental studies are expressed in terms of correlation equations. This enables the fin designs to be intercompared in the whole design space with other variables that affect the thermal-hydraulic efficiency, such as fin pitch, tube diameter, tube pattern and fin thickness. Naturally, in the experimental studies, the authors are reporting values of real existing FTHE designs that are manufactured with applicable machinery. This means that data from uncommon combinations, which are rare in the industry, are absent. In

* Corresponding author.
E-mail addresses: turo.valikangas@tuni.fi (T. Välikangas), miikka.dalmaso@tuni.fi (M. Dal Maso), petteri.peltonen@vtt.fi (P. Peltonen), ville.vuorinen@aalto.fi (V. Vuorinen).

https://doi.org/10.1016/j.applthermaleng.2021.117642
Received 20 May 2021; Received in revised form 30 September 2021; Accepted 3 October 2021
Available online 22 October 2021

Nomenclature

Symbols

$\dot{m}$	Mass flow, kgs^{-1}
$\overline{h}$	Overall average heat transfer coefficient, $Wm^{-2}\ K^{-1}$
A	Wet area, m^2
$A_{freeflow}$	Free flow area, m^2
A_{front}	Front inlet area, m^2
C_f^p	Specific heat of the air, $Jkg^{-1}\ K^{-1}$
C_s	Specific heat of the fin, $Jkg^{-1}\ K^{-1}$
D	Tube diameter after expansion, m
D_h	Hydraulic diameter, based on free flow and wet area, m
D_c	Tube collar diameter, m
D_{in}	Tube inner diameter, m
f	Fanning friction factor
F_p	Fin pitch, m
G_k	Production term for k, $kgm^{-1}s^{-3}$
G_ω	Production term for ω, $kgm^{-3}s^{-2}$
j	Colburn j-factor
JF	JF performance ratio
k	Turbulence kinetic energy, m^2s^{-2}
L	Depth of the heat exchanger in flow direction, m
Nu	Nusselt number
P_d	Diagonal tube pitch, m
P_l	Longitudinal tube pitch, m
P_t	Transversal tube pitch, m
Pr	Prandtl number
Q	Overall transferred heat to the air, W
q	Heat flux, $Wm^{-2}s^{-1}$
Re_{D_c}	Reynolds number, based on hydraulic diameter D_c
Re_{D_h}	Reynolds number, based on hydraulic diameter D_h
T	Temperature, K
T_f	Temperature of the fluid, K
T_s	Temperature on the surface, K
T_w	Temperature at the wall, K
T_{inlet}	Temperature at the inlet, K
T_{lm}	Logarithmic mean temperature difference, K
T_{outlet}	Temperature at the outlet, K
u	Velocity in the direction of x axis, ms^{-1}
u_i	Velocity in the direction of each cartesian directions, ms^{-1}
u_{core}	Velocity in the minimum cross-sectional flow area, ms^{-1}
v	Velocity in the direction of y axis, ms^{-1}
w	Velocity in the direction of z axis, ms^{-1}
x_i	Cartesian coordinates x,y,z, m

Greek symbols

Δp	Pressure loss, Pa
η	Fin efficiency
Γ	Turbulent viscosity, $kgm^{-1}s^{-1}$
κ	Air thermal diffusivity, $Wm^{-1}s^{-1}$
λ_f	Thermal conductivity of the air, $Wm^{-1}K^{-1}$
λ_s	Thermal conductivity of the fin, $Wm^{-1}K^{-1}$
μ	Dynamic viscosity of air, $kgm^{-1}s^{-1}$
ν	Kinematic viscosity of the air, m^2s^{-1}
ω	Turbulence specific dissipation, s^{-1}
ρ	Density of the air, kgm^{-3}
θ	Non-dimensionalized temperature

Subscripts

f	Fluid
i, j, k	Cartesian coordinate directions, -
s	Solid

Superscripts

p	Constant pressure

addition to this, not all possible combinations have been measured and therefore the real relation between the fin shape and design parameters and their effect on the thermal-hydraulic efficiency is obscured. In other words, the variables used in the designs are not selected evenly to cover all parts of the design space in an equal and unbiased manner. Therefore, such literature data may be biased towards certain designs.

Ameel et al. [17] showed that a lighter and smaller FTHE can be made with a smaller fin pitch. However, there is often an application specific threshold that enforces the use of a wider fin spacing. Therefore, in cooling coils with high condensation rates, often only plain fin types with relatively high fin pitches are used. Such occasions are for example hygiene-related applications that are used in hospital environments. Other examples include applications with higher amounts of condensate rate [18], hazardous air with increased fouling propensity [19] or the risk of ice formation [20] on the fins. Hence, the tube arrangement needs to be specifically optimized for each application-specific fin spacing and inlet velocity. Therefore, as noted in the present study, it may be important for the manufacturer of the FTHE to know which tube arrangements are the best for a given application.

As mentioned earlier, in experimental FTHE studies the designs are very often biased towards the pre-existing portfolio that is being manufactured already in the industry. In contrast, in CFD-based FTHE studies the manufacturing restrictions or difficulties are often neglected. For example, a very common rule that is followed in the industry is to use a tube pattern that has the ratio of traversal tube pitch to longitudinal tube pitch $P_t/P_l = 1.1547$. This enables the manufacturer to use only one kind of U-bend tubes in the process of soldering the circuits. Experimental studies found in the literature on the thermal-hydraulic efficiency of FTHE with plain fins [13,14,21–25] have a 61% portion with the aforementioned ratio. Another popular tube arrangement ratio was $P_t/P_l = 1.333$ with 24% of all the designs. We do not have an explanation for the use of the latter ratio but the first one is further analyzed in Section 4 where its effect on the thermal-hydraulic efficiency is illustrated.

Based on the literature, previous dimensional characterizations of FTHE's have been done mostly on ad-hoc principles following traditional guidelines. Here, we make an attempt to systematically assess such FTHE design by CFD, utilizing a novel open source meshing tool called Swiftblock along with the open source CFD library OpenFOAM. The main objectives of this study are as follows: 1) Develop a parametric computational conjugate heat transfer model to explore different fin spacings and tube arrangements. 2) Carry out a systematic parameter sweep for transverse ($P_t = 14{-}38$ mm) and longitudinal ($P_l = 14{-}78$ mm) tube distances. Repeat the parametric sweep for two

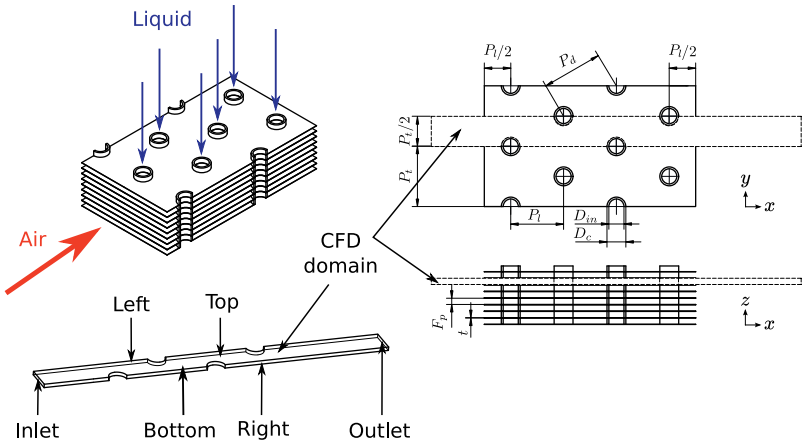

Fig. 1. Illustration of the simulated geometry between the fins and tubes of the fin-and-tube heat exchanger. The main parameters studied herein are P_l and P_t for two different fin pitches F_p.

different fin pitch values. A typical marine application design point with the velocity of $u = 3\,\mathrm{m\,s^{-1}}$ was chosen for the inlet boundary condition. Other variables such as number of tube rows $N = 4$, tube diameter $D_c = 10.00\,\mathrm{mm}$ and the fin thickness $t = 0.2\,\mathrm{mm}$ are kept constant. 3) Create a regression model based on performance ratio data. 4) Find the optimal tube pattern value from the model when the manufacturing restrictions have to be followed and when they can be arbitrarily selected based on the goodness of the design.

This study offers a novel approach for creating the computational model with automatic open source meshing, so that larger parametric design spaces can be studied. The study offers a valuable data set outside the previously investigated ranges available in the literature. The published data set can be used to find optimal solutions for various FTHE designs. Additionally, this study illustrates that for maximizing the JF performance ratio, the best design is not found within the current design portfolio broadly used in the industry.

2. Details on the numerical domain and performance parameters

2.1. Plain fin-and-tube heat exchanger simulation domain

The computational domain is designed in a way that it represents the characteristics of the air side heat transfer in any size of heat exchanger inlet area but requires a feasible amount of computational resources. It is expected that by multiplying this to match the face area of arbitrary sized heat exchanger, the air side heat transfer rate scales equally. Therefore, only one flow section between the tubes and the fins is simulated. In Fig. 1 is an illustration of the FTHE and the computational domain that is modeled.

Before and after the heat exchanger we model an inflow and an outflow region with the length of one and two longitudinal tube pitches, respectively.

2.2. Data reduction and performance parameters

In this study, the Reynolds number is defined in two different ways. The first one in Eq. (1) is based on the hydraulic diameter $D_h = \frac{4A_{freeflow}L}{A}$ [26] as the reference length scale and the used reference velocity is the average velocity in the minimum cross section called the core velocity u_{core}.

$$Re_{D_h} = \frac{u_{core} D_h}{\nu} \tag{1}$$

The second is used when the CFD values are compared to the experimental results in Section 3.3 and is therefore defined as:

$$Re_{D_c} = \frac{u_{core} D_c}{\nu} \tag{2}$$

where $D_c = 10.00\,\mathrm{mm}$ is the collar tube diameter, which can be calculated as $D_c = D + 2 * t$. The overall average heat transfer coefficient in the case of a FTHE is calculated as:

$$\overline{h} = \frac{Q}{A \Delta T_{lm}} \tag{3}$$

where $Q = \dot{m} C_f^p (T_{inlet} - T_{outlet})$ is the overall transferred heat to the air and ΔT_{lm} is the logarithmic mean temperature difference between the inside diameter of the tube and the air.

The results in this study are illustrated in the form of a non-dimensional pressure drop, the Fanning friction factor f [27,28], and the non-dimensional heat transfer, Colburn j-factor [29], which are calculated as follows.

$$j = \frac{Nu}{Re_{D_h} Pr^{1/3}} = \frac{\frac{\overline{h} D_h}{\lambda_f}}{\frac{\rho u_{core} D_h}{\mu}} Pr^{2/3} \tag{4}$$

$$f = \frac{\Delta p}{\frac{1}{2}\rho u_{core}^2} \times \frac{D_h}{4L} \tag{5}$$

In general, increase in heat transfer yields an increase in pressure drop. This means that one must consider the trade-off between the increase in heat transfer and increase on the pressure drop when evaluating the performance of the heat exchanger. Traditionally the performance of the fin shapes are compared with goodness factors such as area [30,31] or volume goodness [30,32,33]. However, using these presents some difficulties when the reference length and/or velocity scales are different between the cases [34]. In this study, all the reference variables change between the cases. Therefore, it is desirable to use a performance criterion that has a numerical value that increases with improved performance, regardless of reference scales. One such performance criterion is the JF performance rate, as defined by Shi et al. [35] and Yun and Lee [36] (see references for the derivation). We apply a version of the JF performance ratio in which the reference variables are not subtracted from the equation. JF is defined as the ratio of two other important ratios obtained between a studied heat exchanger and a reference heat exchanger. One is the ratio of the heat transfer rate per unit temperature difference, per unit surface area, and

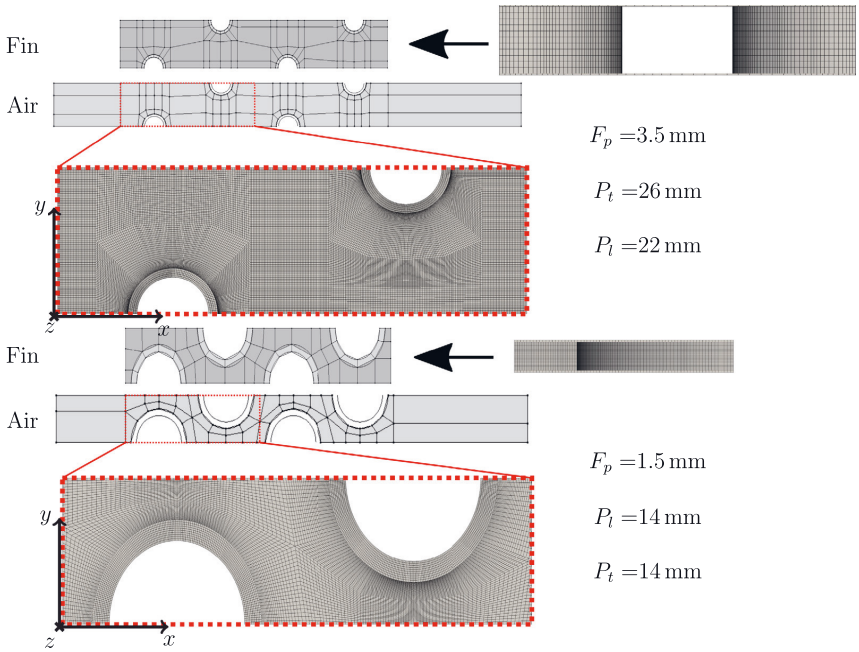

Fig. 2. Illustration of the two different blocking strategies used for the fin and air mesh.

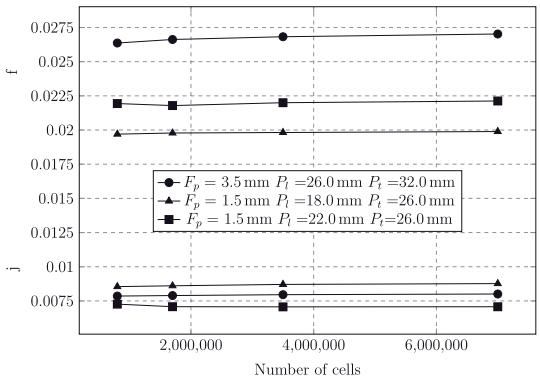

Fig. 3. Mesh sensitivity of the non-dimensional pressure drop (Fanning friction factor f) and heat transfer (Colburn j-factor j). Overall root mean square percentage error respect to the finest grid was 1.97% for 800k mesh, 1.4% for 1.7 million cell mesh and 0.79% for the 3.5 million cell mesh.

the other is the ratio of the friction power dissipated per unit surface area.

The ratio of the heat transfer rate per unit temperature, per unit area of studied heat exchanger and reference heat exchanger is shown in Eq. (6).

$$\frac{\overline{h}}{\overline{h}_R} = \frac{j}{j_R} \times \frac{(Re_{D_h}/D_h)}{(Re_{D_h}/D_h)_R} \tag{6}$$

The ratio of the friction power dissipated per unit area of studied heat exchanger and reference heat exchanger is shown in Eq. (7).

$$\frac{(P/A)}{(P/A)_R} = \frac{f}{f_R} \times \frac{(Re_{D_h}/D_h)^3}{(Re_{D_h}/D_h)^3_R} \times \frac{A_{front}}{A_{frontR}} \times \frac{A_R}{A} \tag{7}$$

Therefore, we define the JF performance ratio as

$$JF = \frac{\frac{\overline{h}}{\overline{h}_R}}{(\frac{(P/A)}{(P/A)_R})^{1/3}} = \frac{\frac{j}{j_R} \times \frac{(Re_{D_h}/D_h)}{(Re_{D_h}/D_h)_R}}{(\frac{f}{f_R} \times \frac{(Re_{D_h}/D_h)^3}{(Re_{D_h}/D_h)^3_R} \times \frac{A_{front}}{A_{frontR}} \times \frac{A_R}{A})^{1/3}} \tag{8}$$

where the A_{front} is the inlet area of the flow domain and A is the heat transfer area of the FTHE. The subscript R refers to the reference design, which is chosen as the one with P_l = 14 mm, P_t = 14 mm and F_p = 1.5 mm.

2.3. Governing equations and boundary conditions

The equations describe a steady-state, incompressible, three-dimensional flow with no sink or source terms. The governing equations that describe the conjugate heat transfer process in the fin-and-tube heat exchanger are the continuity equation in Eq. (9), momentum equation in Eq. (10) and the energy equation for fluid in Eq. (11) as well as for solid regions in Eq. (14). Turbulence is modeled with the $k-\omega$ Shear-Stress Transport (SST) model, which considers the enhanced wall treatment as default and is widely used in FTHE simulations [37–39]. The transport equation for turbulence kinetic energy is shown in Eq. (12) and for the specific turbulence dissipation rate in Eq. (13).

1. Continuity equation

$$\frac{\partial(\rho u_i)}{\partial x_i} = 0 \tag{9}$$

2. Momentum equation

$$\frac{\partial}{\partial x_i}(\rho u_i u_j) = \frac{\partial}{\partial x_i}(\mu \frac{\partial u_j}{\partial x_i}) - \frac{\partial p}{\partial x_j} \tag{10}$$

3. Energy equation for fluid region

$$\frac{\partial}{\partial x_i}(\rho C_f^p u_i T) = \frac{\partial}{\partial x_i}(\lambda_f \frac{\partial T}{\partial x_i}) \tag{11}$$

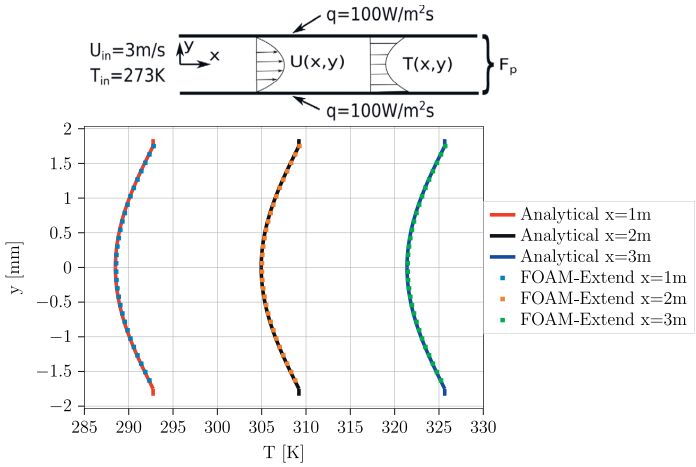

Fig. 4. Temperature profile comparison between the analytic and CFD results for laminar channel flow with conjugate heat transfer in a 2D channel flow with constant heat flux for which an analytic solution exists.

Table 1
Boundary conditions used for the computational model.

Boundary name	Boundary condition
Inlet	$u = constant, v = w = 0, T = 273$ K
Outlet	$\frac{\partial u_i}{\partial x} = \frac{\partial T}{\partial x} = 0$
Inflow and outflow regions	
Top and bottom	$\frac{\partial u}{\partial z} = \frac{\partial v}{\partial z}, w = 0, \frac{\partial T}{\partial z} = 0$
Left and right	$\frac{\partial u}{\partial y} = \frac{\partial w}{\partial y}, v = 0, \frac{\partial T}{\partial y} = 0$
Fin region	
Top and bottom	$\frac{\partial u}{\partial z} = \frac{\partial v}{\partial z}, w = 0, \frac{\partial T}{\partial z} = 0$
Left and right	Tube inner surface $u = v = w = 0, T = 333$ K Fin region $u = v = w = 0, \frac{\partial T}{\partial y} = 0$ Fluid region $\frac{\partial u}{\partial y} = \frac{\partial w}{\partial y}, \frac{\partial T}{\partial y} = 0$
Fluid–solid interface	$T_s = T_f, -\lambda_s \frac{\partial T_s}{\partial n} = -\lambda \frac{\partial T_f}{\partial n}$

4. Transport equation for the turbulence kinetic energy, k

$$\frac{\partial}{\partial x_i}(\rho k u_i) = \frac{\partial}{\partial x_j}(\Gamma_k \frac{\partial k}{\partial x_j}) + G_k \tag{12}$$

5. Transport equation for the specific turbulence dissipation rate, ω

$$\frac{\partial}{\partial x_i}(\rho \omega u_i) = \frac{\partial}{\partial x_j}(\Gamma_\omega \frac{\partial \omega}{\partial x_j}) + G_\omega \tag{13}$$

6. Energy equation for solid region

$$\frac{\partial}{\partial x_i}(\lambda_s \frac{\partial T}{\partial x_i}) = 0 \tag{14}$$

The boundary conditions used in the computational domain are defined in Table 1. Please see the locations of inlet, outlet, top, bottom, left and right boundaries in Fig. 1.

The governing equations are solved with a solver called conjugateHeatSimpleFoam from the foam-extend 4.0 [40] a community driven version of the OpenFOAM library.

3. Meshing and model validation

3.1. Parametric structured meshing

Altogether 198 simulations are carried out by varying the fin pitch and tube pattern inside the FTHE. In a parametric FTHE study, where

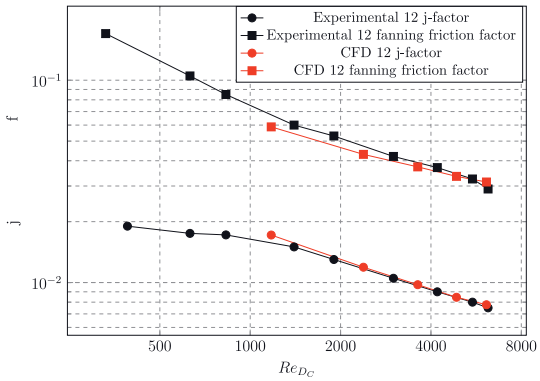

Fig. 5. Model validation by comparing the results of CFD pressure drop and heat transfer to the experimental results by Wang et al. [27].

only a few of the parameters are changed at once and rest of the design stays the same, parametric structured meshing can be superior over unstructured meshing strategies. For this purpose, a novel parametric open source meshing tool Swiftblock developed by the authors (https://swiftblock.readthedocs.io/) was used. The authors have successfully used the meshing tool in multiple different studies in the past [41–43]. The blocking strategies that were created for the plain fin FTHE are illustrated in Fig. 2. The lower two blockings for fin and air are used for cases with P_l = 14.00–22.00 mm in conjunction with P_t = 14.00–20.00 mm. The upper two figures are used for the rest of the designs.

3.2. Mesh sensitivity

As no wall function were used in the simulations, a fine mesh was used at the wall to assure accurately resolved boundary layer on the heat transfer surfaces. A y-value that translates to the average y^+-value of 0.25 was chosen with the maximum of around $y^+ = 2$ in the whole domain. Then a mesh sensitivity analysis was performed by changing the maximum cell size and keeping the y-value constant at the wall.

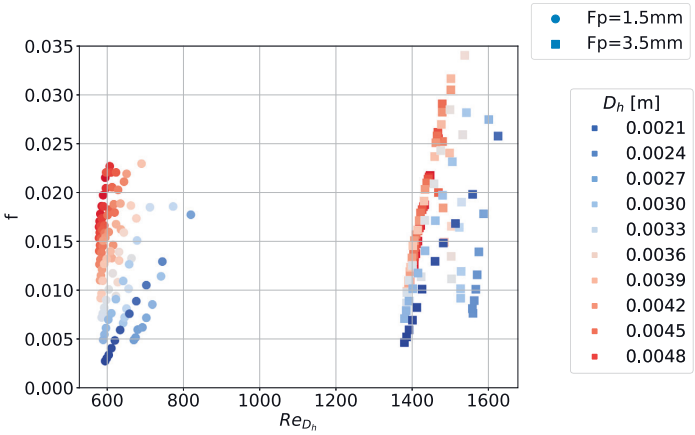

Fig. 6. Fanning friction factor observed in the present 198 simulated data points. The left cluster corresponds to the smaller fin pitch $F_p = 1.5\,\text{mm}$ while the right cluster corresponds to the larger pitch value $F_p = 3.5\,\text{mm}$. No clear difference in pressure drop can be seen between the fin pitches.

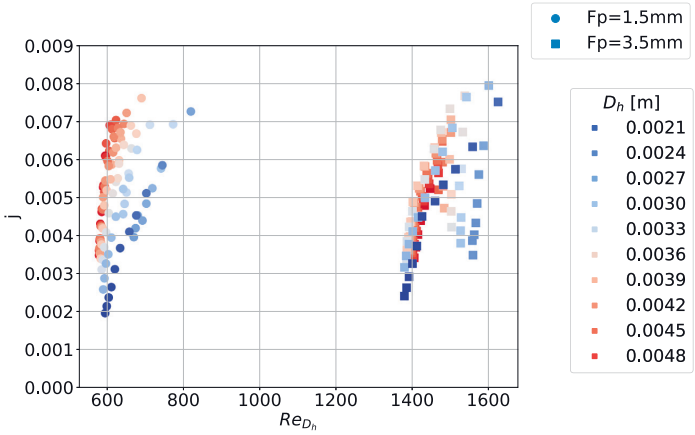

Fig. 7. Colburn j-factors observed in the present 198 simulated data points. Left cluster for smaller fin pitch $F_p = 1.5\,\text{mm}$ and right cluster for larger $F_p = 3.5\,\text{mm}$. No clear difference in heat transfer can be seen between the fin pitches.

The results are shown in Fig. 3 for pressure drop and heat transfer over the heat exchanger with the studied design variables.

Overall root mean square percentage error respect to the finest grid was 1.97% for 800 k mesh, 1.4% for 1.7 million cell mesh and 0.79% for the 3.5 million cell mesh. For a feasible trade off between computational resources and accuracy, first the data simulations for the surrogate models are made with 1.7 million cell mesh and then the maximum values are simulated with the 3.5 million cell size mesh.

3.3. Solver verification and model validation

In Fig. 4, the solver was verified by comparing the CFD results computed with foam-extend to the analytical results for conjugate heat transfer of laminar channel flow with constant heat flux boundary condition illustrated in Eq. (15) for air and for solid in Eq. (16). [44,45]

$$T_f(x,y) = T_{mi} - \frac{3q}{\kappa F_p}\left(\frac{y^4}{3F_p^2} - \frac{y^2}{2} + \frac{5F_p^2}{48}\right) + \frac{17}{70}\frac{F_p q}{\kappa} + \frac{qP}{\dot{m}C_f^p}x \tag{15}$$

$$T_s(x,y) = T_w + \frac{q}{\lambda_s}y \tag{16}$$

All the material properties used for the solver validation in this study are identical to the ones tabulated in Appendix in Table 2 and the used fin pitch was $F_p = 3.5\,\text{mm}$ and fin thickness $t = 0.2\,\text{mm}$.

In Fig. 5, the computational model is validated by comparing the results over the heat exchanger to the experimental values created by Wang et al. [27]. The compared design was the number 12 in the study with $D_c = 10.23\,\text{mm}$, $t = 0.2\,\text{mm}$, $F_p = 1.77\,\text{mm}$, $P_t = 25.4\,\text{mm}$ and $P_l = 22.0\,\text{mm}$. As opposed to all other calculations in this study, for the model validation, the fin efficiency $\eta = 0.93 - 0.85$ was excluded from the heat transfer coefficient calculation to be consistent with the experimental results [27]. All other parameters and numerical details were chosen to be identical with the ones used in this study.

Acceptable agreement was seen between the CFD and the experimental results with the root mean square error of 0.00067 (5.0%) for j-factor and 0.003 (6.4%) for friction factor. Therefore, a conclusion is made that the model can be used for the analysis of thermal-hydraulic efficiency of the FTHE.

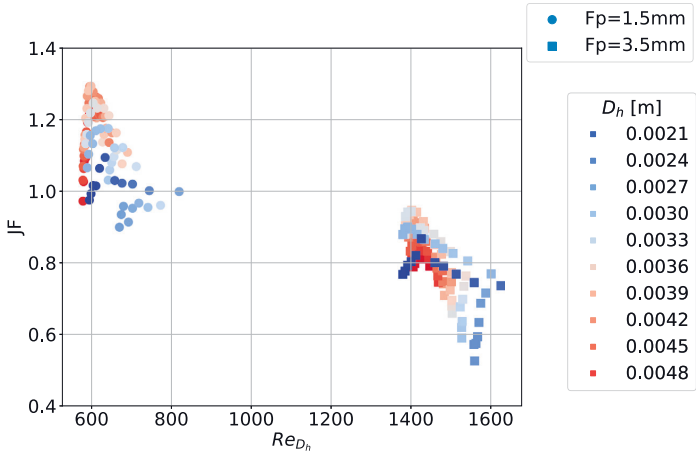

Fig. 8. JF performance ratio respect to the Reynolds number observed in the present 198 simulated data points. Left cluster represents a smaller fin pitch $F_p = 1.5\,\text{mm}$ while the right cluster the larger value $F_p = 3.5\,\text{mm}$. Left cluster clearly outperforms the right cluster in terms of the JF performance ratio.

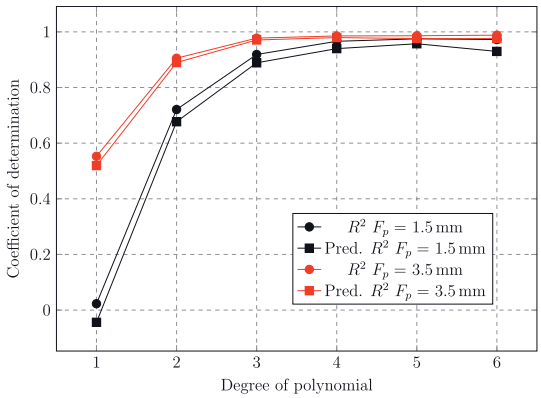

Fig. 9. Coefficient of determination R^2 and predictive R^2 with different degrees of polynomial regression models.

4. Results and discussion

4.1. Thermal-hydraulic performance of the simulated designs

In order to understand the thermal and hydraulic features of the different designs simulated in this study, all the CFD-results are first plotted as a function of the Reynolds number and colored with the hydraulic length scale $D_h = \frac{4A_{freeflow}L}{A}$. Traditionally this is the standard approach for investigating the characteristics of different FTHE designs. In fact, FTHE correlation equations are commonly based on Re_{D_h}, D_h and other physical parameters. The Fanning friction factor for all the simulated cases at different Reynolds numbers is shown in Fig. 6 (see Eq. (5)).

In Fig. 6, it is noted that friction factor values with the larger fin pitch seem to span a larger area than with the smaller fin pitch. When the coloring of the values is investigated in more detail, it can be seen that the larger hydraulic length scale values tend to accumulate in the north-east of the stack where as smaller hydraulic length scale values are seen on the south-west side of the stack. This observation applies to the bigger fin pitch as well but with a few outliers in the data. Due to the different length scales and reference velocities in each design, no clear correlation between the friction factor, Reynolds number and hydraulic length scale can be observed. The non-dimensional heat transfer parameter, the Colburn j-factor (see Eq. (4)), calculated for all cases is shown in Fig. 7 and the data points are again colored with the hydraulic length scale. Similar to the above, no clear correlation between j-factor and Reynolds number can be observed.

In order to see if the best performing tube pattern correlates with the Reynolds number or the hydraulic length scale, the JF performance ratio of the plain fin shape with all the different tube arrangement combinations calculated in this study are shown in Fig. 8. The left cluster with the smaller fin pitch $F_p = 1.5\,\text{mm}$ can be seen to clearly outperform the right cluster with the larger fin pitch $F_p = 3.5\,\text{mm}$. In other words, the larger the distance between the planar fins, and therefore larger heat transfer area, the worse the JF performance indicator for majority of the studied data points.

No similar trend can be found with the JF performance ratio and hydraulic length scale as was seen with j-factor and friction factor. As it was seen, there was no big difference between the thermal-hydraulic characteristics of the two different fin pitches, the difference in the JF performance ratio has to originate from geometric dimensions such as the inlet area and heat transfer area of the designs. Evidently, it is challenging to draw any direct conclusions on the relationship between the Reynolds number, the hydraulic length scale and the JF ratio in terms of the thermal-hydraulic performance of the different tube patterns in each fin pitch. For this reason, next a regression model is fitted on the data and visualized as a function of P_l and P_t separately for both fin pitches.

4.2. Regression model

Next, we aim at finding a polynomial regression to the data points. The benefit of such a regression model would be to find maximal JF performance ratio for a FTHE design. The regression polynomial is illustrated in Eq. (17):

$$\begin{aligned} y = {} & b_0 + b_1 P_l + b_2 P_t + b_{11} P_l^2 + b_{12} P_l P_t + b_{22} P_t^2 + b_{111} P_l^3 + b_{112} P_l^2 P_t \\ & + b_{122} P_l P_t^2 + b_{222} P_t^3 + b_{1111} P_l^4 + b_{1112} P_l^3 P_t + b_{1122} P_l^2 P_t^2 \\ & + b_{1222} P_l P_t^3 + b_{2222} P_t^4 \end{aligned} \tag{17}$$

where y is the response and b_1, b_{ii}, b_{iii}, b_{iiii}, b_{ij}, b_{iij}, b_{ijj}, b_{iiij}, b_{ijjj} and b_{ijjj} are the linear regression coefficients. The quality of the

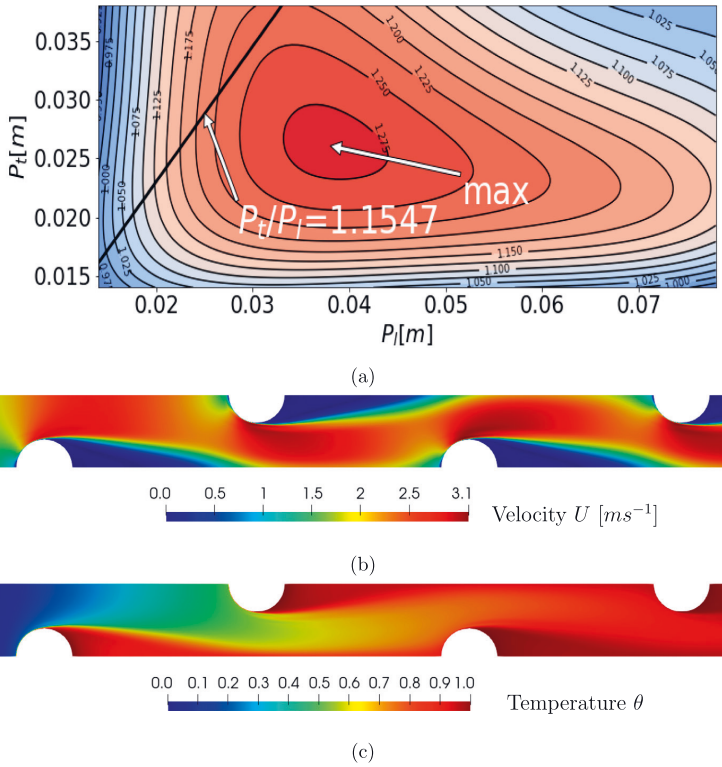

Fig. 10. (a) JF performance criteria response surface for F_p = 1.5 mm. The P_t/P_l = 1.1547 tube pattern ratio is illustrated with a black line. (b) Velocity in the middle of the channel in the design with F_p = 1.5 mm, P_l = 38.04 mm and P_t = 26.05 mm (c) Temperature in the middle of the channel in the design with F_p = 1.5 mm, P_l = 38.04 mm and P_t = 26.05 mm.

mathematical models is measured with the coefficient of determination R^2 which is the proportion of the variance in the dependent variable that is predictable from the independent variables. It is defined as

$$R^2 = 1 - \frac{SS_{res}}{SS_{tot}} \tag{18}$$

where $SS_{tot} = \sum_{n=i}(y_i - \bar{y})^2$ is the total sum of squares which is proportional to overall variance of the data and $SS_{res} = \sum_{n=i}(y_i - f_i)^2$ is the residual sum of squares. In regression, the R^2 coefficient of determination is a statistical measure of how well the regression predictions approximate the real data points. An R^2 of 1 indicates that the regression predictions perfectly fit the data. The predictive R^2 is calculated by removing each experiment separately, calculating the regression coefficients again and determining how well the model predicts the removed observation. The values of R^2 and predictive R^2 with different degrees of polynomial regression models can be seen in Fig. 9.

The 4th degree polynomial regression model was chosen and the coefficients of the model can be seen in Appendix in Table 3.

4.3. Results and discussions

The regression models are then used to visualize and locate the maximum value for the JF performance ratio for each fin pitch separately. In the present study, a sequential least squares quadratic programming (SLSQP) algorithm is used [46] to locate the maximum. SLSQP is an iterative method for constrained nonlinear optimization. In Fig. 10(a), the JF performance ratio for F_p = 1.5 mm can be seen to reach its maximum value of JF = 1.28 (j = 0.0061 , f = 0.0176). This corresponds to the longitudinal tube pitch of P_l = 38.04 mm ($3.8D_c$, $25.4F_p^{1.5\ \mathrm{mm}}$) and the traversal tube pitch of P_t = 26.05 mm ($2.6D_c$, $17.4F_p^{1.5\ \mathrm{mm}}$). The velocity and temperature fields of this design at the maximum JF performance ratio are then illustrated in Figs. 10(b) and 10(c). The temperature is non-dimensionalized according to the Eq. (19).

$$\theta = \frac{T - T_{inlet}}{T_w - T_{inlet}} \tag{19}$$

In Fig. 11(a), the JF performance ratio surface for F_p = 3.5 mm can be seen within the studied design space with the maximum value of JF = 0.94 (j = 0.0046 , f = 0.0129). This corresponds to the longitudinal tube pitch of P_l = 55.77 mm ($5.6D_c$, $15.9F_p^{3.5\ \mathrm{mm}}$) and the traversal tube pitch of P_t = 21.56 mm ($2.16D_c$, $6.16F_p^{3.5\ \mathrm{mm}}$). The velocity and temperature fields of this design in the middle of the channel are then illustrated in Figs. 11(b) and 11(c).

It can be seen that the design with the maximum JF performance ratio for the larger fin pitch has a larger longitudinal tube distance than with the one with the smaller fin pitch. On the contrary the best performing smaller fin pitch design has a larger transversal tube distance compared to the larger fin pitch. The best performing design in Figs. 10(b) and 10(c) with the smaller fin pitch has a relatively smooth velocity field with no clearly visible secondary flows that could enhance the heat transfer process. But in contrast, in the best performing design with larger fin pitch in Figs. 11(b) and 11(c), there is clearly two separate flow patterns that most likely increase the rate of heat transfer. In both design, the recirculation zone behind the tubes reaches the same level with the next tube row. It was already discussed that a smaller fin

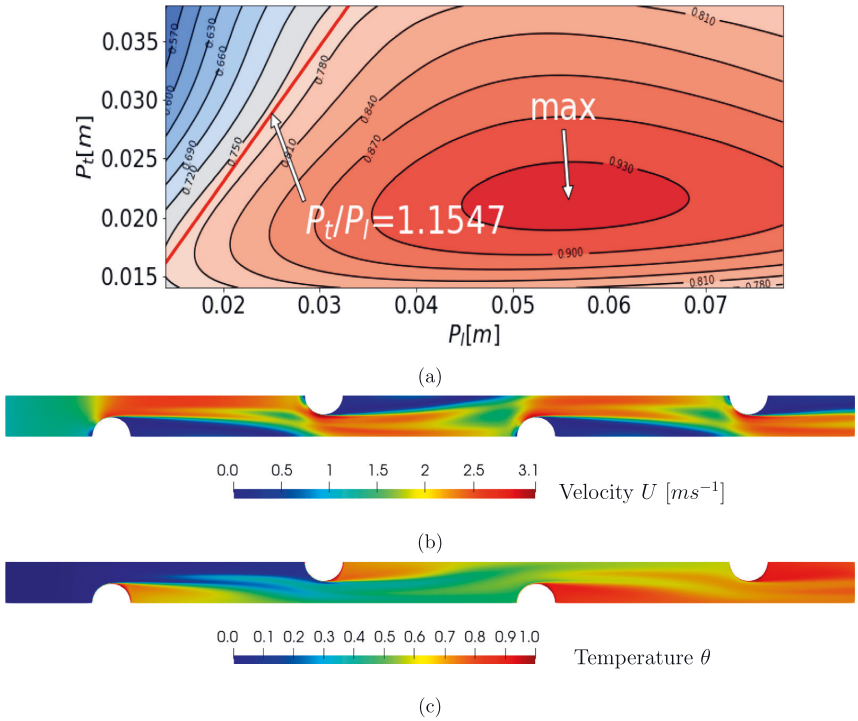

Fig. 11. (a) JF performance ratio response surface for F_p = 3.5 mm. The P_t/P_l = 1.1547 tube pattern ratio is illustrated with a red line. (b) Velocity in the middle of the channel in the design with F_p = 3.5 mm, P_l = 55.77 mm and P_t = 21.56 mm c) Temperature in the middle of the channel in the design with F_p = 3.5 mm, P_l = 55.77 mm and P_t = 21.56 mm.

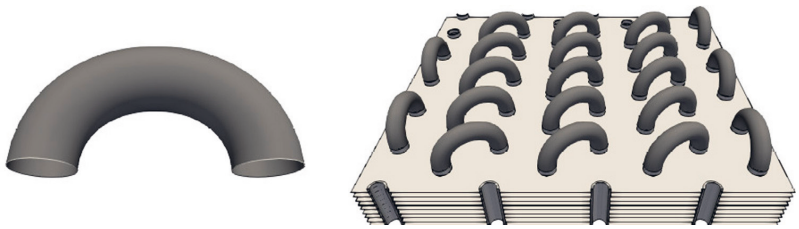

Fig. 12. Illustration of a one size U-bend in a situation where the $P_d = P_t$, therefore the same U-bend can be used to connect tubes vertically as well as tube rows horizontally to each other.

pitch enables lighter and smaller heat exchangers to be made [17]. In this study, the tube pattern with the highest performance ratio with the fin pitch of F_p = 1.5 mm can have a 36% higher JF performance ratio than the best performing tube pattern with fin pitch of F_p = 3.5 mm. This observation has a 32.6% higher j-factor and 36.4% higher friction factor.

In Figs. 10(a) and 11(a), the black and red line represents a manufacturing restriction that is widely followed in the industry. By using tube patterns that corresponds to the ratio of P_t/P_l = 1.1547, the transversal tube distance equals to the diagonal distance of the tube rows $P_t = P_d$ and therefore only one kind of U-bends can be used in the soldering process of the tube circuits. This means that the same U-bend can be used to connect tubes vertically as well as tube rows horizontally to each other as shown in Fig. 12. The values on along the line that follows the ratio of P_t/P_l = 1.1547 in two dimensional space can be found in Fig. 13.

If the FTHE is designed for an application with dry filtered air a smaller fin pitch of F_p = 1.5 mm can be used. Therefore, when the manufacturing restrictions related to the radius of the U-bends are neglected (i.e. the ratio P_t/P_l = 1.1547 is not enforced), a design with a 4% higher JF performance ratio can be achieved. The observation has a 7.6% lower j-factor and 6.0% higher friction factor. In an application with a high condensation rate, requiring a larger fin pitch of F_p = 3.5 mm, a 23% higher JF performance ratio can be achieved when deviating from the P_t/P_l = 1.1547 ratio. The unrestricted design has a 34.3% lower j-factor and 49% lower friction factor than the restricted design. The final decision of following the tube pattern ratio rule has to be made based on the extra cost related to manufacturing of two

Table 2
Thermophysical properties.

Property name	Variable	Value	Units
Fin thermal conductivity	λ_s	220	W m^{-1} K^{-1}
Air density	ρ_a	1.15	kg m^{-3}
Air Prandtl number	Pr	0.72	–
Air kinematic viscosity	ν	1.6e−5	m^{2}s^{-1}
Air heat capacity	C_f^p	1007	kg m^2 s^{-2} K^{-1}
Air thermal diffusivity	$\kappa = \rho_a C_f^p \nu / Pr$	0.025734	W m^{-1} K^{-1}

different U-bend sizes and the benefit gained by higher JF performance ratio of such heat exchangers.

With the wider fin pitch of $F_p = 3.5$ mm, there seems to be only a small difference between different tube patterns. The local maximum was seen to be $JF = 0.77$ ($j = 0.0070$, $f = 0.0253$) with $P_l = 17.58$ mm ($1.76D_c$, $5.02F_p^{3.5\ \mathrm{mm}}$) and $P_t = 20.22$ mm ($2.02D_c$, $5.78F_p^{3.5\ \mathrm{mm}}$). With the smaller fin pitch of $F_p = 1.5$ mm, there is a clear local maximum to be found at $P_l = 29.79$ mm ($2.98D_c$, $19.86F_p^{1.5\ \mathrm{mm}}$) and $P_t = 34.26$ mm ($3.43D_c$, $22.84F_p^{1.5\ \mathrm{mm}}$) with the value of JF =1.24 ($j = 0.0066$, $f = 0.0166$). Illustration of both these designs are shown in Fig. 14.

The best performing design that follows $P_t/P_l = 1.1547$ rule with the smaller fin pitch in Figs. 14(a) and 14(b) has a similar smooth velocity and temperature field with only one primary flow in the middle of the channel. This is similar to the best design without restrictions in Figs. 10(b) and 10(c). The best performing design that follows $P_t/P_l = 1.1547$ rule with the larger fin pitch in Figs. 14(c) and 14(d) in contrast has a much narrower flow path and the re-circulation zone extends much further downstream when compared to all the other best performing designs.

In a situation where the $P_t/P_l = 1.1547$ tube pattern rule is followed, the tube pattern with highest performance ratio with the smaller fin pitch $F_p = 1.5$ mm has a 61% higher JF performance ratio than with the larger fin pitch of $F_p = 3.5$ mm. The observation can be largely explained by a 5.7% reduction in j-factor and 34.4% reduction in friction factor. This is consistent with the literature although such absolute comparison has not been made before for a specific application that has a collection of design restrictions. We assume that these findings can be reproduced for each tube size independently. Only then, a comprehensive comparison can be made between the best performing tube pattern of each tube size, inlet velocity and fin pitch combination. This would enable the manufacturers of the heat exchangers to make a direct comparison between the benefits gained from only changing the tube pattern and changing both the tube size and the tube pattern.

From all the numerical data in this study, a conclusion can be made that the maximum possible performance ratio JF for plain fins with a tube diameter of $D_c = 10.00$ mm is not found in the area of the current portfolio that is manufactured in the industry and the experimental data available in the literature. Therefore, it is possible that the correlation equations that are used in the industry and are made based on the experimental data, cannot predict the performance of unorthodox tube patterns correctly. This means that by performing an optimization study based on the correlation equations, as is commonly done in the industry, it is unlikely to find the same optimal tube patterns that were shown in this study. As the amount of CFD results in the literature is increasing with a rapid pace, a similar correlation study should be performed and correlation equations should be made for computational results. This study contributes a comprehensive and systematic collection of 198 data points for the specific part of the design space with one inlet velocity of $u = 3\,\mathrm{m\,s^{-1}}$, two different fin pitches $F_p = 1.5$ mm and $F_p = 3.5$ mm, number of tube rows $N = 4$, tube diameter $D = 10.00$ mm, the fin thickness $t = 0.2$ mm and the range of longitudinal tube pitch $P_l = 14{-}78$ mm and transverse tube pitch $P_t = 14{-}38$ mm.

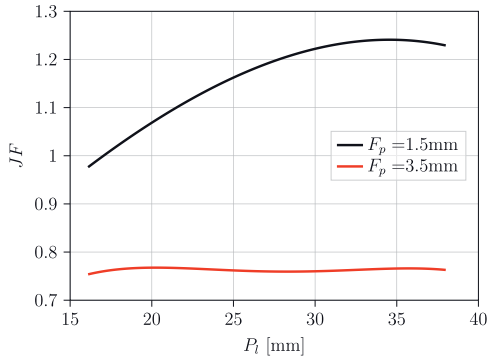

Fig. 13. JF performance ratio regression model for following the $P_t/P_l = 1.1547$ ratio.

5. Conclusions

In this study, we investigated the optimal tube arrangements for a fin-and-tube (FTHE) heat exchanger with plain fins for two application-specific fin pitches $F_p = 1.5$ mm and 3.5 mm. The smaller fin pitch represents a FTHE design for dry filtered air. In contrast, the larger fin pitch represents a typical design with high condensation rate and unfiltered air. Both cases are relevant to marine HVAC applications with a typical design inlet velocity of $u = 3\,\mathrm{m\,s^{-1}}$. The thermal-hydraulic efficiency of the FTHE design was measured by comparing the JF performance ratio of each design. The selection of different tube patterns covered longitudinal tube pitch $P_l = 14{-}78$ mm and transverse tube pitch $P_t = 14{-}38$ mm, resulting in 198 simulated designs. From this, the following conclusions are made:

1. If application-specific additional constraints, related to air with high humidity or impurities, are not applied, the smaller fin pitch $F_p = 1.5$ mm may offer 36% better JF performance ratio than the design $F_p = 3.5$ mm.
2. For unconstrained tube arrangements, the local maximum performance ratio of $JF = 1.28$ for the fin pitch $F_p = 1.5$ mm is found and for the fin pitch $F_p = 3.5$ mm the maximum performance ratio of $JF = 0.94$ can be achieved.
3. For constrained tube arrangements, $P_t/P_l = 1.1547$, the local maximum of the performance ratio is $JF = 1.24$ for the fin pitch $F_p = 1.5$ mm and for the fin pitch $F_p = 3.5$ mm the maximum performance ratio of $JF = 0.77$ can be achieved.
4. Thus, by neglecting the manufacturing restrictions related to the radius of the hairpins in the soldering process of the tube circuits, a 4% higher JF performance ratio for fin pitch $F_p = 1.5$ mm and 23% higher JF performance ratio for fin pitch $F_p = 3.5$ mm can be achieved.
5. The results indicate that unconventional tube arrangement ratio values $P_t/P_l \neq 1.1547$ may offer better performance with regard to the JF performance ratio. We propose that such values should be considered in future FTHE designs.

Regarding all the numerical data in this study, a conclusion can be made that the maximum possible performance ratio JF for plain fins with a tube diameter of $D_c = 10.00$ mm is not found in the area of the current portfolio that is manufactured in the industry. Based on the computational results presented in this study, the new tube patterns should be manufactured, measured and new improved correlation equations should be created for the industry. This could enable the industry to manufacture better performing application specific heat exchangers in the future. The results are shared as a comma-separated value (csv) file. The data should be used as a part of a data bank

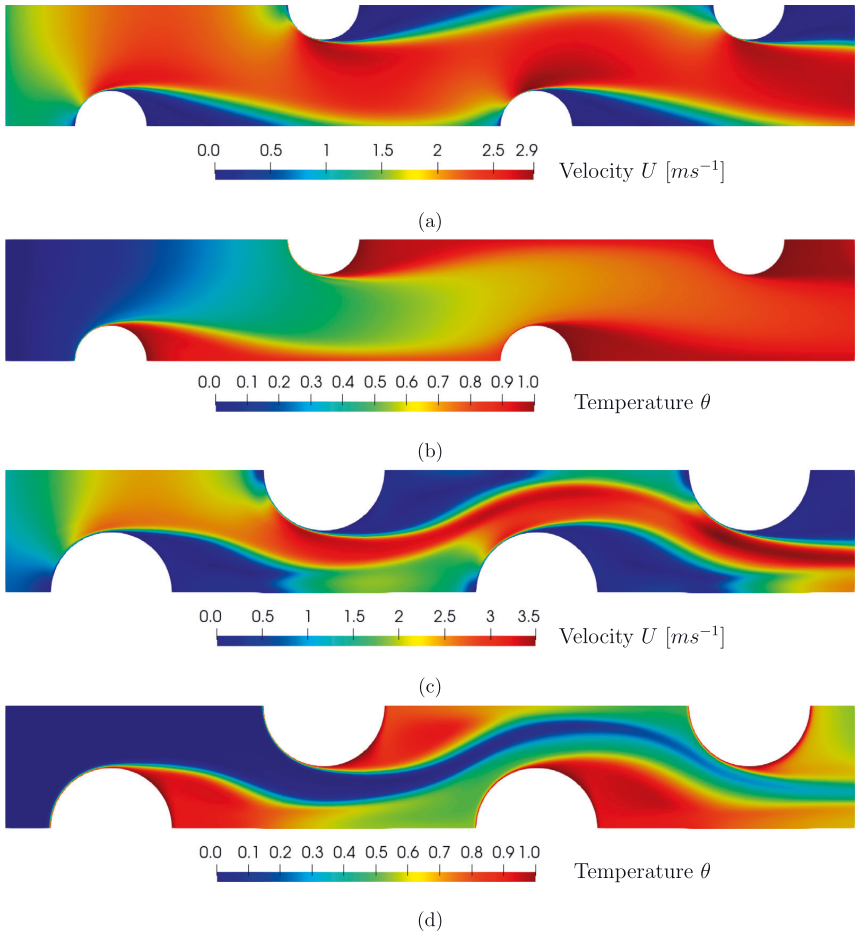

Fig. 14. (a) Velocity in the middle of the channel with F_p = 1.5 mm, P_l = 29.79 mm and P_t = 34.26 mm (b) Temperature in the middle of the channel with F_p = 1.5 mm, P_l = 29.79 mm and P_t = 34.26 mm (c) Velocity in the middle of the channel with F_p = 3.5 mm, P_l = 17.58 mm and P_t = 20.22 mm (d) Temperature in the middle of the channel with F_p = 3.5 mm, P_l = 17.58 mm and P_t = 20.22 mm.

Table 3
Coefficients and the quality indicators of the regression models.

Responses	F_p = 1.5 mm		F_p = 3.5 mm	
	Coefficient	Std err	Coefficient	Std err
b_0	0.48	0.42	−0.32	0.26
b_1	−23.69	11.10	23.19	6.98
b_2	55.12	64.87	188.13	40.79
b_{11}	−659.77	275.31	78.34	173.13
b_{12}	−6798.87	767.68	3307.57	482.75
b_{22}	−5540.69	3828.94	1240.29	2497.83
b_{111}	17077.78	3665.94	997.29	2305.33
b_{112}	72750.02	7884.42	−26166.21	4958.12
b_{122}	−125539.79	23545.95	−62106.19	14806.86
b_{222}	147477.31	99063.08	303669.22	62295.79
b_{1111}	−104797.69	19160.09	−6732.87	12048.82
b_{1112}	294342.54	40918.26	66435.03	25731.43
b_{1122}	529892.66	10540.53	261357.07	66284.12
b_{1222}	816672.01	275148.25	338885.09	173026.90
b_{2222}	1281645.61	944518.36	−2583721.16	593960.10
R^2	0.967		0.985	
Pred. R^2	0.942		0.979	

for generating more accurate surrogate models for the industry of manufacturing fin-and-tube heat exchangers.

Declaration of competing interest

The authors declare that they have no known competing financial interests or personal relationships that could have appeared to influence the work reported in this paper.

Acknowledgment

The authors wish to acknowledge CSC – IT Center for Science, Finland, for computational resources and Koja Oy, for financial support.

Appendix

See Tables 2 and 3.

References

[1] T. Cao, H. Lee, Y. Hwang, R. Radermacher, H.-H. Chun, Performance investigation of engine waste heat powered absorption cycle cooling system for shipboard applications, Appl. Therm. Eng. (ISSN: 1359-4311) 90 (2015) 820–830, http://dx.doi.org/10.1016/j.applthermaleng.2015.07.070, URL http://www.sciencedirect.com/science/article/pii/S135943111500767X.

[2] F. Baldi, F. Ahlgren, T.-V. Nguyen, M. Thern, K. Andersson, Energy and exergy analysis of a cruise ship, Energies 11 (10) (2018) 2508.

[3] G. Barone, A. Buonomano, C. Forzano, A. Palombo, M. Vicidomini, Sustainable energy design of cruise ships through dynamic simulations: Multi-objective optimization for waste heat recovery, Energy Convers. Manage. (ISSN: 0196-8904) 221 (2020) 113166, http://dx.doi.org/10.1016/j.enconman.2020.113166, URL http://www.sciencedirect.com/science/article/pii/S019689042030710X.

[4] G. Xie, Q. Wang, B. Sunden, Parametric study and multiple correlations on air-side heat transfer and friction characteristics of fin-and-tube heat exchangers with large number of large-diameter tube rows, Appl. Therm. Eng. (ISSN: 1359-4311) 29 (1) (2009) 1–16, http://dx.doi.org/10.1016/j.applthermaleng.2008.01.014, URL https://www.sciencedirect.com/science/article/pii/S135943110800029X.

[5] R. Borrajo-Pelaez, J. Ortega-Casanova, J. Cejudo-Lopez, A three-dimensional numerical study and comparison between the air side model and the air/water side model of a plain fin-and-tube heat exchanger, Appl. Therm. Eng. (ISSN: 1359-4311) 30 (13) (2010) 1608–1615, http://dx.doi.org/10.1016/j.applthermaleng.2010.03.018, URL https://www.sciencedirect.com/science/article/pii/S1359431110001286.

[6] C.-T. Hsieh, J.-Y. Jang, Parametric study and optimization of louver finned-tube heat exchangers by taguchi method, Appl. Therm. Eng. (ISSN: 1359-4311) 42 (2012) 101–110, http://dx.doi.org/10.1016/j.applthermaleng.2012.03.003, Heat Powered Cycles Conference, 2009. URL https://www.sciencedirect.com/science/article/pii/S1359431112001585.

[7] A.A. Bhuiyan, M.R. Amin, A.S. Islam, Three-dimensional performance analysis of plain fin tube heat exchangers in transitional regime, Appl. Therm. Eng. (ISSN: 1359-4311) 50 (1) (2013) 445–454, http://dx.doi.org/10.1016/j.applthermaleng.2012.07.034, URL https://www.sciencedirect.com/science/article/pii/S1359431112005169.

[8] R. Yun, Y. Kim, Y. Kim, Air side heat transfer characteristics of plate finned tube heat exchangers with slit fin configuration under wet conditions, Appl. Therm. Eng. (ISSN: 1359-4311) 29 (14) (2009) 3014–3020, http://dx.doi.org/10.1016/j.applthermaleng.2009.03.017, URL https://www.sciencedirect.com/science/article/pii/S1359431109000994.

[9] W. Ding, J. Fan, Y. He, W. Tao, Y. Zheng, Y. Gao, J. Song, A general simulation model for performance prediction of plate fin-and-tube heat exchanger with complex circuit configuration, Appl. Therm. Eng. (ISSN: 1359-4311) 31 (16) (2011) 3106–3116, http://dx.doi.org/10.1016/j.applthermaleng.2011.01.045, URL https://www.sciencedirect.com/science/article/pii/S1359431111000706.

[10] J. Wu, W. Tao, Investigation on laminar convection heat transfer in fin-and-tube heat exchanger in aligned arrangement with longitudinal vortex generator from the viewpoint of field synergy principle, Appl. Therm. Eng. (ISSN: 1359-4311) 27 (14) (2007) 2609–2617, http://dx.doi.org/10.1016/j.applthermaleng.2007.01.025, URL https://www.sciencedirect.com/science/article/pii/S1359431107000488.

[11] M. Li, H. Zhang, J. Zhang, Y. Mu, E. Tian, D. Dan, X. Zhang, W. Tao, Experimental and numerical study and comparison of performance for wavy fin and a plain fin with radiantly arranged winglets around each tube in fin-and-tube heat exchangers, Appl. Therm. Eng. (ISSN: 1359-4311) 133 (2018) 298–307, http://dx.doi.org/10.1016/j.applthermaleng.2018.01.012.

[12] C.-C. Wang, K.-Y. Chi, C.-J. Chang, Heat transfer and friction characteristics of plain fin-and-tube heat exchangers, part II: Correlation, Int. J. Heat Mass Transfer (ISSN: 0017-9310) 43 (15) (2000) 2693–2700, http://dx.doi.org/10.1016/S0017-9310(99)00333-6.

[13] C.-C. Wang, K.-Y. Chi, C.-J. Chang, Heat transfer and friction characteristics of plain fin-and-tube heat exchangers, part II: Correlation, Int. J. Heat Mass Transfer 43 (15) (2000) 2693–2700.

[14] C.-C. Wang, Y.-J. Chang, Y.-C. Hsieh, Y.-T. Lin, Sensible heat and friction characteristics of plate fin-and-tube heat exchangers having plane fins, Int. J. Refrig. 19 (4) (1996) 223–230.

[15] C.-C. Wang, Y.-M. Hwang, Y.-T. Lin, Empirical correlations for heat transfer and flow friction characteristics of herringbone wavy fin-and-tube heat exchangers, Int. J. Refrig. 25 (5) (2002) 673–680.

[16] C.-C. Wang, W.-S. Lee, W.-J. Sheu, A comparative study of compact enhanced fin-and-tube heat exchangers, Int. J. Heat Mass Transfer 44 (18) (2001) 3565–3573.

[17] B. Ameel, J. Degroote, H. Huisseune, J. Vierendeels, M.D. Paepe, Interaction effects between parameters in a vortex generator and louvered fin compact heat exchanger, Int. J. Heat Mass Transfer (ISSN: 0017-9310) 77 (2014) 247–256, http://dx.doi.org/10.1016/j.ijheatmasstransfer.2014.04.073, URL http://www.sciencedirect.com/science/article/pii/S0017931014003913.

[18] C.-C. Wang, Y.-J. Du, Y.-J. Chang, W.-H. Tao, Airside performance of herringbone fin-and-tube heat exchangers in wet conditions, Can. J. Chem. Eng. 77 (6) (1999) 1225–1230.

[19] J.A. Siegel, W.W. Nazaroff, Predicting particle deposition on HVAC heat exchangers, Atmos. Environ. (ISSN: 1352-2310) 37 (39) (2003) 5587–5596, http://dx.doi.org/10.1016/j.atmosenv.2003.09.033, Indoor Air Chemistry and Physics: Papers from Indoor Air 2002.

[20] Y. Xia, Y. Zhong, P. Hrnjak, A. Jacobi, Frost, defrost, and refrost and its impact on the air-side thermal-hydraulic performance of louvered-fin, flat-tube heat exchangers, Int. J. Refrig. (ISSN: 0140-7007) 29 (7) (2006) 1066–1079, http://dx.doi.org/10.1016/j.ijrefrig.2006.03.005, URL http://www.sciencedirect.com/science/article/pii/S0140700706000648.

[21] C.-C. Wang, C.-J. Lee, C.-T. Chang, Y.-J. Chang, Some aspects of plate fin-and-tube heat exchangers: with and without louvers, J. Enhanc. Heat Transf. 6 (5) (1999).

[22] C.-C. Wang, J.-Y. Chang, N.-F. Chiou, Effects of waffle height on the air-side performance of wavy fin-and-tube heat exchangers, Heat Transf. Eng. 20 (3) (1999) 45–56.

[23] D.G. Rich, The effect of fin spacing on the heat transfer and friction performance of multi-row, smooth plate fin-and-tube heat exchangers, AsHRAE Trans. 79 (2) (1973) 135–145.

[24] D.G. Rich, The effect of the number of tube rows on heat transfer performance of smooth plate fin-and-tube heat exchangers, 1975, Unknown.

[25] Y. Seshimo, M. Fujii, An experimental study on the performance of plate fin and tube heat exchangers at low Reynolds numbers, in: Proceedings of the 1991 ASME JSME Thermal Engineering Joint Conference, 1991, pp. 673–680.

[26] M.-Y. Wen, C.-Y. Ho, Heat-transfer enhancement in fin-and-tube heat exchanger with improved fin design, Appl. Therm. Eng. (ISSN: 1359-4311) 29 (5) (2009) 1050–1057, http://dx.doi.org/10.1016/j.applthermaleng.2008.05.019, URL https://www.sciencedirect.com/science/article/pii/S1359431108002457.

[27] C.-C. Wang, Y.-J. Chang, Y.-C. Hsieh, Y.-T. Lin, Sensible heat and friction characteristics of plate fin-and-tube heat exchangers having plane fins, Int. J. Refrig. 19 (4) (1996) 223–230.

[28] C. Luo, S. Wu, K. Song, L. Hua, L. Wang, Thermo-hydraulic performance optimization of wavy fin heat exchanger by combining delta winglet vortex generators, Appl. Therm. Eng. (ISSN: 1359-4311) 163 (2019) 114343, http://dx.doi.org/10.1016/j.applthermaleng.2019.114343, URL https://www.sciencedirect.com/science/article/pii/S1359431119322781.

[29] G. C., Transport Processes and Separation Process Principles (Includes Unit Operations), Prentice Hall Press, 2003.

[30] W.M. Kays, A.L. London, Compact Heat Exchangers, Vol. 196, McGraw-Hill New York, 1958.

[31] R.L. Webb, N. Kim, Enhanced Heat Transfer, Taylor and Francis, NY, 2005.

[32] A. London, C. Ferguson, Test results of high-performance heat exchanger surfaces used in aircraft intercoolers and their significance for gas-turbine regenerator design, Trans. ASME 71 (1949) 17–26.

[33] R.K. Shah, A.L. London, Flow Forced Convection Heat Transfer and Flow Friction in Straight and Curved Ducts - A Summary of Analytical Solutions, Vol. 1, No. 1, Academic Press, ISBN: 1483191303, 1972, p. 311.

[34] K. Stone, Review of Literature on Heat Transfer Enhancement in Compact Heat Exchangers, Tech. Rep., Air Conditioning and Refrigeration Center. College of Engineering, 1996.

[35] B. Shi, L. Wang, F. Gen, Y. Zhang, The optimal fin spacing for three-row flat tube bank fin mounted with vortex generators, Heat Mass Transf. 43 (1) (2006) 91–101.

[36] J.-Y. Yun, K.-S. Lee, Influence of design parameters on the heat transfer and flow friction characteristics of the heat exchanger with slit fins, Int. J. Heat Mass Transfer 43 (14) (2000) 2529–2539.

[37] L.O. Salviano, D.J. Dezan, J.I. Yanagihara, Optimization of winglet-type vortex generator positions and angles in plate-fin compact heat exchanger: Response Surface Methodology and Direct Optimization, Int. J. Heat Mass Transfer (ISSN: 0017-9310) 82 (2015) 373–387, http://dx.doi.org/10.1016/j.ijheatmasstransfer.2014.10.072, URL https://www.sciencedirect.com/science/article/pii/S0017931014009727.

[38] L.O. Salviano, D.J. Dezan, J.I. Yanagihara, Thermal-hydraulic performance optimization of inline and staggered fin-tube compact heat exchangers applying longitudinal vortex generators, Appl. Therm. Eng. (ISSN: 1359-4311) 95 (2016) 311–329, http://dx.doi.org/10.1016/j.applthermaleng.2015.11.069, URL https://www.sciencedirect.com/science/article/pii/S1359431115013150.

[39] M.F. Md Salleh, H.A. Mohammed, M.A. Wahid, Thermal and hydraulic characteristics of trapezoidal winglet across fin-and-tube heat exchanger (FTHE), Appl. Therm. Eng. (ISSN: 1359-4311) 149 (2019) 1379–1393, http://dx.doi.org/10.1016/j.applthermaleng.2018.12.098, URL https://www.sciencedirect.com/science/article/pii/S1359431118358034.

[40] FOAM-extend, FOAM-extend, 2017, URL http://foam-extend.org/.

[41] T. Välikangas, R. Karvinen, Conjugated heat transfer simulation of a fin-and-tube heat exchanger, Heat Transf. Eng. 39 (13–14) (2018) 1192–1200.

[42] T. Välikangas, S. Singh, K. Sørensen, T. Condra, Fin-and-tube heat exchanger enhancement with a combined herringbone and vortex generator design, Int. J. Heat Mass Transfer (ISSN: 0017-9310) 118 (2018) 602–616, http://dx.doi.org/10.1016/j.ijheatmasstransfer.2017.11.006.

[43] T. Välikangas, J. Hærvig, H. Kuuluvainen, M.D. Maso, P. Peltonen, V. Vuorinen, Deposition of dry particles on a fin-and-tube heat exchanger by a coupled soft-sphere DEM and CFD, Int. J. Heat Mass Transfer (ISSN: 0017-9310) 149 (2020) 119046, http://dx.doi.org/10.1016/j.ijheatmasstransfer.2019.119046.

[44] T.L. Bergman, F.P. Incropera, D.P. DeWitt, A.S. Lavine, Fundamentals of Heat and Mass Transfer, John Wiley & Sons, 2011.

[45] S. Patankar, C. Liu, E.M. Sparrow, Fully developed flow and heat transfer in ducts having streamwise-periodic variations of cross-sectional area, J. Heat Transfer (1977).

[46] C.T. Lawrence, A.L. Tits, A computationally efficient feasible sequential quadratic programming algorithm, SIAM J. Optim. 11 (4) (2001) 1092–1118.

Publication 4

Välikangas T., Hærvig J., Kuuluvainen H., Dal Maso M., Peltonen P. and Vuorinen V. (2020). Deposition of dry particles on a fin-and-tube heat exchanger by a coupled soft-sphere DEM and CFD. *International Journal of Heat and Mass Transfer*, vol. 149, pp. 119046, DOI: 10.1016/j.ijheatmasstransfer.2019.119046

International Journal of Heat and Mass Transfer 149 (2020) 119046

Contents lists available at ScienceDirect

International Journal of Heat and Mass Transfer

journal homepage: www.elsevier.com/locate/hmt

Deposition of dry particles on a fin-and-tube heat exchanger by a coupled soft-sphere DEM and CFD

Turo Välikangas[a,*], Jakob Hærvig[c], Heino Kuuluvainen[a], Miikka Dal Maso[a], Petteri Peltonen[b], Ville Vuorinen[b]

[a] Aerosol Physics Laboratory, Physics Unit, Tampere University, Finland
[b] Department of Mechanical Engineering, Aalto University, Finland
[c] Department of Energy Technology, Aalborg University, Denmark

ARTICLE INFO

Article history:
Received 26 August 2019
Revised 24 October 2019
Accepted 12 November 2019
Available online 21 November 2019

Keywords:
Fin-and-tube heat exchanger
Herringbone fin
Plain fin
CFD-DEM
Soft sphere
Dry-particle
Fouling
Large-eddy simulation

ABSTRACT

In this study, a novel computational model is utilized for investigating fouling of two commonly encountered heat exchanger fin shapes in an air-conditioning application. The computational method utilizes the discrete element method (DEM) coupled with a large-eddy simulation (LES) framework. The fin-and-tube heat exchangers (FTHE) are investigated for three different Reynolds numbers (Re_{D_h} =243, 528, 793), three different particle sizes (D_p = 5, 10, 20 μm) and two different adhesive particle types based on the experimental values in the literature. The code is first benchmarked from the CFD and DEM viewpoints. A comprehensive fouling study of the FTHE's, consisting of altogether 36 simulations, is then carried out. The major numerical findings of the paper consist of the following four features. First, with low adhesive particles, the plain fin shape has a 3.45 higher volume fouling rate with Re_{D_h} =793 than at Re_{D_h} =264. With the herringbone fin shape, and the low adhesive particles, the volume fouling rate is 1.76 higher with Re_{D_h} =793 than at Re_{D_h} =264. Second, for the high adhesive particles, the plain fin has a 5.4 times higher volume fouling rate at Re_{D_h} =793 than for Re_{D_h} =264. The herringbone fin shape has a 3.92 times higher volume fouling rate with the highest Reynolds number of Re_{D_h} =793 compared to Re_{D_h} =264. Third, high adhesive particles have 3.0 times higher volume fouling rate than low adhesive particles for both fin shapes, all particle sizes and all Reynolds numbers combined. And finally, herringbone fins have 1.74 times higher volume fouling rate than plain fins for low adhesive particles. For high adhesive particles, herringbone has 1.8 times higher volume fouling rate and when both particle types are summed together, herringbone has a 1.78 times higher volume fouling rate than the plain fin shape. As a major finding of the study, the high adhesive particle collection efficiency increases monotonously with the Stokes and Reynolds numbers while low adhesive particle collection efficiency poses a non-monotonous trend.

1. Introduction

Globally around 10 – 20% of the energy consumption in developed countries is used by the Heating Ventilation and Air Conditioning (HVAC) systems of buildings [1]. Almost half of the total energy consumption in buildings is due to air conditioning [1]. Commonly used type of a heat exchanger in the air conditioning unit is a Fin-and-Tube Heat Exchanger (FTHE). Inside the FTHE, heat is exchanged between the flowing air between the fins and the fluid flow in the tubes. The efficiency of a heat exchanger is defined as the ratio between the exchanged heat and the induced pressure drop [2]. Considering the complete heat transfer process, around 60 – 80% of the resistance has shown to be on the air side [3,4]. The most traditional design of a FTHE with plain fins [5,6] can be made smaller by making the fin wavy [7–9]. In this way, smaller heat exchangers could be designed. Later, as enabled by louvered [10] and slit [11] fins even more compact heat exchangers have been made for various different air conditioning applications. Quite recently, vortex generators [12,13] including winglet type flow actuators [14] have been proposed for enhancing heat transfer. Most of the previous CFD studies are conducted with ideal air without impurities. Therefore, new designs obtained with CFD are only valid for a new heat exchanger for a short period of time.

After long term operation, air impurities begin to accumulate inside the heat exchanger [15–17], commonly denoted fouling.

* I am corresponding author.
E-mail addresses: turo.valikangas@tuni.fi (T. Välikangas), jah@et.aau.dk (J. Hærvig), heino.kuuluvainen@tuni.fi (H. Kuuluvainen), miikka.dalmaso@tuni.fi (M. Dal Maso), petteri.peltonen@aalto.fi (P. Peltonen), ville.vuorinen@aalto.fi (V. Vuorinen).

https://doi.org/10.1016/j.ijheatmasstransfer.2019.119046
0017-9310/

Nomenclature

Symbols

$\mathbf{u}$	Fluid velocity, ms^{-1}
A_{inlet}	Area of the inlet boundary
$A_{\min}$	Area of the minimum cross section inside the heat exchanger
R_{pf}	local fluid volume fraction, m
u	Velocity, ms^{-1}
U_{inlet}	Inlet flow velocity
$U_{max,\ avg}$	Maximum average flow velocity
V	Volume of the cell, ms^3
v	Particle velocity, ms^{-1}
x	Cartesian location, m
a	Contact area, m^2
C	Collection efficiency
D_{h}	Hydraulic diameter, mm
E	Young's modulus, Pa
F_{number}	Number fouling rate
F_{volume}	Volume fouling rate
$F_{\mathrm{i,fluid}}$	Particle force, N
n	Surface normal vector
R	Effective particle radius, m
S_n	Material properties parameter for normal direction
S_t	Material properties parameter for tangential direction
w	Adhesion work

Greek symbols

α_f	Local fluid volume fraction, -
μ	Dynamic viscosity of air, $kgm^{-1}s^{-1}$
μ_{sgs}	Eddy viscosity, $kgm^{-1}s^{-1}$
ρ_f	Density of fluid, kgm^{-3}
β	Coefficient restitution parameter
ν	Poisson's ratio

Such fouling processes can be classified into wet and dry particulate fouling. The present work focuses on the dry particulate fouling. Dry particulate fouling process can be further divided into the nucleate and bulk fouling regimes [18]. Every fouling process will initially start with the nucleation regime where particles accumulate on the surface and form a deposition distribution. Later on, once the surfaces have been initially deposited by particles, the nucleation regime transitions typically towards the bulk fouling regime. At this stage the induced pressure drop from fouling is at its maximum in a specific operation point.

In HVAC applications, typical substances that contribute to fouling are dust and fibres that can originate from clothes, furniture and fur of domestic animals [19]. Fouling in dry FTHE environments occurs mainly in the flow stagnation and recirculation regions [20]. Li et al. [21] propose that both particle size, shape and properties are important factors in the fouling process. While fouling of larger particles is dominated by inertial impact, smaller particles deposit by eddy transport and thermophoresis [22]. Due to the rather low temperature gradients in HVAC systems, thermophoresis is often negligible as one of the fouling mechanisms [23].

The challenges of studying FTHE by analytical and empirical means was pointed out by Siegel and Nazaroff [24]. They present a deterministic model for FTHE fouling with particle impaction, gravitational settling and Brownian diffusion. The authors pointed out deficiencies in the model for particles in the range of 5–20 µm scale particles having rather large initial velocity [24]. Another computational model by Inamdar et al. [25] was compared against the experimental results. The model was shown to predict the fouling trends in various different heat exchangers to an acceptable precision along with a qualitative estimation of the deposition distribution.

Experimental application field studies have been conducted to study the effect of the real fouling environment and the effect of fouling on the thermal hydraulic efficiency of the FTHE. Ahn et al. [19] showed that, in residential buildings, the mean fouling particle diameters typically range between 1–20 µm. In their study, they concluded that after 7 years, in both dry and wet cycle heat exchanger, the fouling can cause the pressure drop over the heat exchanger to increase up to 44% while the cooling capacity decreases $10-15\%$ [19]. Another study by Park et al. [26] shows that dry particle fouling causes $4-12\%$ decrease in heat transfer coefficient whereas, the pressure drop increases by $22-37\%$.

Above, FTHE's in HVAC context was discussed. Another branch of FTHE fouling investigations is related to heat recovery boilers. In such applications, the heat exchangers are exposed to ash and particulates originating from combustion processes. [27–30]. The properties of the fouling particles in combustion fumes obviously differ drastically from the normal indoor fouling particle properties. The effect of fouling have been experimentally studied in the laboratory environment with various different standard dust types by various authors. An experimental study by Zhang et al. [31] for air conditioning application, concluded that interrupted louvre fin shapes are more prone to fouling in a microchannel design than a planar fin. One of their main conclusions was that the interior of the heat exchanger with louvre fin is more vulnerable to fouling, whereas with the plain fin, the fouling occurs in the front surfaces. They emphasized that the type of the fin plays a prominent role in the fouling characteristics of the heat exchanger [31]. The microchannel heat exchanger and dry coolers were studied by Bell et al. [32,33], who concluded an increase of up to 50% due to fouling on the pressure drop on the air side. Zhan et al. [34] studied the wavy fin-and-tube heat exchanger and concluded that areas that are most prone to fouling are the leading edge of the fins and the front part of the tubes. A very recent experimental study by Zhan et al. [18] investigated the fouling mechanism of wet-particle deposition and concluded that louvered fins are the most conducive to wet-particle deposition. They also pointed out that dry-particle and wet-particle fouling share several similarities. Yet, the fouling rate in dehumidifying conditions can be a factor of 5 to 7 times higher than the dry particle environment.

The numerical fouling studies conducted on an air conditioning application are very few. Zhan et al. [35] studied the bulk regime fouling with 50 µm particles with Reynolds–Averaged Navier–Stokes flow simulation and developed a model for the fouling thickness. The effect of particles sizes on the deposition areas on a metal foam heat exchanger has been studied by Sauret and Hooman [36] in laminar conditions. Kuruneru et al. [37] has developed and validated a CFD-DEM model to study fouling of a metal foam heat exhchanger. Kuruneru et al. [38] studied the fouling bulk regime of 25 µm particles in an oscillating unsteady laminar flow and made a comparison study between sawdust and sandstone type particles [39] in the metal foam heat exchanger. Kuruneru et al. [40] also studied fouling with 50 µm and with very low inlet velocity of around $0.1m/s$, which is very rarely encountered in HVAC application. All these studies focus on the bulk regime fouling for a very simple tube bank geometry with surrounding metal foam porous area.

Based on the literature survey, fouling of the heat transfer surfaces is an important concern in heat exchanger design. There is a clear research gap for better understanding FTHE fouling processes by simulations which, not only model the fluid flow by CFD, but also model the particle phase and the particle-surface interactions. The main objectives of the present study are listed as follows. First,

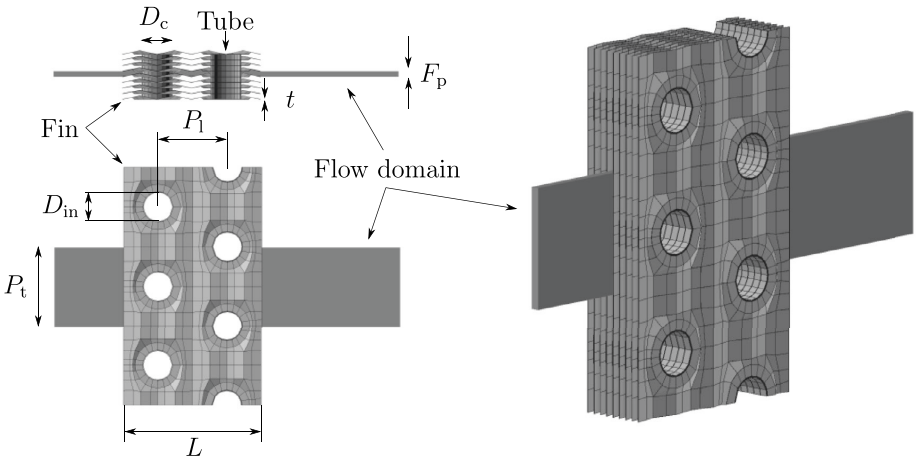

Fig. 1. Illustration of the fin-and-tube heat exchanger geometry being simulated.

a CFD-DEM model is benchmarked to model fouling processes in heat exchangers. Second, two different fin shapes with three different particle sizes, 3 typical inlet velocities and two different particle adhesive types are simulated to illustrate and to quantify, via a pioneering research approach, the fouling rate in the nucleation regime of the heat transfer surfaces. The first fin shape is a plain fin without fin forming. The other, very common fin shape used in the industry, is called the herringbone. The overall motivation is to find quantitative results, which can be used to asses the amount of fouling between the different fin shapes. Thereby, in larger scope, the study demonstrates a next level approach to develop enhanced heat transfer surfaces with lower pressure drop and higher heat transfer rates.

2. Details on the numerical domain and setup

The geometry in the present study is widely used in HVAC industry and has been studied by others as well Chokeman and Wongwises [9], Pirompugd et al. [41]. Two fin types are studied to illustrate the geometry effects on the fouling characteristics.

2.1. Computational domain

The computational domain is limited to one channel between the fins. The simulation domain is shown in Fig. 1 for the herringbone fins. For the plain fins, the geometry is otherwise exactly the same.

The inlet is placed a distance of P_l upstream from the heat exchanger geometry to make sure the deposition process is independent of the inlet position. Similarly, the outlet is placed $2P_l$ downstream of the heat exchanger geometry. Further details on the geometries are provided in Table 1.

Throughout this study, the hydraulic diameter is used as a characteristic length scale of the flow. The hydraulic diameter is defined as:

$$D_h = \frac{4 \cdot \text{free flow volume}}{\text{wetted area}} = \frac{4 \cdot \text{free flow area} \cdot \text{depth of the FTHE}}{\text{fin surface area} + \text{tube surface area}} = \frac{4(F_h)(P_t - D_c)(2P_l)}{(4P_lP_t - 4\pi(\frac{D_c}{2})^2) + ((F_h)2\pi D_c)} = 2.28 \quad \text{mm} \tag{1}$$

Table 1
Geometric dimensions for herringbone and plain fin shape.

Parameter	Symbol/unit	Value
Outside diameter of tube collar	D_c	9.76 mm
Longitudinal tube distance	P_l	22.0 mm
Transverse tube distance	P_t	25.4 mm
Number of tube row	n	2
Fin length along flow direction	L	44.0 mm
Fin pitch	F_p	1.81 mm
Fin thickness	t	0.115 mm
Herringbone amplitude	P_d	1.19 mm
Herringbone half wave length	X_f	5.5 mm

where the flow is in a channel with the length $L = 2P_l = 44$ mm, height $F_h = F_p - t = 1.695$ mm and width $P_t = 25.4$ mm. In the normal direction of the fin, a staggered tube array is penetrated through the fin pack with the diameter of $D_c = 9.76$ mm, longitudinal tube pitch $P_l = 22$ mm and transverse tube pitch $P_t = 25.4$ mm. In this type of a flow, the flow length scale can be calculated as shown in Eq. [1]. The geometry details are shown in Table 1. The reference velocity used in this study is the average flow velocity at the minimum cross sectional area calculated as $U_{max,avg} = U_{inlet}\frac{A_{inlet}}{A_{min}}$, where $U_{max,avg}$ is the maximum average flow velocity, U_{inlet} is the inlet flow velocity, A_{inlet} is the area of the inlet boundary and A_{min} is the area of the minimum cross section inside the heat exchanger.

In the present study, we use the no-slip boundary condition for velocity at the solid boundaries. Respectively, for pressure the zero gradient boundary condition is utilized at the walls. At the inlet of the domain, constant velocity is prescribed while the zero gradient boundary condition is used at the outlet. At the lateral boundaries, periodic boundary conditions are used. The pressure is fixed at the outlet and assumed zero gradient at the inlet.

2.2. Governing equations for fluid flow

The governing equations for three-dimensional, incompressible, transient viscous flow with two-way coupling between the particle phase and the fluid through the heat exchanger are the continuity

(2) and the momentum equations (3).

$$\frac{\partial(\alpha_{\mathrm{f}}\overline{u}_{\mathrm{i}})}{\partial x_{\mathrm{i}}} = 0 \tag{2}$$

$$\frac{\partial(\alpha_{\mathrm{f}}\overline{u}_{\mathrm{i}})}{\partial t} + \frac{\partial(\alpha_{\mathrm{f}}\overline{u}_{\mathrm{i}}\overline{u}_{\mathrm{j}})}{\partial x_{\mathrm{j}}} + = -\frac{\alpha_{\mathrm{f}}}{\rho_{\mathrm{f}}}\frac{\partial \overline{p}}{\partial x_{\mathrm{i}}} + \alpha_{\mathrm{f}}\frac{\partial}{\partial x_{\mathrm{j}}}((\nu + \nu_{\mathrm{sgs}})\frac{\partial \overline{u}_{\mathrm{i}}}{\partial x_{\mathrm{j}}}) - \frac{R_{\mathrm{pf}}}{\rho_{\mathrm{f}}} \tag{3}$$

where α_{f} is the local fluid volume fraction, $R_{\mathrm{pf}} = K_{\mathrm{pf}}(\mathbf{u} - \langle v \rangle)$ is the momentum exchanger with the particle phase. For the momentum exchange between the domains an implicit second-order accurate Crank–Nicolson scheme is used. The source of the momentum equation is the sum of the local particle-fluid forces ($F_{\mathrm{i,fluid}}$)

$$K_{\mathrm{pf}} = \frac{\alpha_{\mathrm{f}}|\sum_{\mathrm{i}} \mathbf{F}_{\mathrm{i,fluid}}|}{V|\mathbf{u} - \langle v \rangle|}. \tag{4}$$

In practice, the studied particle volume concentrations are in the order of $\phi = 5 \times 10^{-5}$, which corresponds to the 1-way coupling regime [42]. R_{pf} is small compared to the other terms and is neglected in the present study resulting in a 1-way coupling.

The governing equations are discretized by using a finite volume method and spatial terms are discretized by a second order accurate discretization scheme. The PISO (Pressure-Implicit with Splitting of Operators) [43] algorithm is used to couple the pressure and velocity fields. The CFD-DEM simulations are carried out with the open-source CFD-DEM solver called CFDEM (version 3.8.0) [44], which combines the CFD (version 5.0) toolbox OpenFOAM [45] with the DEM solver LIGGGHTS [46].

For accurate prediction of the trajectory calculation for the deposited particles, it is important to solve the flow field and the turbulence quantities correctly [20]. Because the particles are influenced by the largest, energy containing turbulent eddies throughout the flow, the larger eddies are resolved but the smaller ones are modelled. Such an approach is called Large Eddy Simulation (LES), where only the smallest scales of the turbulence structures are modelled while the larger scales are resolved directly. The subgrid scale viscosity ν_{sgs} in this study is modelled by using a Wall-Adapting Local Eddy-viscosity (WALE) model with default parameters by Nicoud and Ducros [47], which is suited for wall-bounded flows as the eddy viscosity naturally goes to zero at the walls Mirzaei et al. [48].

As Nagaosa [49] concluded in the turbulence-model free study of a plain FTHE, the flow field inside the FTHE is fully laminar for $\mathrm{Re}_{D_h} = 400$ (converted from Nagaosa [49] using the reference velocity and length scale as defined in the present study). A transition regime with both laminar and turbulent regions was reported for $\mathrm{Re}_{D_h} = 400$–2000 and fully turbulent flow was observed for $\mathrm{Re}_{D_h} = 2400$–3200. As a remark, in the present work $\mathrm{Re}_{D_h} = 243$–793 which may involve both laminar and turbulent features. For the herringbone fin shape, the wavy fin shape induces a new lateral deviation to the flow field. Therefore, it will shift the spatial location of the transition as well as the critical Reynolds number for the transition.

2.3. Governing equations for particles

The collisions between the particles with each other and the fin surface is modelled with the soft-sphere discrete element method (DEM) approach [50]. If a particle i with the mass m_i and radius r_i, then the mass momentum of inertia can be calculated as $I_{\mathrm{i}} = (2/5)m_{\mathrm{i}}r_{\mathrm{i}}^2$. The governing equation for the location $\boldsymbol{x}_{\mathrm{i}}$ is given by 5 :

$$m_{\mathrm{i}}\frac{\mathrm{d}^2\boldsymbol{x}_{\mathrm{i}}}{\mathrm{d}t^2} = \boldsymbol{F}_{\mathrm{i,con}} + \boldsymbol{F}_{\mathrm{i,fluid}} \tag{5}$$

where the $\boldsymbol{F}_{\mathrm{con}}$ is a contact force upon collision and $\boldsymbol{F}_{\mathrm{fluid}}$ is the combined fluid force acting on the particle.

2.4. Fluid forces on particles

A Lagrangian approach is used to track the particles as they flow through the heat exchanger. In this study, particles with diameters of $d_{\mathrm{p}} = 5$ µm, $d_{\mathrm{p}} = 10$ µm and $d_{\mathrm{p}} = 20$ µm and with density of $\rho_{\mathrm{p}} = 2500$ kg m^{-3} are being considered.

Here, we use the particle drag formulation by Benyahia et al. [51], which is based on the simulations by Hill et al. [52] and Koch and Hill [53], where the modified Stokes drag is defined as $C_d = (24/Re_p)F$, where $F = f(Re_p, \alpha_f)$. In the definition, Re_p corresponds to the particle Reynolds number while α_f corresponds to the particle volume fraction. By using this definition, a larger range of Reynolds numbers and particle volume fractions are covered.

2.4.1. Contact forces

The adhesive force between two spherical particles was originally studied by Hamaker [54]. Hamaker concluded that the dominant forces of adhesion for two materials are the van der Waals and electrostatic forces. They originate from the continuous change of the electrical potential of atoms as the electrons circle around the core. The model that describes these forces is the Johnson–Kendall–Roberts (JKR) model that was originally developed by Johnson et al. [55]. The JKR model is suitable for the specific type of collision for which the Tabor parameter $\lambda_T = (4R\gamma^2/E^2D_{\mathrm{min}}^3) > 3$ [56], where γ is the surface energy density, which is defined as half of the energy required to separate two particles in contact and D_{min} is the minimum separation distance, usually assumed to be 1.65 Å [57,58].

Since the surface energy density is defined for a specific material to interact with itself, it is important to notice that the value cannot be used directly in the collision computations between two different materials. For this a new property called adhesion work $w = \sqrt{\gamma_1\gamma_2}$ [59] is used.

The contact forces in the normal direction of the surface that are modelled with the JKR model are the spring force $\boldsymbol{F}_{\mathrm{spring,n}}$, the adhesive force $\boldsymbol{F}_{\mathrm{jkr,n}}$ and the damping force $\boldsymbol{F}_{\mathrm{damp,n}}$:

$$\boldsymbol{F}_{\mathrm{spring,n}} = -\frac{4E}{3R}a^3\boldsymbol{n} \tag{6}$$

where n is the surface normal vector and a is the contact area.

$$\boldsymbol{F}_{\mathrm{jkr,n}} = 4\sqrt{\pi\gamma E a^3}\boldsymbol{n} \tag{7}$$

The effective Young's modulus is defined as $\frac{1}{E_{\mathrm{eff}}} = \frac{1-\nu_{\mathrm{i}}^2}{E_{\mathrm{i}}} + \frac{1-\nu_j^2}{E_j}$ and the effective radius $\frac{1}{R} = \frac{1}{r_{\mathrm{i}}} + \frac{1}{r_{\mathrm{j}}}$ for particle collision between two materials where E and ν are the Young's modulus and Poisson's ratio and the subscript corresponds to the colliding materials i and j. In order to model the dissipation of kinetic energy upon collision, a damping force $\boldsymbol{F}_{\mathrm{damp,n}}$ is used:

$$\boldsymbol{F}_{\mathrm{damp,n}} = -2\sqrt{\frac{5}{6}}\beta\sqrt{S_{\mathrm{n}}}\boldsymbol{v}_{\mathrm{n}} \tag{8}$$

where $\boldsymbol{v}_{\mathrm{n}}$ is the relative normal velocity, β is a parameter that takes into account the coefficient of restitution e as:

$$\beta = \frac{\ln(\mathrm{e})}{\sqrt{\ln^2(2) + \pi^2}} \tag{9}$$

S_{n} is parameter that takes into account the material properties as:

$$S_{\mathrm{n}} = 2E\sqrt{R\delta_{\mathrm{n}}} \tag{10}$$

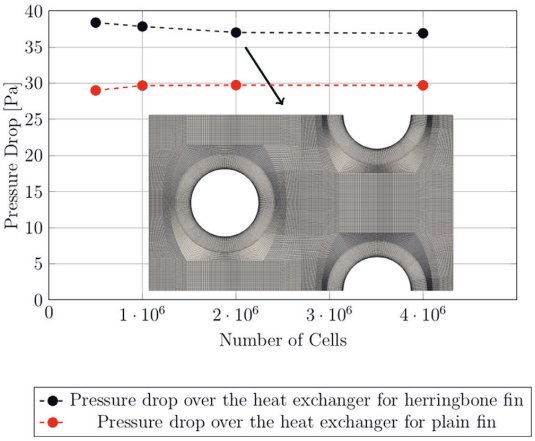

Fig. 2. Pressure drop over the heat exchanger with respect to the cell count of the mesh with $Re_{D_h} = 793$ is shown as well as the chosen mesh resolution.

where δ_n is the overlap distance. In the tangential direction of the contact, the spring force $\boldsymbol{F}_{\text{spring,t}}$ is used:

$$\mathbf{F}_{\text{spring,t}} = -S_t \Delta s_t \tag{11}$$

where $S_t = 8G\sqrt{R\delta_{s_t}}$ is a parameter for the particle properties and the δ_{s_t} is the tangential overlap. The effective shear modulus is calculated as $\frac{1}{G} = \frac{2-\nu_i}{G_i} + \frac{2-\nu_j}{G_j}$. As was done for the normal direction, a similar damping force $\boldsymbol{F}_{\text{damp,t}}$ for the tangential direction is used:

$$\mathbf{F}_{\text{damp,t}} = 2 - \sqrt{\frac{5}{6}}\beta\sqrt{S_t m}\mathbf{v}_t \tag{12}$$

where the $1/m = 1/m_i + 1/m_j$ is the effective mass and $\boldsymbol{v}_t$ is the tangential velocity respect to the surface.

3. Computational model validation

Next, model validation results are discussed. First, a mesh sensitivity analysis on the pressure drop over both fin shapes is presented. Second, the collection efficiency of the FTHE for low adhesive particles at relevant particle sizes and two fin shapes is considered for different mesh resolutions. Additionally, the overall fluid dynamics and turbulence modelling is validated for a three-dimensional cylinder in crossflow. Third, the flow field inside the FTHE is validated against experimental results available in the literature. Fourth, the contact mechanics model is validated. Finally, the drag experienced by the particles is compared with the analytical Stokes equation and a particle number sensitivity study is carried out.

3.1. Mesh sensitivity assessment for fin-and-tube heat exchanger

In LES, it is of high priority to assess the mesh sensitivity of the results. From the viewpoint of particle transport, the energy containing flow scales should be resolved in order to capture the deposition process reliably [60,61]. In the present study, we aim at resolving the flow field well, in order to capture the particle dispersion adequately. Thereby the sub-grid scale effect on particle dispersion is neglected. First, four different mesh resolutions are investigated by showing the pressure drop over the FTHE in Fig. 2 and the chosen mesh resolution is illustrated.

Next, the collection efficiency for low adhesive particles for the highest Reynolds number is shown for both fin shapes and three different particle sizes in Fig. 3. The same mesh resolution is used for the plain and herringbone fin shape, which was illustrated in Fig. 2. More information about the adhesiveness of the particle types is provided in Table 2.

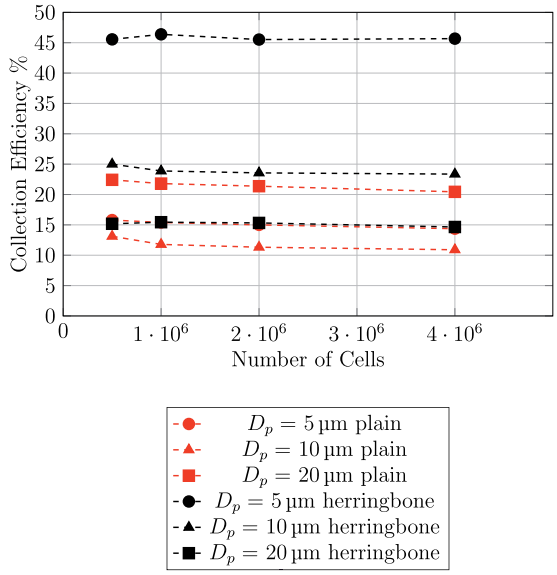

Fig. 3. Mesh sensitivity study with respect to the cell count of the mesh with low-adhesive particles and $Re_{D_h} = 793$.

Based on the mesh sensitivity study, the results with the 2 million cell mesh in Fig. 3 deviate only 3% on average from the results with the 4 million cell mesh for the highest Reynolds number and low-adhesive particles. Such a scenario can be considered as the most conservative simulation case. Therefore, we conclude that the scales resolved by the 2 million cell mesh are sufficient to capture the particle transport in the present Reynolds number range. The low-adhesive particles are expected to bounce multiple times more from the surface in contrast to the high-adhesive ones and therefore the low-adhesive particles are influenced by the turbulent scales for a relatively long period of time. Thereby, we assume that the mesh resolution is sufficient for high-adhesive particles as well.

3.2. Single cylinder flow validation

In the previous section, the mesh with around 2 million cells was noted to provide acceptable accuracy. Next, using the same spatial resolution, the flow around a single cylinder is confirmed for the range of Reynolds numbers in Figs. 4 and 5. The boundary layer flow around a cylinder is validated by comparing the drag coefficient and Strouhal number of a cylinder in a cross flow to the numerical results found from the literature for CFD studies [62–64] and experimental results [65]. The same y^+-value and maximum cell size was chosen as was selected to be sufficient in the mesh sensitivity study in Section 3.1. The computational domain is 4D deep, 20D wide and 30D long.

3.3. Flow field validation inside a fin-and-tube heat exchanger

Model validation for the flow field inside the FTHE is carried out in Fig. 6 out by comparing the pressure drop over the heat exchanger to the experimental values by Chokeman and Wongwises

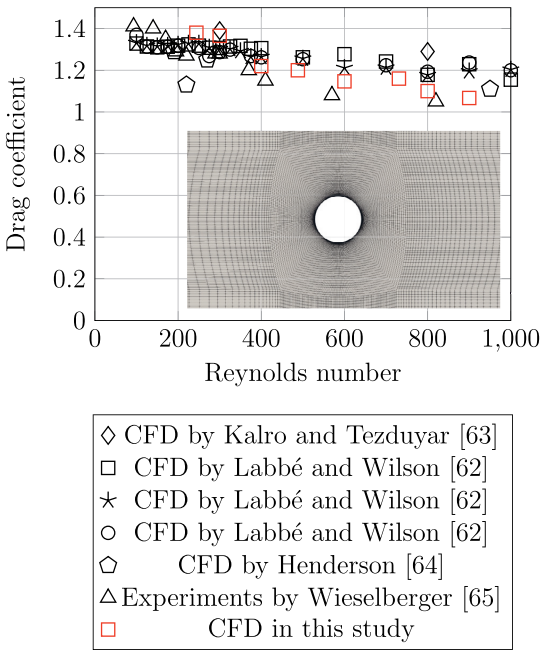

Fig. 4. Comparison of the simulated three-dimensional drag coefficient and a boundary layer mesh illustration for flow around a cylinder without particles.

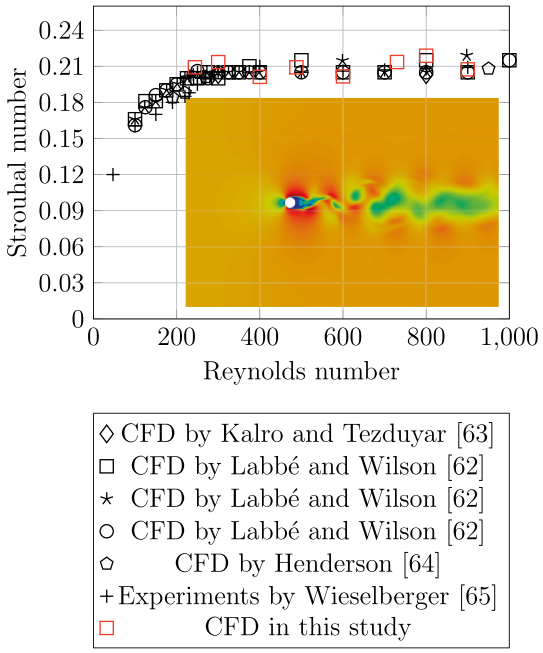

Fig. 5. Comparison of the simulated three-dimensional Strouhal number and flow field illustration with $Re_D = 900$ for flow around a cylinder without particles.

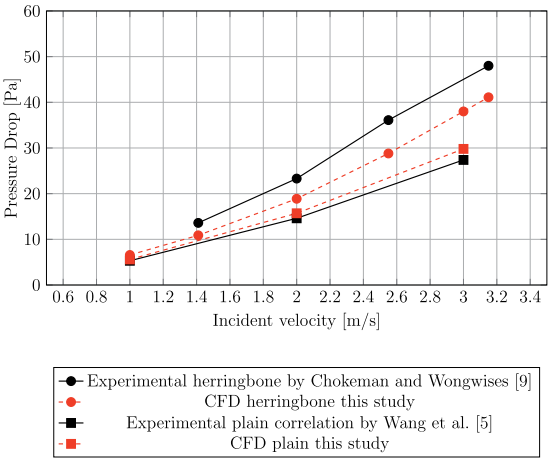

Fig. 6. Simulated pressure drop over the heat exchanger compared to the experimental results found from the literature for both plain and herringbone fin shape.

[9] and Wang et al. [5]. The incident velocity range $U_{in} \in [1, 3]$ m/s corresponds to the $Re \in [243, 793]$.

The agreement with the experiments Wang et al. [5] and the simulated plain fin is good. Slightly more deviation can be seen for the herringbone fin shape [9]. The difference can be caused by the non-matching boundary conditions such as the turbulence level of the inlet flow. However, based on the numerical results presented in Fig. 6, we conclude the present model to be quantitatively reliable.

3.4. Particle number sensitivity study

A simple comparison was first performed between the analytical equations and the CFD-DEM framework to validate the drag force for individual particles. Settling velocity for all particle sizes and the stopping distance for all particle sizes with the corresponding initial velocities used in present study was compared to the analytical values derived from the Stokes drag law. A mean error of 1% was seen between the analytical and the value calculated with the CFD-DEM model used in present study.

To ensure that the collection efficiencies being reported are independent of the number of particles being simulated, simulations with 2500, 5000, 10,0000, and 20,000 particles was performed. The amount of particles is closely related to the computational resources required to perform the simulations. Therefore it is important to inject as few particles as possible to save in computational expenses. The collection efficiencies are $C_{20000} = 23.43\%$, $C_{10000} = 23.64\%$, $C_{5000} = 22.86\%$ and $C_{2500} = 23.08\%$ as shown in Fig. 7. For good visual illustration with reasonable computational cost, 10,000 particles were chosen for the number of simulated particles in all simulations.

3.5. Contact mechanics validation

As a last demonstration of the model functionality, the contact mechanics between a particle and surface is validated in Fig. 8 by investigating the bouncing motion of a 6mm Teflon particle impacting a soda glass surface. The material properties used for the comparison are tabulated in Table 3 in the Appendix.

The height of each individual bounce was seen to be almost identical with the reference values found from the literature

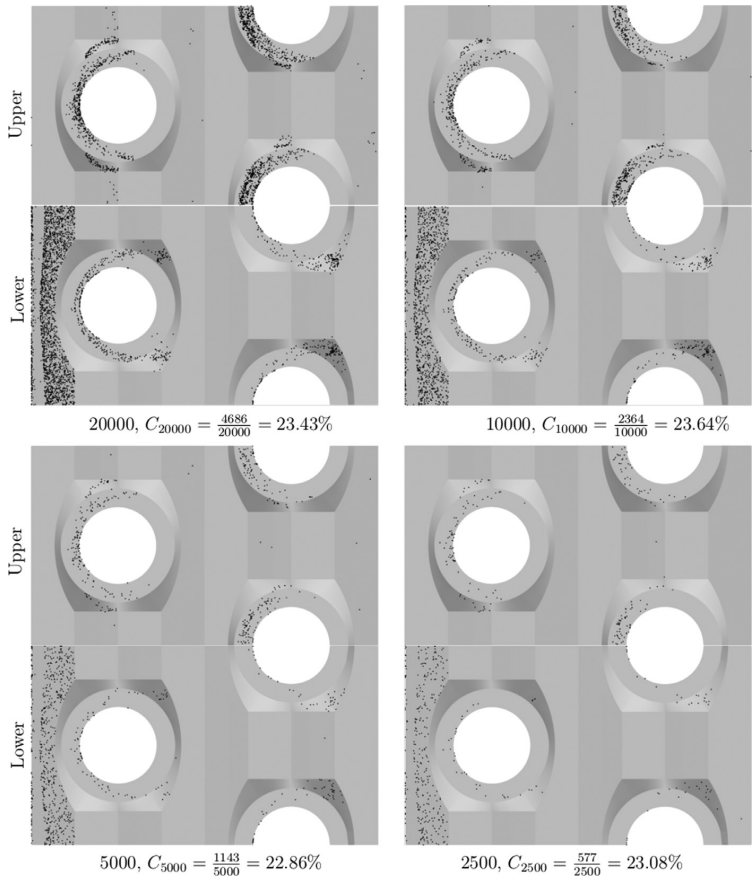

Fig. 7. Illustration of the deposition distributions for both upper and lower fin for different amounts of $D_p = 10$ μm low adhesive particles and $Re_{D_h} = 732$, from left to right and upper to lower, 20000, 10000, 5000 and 2500 particles (size of the particles is multiplied by a factor of 30).

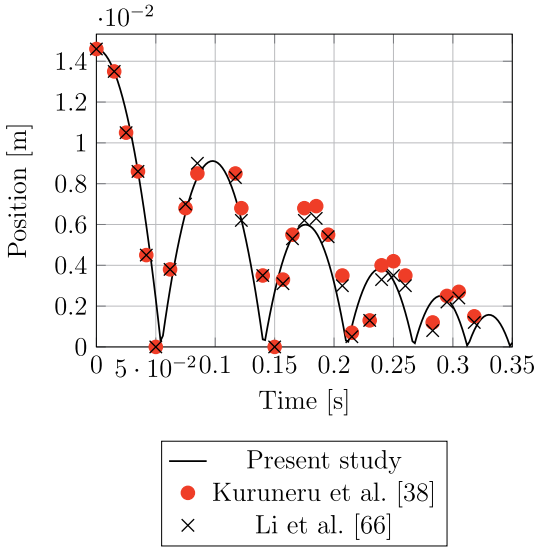

Fig. 8. The position of a 6 mm Teflon ball respect to a soda glass surface.

[38,66]. Thereby, we conclude that the contact mechanics for the particle impact with a wall surface is correctly implemented.

4. Particle property selection based on critical velocity measurements

In the context of particle-surface impact, the term 'critical velocity' refers to the incident velocity threshold under which a particle will stick to the surface. In practice, critical velocity depends on the particle properties (size, density, Young's modulus, Poisson's ratio, surface energy density and shape) as well as surface properties (Young's modulus, Poisson's ratio, surface energy density and surface roughness) [59]. Herein, a major effort is carried out to collect literature data on critical velocities in order to deduce and justify a meaningful parameter range for the simulations.

4.1. Description of the simulated properties

The particle concentration, size distribution and HVAC working conditions of the FTHE can be arbitrary. The fouling process is very slow and can be measured in months or years. A fouling process consists of a chain of events, where first, the smaller particles with higher critical velocity will start to deposit on the surface. For a clean surface, the critical velocity of larger particles is too low and therefore they will just rebound on the surface and re-entrain to

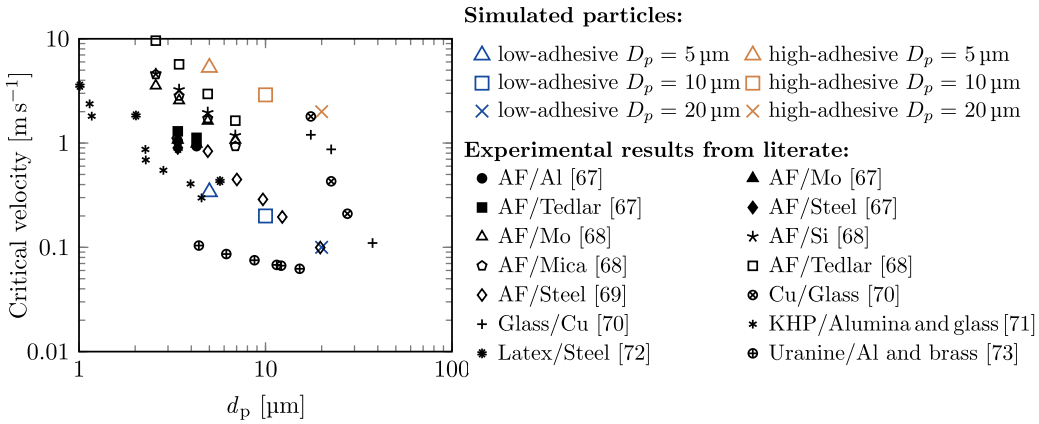

Fig. 9. Comparison between experimental results from the literature and simulated particles in this study.

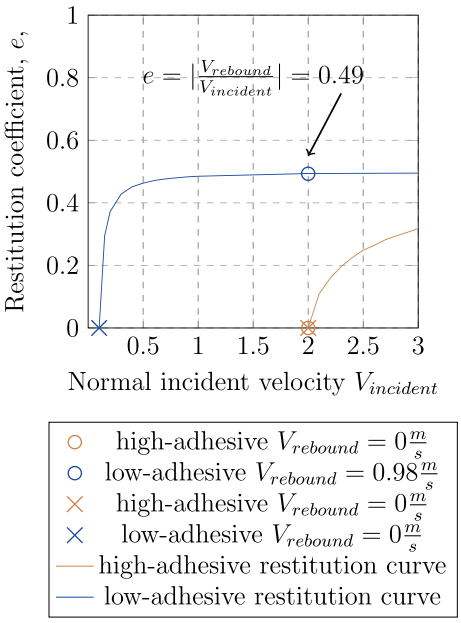

Fig. 10. Restitution coefficient with respect to the incident velocity for the corresponding 20µm particles illustrated described in Fig. 9.

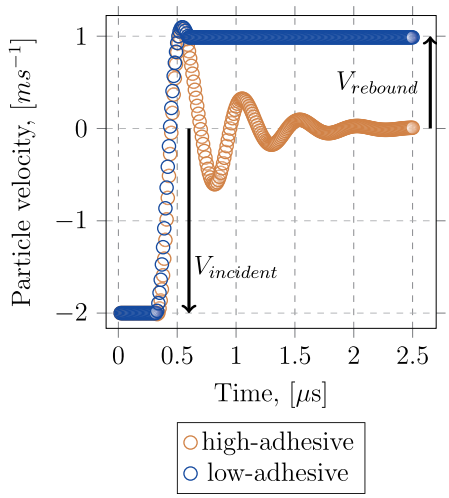

Fig. 11. Velocity of particles during the impact for the corresponding particles described in Fig. 10.

the flow. This means that in the start of the nucleation regime, the smaller particles start to deposit on the surface and change the adhesion mechanics of the surface for the larger particles. This increases the critical velocity and therefore increases the amount of deposited larger particles. Because of the complexity of the fouling process and the variety in particle properties in the real application, it is essential to simplify the process of selecting the material properties so that the results are repeatable and comparable.

The material properties selection process is based on the critical velocity of a specific particle size. The information found in the literature on different particle and surface pairs and their critical velocity is shown in Fig. 9 [67–73]. Based on this figure, the critical velocities are typically in the range of $U_{crit} \in [0.1, 5]$ for $D_p \in [1, 20]$ µm. A relation between the particle diameter and the critical velocity can be observed from this data. Therefore, even with no information on the material of the particles or the deposition surface, we can assume that by using values that corresponds to the minimum and maximum of the data set, the results will represent both extremes of the particle types encountered in the real application. When the contact mechanics of the chosen properties for a specific particle size are investigated further in Fig. 10, we can observe the restitution curve for each particle-surface pair, here for the $D_p = 20$ µm. Finally, in Fig. 11, the impact kinetics of the collision with the aforementioned properties is illustrated for both adhesive levels with the same incident velocity. All the chosen pairs that lead to the size specific critical velocity are tabulated in the Appendix in Table 4.

4.2. Non-dimensional groups

A fouling process of a FTHE can be characterized by six parameters, namely the flow Reynolds number Re_{D_h}, the particle Stokes

Table 2
Details of the simulations performed in this study: ID is the identifier number of each case, non-dimensional particle diameter $\epsilon = d_p/D_h$, flow Reynolds number $Re_{D_h} = U_{max}D_h/\nu$, Stokes number based on the eddy turnover time $St_e = \rho_p d_p^2 U_{max}/(18\mu_f D_h)$, the elasticity parameter $\lambda = E_{eff}/(\rho_p U_{max}^2)$, the adhesion parameter $Ad = w/(\rho_p U_{max}^2 d_p)$ and name of the fin shape.

Re_{D_h}=264		Re_{D_h}=528		Re_{D_h}=793		Fin shape
		ϵ=0.0021				
St_e=0.16 λ=14.4 × 10^5		St_e=0.31 λ=3.6 × 10^5		St_e=0.47 λ=1.6 × 10^5		
ID	Ad	ID	Ad	ID	Ad	
1	0.82	2	0.2	3	0.09	Plain
4	27.7	5	6.9	6	3.1	Plain
7	0.82	8	0.2	9	0.09	Herringbone
10	27.7	11	6.9	12	3.1	Herringbone
		ϵ=0.0043				
St_e=0.62 λ=14.4 × 10^5		St_e=1.24 λ=3.6 × 10^5		St_e=1.86 λ=1.6 × 10^5		
ID	Ad	ID	Ad	ID	Ad	
13	0.41	14	0.1	15	0.046	Plain
16	13.8	17	3.45	18	1.53	Plain
19	0.41	20	0.1	21	0.046	Herringbone
22	13.8	23	3.45	24	1.53	Herringbone
		ϵ=0.0087				
St_e=2.49 λ=14.4 × 10^5		St_e=4.97 λ=3.6 × 10^5		St_e=7.47 λ=1.6 × 10^5		
ID	Ad	ID	Ad	ID	Ad	
25	0.2	26	0.05	27	0.022	Plain
28	6.91	29	1.73	30	0.77	Plain
31	0.2	32	0.05	33	0.022	Herringbone
34	6.91	35	1.73	36	0.77	Herringbone

number St_{τ_e}, the adhesion parameter Ad, the elasticity parameter λ, the density ratio χ and the particle to hydraulic diameter ratio ϵ further discussed in what follows.

The Reynolds number is defined as $Re_{D_h} = U_{max}D_h/\nu$. Note that the used definition is based on the hydraulic diameter calculated in Eq. (1), the characteristic velocity at the minimum cross sectional area $U_{max,avg}$ and the dynamic viscosity $\nu = 15$ μm^2/s. The Stokes number $St_{\tau_e} = \tau_e/\tau_f$. The parameters that define the adhesiveness of the particles are the adhesion coefficient and elasticity parameter that are defined as $Ad = \frac{\gamma}{U_{max}^2 \ \rho_p \ d_p}$ and $\lambda = \frac{E_{eff}}{U_{max}^2 \ \rho_p}$ [59]. Finally, the density ratio $\chi = \rho_f/\rho_p = 0.0005$ and the particle diameter $\epsilon = d_p/D_h$.

Although the fouling process is a slow process, the computational resources allow us to perform LES simulations of few-tenth of a second. For this reason, the volume fraction $\phi = \dot{V}_p/(\dot{V}_p + \dot{V}_f)$ of the particles at the inlet is increased to a higher value and kept constant between the different cases. The concentration value is kept low enough so that its effect on the flow field is negligible. The volume fraction being $\phi = 5 \cdot 10^{-5}$ for all the simulations. As these values are smaller than 10^{-4}, their effect on the flow field can be neglected [67]. The mass coupling parameter for the simulations is kept under 0.1 for all simulations to ensure that the mass coupling effects are unimportant [68]. The coefficient of restitution $e = 0.5$ is kept constant for all the particle types. An overview of the simulations carried out in this study is provided in Table 2.

5. Results and discussion

First, the flow field inside the FTHE is visualised. Then the collection efficiency is shown with respect to the Reynolds number as well as Stokes number and adhesion parameter. Finally, an example is provided on the practical relevance and applicability of the present results.

5.1. Flow visualisation

Particles are inserted to the computational domain with the mean inflow velocity. An illustration of the flow field inside the heat exchanger and the upper and lower fins is provided in Fig. 12.

It is noted how the laminar inflow impinges on the tube surface (I). Based on the literature, this point corresponds to a major region of particle deposition in various FTHE applications [34,35]. Behind the tubes, a recirculation region (II) is formed. Such regions experience typically rather poor heat transfer characteristics [12]. Then, the flow undergoes transition from laminar to turbulent (III) while the flow is qualitatively relatively turbulent with incoherent features close to the outlet boundary (IV). We note that the channel height and cylinder diameter based Reynolds numbers are respectively 312 and 1800. Hence, the flow is not fully turbulent from the viewpoint of standard channel flow but, instead, the unsteady cylinder wake provokes dynamic and incoherent flow features. Please see Nagaosa [49] for further information.

5.2. Fouling locations

The deposition locations for plain fins are shown from the upstream side in Figs. 13 and 14. The results with $D_p = 10$ μm particles ($0.62 \leq St \leq 1.86$) are shown in Fig. 13. For $St = 0.62$ the particle timescale is small from the flow timescale viewpoint and hence they will most likely follow the flow streamlines. For $St = 1.24$, the particle timescale is of intermediate size and it is more likely for the particles to deviate from the streamline. For $St = 1.86$, the directional change of the flow, due to e.g. tubes in the flow, enables large proportion of the particles to escape from the streamline and collide with the surface. After the particles have deviated from the streamline, the low-adhesive particles that hit the surface will bounce away from the surface and only stick during the next consecutive collisions. If the momentum of the particles is low enough, the particles will bounce multiple times on the tube surface and stick when the impact velocity is lower than the critical velocity. (I) If the momentum is high enough, the particles will bounce from the tube surface and reach the fin surface. Higher initial momentum will lead to larger amount of deposited particles on the fin and lower amount on the tube surface (II and III). In contrast, the high adhesive particles will most likely stick at the first collision, excluding the ones that have accelerated with the flow to achieve an impact velocity high enough to enable the particles to bounce, re-entrain to the flow and even hit the fin surface (IV). In fact, we have noted that the

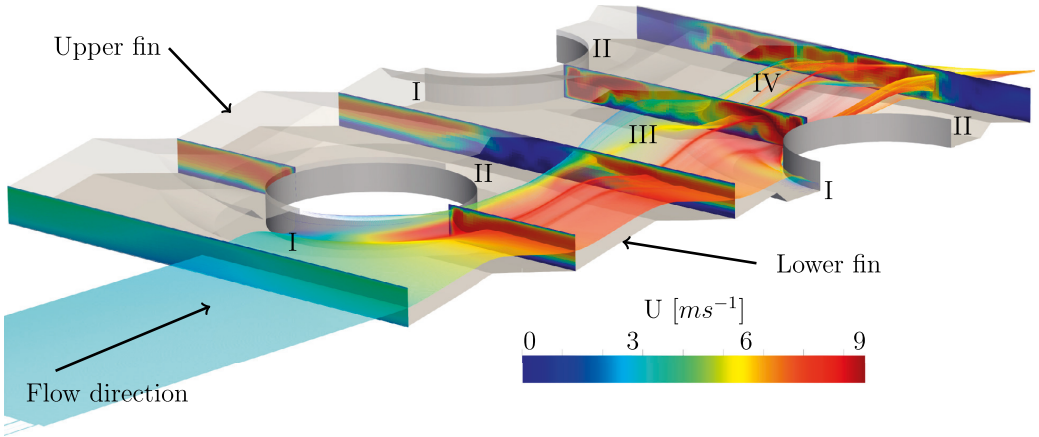

Fig. 12. Illustration of the flow field and the upper and lower fin with respect to the flow direction with $Re = 793$.

qualitatively, very similar trends on particle deposition would be noted for 5 μm ($0.16 \leq St \leq 0.47$) and 20 μm ($2.49 \leq St \leq 7.47$) particles. Fig. 13 shows deposition locations for plain fins, for particles with different characteristic features such as ID, *Re, St,* λ and *Ad*. The non-dimensional numbers and the ID of the simulation corresponds to the ones tabulated in Table. 2. Fouling locations for IDs 1–12 ($D_p = 5$ μm) and 24–36 ($D_p = 20$ μm) are provided in the Appendix in Figs. A1, A2, A3 and A4.

For all parameter values the qualitative trends are rather similar: most particles will deposit on the front side of the tubes. The deposition location results illustrate that with the ID =13, with the lowest Reynolds number and low adhesiveness, the particles at the center of the flow field will have just enough momentum so that they will bounce once and only deposit if they will hit the surface multiple times. Therefore only few particles will deposit in the middle of the tube. With the higher Reynolds number (ID=14 and ID=15) the particle inertia increases to a level that is enough for the particles to escape from the surface after the collision and therefore the tube surface will have less and less deposited particles. When the ID=15 is compared to ID=14, it can be seen that when the Reynolds number is even higher, the particles will start to deposit on the fin after the collision with the tube surface. With the higher adhesion levels (ID=16-18), the particles will deposit on the tube when they deviate from the streamlines and only rarely bounce back and deposit on the fin. For ID=18, an empty region can be seen on the second tube row where less particles have deposited on the middle of the tube. This is due to the fact that as the flow speed is increased in the middle of the channel between the fins, the particles will have just high enough impact velocity so that they will bounce back, even though there exists a strong adhesive force between the particles and the fin. The low adhesive case with the highest Reynolds number, ID=21, is the only case where no particles are not deposited on the downwind side of the second tube row.

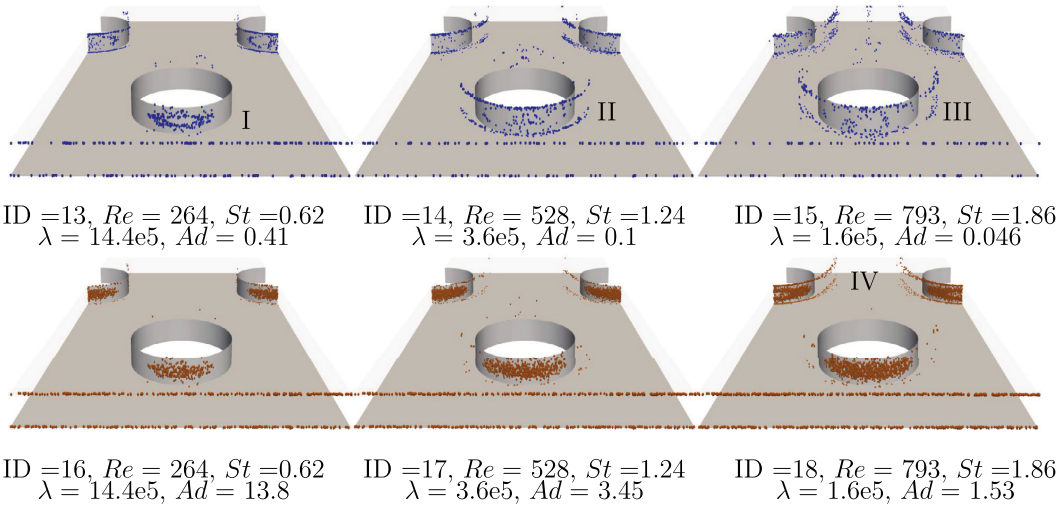

Fig. 13. Deposition locations for plain fin with $D_p = 10$ μm low-adhesive and high-adhesive particles (size of particles increased by a factor of 30).

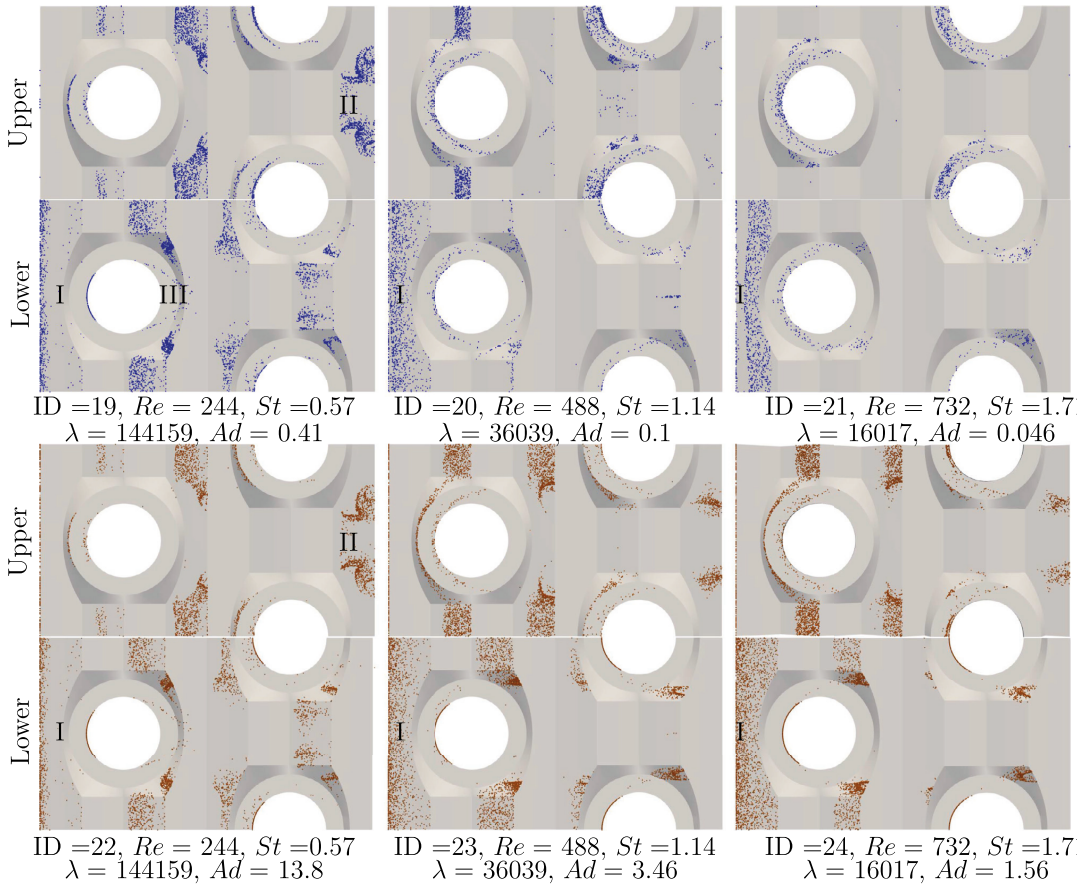

Fig. 14. Deposition locations for lower and upper fin separately with D_p = 10 μm low-adhesive and high-adhesive particles.

For the herringbone fins, the deposition locations are demonstrated for both upper and lower fins separately. The findings for the herringbone case are consistent with the plain fin cases above. Due to its wavy shape, the number of deposited particles is observed to be higher for the herringbone fin cases. As the particles enter the heat exchanger, the flow is initially guided towards the upper fin while most of the particles first hit the first wave of the lower fin (I). As for the ID=19 and ID=22, the deposition locations are almost identical between the cases. This means that in these cases, when the particle hits the surface, the impact velocity is under the corresponding critical velocity. Therefore, the adhesiveness of the particle does not affect the fouling process in these situations. The deposition surface at the trailing edge of the upper fin (II) shows how the fin shape is mixing the flow and causing the particles to hit the surface in a chaotic manner. For the low Reynolds number cases, particles are seen to deposit behind the tubes (III), in contrast to the higher Reynolds number cases where almost no particles are seen in the recirculation region. When the Reynolds number is increased, for low-adhesive particles, the flow accelerates particles impact velocities over the critical velocity and therefore, less particles deposit on the surface of the fin. The results for ID=19-24 are shown in Fig. 14.

5.3. Collection efficiencies

The fin collection efficiency can be defined as the ratio of the deposited and the inserted particles. It is clearly noted from Figs. 15 and 16 that, for high adhesive particles the collection efficiency will increase along with Reynolds number. The main reason for this phenomenon is the Stokes number, which increases along with the Reynolds number: the higher the Stokes number the more likely a particle deviates from the streamline. For low adhesive particles, the deposition process is much more complicated since the deposition rarely takes place at the first collision. The process can be described with a series of collisions that eventually lead to the deposition of a particle. Based on the results on Figs. 15 and 16 there exists a non-monotonous trend between the Reynolds number and the collection efficiency. A maximum in the collection efficiency for the low-adhesive particles is observed between the ID=9 (D_p = 5 μm Re_{D_h} = 793, St = 0.47, Ad = 0.09 and $\lambda = 1.6 \times 10^5$) and ID=19 ($D_p$ = 10 μm, Re_{D_h} = 264, St = 0.62, Ad = 0.41 and $\lambda = 14.4 \times 10^5$). The results regarding the collection efficiency are reported in Figs. 15–17 with respect to the Stokes number. It can be noted that a higher Stokes number does not necessarily lead to a higher collection efficiency or higher rate of fouling.

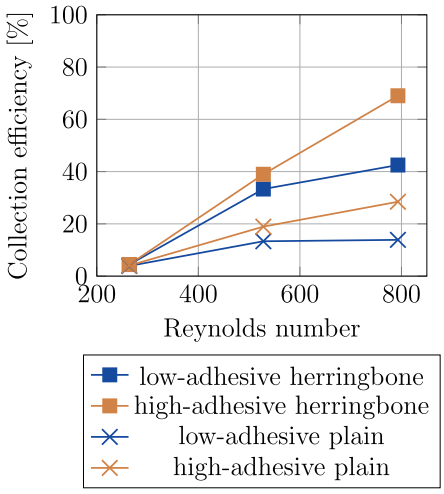

Fig. 15. Collection efficiencies for $D_p = 5$ µm.

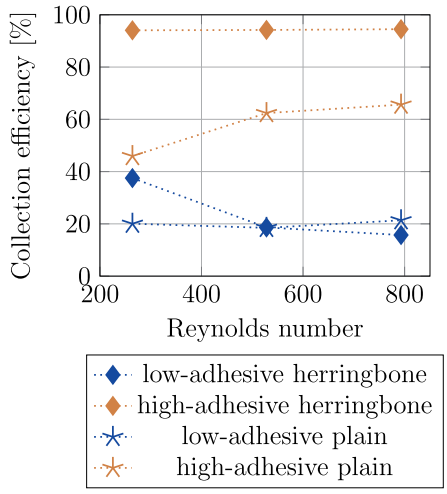

Fig. 17. Collection efficiencies for $D_p = 20$ µm.

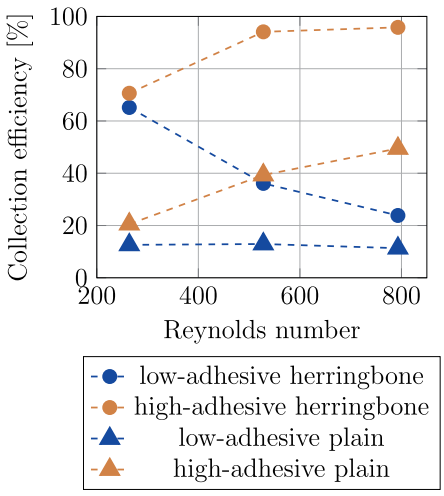

Fig. 16. Collection efficiencies for $D_p = 10$ µm.

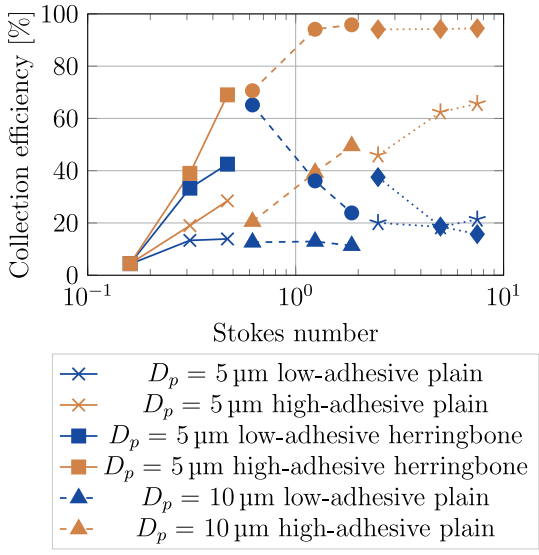

Fig. 18. Collection efficiency of all the simulated cases with respect to the Stokes number.

In Fig. 18, the collection efficiency is shown with respect to the Stokes number. A conclusion can be made that a higher Stokes number does not always correlate to a higher collection efficiency and therefore a higher rate of fouling. For high adhesive particles the collection efficiency is shown to be a function of the Stokes number. But when investigated more carefully, different particle size classes will lead to a small difference in the adhesive properties and therefore to a discontinuation in the collection efficiency. Thus, in fouling investigations, one should not only consider St and Re but also take into account the particle adhesiveness (Ad) and the elasticity parameter (λ) which further depend on the adhesion work, Young's modulus, particle size and the density of the particle as seen in Eqs. (6)–(12). Finally on the Fig. 19, the collection efficiency is illustrated with respect to the adhesion parameter. It is clearly seen that a higher adhesion parameter does not correlate directly with a higher collection efficiency but in fact the opposite seems to be true. This is because the adhesion parameter is the measure between adhesive force and the particle inertia [59]. In other words, the parameter acts as a relative measure of the impact process between the particle and the fin. The fouling process of a FTHE is not only a function of the adhesion parameter but also a function of the Stokes number, Reynolds number and the elasticity parameter as shown in this study.

5.4. Fouling rate prediction from air quality measurements

In the earlier sections, the presented numerical results indicated that the fouling process of a FTHE depends monotonically on the Reynolds and Stokes numbers for high-adhesive particles. In contrast, for the low adhesive particles, a non-monotonic relationship was observed. As expected, it was noted that the

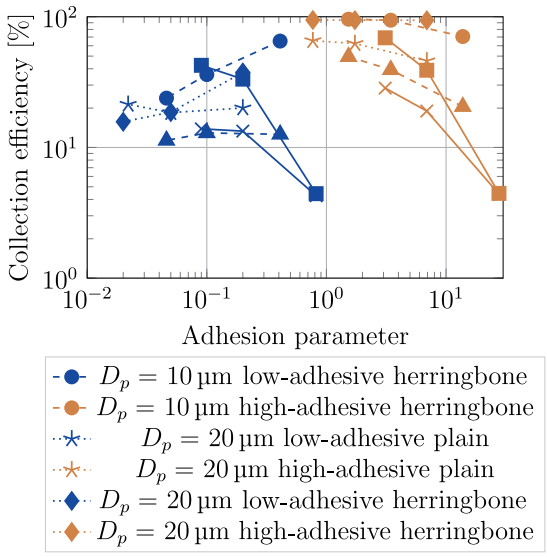

Fig. 19. Collection efficiency of all the simulated cases with respect to the Adhesion parameter.

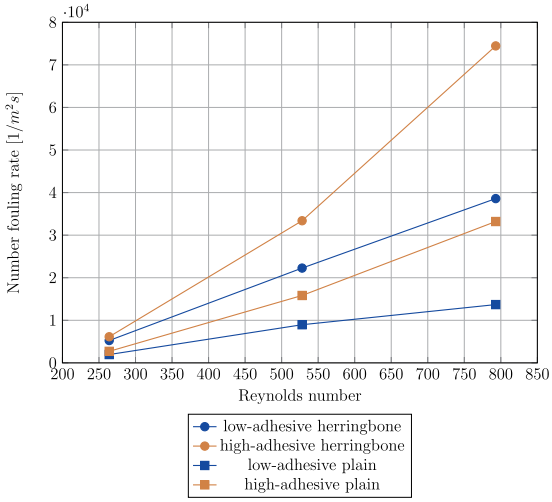

Fig. 20. Estimate on the number of overall deposited particles for FTHEs at the Taipei train station.

adhesion and elasticity parameters are equally important in the fouling process. Next, the results will be applied to estimate the fouling rate in a certain FTHE application. The air quality and the particle size distribution of the ambient environment can vary drastically between different applications. For example, the outdoor air during a sandstorm most likely has a much higher concentration of low adhesive particles compared to the indoor air of an average school with high adhesive clothing fibers and other organic substances that are circulated through the heat exchanger. Therefore, when a fouling rate comparison between different fin shapes is performed, it is important to define the particle size distribution and the adhesion properties of the particles in the air.

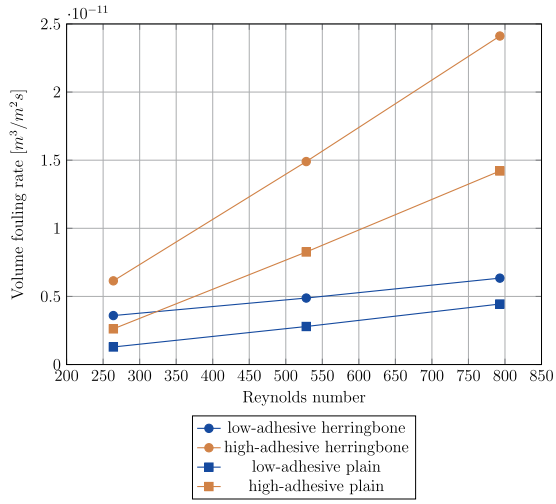

Fig. 21. Estimate on the volume of overall deposited particles for FTHEs at the Taipei train station.

Next, the present numerical results are applied in the context of the data provided by Cheng and Lin [69]. The data includes the average particle mass size distribution of the air at the Taipei main station during January - February 2008. The measured average particle mass concentrations were $m_c^{4-5\mu m} = 4.37$ µg/ m^3, $m_c^{7.5-10\mu m} = 7.42$ µg/ m^3 and $m_c^{15-20\mu m} = 10.55$ µg/ m^3. The number concentration can then be calculated as $N = m_c/m_p$ where m_p is the weight of one particle. We assume here the diameter of the particle to be the maximum from the size range and its corresponding weight. ($D_p = 5,\ 10,\ 20$ µm) The respective concentrations can then be easily calculated to be $N^{4-5\mu m} = 267071$ /m^3, $N^{7.5-10\mu m} = 56681$ / m^3 and $N^{15-20\mu m} = 10071$ / m^3. By knowing the particle concentration N^{d_p} and the corresponding collection efficiency C^{d_p} and the inlet velocity U_{inlet} in Figs. 15, 16 and 17, it is straightforward to calculate the number fouling rate $F_{number} = N^{d_p} C^{d_p} U_{inlet}$ and the results are shown in Fig. 20.

The thickness of the fouling layer decreases the thermal-hydraulic efficiency of the FTHE in two different ways. First, the fouling layer acts as an insulation in the heat transfer process between the air and the fluid in the tubes. Second, the thickness of the fouling layer will decrease the minimum cross sectional area of the flow and therefore increase the pressure drop over the FTHE. By knowing the volume of each particle size (V_{d_p}), the volume fouling rate can be calculated as $F_{volume} = V_{d_p} F_{number}$. The volume of the deposited particles in unit time for a frontal area of the FTHE can be seen in Fig. 21.

First, it is noted that low adhesive particles have a lower volume fouling rate than the high adhesive particles. Second, for a given adhesive type, the plain fin has a lower volume fouling rate than the herringbone fin. It is clear that the volume fouling rate increases with the Reynolds number. If the Reynolds increases by factor 3, the fouling rate is not desired to increase more than by factor 3. The volume fouling rate for low adhesive particles is noted to be 3.45 times higher for $Re_{D_h} = 793$ than at $Re_{D_h} = 264$ in the case of the plain fin shape. In contrast, the herringbone fin shape at $Re_{D_h} = 793$, has a 1.76 times higher volume fouling rate than at $Re_{D_h} = 264$. When the values for the high adhesive particles are compared, the plain fin has a 5.4 times higher volume fouling rate with the highest velocity compared to the lowest. The herringbone has 3.92 times higher volume fouling rate with the

highest velocity compared to the lowest. The main conclusion of the analysis is that the volume fouling rate increases more than by factor 3 in all cases except the herringbone fins with low adhesive particles. As another conclusion, we note that, in the effort to avoid fouling, lower inlet velocities should be used. Indeed, the present results indicate the trade-off between FTHE Reynolds number and the fouling rate. Furthermore, fouling also deteriorates the heat transfer coefficient of a FTHE. Optimally, various parameters including fin type, Reynolds number, air quality, size distribution and particle type should all be known in the design phase.

Last, we note that in practice FTHEs may need to operate in different ambient conditions. Therefore, based on the numerical findings, the type of particles can affect the choice of the optimal fin type. In fact, such design guidelines are already followed in the industry by practical experiences without detailed knowledge on the phenomena. By summing over the fin types and the Reynolds numbers, the fouling volume rate was found to be approximately 3 times higher for the high adhesive particles than for the low adhesive ones.

As discussed earlier, enhanced fin shapes such as herringbone are used to increase the heat transfer on the air side. In an environment with low adhesive particles the volume fouling rate in the nucleation regime is 1.74 times higher for the herringbone fin shape when compared to the plain fin. For the high adhesive particles, the volume fouling rate is 1.8 times higher with herringbone. Together, when both adhesion levels are summed together, the volume fouling rate for the herringbone fin shape is 1.78 times higher when compared to the plain fin FTHE. The presented numerical results indicate the relevance of combined CFD-DEM studies regarding the fouling rate and the performance of the fin during the lifetime of the FTHE [70–76].

6. Conclusions

In this study, the deposition of dry particles on a fin-and-tube heat exchanger by a coupled soft-sphere DEM and CFD was performed. The novel selection of material properties for the fouling particles is done such that a representative range of Reynolds numbers, Stokes numbers, elasticity and adhesion parameters is covered. The material selection in this study will lead to critical velocities between the particles and the fin surface that corresponds to the measurements performed for various material combinations and therefore different fouling characteristics. All the different models used for the calculation of the flow field and particle drag were validated. A comparison was carried out between low adhesive and high adhesive particle environments, with particle sizes of $D_p = 5$, 10, 20 μm, with three typical FTHE Reynolds numbers $Re_{D_h} = 243$, 528, 793 and two different fin shapes found in the contemporary HVAC industry. The major findings of this study are summarized below.

1. Novel method for the selection of adhesion properties such as particle size, particle density, effective Young's modulus, Poisson's ratio and adhesion work is demonstrated so that the corresponding critical velocity of the particles represent both ends of the spectrum in the real world fouling environments. The CFD code was validated by comparing the C_d and Strouhal numbers for a free cylinder against literature values. The CFD-DEM code was validated by comparing the particle drag to the analytical values and the DEM code was validated by comparing the critical velocity of the adhesion process to the experimental values reported in the literature.
2. This method enables the comparison of the volume fouling rate of the fin-and-tube heat exchanger fin shapes in different environments.
3. With low adhesive particles, plain fin volume fouling rate is 3.45 times higher with $Re_{D_h} = 793$ than at $Re_{D_h} = 264$. The herringbone fin shape has a volume fouling rate of 1.76 times higher with $Re_{D_h} = 793$ than at $Re_{D_h} = 264$.
4. With high adhesive particles, plain fin volume fouling rate is 5.4 times higher with $Re_{D_h} = 793$ than at $Re_{D_h} = 264$. The herringbone fin shape has a volume fouling rate of 3.92 times higher with $Re_{D_h} = 793$ than at $Re_{D_h} = 264$.
5. High adhesive particles will have 3.0 times higher volume fouling rate than low adhesive particles for both fin shapes, particle sizes and all Reynolds numbers combined.
6. Herringbone fins have 1.74 higher volume fouling rate than plain fin shape for low adhesive type particles. For high adhesive particles, herringbone has 1.8 times higher volume fouling rate and when both particle types are summed together, herringbone has 1.78 times higher volume fouling rate than the plain fin shape.

In the future, the investigated CFD-DEM method could be used for further studies on different fin shapes under different operating conditions and particle properties. Such results would be of high value in design of FTHE's. Novel topics for future research on fouling are different flow control strategies and fin shape optimization. Consequently, it is of constant interest to better manage the costs of FTHE life cycle.

Declaration of Competing Interest

We wish to confirm that there are no known conflicts of interest associated with this publication and there has been no significant financial support for this work that could have influenced its outcome.

Acknowledgments

The authors wish to acknowledge CSC - IT Center for Science, Finland, for computational resources and Koja Oy, for financial support.

Appendix A. Deposition locations

Table 3
Collision material properties for Teflon particle and a soda glass wall.

Material	E (GPa)	ν	ρ (kg m^{-3})	w (J m^{-2})	e
Teflon particle 6mm	0.4	0.46	2150	0.35	0.8
Soda glass wall	60	0.24	2526	0.13	0.97

Table 4
Collision material properties.

Material	E_{eff} (GPa)	ν	ρ (kg m^{-3})	w (J m^{-2})	e	V_{crit} (ms^{-1})
high-adhesive 5 μm	1.08	0.3	2500	1.04	0.5	5.3
high-adhesive 10 μm	1.08	0.3	2500	1.04	0.5	2.9
high-adhesive 20 μm	1.08	0.3	2500	1.04	0.5	2
low-adhesive 5 μm	1.08	0.3	2500	0.031	0.5	0.34
low-adhesive 10 μm	1.08	0.3	2500	0.031	0.5	0.2
low-adhesive 20 μm	1.08	0.3	2500	0.031	0.5	0.1

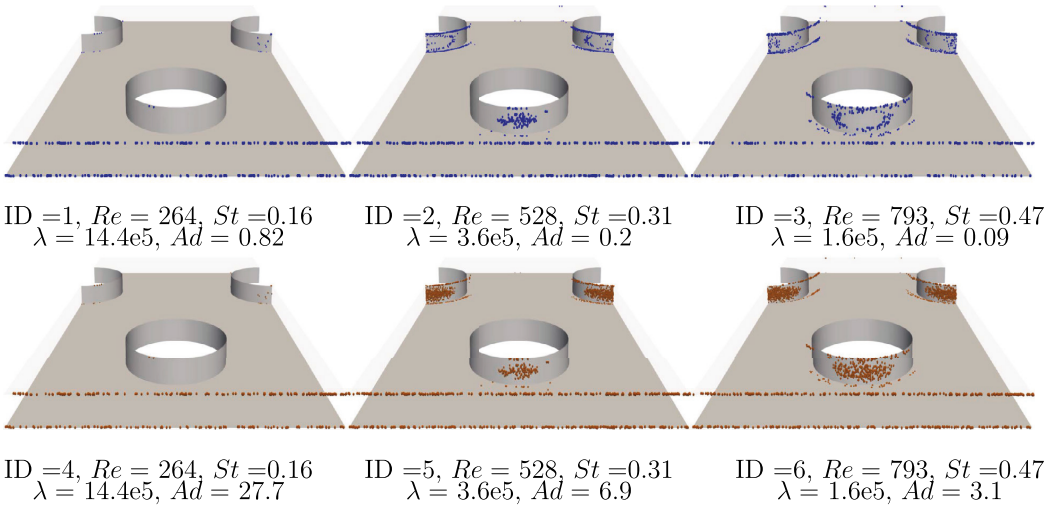

Fig. A1. Deposition locations for plain fin with $D_p = 5$ µm • low-adhesive and • high-adhesive particles (size of particles increased by a factor of 60).

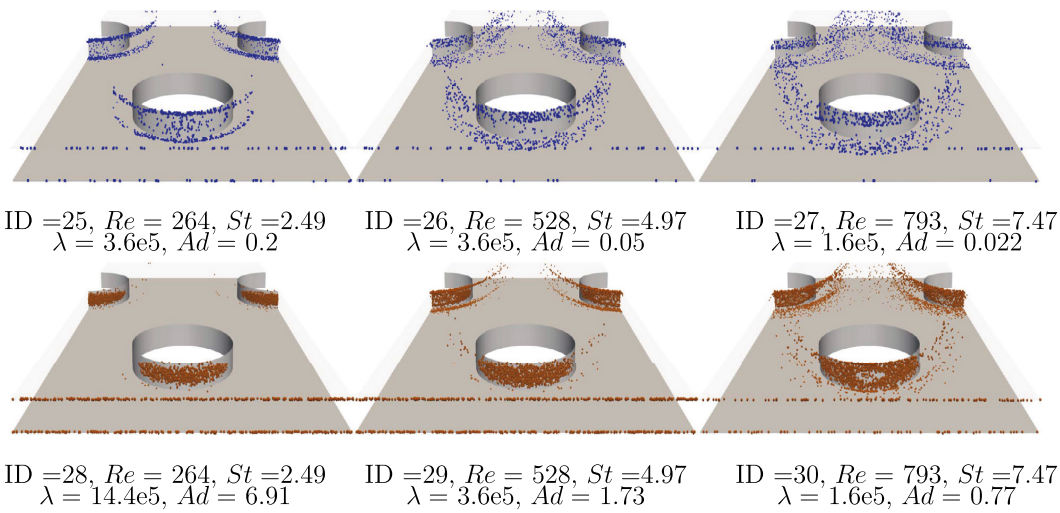

Fig. A2. Deposition locations for plain fin with $D_p = 20$ µm • low-adhesive and • high-adhesive particles (size of particles increased by a factor of 15).

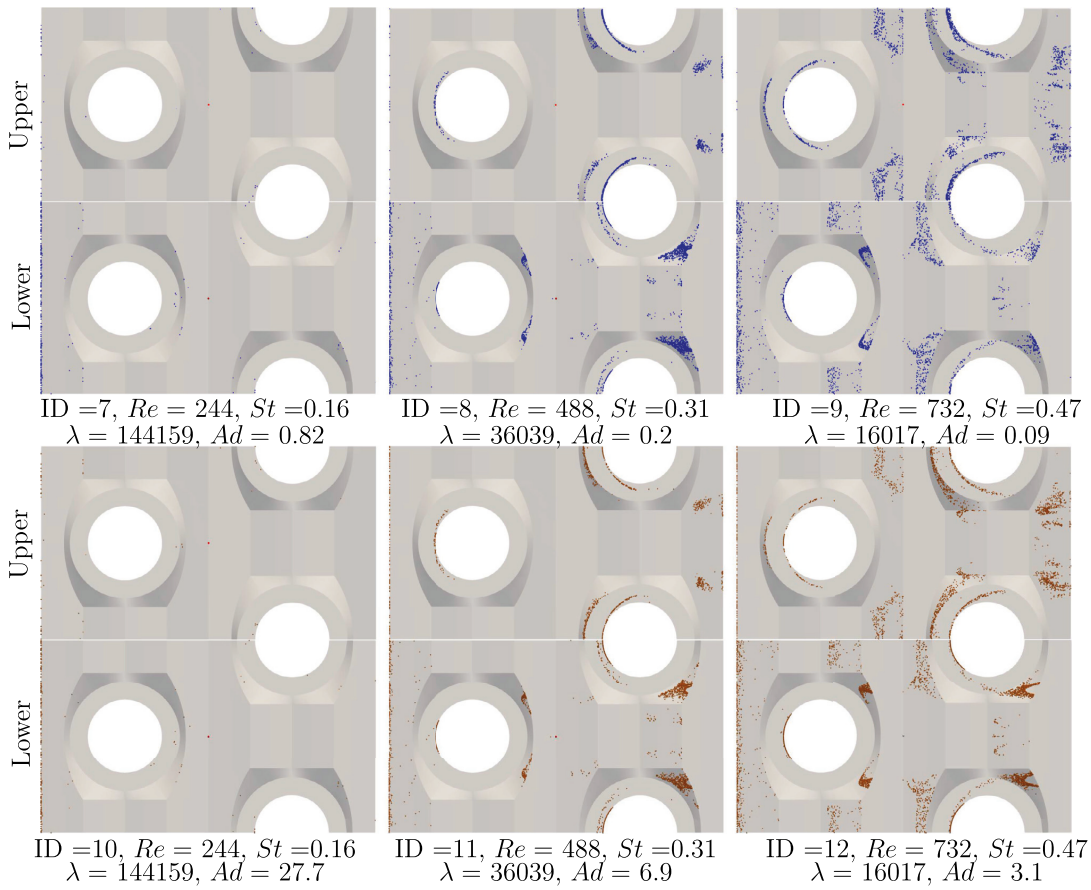

Fig. A3. Deposition locations for lower and upper fin separately with $D_p = 5$ µm • low-adhesive and • high-adhesive particles (size of particles increased by a factor of 60).

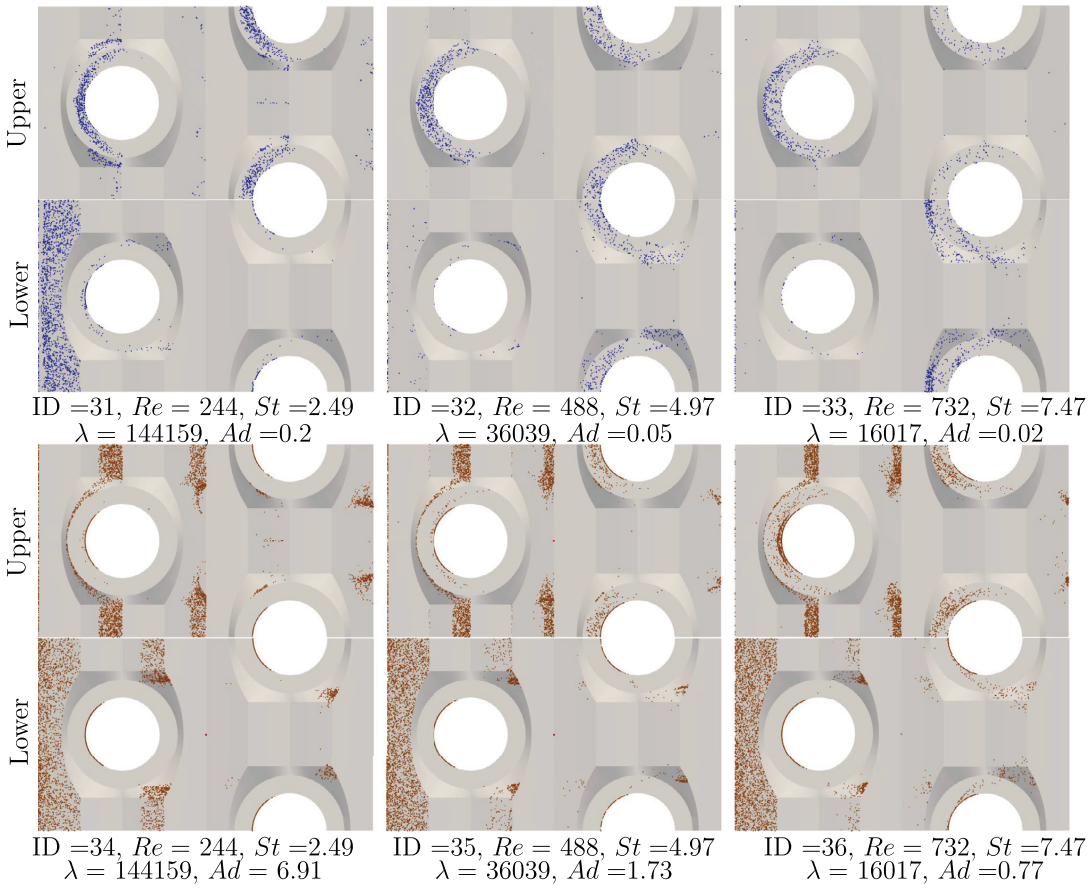

Fig. A4. Deposition locations for lower and upper fin separately with D_p = 20 μm • low-adhesive and • high-adhesive particles (size of particles increased by a factor of 15).

References

[1] L. Pérez-Lombard, J. Ortiz, C. Pout, A review on buildings energy consumption information, Energy Build. 40 (3) (2008) 394–398, doi:10.1016/j.enbuild.2007.03.007.

[2] A.F. Mills, A. Mills, Basic heat and mass transfer, 2, Prentice hall Upper Saddle River, 1999.

[3] J. Jeong, C.N. Kim, B. Youn, A study on the thermal contact conductance in fin-tube heat exchangers with 7mm tube, Int. J. Heat Mass Transf. 49 (7) (2006) 1547–1555, doi:10.1016/j.ijheatmasstransfer.2005.10.042.

[4] C.-C. Wang, R.L. Webb, K.-Y. Chi, Data reduction for air-side performance of fin-and-tube heat exchangers, Exp. Thermal Fluid Sci. 21 (4) (2000) 218–226, doi:10.1016/S0894-1777(00)00005-4.

[5] C.-C. Wang, K.-Y. Chi, C.-J. Chang, Heat transfer and friction characteristics of plain fin-and-tube heat exchangers, part ii: correlation, Int. J. Heat Mass Transf. 43 (15) (2000) 2693–2700, doi:10.1016/S0017-9310(99)00333-6.

[6] T. Vlikangas, R. Karvinen, Selected papers from the 9th international conference on computational heat and mass transfer, Heat Transf. Eng. (2016).

[7] Y.-T. Lin, Y.-M. Hwang, C.-C. Wang, Performance of the herringbone wavy fin under dehumidifying conditions, Int. J. Heat Mass Transf. 45 (25) (2002) 5035–5044, doi:10.1016/S0017-9310(02)00193-X.

[8] S. Wongwises, Y. Chokeman, Effect of fin pitch and number of tube rows on the air side performance of herringbone wavy fin and tube heat exchangers, Energy Convers. Manage. 46 (13–14) (2005) 2216–2231, doi:10.1016/j.enconman.2004.09.011.

[9] Y. Chokeman, S. Wongwises, Effect of fin pattern on the air-side performance of herringbone wavy fin-and-tube heat exchangers, Heat Mass Transf./Waerme- Und Stoffuebertragung 41 (7) (2005) 642–650, doi:10.1007/s00231-004-0578-5.

[10] X. Zhang, D. Tafti, Flow efficiency in multi-louvered fins, Int. J. Heat Mass Transf. 46 (10) (2003) 1737–1750, doi:10.1016/S0017-9310(02)00482-9.

[11] J. Yun, K. Lee, Investigation of heat transfer characteristics on various kinds of fin-and-tube heat exchangers with interrupted surfaces, Int. J. Heat Mass Transf. 42 (13) (1999) 2375–2385, doi:10.1016/S0017-9310(98)00310-X.

[12] T. Vlikangas, S. Singh, K. Sørensen, T. Condra, Fin-and-tube heat exchanger enhancement with a combined herringbone and vortex generator design, Int. J. Heat Mass Transf. 118 (2018) 602–616, doi:10.1016/j.ijheatmasstransfer.2017.11.006.

[13] M. Li, H. Zhang, J. Zhang, Y. Mu, E. Tian, D. Dan, X. Zhang, W. Tao, Experimental and numerical study and comparison of performance for wavy fin and a plain fin with radiantly arranged winglets around each tube in fin-and-tube heat exchangers, Appl. Thermal Eng. 133 (2018) 298–307, doi:10.1016/j.applthermaleng.2018.01.012.

[14] Y. He, H. Han, W. Tao, Y. Zhang, Numerical study of heat-transfer enhancement by punched winglet-type vortex generator arrays in fin-and-tube heat exchangers, Int. J. Heat Mass Transf. 55 (21) (2012) 5449–5458, doi:10.1016/j.ijheatmasstransfer.2012.04.059.

[15] Z. Guan, S. Yu, K. Hooman, H. Gurgenci, J. Barry, Dust characterisation for solar collector deposition and cleaning in a concentrating solar thermal power plant, Heat Exchanger Foul. Clean. (2015) 301–307.

[16] B.E. Lee, C.A. Fletcher, S.H. Shin, S.B. Kwon, Computational study of fouling deposit due to surface-coated particles in coal-fired power utility boilers, Fuel 81 (15) (2002) 2001–2008, doi:10.1016/S0016-2361(02)00127-8.

[17] M. Waring, J.A. Siegel, Particle loading rates for hvac filters, heat exchangers, and ducts, Indoor Air 18 (3) (2008) 209–224.

[18] F. Zhan, D. Zhuang, G. Ding, P. Ju, J. Tang, Influence of wet-particle deposition on air-side heat transfer and pressure drop of fin-and-tube heat exchangers, Int. J. Heat Mass Transf. 124 (2018) 1230–1244, doi:10.1016/j.ijheatmasstransfer.2018.04.049.

[19] Y.-C. Ahn, J.-M. Cho, H.-S. Shin, Y.-J. Hwang, C.-G. Lee, J.-K. Lee, H.-U. Lee, T.-W. Kang, An experimental study of the air-side particulate fouling in fin-and-tube heat exchangers of air conditioners, Korean J. Chem. Eng. 20 (5) (2003) 873–877.

[20] F.-L. Wang, Y.-L. He, Z.-X. Tong, S.-Z. Tang, Real-time fouling characteristics of a typical heat exchanger used in the waste heat recovery systems, Int. J. Heat Mass Transf. 104 (2017) 774–786, doi:10.1016/j.ijheatmasstransfer.2016.08.112.

[21] X. Li, H. Zhou, K. Cen, Influences of various vortex structures on the dispersion and deposition of small ash particles, Fuel 87 (7) (2008) 1379–1382, doi:10.1016/j.fuel.2007.07.007.

[22] L. Mu, L. Zhao, H. Yin, Modelling and measurements of the characteristics of ash deposition and distribution in a hrsg of wastewater incineration plant, Appl. Thermal Eng. 44 (2012) 57–68, doi:10.1016/j.applthermaleng.2012.03.039.

[23] A. Leppnen, H. Tran, R. Taipale, E. Vlimki, A. Oksanen, Numerical modeling of fine particle and deposit formation in a recovery boiler, Fuel 129 (2014) 45–53, doi:10.1016/j.fuel.2014.03.046.

[24] J.A. Siegel, W.W. Nazaroff, Predicting particle deposition on hvac heat exchangers, Atmospheric Environment 37 (39) (2003) 5587–5596, doi:10.1016/j.atmosenv.2003.09.033. Indoor Air Chemistry and Physics: Papers from Indoor Air 2002

[25] H.V. Inamdar, E.A. Groll, J.A. Weibel, S.V. Garimella, Prediction of air-side particulate fouling of hvac&r heat exchangers, Appl. Thermal Eng. 104 (2016) 720–733, doi:10.1016/j.applthermaleng.2016.05.082.

[26] B.C. Pak, E.A. Groll, J.E. Braun, Impact of fouling and cleaning on plate fin and spine fin heat exchanger performance., ASHRAE Trans. 111 (1) (2005).

[27] D. Bouris, G. Bergeles, Numerical calculation of the effect of deposit formation on heat-exchanger efficiency, Int. J. Heat Mass Transf. 40 (17) (1997) 4073–4084, doi:10.1016/S0017-9310(97)00058-6.

[28] H. Han, Y.-L. He, W.-Q. Tao, Y.-S. Li, A parameter study of tube bundle heat exchangers for fouling rate reduction, Int. J. Heat Mass Transf. 72 (2014) 210–221, doi:10.1016/j.ijheatmasstransfer.2014.01.010.

[29] F.-L. Wang, Y.-L. He, S.-Z. Tang, Z.-X. Tong, Parameter study on the fouling characteristics of the h-type finned tube heat exchangers, Int. J. Heat Mass Transf. 112 (Supplement C) (2017) 367–378, doi:10.1016/j.ijheatmasstransfer.2017.04.107.

[30] Y. Wang, G. Tang, Numerical investigation on the coupling of ash deposition and acid vapor condensation on the h-type fin tube bank, Appl. Thermal Eng. 139 (2018) 524–534, doi:10.1016/j.applthermaleng.2018.05.026.

[31] C. Zhang, Z. Tang, Z. Zhang, J. Shi, J. Chen, M. Zhang, Impact of airside fouling on microchannel heat exchangers, Appl. Thermal Eng. 128 (Supplement C) (2018) 42–50, doi:10.1016/j.applthermaleng.2017.08.163.

[32] I.H. Bell, E.A. Groll, H. König, Experimental analysis of the effects of particulate fouling on heat exchanger heat transfer and air-side pressure drop for a hybrid dry cooler, Heat Transf. Eng. 32 (3–4) (2011) 264–271.

[33] I.H. Bell, E.A. Groll, Air-side particulate fouling of microchannel heat exchangers: Experimental comparison of air-side pressure drop and heat transfer with plate-fin heat exchanger, Applied Thermal Engineering 31 (5) (2011) 742–749, doi:10.1016/j.applthermaleng.2010.10.019. MNF 2009 Special Issue

[34] F. Zhan, J. Tang, G. Ding, D. Zhuang, Experimental investigation on particle deposition characteristics of wavy fin-and-tube heat exchangers, Appl. Thermal Eng. 99 (2016) 1039–1047, doi:10.1016/j.applthermaleng.2016.01.136.

[35] F. Zhan, D. Zhuang, G. Ding, J. Tang, Numerical model of particle deposition on fin surface of heat exchanger, Int. J. Refrig. 72 (2016) 27–40, doi:10.1016/j.ijrefrig.2016.07.015.

[36] E. Sauret, K. Hooman, Particle size distribution effects on preferential deposition areas in metal foam wrapped tube bundle, Int. J. Heat Mass Transf. 79 (2014) 905–915, doi:10.1016/j.ijheatmasstransfer.2014.08.038.

[37] S.T. Kuruneru, E. Sauret, S.C. Saha, Y.T. Gu, A coupled finite volume & discrete element method to examine particulate foulant transport in metal foam heat exchangers, Int. J. Heat Mass Transf. 115 (2017) 43–61.

[38] S.T. Kuruneru, E. Sauret, S.C. Saha, Y. Gu, Coupled cfd-dem simulation of oscillatory particle-laden fluid flow through a porous metal foam heat exchanger: mitigation of particulate fouling, Chem. Eng. Sci. 179 (2018) 32–52, doi:10.1016/j.ces.2018.01.006.

[39] S.T. Kuruneru, E. Sauret, S.C. Saha, Y.T. Gu, A coupled finite volume & discrete element method to examine particulate foulant transport in metal foam heat exchangers, Int. J. Heat Mass Transf. 115 (2017) 43–61, doi:10.1016/j.ijheatmasstransfer.2017.07.027.

[40] S.T. Kuruneru, E. Sauret, K. Vafai, S.C. Saha, Y. Gu, Analysis of particle-laden fluid flows, tortuosity and particle-fluid behaviour in metal foam heat exchangers, Chem. Eng. Sci. 172 (2017) 677–687, doi:10.1016/j.ces.2017.07.027.

[41] W. Pirompugd, C.-C. Wang, S. Wongwises, Correlations for wet surface ratio of fin-and-tube heat exchangers, Int. J. Heat Mass Transf. 53 (1) (2010) 568–573, doi:10.1016/j.ijheatmasstransfer.2009.09.025.

[42] S. Elgobashi, An updated classification map of particle-laden turbulent flows, in: IUTAM Symposium on Computational Approaches to Multiphase Flow, Springer, 2006, pp. 3–10.

[43] R.I. Issa, Solution of the implicitly discretised fluid flow equations by operator-splitting, J. Comput. Phys. 62 (1) (1986) 40–65.

[44] C. Goniva, C. Kloss, N.G. Deen, J.A. Kuipers, S. Pirker, Influence of rolling friction on single spout fluidized bed simulation, Particuology 10 (5) (2012) 582–591.

[45] T.O. Foundation, The openfoam documentation, 2017.

[46] C. Kloss, C. Goniva, A. Hager, S. Amberger, S. Pirker, Models, algorithms and validation for opensource dem and cfd–dem, Progr. Comput. Fluid Dyn.Int. J. 12 (2–3) (2012) 140–152.

[47] F. Nicoud, F. Ducros, Subgrid-scale stress modelling based on the square of the velocity gradient tensor, Flow Turbul. Combus. 62 (3) (1999) 183–200.

[48] M. Mirzaei, A. Sohankar, L. Davidson, F. Innings, Large eddy simulation of the flow and heat transfer in a half-corrugated channel with various wave amplitudes, Int. J. Heat Mass Transf. 76 (2014) 432–446, doi:10.1016/j.ijheatmasstransfer.2014.04.018.

[49] R. Nagaosa, Turbulence model-free approach for predictions of air flow dynamics and heat transfer in a fin-and-tube exchanger, Energy Conversion and Management 142 (2017) 414–425, doi:10.1016/j.enconman.2017.03.063. Cited By 0

[50] P.A. Cundall, O.D. Strack, A discrete numerical model for granular assemblies, geotechnique 29 (1) (1979) 47–65.

[51] S. Benyahia, M. Syamlal, T.J. O'Brien, Extension of hill-koch-ladd drag correlation over all ranges of reynolds number and solids volume fraction, Powder Technol. 162 (2) (2006) 166–174, doi:10.1016/j.powtec.2005.12.014.

[52] R.J. Hill, D.L. Koch, A.J. Ladd, The first effects of fluid inertia on flows in ordered and random arrays of spheres, J. Fluid Mech. 448 (2001) 213–241.

[53] D.L. Koch, R.J. Hill, Inertial effects in suspension and porous-media flows, Annu. Rev. Fluid Mech. 33 (1) (2001) 619–647.

[54] H. Hamaker, The london van der waals attraction between spherical particles, Physica 4 (10) (1937) 1058–1072.

[55] K.L. Johnson, K. Kendall, A. Roberts, Surface energy and the contact of elastic solids, Proc. R. Soc. Lond. A 324 (1558) (1971) 301–313.

[56] D. Tabor, Surface forces and surface interactions, in: Plenary and Invited Lectures, Elsevier, 1977, pp. 3–14.

[57] J.N. Israelachvili, Intermolecular and Surface Forces, Academic press, 2011.
[58] E.J. Parteli, J. Schmidt, C. Blümel, K.-E. Wirth, W. Peukert, T. Pöschel, Attractive particle interaction forces and packing density of fine glass powders, Scientif. Rep. 4 (2014) 6227.
[59] J.S. Marshall, S. Li, Adhesive Particle Flow, Cambridge University Press, 2014.
[60] V. Armenio, U. Piomelli, V. Fiorotto, Effect of the subgrid scales on particle motion, Phys. Fluids 11 (10) (1999) 3030–3042.
[61] J. Hærvig, K. Sørensen, T. Condra, Early stages of agglomeration of adhesive particles in fully-developed turbulent pipe flows, Int. J. Multiph. Flow 106 (2018) 254–267, doi:10.1016/j.ijmultiphaseflow.2018.04.017.
[62] D. Labbé, P. Wilson, A numerical investigation of the effects of the spanwise length on the 3-d wake of a circular cylinder, J. Fluids Struct. 23 (8) (2007) 1168–1188, doi:10.1016/j.jfluidstructs.2007.05.005.
[63] V. Kalro, T. Tezduyar, Parallel 3d computation of unsteady flows around circular cylinders, Parallel Computing 23 (9) (1997) 1235–1248, doi:10.1016/S0167-8191(97)00050-1. Parallel computing methods in applied fluid mechanics.
[64] R.D. Henderson, Nonlinear dynamics and pattern formation in turbulent wake transition, J. Fluid Mech. 352 (1997) 65–112.
[65] C. Wieselberger, 'neurere feststellungen über die gesetze des flussigkeitsund luftwiederstands, 1921.
[66] L. Li, B. Li, Z. Liu, Modeling of spout-fluidized beds and investigation of drag closures using openfoam, Powder Technol. 305 (2017) 364–376, doi:10.1016/j.powtec.2016.10.005.
[67] J. Derksen, H. Van den Akker, S. Sundaresan, Two-way coupled large-eddy simulations of the gas-solid flow in cyclone separators, AIChE J. 54 (4) (2008) 872–885.
[68] J.D. Schwarzkopf, M. Sommerfeld, C.T. Crowe, Y. Tsuji, Multiphase Flows with Droplets and Particles, CRC press, 2011.
[69] Y.-H. Cheng, Y.-L. Lin, Measurement of particle mass concentrations and size distributions in an underground station, Aerosol Air Qual. Res. 10 (2010) 22–29.
[70] H. Kuuluvainen, A. Arffman, A. Järvinen, J. Harra, J. Keskinen, The effect of materials and obliquity of the impact on the critical velocity of rebound, Aerosol Sci. Technol. 51 (3) (2017) 301–310.
[71] S. Wall, W. John, H.-C. Wang, S.L. Goren, Measurements of kinetic energy loss for particles impacting surfaces, Aerosol Sci. Technol. 12 (4) (1990) 926–946.
[72] H.-C. Wang, W. John, Dynamic contact charge transfer considering plastic deformation, J. Aerosol Sci. 19 (4) (1988) 399–411.
[73] L. Rogers, J. Reed, The adhesion of particles undergoing an elastic-plastic impact with a surface, J. Phys. D: Appl. Phys. 17 (4) (1984) 677.
[74] T. D'Ottavio, S.L. Goren, Aerosol capture in granular beds in the impaction dominated regime, Aerosol Sci. Technol. 2 (2) (1982) 91–108.
[75] Y.-S. Cheng, H.-C. Yeh, Particle bounce in cascade impactors, Environ. Sci. Technol. 13 (11) (1979) 1392–1396.
[76] N.A. Esmen, P. Ziegler, R. Whitfield, The adhesion of particles upon impaction, J. Aerosol Sci. 9 (6) (1978) 547–556.